Dual Modulation of Chikungunya Virus nsP2 Protease: Peptide-Mediated Inhibition and Nucleic Acid-Induced Activation

Inaugural-Dissertation

zur Erlangung des Doktorgrades
der Mathematisch-Naturwissenschaftlichen Fakultät
der Heinrich-Heine-Universität Düsseldorf

vorgelegt von

Mohammadamin Mastalipour
aus Teheran, Iran

Aachen, Juli 2025

aus dem Institut für Physikalische Biologie
der Heinrich-Heine-Universität Düsseldorf

Gedruckt mit der Genehmigung der
Mathematisch-Naturwissenschaftlichen Fakultät der
Heinrich-Heine-Universität Düsseldorf

Berichterstatter:

1. Prof. Dr. Dieter Willbold

2. Apl. Prof. Dr. Andrew Dingley

Tag der mündlichen Prüfung: 10.10.2025

Eidesstattliche Erklärung

Ich, Mohammadamin Mastalipour, versichere an Eides statt, dass die vorliegende Dissertation von mir selbstständig und ohne unzulässige fremde Hilfe unter Beachtung der „Grundsätze zur Sicherung guter wissenschaftlicher Praxis an der Heinrich-Heine-Universität Düsseldorf“ erstellt worden ist.

Aachen, den

_____

Mohammadamin Mastalipour

Contents

Acknowledgements

I would like to take this opportunity to express my deep gratitude to my supervisor, Prof. Dr. Dieter Willbold, for his continuous support and valuable guidance throughout my doctoral research. I would also like to thank Prof. Dr. Andrew Dingley for his mentorship, insightful comments, and encouragement during this work.

I owe my heartfelt thanks to my co-supervisor, Dr. Raphael Eberle, for his unwavering support, constructive feedback, and encouragement. I am also very grateful to Dr. Monika A. Conrado for her generous assistance, helpful discussions, and kind support during my work. Without their help and dedication, this dissertation would not have been possible.

I sincerely thank Ian Gering for his help and technical support during the course of my research. My appreciation also extends to all the members of IBI-7, the IPB institute, and everyone else who contributed to this work with their time, knowledge, and assistance.

My deepest gratitude goes to my family especially my parents for their unconditional love and support. I am profoundly thankful to my partner Miriam and our beloved son Maxi, whose patience and encouragement sustained me through the most challenging moments. I would also like to thank my dear friends Pelin, Sara, Verena, and Felix for their continuous belief in me and their emotional support, not only during this project, but throughout my life.

Finally, thank you to everyone who, in ways big or small, contributed to the realization of this dissertation.

I dedicate this work to the hope for peace in the world. May knowledge, cooperation, and compassion guide us toward a better future for all.

List of Abbreviations

Abbreviation	Full term
µM	Micromolar
$3CL^{pro}$	3-chymotrypsin-like protease
Aβ	Amyloid beta
CDC	Centers for Disease Control and Prevention
CHIKV	Chikungunya virus
CPV	Cytopathic vacuole
Cys	Cysteine
DAC	DNA against CHIKV
DENV	Dengue virus
DMSO	Dimethyl sulfoxide
dsRNA	Double-stranded RNA
EC_{50}	Half maximal effective concentration
ECDC	European Centre for Disease Prevention and Control
E.coli	*Escherichia coli*
ELISA	Enzyme-linked immunosorbent assay
ER	Endoplasmic reticulum
FDA	Food and Drug Administration
Fig.	Figure
JEV	Japanese encephalitis virus
His	Histidine
HiTS-FLIP	High-throughput sequencing-fluorescent ligand interaction profiling
HSD	Hesperidin
HST	Hesperetin
IC_{50}	Half maximal inhibitory concentration
IgG	Immunoglobulin G
IgM	Immunoglobulin M
K_m	Michaelis-Menten constant
MD	Molecular dynamics
MHC-I	Major histocompatibility complex class I
MRI	Magnetic resonance imaging
mRNA	Messenger RNA
MST	Microscale thermophoresis
MTT	MTT assay 3-(4,5-dimethylthiazol-2-yl)-2,5-diphenyltetrazolium bromide
MXRA8	Matrix remodeling associated protein 8
MAYV	Mayaro virus
NGS	Next generation sequencing
nM	Nanomolar
nm	Nanometer
nsP	Non-structural protein
ORF	Open reading frame
PAHO	Pan American Health Organization
PDB	Protein Data Bank
pro	Protease
RAC	RNA against CHIKV
RRV	Ross River virus

RT-PCR	Reverse transcription polymerase chain reaction
SINV	Sindis virus
SLEV	St. Louis encephalitis virus
spp.	Species
ssDNA	Single-stranded DNA
ssRNA	Single-stranded RNA
VEEV	Venezuelan equine encephalitis virus
WEEV	Western equine encephalitis virus
WNV	West Nile virus
WHO	World Health Organization
YFV	Yellow fever virus
ZIKV	Zika virus

List of Figures

List of Tables

Abstract

Climate change favors the proliferation and spread of arthropod-borne viruses (arboviruses) around the globe. Chikungunya virus (CHIKV) is a re-emerging arbovirus from the genus *Alphavirus,* which is mainly transmitted by *Aedes* species mosquitoes. Due to climate change, the vector is now present in various regions, including the Americas, Africa, Europe, and Asia, and causes a rapid increase in CHIKV infections. The first approved vaccine was introduced against CHIKV in 2023. However, the vaccine has its limitations and is not beneficial for individuals already infected. This highlights the need for treatment against CHIKV. CHIKV is a positive-sense, single-stranded RNA virus, whose replication depends on the cleavage of the nonstructural polyprotein P1234 by the protease activity of non-structural protein 2 ($nsP2^{pro}$). In addition to its essential role in viral replication, $nsP2^{pro}$ is also involved in the downregulation of the host immune response, including suppression of the interferon response and disruption of major histocompatibility complex class I (MHC-I). The crucial role of $nsP2^{pro}$ in viral replication makes it a promising target for the development of antiviral therapies. In order to identify potential inhibitors against CHIKV $nsP2^{pro}$, two distinct approaches, including a phage display technique and the screening of animal venom-based peptides, were employed. Through phage display four peptides were identified with the potential to inhibit $nsP2^{pro}$. Biochemical analysis showed that peptide P1 had the strongest inhibitory effect among the four peptides, with a half-maximal inhibitory concentration (IC_{50}) of 4.6 ± 1.9 µM. Further *in vitro* and *in silico* studies revealed that peptide P1 has low cytotoxicity up to 100 µM and acts as a competitive inhibitor with micromolar-range affinity. The second potential candidate is pantinin-1, a peptide derived from the scorpion *Pandinus imperator,* with a broad antimicrobial spectrum. Inhibition assays demonstrated that pantinin-1 is capable of inhibiting the catalytic activity of $nsP2^{pro}$ with an IC_{50} value of 6.4 ± 2.04 µM and complete inhibition at a concentration of 175 µM. Various predictions with three docking programs (Galaxy TongDock, ClusPro, and HDock) showed that pantinin-1 interacts with the protease active site. However, some models predicted binding at a site opposite to the active site of $nsP2^{pro}$. In contrast, inhibition mode assay showed that pantinin-1 decreases the Michaelis-Menten constant (k_m) without affecting the reaction velocity, which is characteristic of a competitive inhibitor. The cell cytotoxicity assay revealed that pantinin-1 has no toxic effects at concentrations around three times higher than its $IC_{50;}$ however, toxicity was observed at concentrations of 40 µM and higher. Nucleic acids are an important factor influencing viral protein activity. Various studies have shown that certain viral proteins can interact with nucleic acids (DNA or RNA) from either the viral genome or the host cell. These interactions can affect the structure, stability, and function of viral proteins, particularly those involved in replication and assembly. In some cases, such interactions can enhance viral protease activity, which in turn impacts viral replication and host

infection. Based on this knowledge, The effects of different nucleic acids, including single- and double-stranded DNA, selected DNA aptamers through high-throughput sequencing-fluorescent ligand interaction profiling, and random nucleic acids, was evaluated on CHIKV $nsP2^{pro}$ activity. The analysis showed that both specifically selected and non-specific single-stranded nucleic acids enhance the activity of the protease. Moreover, it was shown that double-stranded DNA could not enhance protease activity. Additionally, the enhancement depends on buffer composition. At high salt concentration (400 mM NaCl), no enhancement in activity occurred. The molecular docking results predicted that single-stranded nucleic acids likely bind at the methyltransferase domain of the $nsP2^{pro}$. Finally, the effect of the single-stranded nucleic acids on the inhibitory effect of peptide P1 was evaluated. It was shown that in the presence of single-stranded nucleic acids, the inhibitory effect of peptide P1 decreased. This suggests a potential modulatory role of nucleic acids that should be taken into account when developing inhibitors against CHIKV $nsP2^{pro}$. However, further in-depth studies are necessary to confirm this observation and to determine whether this effect is broadly applicable.

Zusammenfassung

Der Klimawandel begünstigt die Vermehrung und weltweite Ausbreitung von Arthropoden-übertragenen Viren (Arboviren). Das Chikungunya-Virus (CHIKV) ist ein wiederauftretendes Arbovirus aus der Gattung *Alphavirus* und wird hauptsächlich durch Stechmücken der Gattung *Aedes* übertragen. Aufgrund veränderter klimatischer Bedingungen haben sich diese Vektoren mittlerweile in verschiedenen Regionen etabliert, darunter Amerika, Afrika, Europa und Asien, was zu einem raschen Anstieg von CHIKV-Infektionen führt. Im Jahr 2023 wurde der erste zugelassene Impfstoff gegen CHIKV eingeführt. Dieser Impfstoff weist jedoch Einschränkungen auf und ist für bereits infizierte Personen nicht wirksam, was die Notwendigkeit antiviraler Behandlungsstrategien unterstreicht. CHIKV ist ein RNA-Virus mit einzel- und positivsträngigem Erbgut, dessen Replikation von der Spaltung des nichtstrukturellen Polyproteins P1234 durch die Proteaseaktivität des nichtstrukturellen Proteins 2 ($nsP2^{pro}$) abhängt. Neben seiner zentralen Rolle in der viralen Replikation ist $nsP2^{pro}$ auch an der Umgehung der Immunantwort beteiligt, unter anderem durch die Suppression der Interferon-Antwort und die Störung der Expression des Haupthistokompatibilitätskomplexes Klasse I (MHC-I). Aufgrund seiner Schlüsselrolle stellt $nsP2^{pro}$ ein vielversprechendes Ziel für die Entwicklung antiviraler Wirkstoffe dar.

Zur Identifikation potenzieller Inhibitoren von CHIKV $nsP2^{pro}$ wurden zwei komplementäre Ansätze verfolgt: ein *phage display technology* sowie die Untersuchung von Peptiden tierischen Ursprungs. Das *phage display* identifizierte vier Peptide mit potenziell inhibitorischer Wirkung auf $nsP2^{pro}$. Unter diesen zeigte Peptid P1 die stärkste Hemmwirkung mit einer halbmaximalen inhibitorischen Konzentration (IC_{50}) von 4,6 ± 1,9 µM. Weitere *in vitro*- *und in silico*-Analysen zeigten, dass P1 bis zu einer Konzentration von 100 µM eine geringe Zytotoxizität aufweist und als kompetitiver Inhibitor mit mikromolarer Affinität wirkt. Ein zweiter vielversprechender Kandidat ist Pantinin-1, ein Peptid aus dem Skorpion *Pandinus imperator*, das ein breites antimikrobielles Spektrum aufweist. Enzymatische Hemmtests zeigten, dass Pantinin-1 die Aktivität von $nsP2^{pro}$ mit einer IC_{50} von 6,4 ± 2,04 µM hemmt; bei einer Konzentration von 175 µM wurde eine vollständige Inhibition beobachtet. Molekulare Docking-Studien mit drei Programmen (GalaxyTongDock, ClusPro und HDOCK) ergaben, dass Pantinin-1 vermutlich an der aktiven Stelle der Protease bindet; einige Modelle deuteten jedoch auch auf eine alternative Bindung gegenüber der aktiven Stelle hin. Im Gegensatz dazu zeigte die kinetische Analyse, dass Pantinin-1 den Michaelis-Konstanten (K_m) senkt, ohne die Reaktionsgeschwindigkeit zu beeinflussen - ein typisches Merkmal kompetitiver Inhibitoren. Zytotoxizitätsanalysen zeigten, dass Pantinin-1 bis zum Dreifachen seiner IC_{50} keine toxischen Effekte aufweist, jedoch ab einer Konzentration von 40 µM eine Toxizität erkennbar ist. Nukleinsäuren stellen einen wichtigen Faktor dar, der die Aktivität viraler

Proteine beeinflussen kann. Verschiedene Studien haben gezeigt, dass bestimmte virale Proteine mit Nukleinsäuren (DNA oder RNA) aus dem viralen Genom oder der Wirtszelle interagieren können. Diese Interaktionen können die Struktur, Stabilität und Funktion viraler Proteine beeinflussen, insbesondere solcher, die an der Replikation und Assemblierung beteiligt sind. In einigen Fällen können diese Wechselwirkungen die Aktivität viraler Proteasen steigern und somit die virale Replikation sowie die Infektion von Wirtszellen fördern. Auf Grundlage dieser Erkenntnisse wurde der Einfluss verschiedener Nukleinsäuren - darunter Einzel- und Doppelstrang-DNA, selektierte DNA-Aptamere (identifiziert mittels Hochdurchsatz-Sequenzierung und fluoreszenzbasierter Liganden-Interaktions-Analyse) sowie zufällige Nukleinsäuren - auf die Aktivität von CHIKV nsP2^{pro} untersucht. Die Analyse zeigte, dass sowohl spezifisch selektierte als auch unspezifische einzelsträngige Nukleinsäuren die Proteaseaktivität steigern können, während Doppelstrang-DNA diesen Effekt nicht zeigte. Darüber hinaus wurde festgestellt, dass die Aktivitätssteigerung vom Puffer abhängig ist: Bei hoher Salzkonzentration (400 mM NaCl) war keine Aktivitätssteigerung nachweisbar. Molekulare Docking-Analysen deuten darauf hin, dass einzelsträngige Nukleinsäuren wahrscheinlich an die Methyltransferase-Domäne von nsP2^{pro} binden. Abschließend wurde der Einfluss einzelsträngiger Nukleinsäuren auf die inhibitorische Wirkung von Peptid P1 untersucht. Es zeigte sich, dass in Anwesenheit dieser Nukleinsäuren die Hemmwirkung von P1 reduziert war. Dies weist auf eine mögliche modulierende Rolle von Nukleinsäuren hin, die bei der Entwicklung von Inhibitoren gegen CHIKV nsP2^{pro} berücksichtigt werden sollte. Dennoch sind weiterführende, vertiefte Studien erforderlich, um diese Beobachtung zu bestätigen und zu klären, ob dieser Effekt allgemein übertragbar ist.

.

1. Introduction

1.1 Impact of climate change on infection diseases

Climate change is creating favorable conditions for the spread of pathogens transmitting infectious diseases into new regions and poses a significant threat to global health [1, 2]. These environmental changes influence the transmission dynamics of various diseases, including food-borne, airborne, and vector-borne (arthropod-borne) infections [3]. Among the critical contributing factors is rising temperature, which facilitates the expansion of arthropod populations into new habitats. As a result, the incidence of arboviral diseases is increasing, raising the risk of emerging epidemics (Fig. 1) [4].

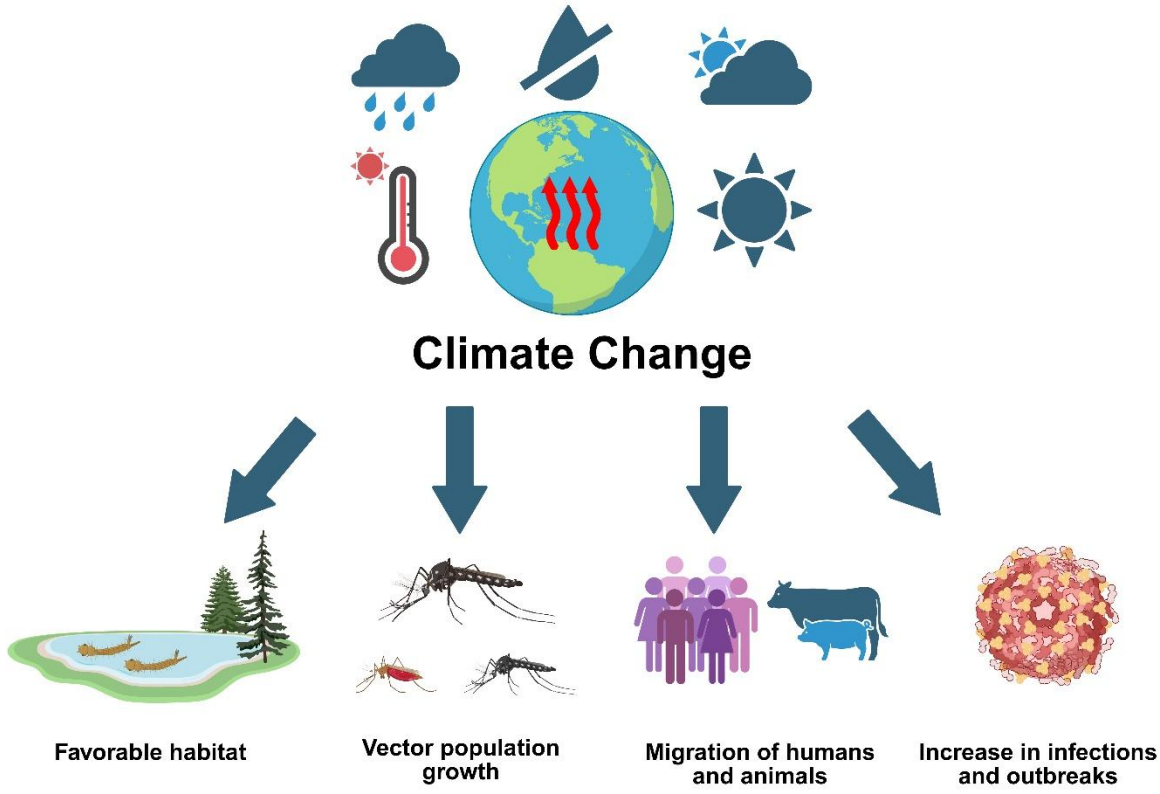

Fig. 1 Impact of climate change on vector-borne disease. The figure demonstrates that climate change creates favorable habitats for vectors and leads to an increase in vector populations. In addition, it shows that climate change drives the movement of humans and animals into new areas. Together, these factors contribute to the rise of new epidemics and outbreaks. The figure was created with BioRender and adapted from Bartlow et al. [5].

1.2 Arbovirus

Arboviruses are arthropod-borne viruses transmitted by blood-sucking arthropods, such as mosquitoes and ticks, from one host to another [6]. According to the Arbovirus Catalog from the Centers for Disease Control and Prevention (CDC), over 500 arboviruses have been identified to date, with many capable of infecting humans or posing a potential threat [7]. Among these, more than 100 are known to cause humans diseases [8]. Arboviruses are primarily RNA viruses and are classified into distinct families based on their genomic characteristics [9]. They are further categorized into three major groups according to their RNA genome structure: positive-sense single-stranded RNA, negative-sense single-stranded RNA, and double-stranded RNA (Table 1) [10, 11].

Table 1. Classification of arboviruses based on RNA genome structure

RNA genome type	Representative genera	Example viruses	Reference
Positive-sense single-stranded RNA	*Alphavirus*	CHIKV, MAYV, VEEV, RRV, WEEV, SINV	[10-12]
	Flavivirus	DENV, YFV, ZIKV, JEV, WNV, SLEV	[10-12]
Negative-sense single-stranded RNA	*Orthobunyavirus*	La Crosse virus, Bunyamwera virus	[10, 13]
Double-stranded RNA	*Orbivirus*, *Coltivirus*	Bluetongue virus, Colorado tick fever virus	[10, 14, 15]

1.3 Chikungunya

Chikungunya (CHIKV) is considered a significant threat among arboviruses. It is the causative agent of chikungunya fever and belongs to the genus *Alphavirus* within the family *Togaviridae* [16]. The first documented outbreak of CHIKV dates back to 1952 in Tanzania and was initially described as a dengue-like fever [17], and in 1953, R.W. Ross reported the isolation and characterization of the chikungunya virus [18]. Since then, CHIKV has been detected in multiple regions across the world (Fig. 2), with numerous major outbreaks documented in Africa, the Americas, Europe, and Asia, as shown in Table 2. According to the Pan American Health Organization (PAHO), between 2018 to 2025, a total of 1,793,179 cases of CHIKV were reported in the Americas, of which 951,091 were confirmed cases [19]. Another report from the European Centre for Disease Prevention and Control (ECDC) indicates that between February 2023 and January 2024, around 10,000 CHIKV cases were reported, most of them in the American, particularly in countries such as Brazil, Paraguay, Bolivia, and Colombia [20]. By March 2025, an additional 80,000 cases had been reported, with 46 deaths [21].

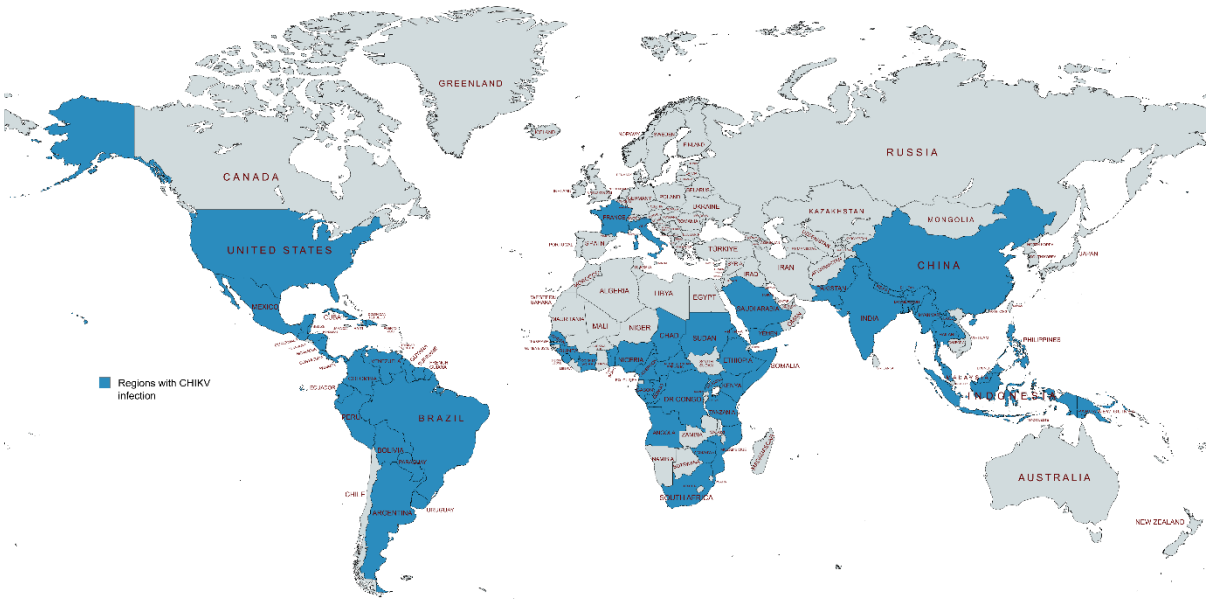

Fig. 2. Regions with reported cases of CHIKV. Areas where CHIKV has been reported are highlighted in blue. The figure was adapted from data provided by the World Health Organization (WHO) and created using the online tool MapChart [25].

The European region has also been affected by CHIKV, including the 2007 outbreak in Italy with 217 confirmed cases [22]. The index case was linked to a traveler returning from India, indicating an imported origin of the virus [22]. In addition to travel-associated cases, local transmission has been reported in several outbreaks, such as those in France in 2010, 2014, and 2017 [23]. These outbreaks were primarily transmitted by *Aedes albopictus* mosquitoes, highlighting the role of local vectors in sustaining CHIKV transmission [23]. More recently, a major epidemic was reported on La Réunion, a French overseas territory, with over 47,500 confirmed cases and more than 170,000 suspected cases between August 2024 and 4 May 2025 [24]. These data show the widespread nature of CHIKV infection and the importance of CHIKV as a re-emerging virus.

Table 2. List of globally occurred CHIKV outbreaks.

Year	Location	Estimated number of cases/Attack rate	Reference
1952-1953	Tanzania	N/A (23% attack rate)	[17, 26]
1958	Thailand (Bangkok)	N/A	[27]
1963, 1973	India	N/A	[28]
2004	Kenya, Lamu	At least 1,300/ 75% attack rate in affected areas	[29]
2005-2006	La Réunion (France)	266,000-300,000	[30]
2006	India	Over 1.25 million suspected cases	[31]
2007	Italy (Ravenna Province)	205	[32]
2019	Republic of the Congo	6,149 suspected	[33]
2024-2025	La Réunion (France)	47,500 confirmed; 170,000+ consultations	[24]

N/A: Not available

1.4 Transmission

CHIKV is primarily transmitted by mosquitoes of the *Aedes* genus, specifically *Aedes aegypti* and *Aedes albopictus* [34]. However, mosquito bites are not the only transmission route; vertical transmission can also occur, potentially leading to impaired neurocognitive development or increased mortality [35, 36]. CHIKV follows two distinct transmission cycles (Fig. 3). The first is the enzootic cycle, also known as the sylvatic cycle, which occurs in forested areas where non-human primates and other *Aedes* species, such as *Aedes africanus*, *Aedes luteocephalus* and *Aedes taylori* are found [37]. The second cycle, known as the urban cycle, occurs in urban areas and involves transmission between humans and *Aedes aegypti* or *Aedes albopictus* [38].

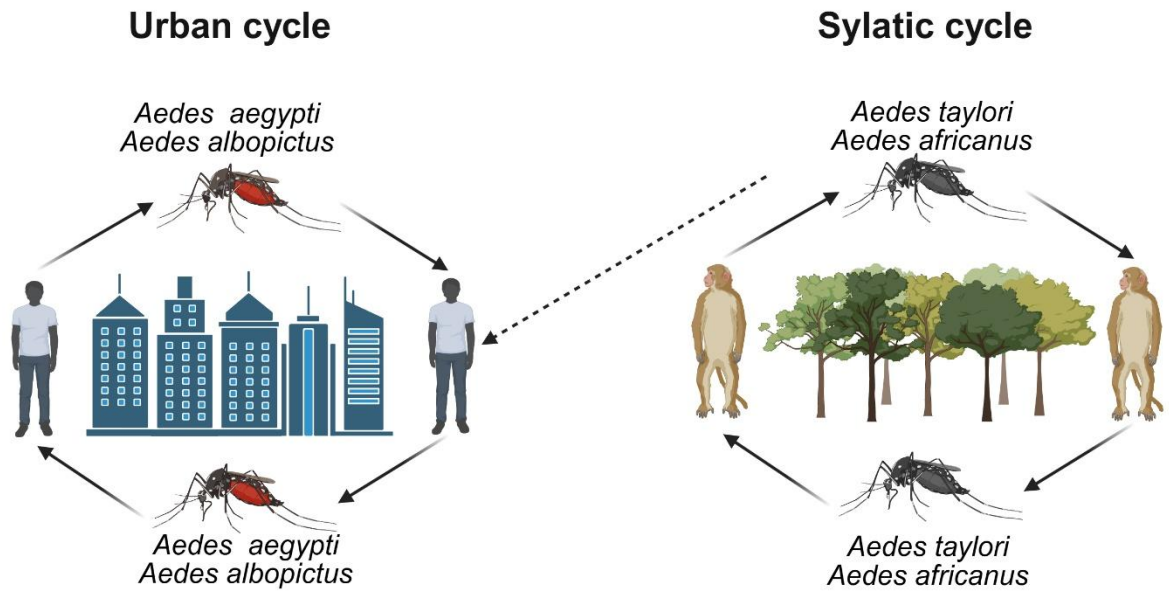

Fig. 3. Transmission cycles of CHIKV. CHIKV is transmitted through two primary cycles: the urban cycle and the sylvatic cycle. The urban cycle involves transmission between humans and *Aedes aegypti* or *Aedes albopictus*. The sylvatic cycle involves non-human primates and other *Aedes* species, such as *Aedes taylori* and *Aedes africanus*,. The figure was created with BioRender and adapted from Power et al. and Diallo et al. [37, 39].

Although transmission to humans is primarily caused by *Aedes aegypti* or *Aedes albopictus,* there are notable differences between these mosquitoes species that influence the efficiency of the transmission of the virus. A 2007 study demonstrated that *Aedes aegypti* exhibits a significantly higher target-attack rate, approximately 30 times higher, and displays more aggressive behavior than *Aedes albopictus* [40]. As previously discussed, climate change impacts the dynamics of arbovirus transmission. Rising temperatures, in particular, affect mosquito vectors by weakening the midgut infection barrier in *Aedes aegypti*, thereby

increasing midgut infection rates and making the species more susceptible to CHIKV infection [41].

1.5 Clinical manifestation of CHIKV

Chikungunya fever has two main phases: an acute phase and a chronic phase [42]. The acute phase begins 2-4 days after the incubation period and may persist up to three weeks [43]. Common symptoms include high fever, skin rash, headache, polyarthralgia, and photophobia [43, 44]. However, approximately 15% of infected individuals remain asymptomatic [45]. Joint pain is the most common and debilitating symptom (~90% of patients) involving the limb joints such as the knees, elbows, fingers and ankles [46]. The second stage of the infection is the chronic phase, which is characterized by persistent arthralgia, myalgia, skin lesions, sleep disorders, and even depression [47]. In approximately 40% to 80% of the cases, the disease progresses to the chronic phase, whose duration can range from three months to several years [43]. The prevalence of the chronic phase varies across studies; however, a review by Silveira-Freitas et al. indicates that between 40% and 60% of patients suffer from persistent arthralgia, one of the main symptoms of the chronic phase [48]. These findings suggest that high proportions of infected individuals are at high risk of chronic Chikungunya infection. Progression to the chronic phase is influenced by several risk factors. A cohort study conducted in the French West Indies found that older individuals and females have a higher probability of developing chronic arthritis and experiencing dehydration during the acute phase, both of which may contribute to the progression to chronic phase [49]. Additionally, a long duration of joint pain during the acute phase has been associated with an increased risk of arthralgia [50].

As illustrated in Fig. 4, CHIKV can affect multiple organs, including the heart, lungs, joint, skin and even the brain [51]. Infection of the brain has a particularly influence and is associated with a range of disorders, such as the Guillain-Barré syndrome, encephalitis, meningoencephalitis, and neonatal hypotonia [52-54]. Although the overall mortality rate of CHIKV infection is low, patients with neurological complications exhibit significantly higher mortality rates, approximately 45% compared to 5% in those without neurological involvement ~5%) [55, 56].

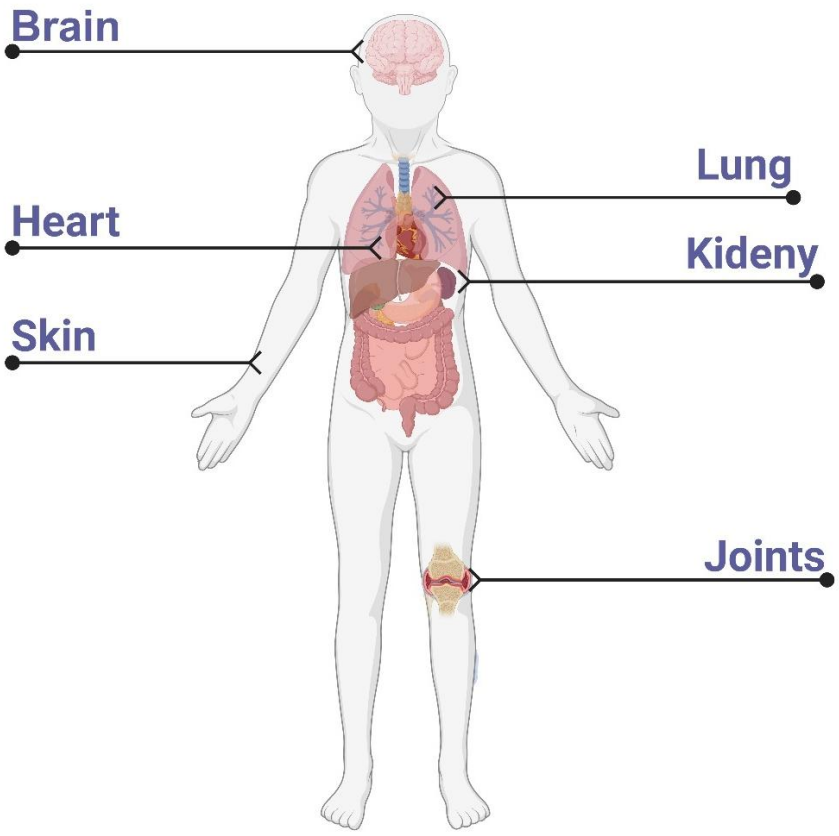

Fig. 4. Organs affected by CHIKV infection in human. The figure illustrates the major organs impacted by CHIKV infection The figure was created with BioRender and adapted from Traverse et al. [51].

1.6 CHIKV genome

CHIKV is an enveloped virus with a positive-sense single-stranded RNA genome consisting of approximately 11,805 nucleotides [57]. The genome is flanked by a 7-methylguanosine cap at the 5′ end and a poly-A tail at the 3′ end [58, 59]. The viral RNA contains two open reading frames (ORFs): ORF1 encoding non-structural proteins (nsPs), while ORF2 encodes structural proteins [60]. The CHIKV genome encodes four non-structural proteins (nsP1-nsP4) and six structural proteins, including the capsid, envelope proteins E1-E3, and 6K all of which play important roles in viral replication (Fig. 5) [61].

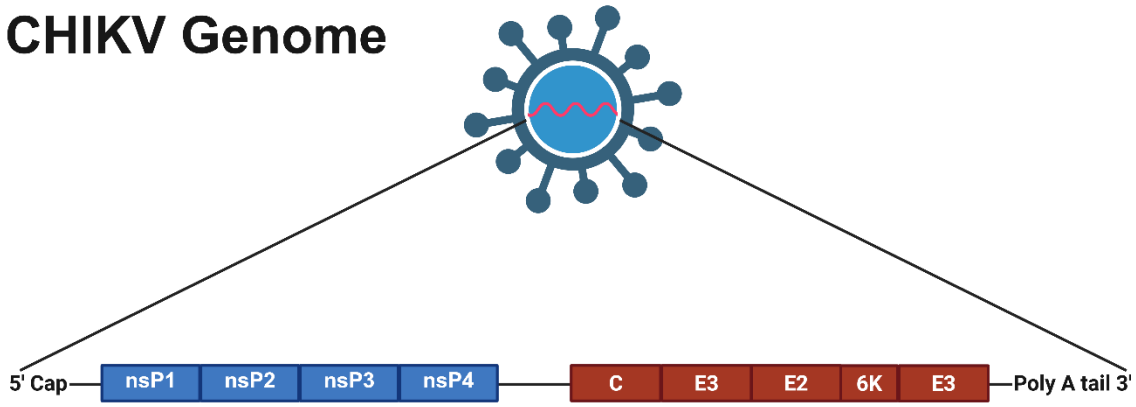

Fig. 5. Structure of the CHIKV genome. The figure illustrates the organization of the CHIKV genome, highlighting the four non-structural proteins (nsP1-nsP4) and the structural proteins, including the capsid (C), envelope protein (E) and 6k leader peptides. The figure was created with BioRender and adapted from Varikkodan et al. [62].

1.6.1 Structural proteins

One of the major structural proteins is the capsid protein, a multifunctional protein primarily responsible for encapsidating the viral genome [63]. It contains an N-terminal RNA-binding domain that inhibits host transcription and facilitates capsid protein dimerization [63]. The C-terminal region anchorages a serine protease domain, which mediates the autocleavage of the capsid from the precursor polyprotein [64, 65].

As illustrated in Fig. 5, CHIKV contains three distinct envelope proteins that play crucial roles in virus attachment and entry. Entry into the host cell is mediated by the interaction between the viral spike protein and specific cell surface receptors [66]. In CHIKV, the spike protein is a heterodimer composed of envelope proteins E1 and E2, which are properly folded with the assistance of the E3 protein. In addition, E1 plays an important role, it facilitates the release of the viral genome into the host cell [67]. The last CHIKV structural protein to mention is the 6K protein, a small polypeptide with around 60 amino acids [68]. This protein predominantly remains in the endoplasmic reticulum (ER) and plays a critical role in proper viral assembly [69]. Additionally, it forms ion channels and modulates membrane permeability [70].

1.6.2 Non-structural protein

CHIKV encodes four distinct non-structural proteins (nsPs). The first, nsP1, exhibits methyltransferase and guanylyltransferase activity, which are essential for the capping of viral RNA [71, 72]. nsP2 is a multifunctional protein that contributes to multiple steps in the viral replication cycle. The N-terminal region contains RNA helicase and 5′-triphosphatase activities, which are essential for RNA processing and capping. The C-terminal region contains

a cysteine protease domain and a methyltransferase-like domain. One of the critical functions of nsP2 is the proteolytic cleavage of the viral nonstructural polyprotein precursor. [73-75]. These functions will be discussed in more detail in section 1.10. Although the function of nsP3 is not completely understood, studies suggest it is involved in genome replication and may contribute to structural protein synthesis [76]. Lastly, nsP4 functions as an RNA-dependent RNA polymerase, responsible for synthesizing the viral RNA [77].

1.7 CHIKV replication

The replication process begins with the attachment of the virus to glycosaminoglycans on the surface of the host cell [78, 79]. The envelope protein E2 interacts with cell receptors such as MXRA8 (Matrix remodeling associated protein 8) and mediates viral entry into via clathrin-mediated endocytosis and subsequent formation of endosomes (Fig. 6A-B) [80]. Following cell entry, the acidification of the endosome triggers a conformational change in the envelope protein E1, allowing it to insert into the endosomal membrane. This process facilitates the release of the viral genome into the host cell cytoplasm (Fig. 6C) [81, 82]. In the next step, the viral genome is translated by host cell translation factors, resulting in the production of the viral polyprotein (Fig. 6D). The polyprotein, known as P1234, is cleaved by nsP2 into individual non-structural proteins [83]. Next, all nsPs, together with viral RNA and host proteins, form on the cell membrane a viral replication compartment known as a spherule, which is essential for viral genome replication and subgenomic transcription (Fig. 6E) [84]. Spherules are then internalized to form a large cytopathic vacuole (CPV-I) (Fig. 6F) [85]. Subsequently, the translation of the structural proteins takes place. Following autocleavage of the capsid, the genomic RNA is encapsidated to form the nucleocapsid, which is transported to the cell membrane. In parallel, the remaining structural proteins are processed by the ER-Golgi apparatus and transported to the cell surface (Fig. 6G) [36]. Finally, viral assembly is completed through the interaction between the nucleocapsid and the envelope proteins (Fig. 6H-J) [36].

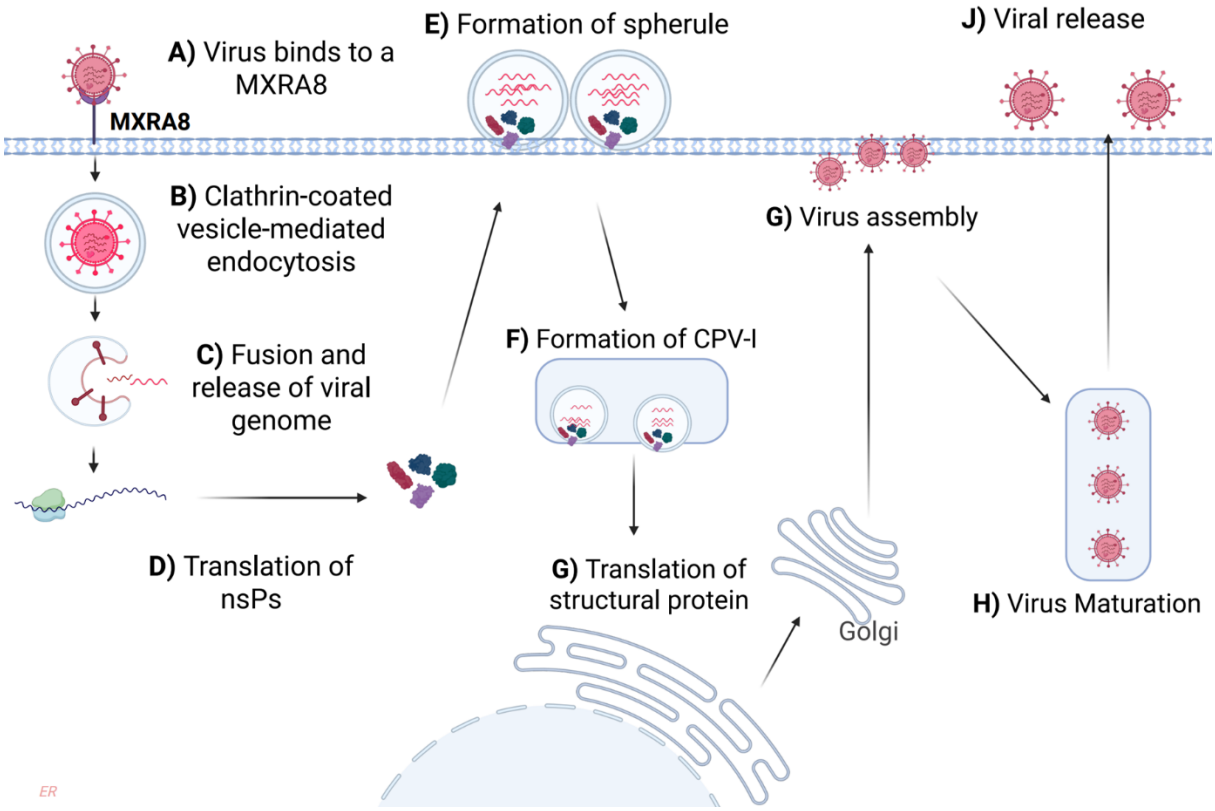

Fig. 6. Replication cycle of CHIKV. The figure was created with BioRender, and adapted and simplified from Silva and Dermody (2017). [36].

1.8 Diagnostic

CHIKV presents a diagnostic challenge due to its clinical similarity to other arboviruses and its potential for co-infection with members of the *flavivirus* family, such as ZIKV and DENV, which share the same mosquito vector [86-89]. These complications can result in misdiagnosis of CHIKV infection and highlight the need for more frequent and precise monitoring [89]. Clinical signs and case reports are the first steps in detecting CHIKV infection, and the use of medical imaging such as magnetic resonance imaging (MRI) can help detect neuroinvasion, while ultrasound can be used to investigate joint inflammation [90, 91]. The main route to confirm an infection is through laboratory testing. For decades, virus culture was used to identify, amplify, and isolate the virus, but it is a time-consuming method and has low sensitivity [92, 93]. Reverse transcription polymerase chain reaction (RT-PCR) is considered the gold-standard method for diagnosing and detecting CHIKV with high sensitivity. This technique was widely employed during the recent COVID-19 pandemic [94]. However, RT-PCR requires specialized laboratories and expensive equipment, making it less practical for use in developing countries where arboviruses are endemic [95]. A more suitable and cost-effective option in developing countries is the use of serological techniques such as ELISA to detects IgG and IgM antibodies. Although this method is more economical and does not require highly

trained personnel, it carries the risk of non-specific binding of antibodies to related antigens and epitopes from the other members of the *Alphavirus* family [96]. A recently developed rapid diagnostic test (Bio-Manguinhos, Fundação Oswaldo Cruz, Brazil) for CHIKV, DENV, and ZIKV provides a quick and simple method for detecting infection [97]. However, the test has demonstrated low sensitivity and moderate specificity during the acute phase, making it more useful in the convalescent phase [97]. Overall, there remains a need for a diagnostic tool that is both precise and cost-effective, with high specificity and sensitivity.

1.9 Prevention and vaccination

Vector control and prevention remain the first line of defense against CHIKV. According to WHO guidelines, wearing long clothes, regularly cleaning and emptying water containers, disposing of waste properly, and using insecticides can help minimize transmission and reduce mosquito population [98]. The development of a vaccine against CHIKV has been a major focus of research. Several candidates (Table 3) have progressed beyond the laboratory and entered clinical trials. Among them, the vaccine VLA1553 (Ixchiq) successfully passed clinical trials and was approved in 2023 by the U.S Food and Drug Administration (FDA) for individuals aged 18 and older. It was later approved by the European Union [99-101]. VLA1553 is a single-dose live-attenuated vaccine that contains a deletion mutation in nsP3 region [100, 102]. Immunogenicity analysis from phase 3 clinical trials showed that in 98.9% of vaccinated participants developed neutralizing antibodies against CHIKV [103]. The vaccine showed that approximately 51% of vaccinated individuals experienced mild to moderate side effects, including arthralgia, headache and fever. However, two individuals developed severe side effects requiring hospitalization [103, 104]. Vimkunya (PXVX0317) is the second vaccine to be approved, receiving authorization in February 2025 from both the USA and the European Union [105]. Vimkunya is a virus-like particle vaccine and, in contrast to VLA1553, is suitable for both adults and children aged 12 years and older. The phase 3 clinical trials analysis reported that 96.8% of participants achieved seroprotective levels of neutralizing antibodies 15 days after immunization with Vimkunya, and this figure increased to 97.8% by the day 22 [105]. The vaccine demonstrated safety profile, with low to moderate adverse effects that resolved within two days [105]. The approval of these vaccines represents a significant advancement in the fight against CHIKV infection. However, children under 12 years are still at risk, and the vaccines are not effective for individuals who are already infected. This highlights the continued need for effective antiviral therapies.

Table 3. List of developed vaccines against CHIKV.

Vaccine	Type	Clinical trials	Approval	Reference
VLA1553	Live attenuated	Phase III	USA, Europe and Brazil	[99, 101]
Vimkunya	Virus-like particle	Phase III	USA and Europe	[105]
VAL-181388	mRNA-based	Phase I	-	[106]
MV-CHIK-202	Live-attenuated measles-virus	Stop after Phase II	-	[107]
ChAdOx1 Chik	Simian adenovirus vectored vaccine	Phase I	-	[108]

1.10 Non-structural protein 2 (nsP2)

The importance of nsP2 in the replication of CHIKV was previously discussed. In this section, we take a closer look at its structure, function, and biological significance. The CHIKV nsP2 is a multifunctional protein involved in several key processes of the viral life cycle. Its N-terminal region exhibits RNA helicase and 5′-triphosphatase activities, while the C-terminal region contains cysteine protease and methyltransferase domains [74, 75]. The helicase activity of nsP2 is essential for unwinding intermediate double-stranded RNA (dsRNA) during viral replication [109, 110]. In addition, CHIKV RNA contains a 5′ cap, the formation of which depends on the triphosphatase activity of nsP2. This enzyme initiates the capping process by removing the γ-phosphate from the 5′ end of the viral RNA [110, 111]. The nsP2 cysteine protease ($nsP2^{pro}$) belongs to the papain-like superfamily and is more specifically classified within the peptidase family C9 of clan CA [112, 113]. The protease activity is essential for cleaving the polyprotein P1234, the precursor of nsP1-nsP4, into individual functional proteins [114, 115]. The active site (Fig. 7A) of $nsP2^{pro}$ contains two conserved amino acids: histidine 548 (His 548) and cysteine 478 (Cys 478) [116]. $nsP2^{pro}$ recognizes three specific sequences in the polyprotein that are critical for identifying the cleavage site (Fig. 7B) [73]. Interestingly, the amino acid glycine is conserved at all cleavage sites and plays a critical role in the cleavage of $nsP2^{pro}$ [83]. Proteolytic cleavage of the polyprotein by $nsP2^{pro}$ occurs in a defined order: nsP4 is released first, followed by nsP3 and then nsP1 (Fig. 7B) [117]. The substrate-binding site of CHIKV $nsP2^{pro}$ is located at the interface between the methyltransferase and cysteine protease domains and consists of four subsites, designated S1-S4 [116]. Beyond the

important role of nsP2 in replication, it also plays a key role in suppressing the host's innate immune system. nsP2 is capable of degrading the Rbp1 subunit of RNA polymerase II, which leads to downregulation of host mRNA transcription and suppression of the antiviral response [118]. In addition, nsP2 inhibits the MDA5/RIG-I signaling pathway, impairing the detection of viral dsRNA and the downregulation of interferon [119]. Although the function of the methyltransferase domain is not fully understood, studies suggest its involvement in suppressing the innate immune response by inhibiting the JAK/STAT signaling pathway, a key component of interferon signaling [120]. Besides that, it can disrupt major histocompatibility complex class I (MHC-I) antigen presentation, thereby helping the virus evade detection by $CD8^+$ T cells [121].

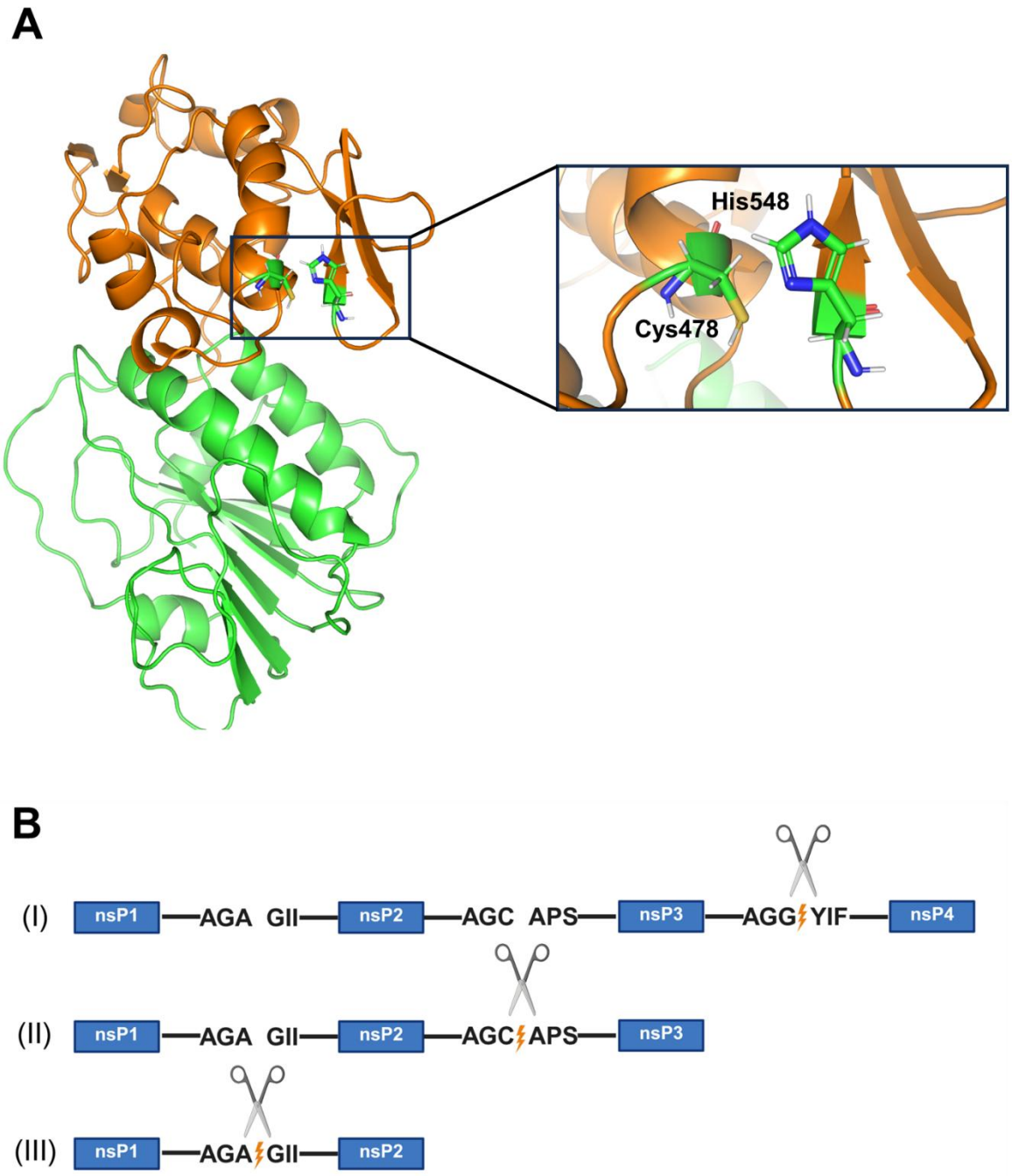

Fig. 7. Structure of nsP2^{pro} and cleavage sites of polyprotein P1234. **(A)** Crystal structure of nsP2^{pro} (PDB 3TRK) with conserved amino acids His548 and Cys478 at the active center. The cysteine protease domain is shown in gold, and the methyltransferase domain in green. **(B)** Cleavage recognition sites of nsP2^{pro} within the polyprotein and the order of cleavage of the non-structural proteins nsP1-nsP4. The cleavage follows a defined sequence: **(I)** nsP4 is cleaved and released first, **(II)** followed by nsP3, **(III)** and finally, nsP1 is released from nsP2.The figure was created with BioRender and is based on data from Ahola and Merits (2016) and Saisawang et al. [73, 122].

1.11 Treatment

Currently there is no approved therapy available for CHIKV infection [123]. However, various studies are underway to develop effective treatment options. The majority of these studies focus on targeting nsP2^{pro} for antiviral therapy, due to its critical role in virus replication, as summarized in Table 4. Various approaches have been employed to identify potential inhibitors, such as small molecule and peptide-based compounds targeting CHIKV nsP2^{pro} activity. However, none of the identified candidates have advanced beyond the laboratory stage [124]. One strategy to inhibit CHIKV involves targeting the nucleophilic residue Cys478 in the active site using an irreversible covalent small-molecule binder [125]. The main limitation of such inhibitors is off-target activity and non-specific binding to host proteases with elementar functions, and this could lead to severe side effects (e.g. toxification) [126]. However, Merten et al. identified a small molecule inhibitor (RA-0002034) from a covalent fragment library of 6,120 compounds, which demonstrated high specificity for the cysteine residue in the active site of nsP2^{pro} [125]. Specificity analysis revealed that RA-0002034 does not interact with other cysteine proteases, except for cathepsin S, where it exhibited low levels of inhibition. However, further analysis is still required to confirm its selectivity and safety profile [125]. Another example of small molecule inhibitors includes Hesperetin (HST) and Hesperidin (HSD), two flavonoids extracted from citrus plants [127-129]. *In vitro* studies demonstrated that both HST and HSD can inhibit nsP2^{pro}, acting as noncompetitive inhibitors with low cytotoxicity [129]. *In silico* screening represents another approach for identifying small molecule inhibitors from compound libraries [130]. Novobiocin and Telmisartan are two *in silico*-selected small molecules from an FDA-approved library that demonstrated promising inhibitory effect on nsP2^{pro} activity [130]. Peptide-based therapy offers another promising route to develop therapy against various diseases, including microbial infections, cancer, and even neurodegenerative disorders such as Alzheimer's disease [131-134]. The advantages of peptides lies in their high target specificity, low toxicity, low immunogenicity, and their ability to bind larger surface areas of the target proteins compared to small molecules [133, 135]. However, despite these benefits, peptide-based therapeutics also have several limitations. These include poor stability due to enzymatic degradation, a short biological half-life, limited membrane permeability, and suboptimal biodistribution [133, 136]. Pep-I and Pep-II are two peptidomimetic inhibitors identified through conformer and pharmacophore-based approaches that specifically target the nsP3/4 cleavage site. These inhibitors are capable of blocking nsP2 protease activity and reducing viral titers in cell culture [137, 138].

Table 4. Example of potential inhibitors against CHIKV nsP2^{pro}.

Compound(s)	Type	Reference
RA-0002034	Small molecule	[125]
1,3 Thiazolbenzamide derivatives	Small molecule	[139]
MBZM-N-IBT	Small molecule	[140]
Hesperidin/ Hesperetin	Small molecule	[129]
Novobiocin/ Telmisartan	Small molecule	[130]
Pep-I/ Pep-II	Peptide	[138]
P1	Peptide	[124]

1.12 Sources and screening methods for peptide discovery

The advantages of peptide-based therapy were outlined in the previous section. Peptides can be selected and screened through various methods, including yeast surface display, phage display, and natural sources like animal venom [141-144]. In addition, screening using recombinant peptide libraries or *in silico* structure-based virtual screening represents two additional promising strategies for peptide selection [145, 146].

Phage display, developed by George P. Smith in 1985, is a high-throughput screening and cost-effective screening method that enables the selection of peptides from a phage library containing billions of phages, each displaying unique peptides on their surfaces (Fig. 8) [147-149]. This method is widely used to develop therapies for various diseases. For example, the phage display derived-peptide PRI-002, which disassembles toxic Aβ oligomers associated with Alzheimer's disease, has shown promising results and has reached phase 1b clinical trial [150]. Furthermore, phage display has been employed in the development and discovery of antimicrobial and antiviral therapies. Notably, peptide inhibitors such as CVL-2, 3CVL-4, and 3CVL-7, derived through phage display, were selected against the main protease of SARS-CoV-2, the 3-chymotrypsin-like protease (3CL^{pro}) [151]. Based on this, phage display was utilized to identify potential peptide binder for CHIKV nsP2^{pro} that targeting its activity [124].

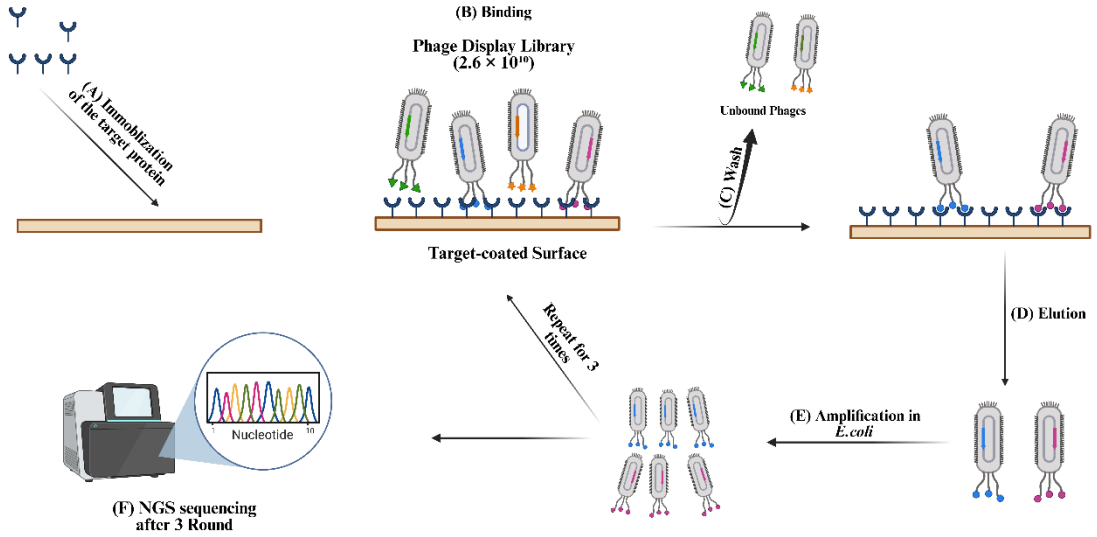

Fig. 8. Overview of the phage display screening process. (A) The process begins with immobilization of the target protein onto the surface of a microplate. **(B)** A phage library (~2.6 × 10^{10}) is then added to allow binding of displayed peptides to the target protein. **(C)** Unbound phages or low-affinity binders are removed through washing steps. **(D)** Bound phages are eluted using an elution buffer and **(E)** subsequently amplified in *E. coli*. **(F)** Finally, the selected phage clones are identified through next-generation sequencing (NGS). The selection cycle is typically repeated at least three times to enrich for high-affinity binders. This figure was created using BioRender and adapted from Mastalipour et al. and Eberle et al. [124, 151]

An alternative approach for peptide-based therapy involves the use of peptides derived from animal venom [152]. Numerous studies across different fields have demonstrated the significant potential of venom derived peptides in the treatment of cancer, bacterial infections, and even viral diseases (see Table 5) [153]. Venom peptides exhibit on one hand good selectivity, stability, in some cases strong cell membrane penetration, and even low susceptibility to drug resistance [154]. However, their therapeutic application is often limited by challenges such as potential cytotoxicity, complex manufacturing and purification processes, and the risk of off-target effects [155]. Despite these limitations, the significant advantages of venom-derived peptides make them a source for the discovery of an antiviral. One of the outstanding venom-derived peptides is pantinin-1, an amphipathic α-helix peptide derived from the scorpion *Pandinus imperator*, with a broad antimicrobial spectrum [156]. Pantinin-1 is formed by 14 amino acids and possess antimicrobial activity against a wide range of microorganisms, including Gram-positive and Gram-negative bacteria, as well as fungi such as *Candida tropicalis* [157]. Its broad-spectrum efficacy makes it a promising candidate for development as a potential inhibitor of CHIKV $nsP2^{pro}$.

Table 5. Summary of venom-derived peptides and their therapeutic potential.

Peptide	Source	Target	Reference
Captopril*	Brazilian pit viper (*Bothrops jararaca*)	Hypertension	[158]
Chlorotoxin	Scorpion (*Leiurus quinquestriatus*)	Brain cancer	[159]
Crotamine derivative peptides (CDP)	Rattlesnake (*Crotalus durissus terrificus*)	SARS-CoV-2	[160]
Echinhibin-1	Snake (*Echis coloratus*)	Sendai virus	[161]
Exenatide (Byetta)*	Gila monster (*Heloderma suspectum*)	Type 2 diabetes	[162, 163]
Melittin	Honeybee (*Apis mellifera*)	HIV-1	[164, 165]
Thanatin	spined soldier bug (*Podisus maculiventris*)	Antibacterial (*E. coli, Salmonella typhimurium, Klebsiella pneumoniae, and Enterobacter cloacae)*	[166]
Ziconotide (Prialt)*	Cone snail (*Conus magus*)	Severe chronic pain	[167, 168]

*FDA approved drug

1.13 Nucleic acids effect on viral protease

Nucleic acid have been shown to influence viral proteins and play a critical role in viral replication. For example, the interaction between adenovirus proteinase and the viral DNA is essential for enzymatic activity, and removal of the DNA leads to the loss of the proteinase activity [169]. Nucleic acids-protein interactions are not limited to DNA. As demonstrated by Hartl et al. foamy virus protease is activated only in the presence of RNA, not DNA [170]. Additionally, *in vitro* studies have shown that RNA enhances the activity of both HIV-1 protease and the 3C protease ($3C^{pro}$) of poliovirus [171, 172]. Nucleic acid-protein interactions are not always advantageous for viruses; rather than enhancing activity, they can also lead to inhibition. For example, aptamers, single-stranded DNA or RNA molecules with defined structures, have demonstrated inhibitory effects against the hepatitis C virus non-structural protein 3 (NS3) and its envelope proteins E1 and E2 [173-176]. These findings highlight the importance of nucleic acid interactions in viral replication. To identify such nucleic acid binders, various selection methods have been developed. One widely used approach is High-throughput sequencing fluorescent ligand interaction profiling (HiTS-FLIP). In this method, a large library of DNA or RNA (containing millions of sequences) is immobilized onto a flow cell, and a fluorescently labeled target protein is introduced to the nucleic acids. Binding between the protein and specific nucleic acid sequences results in bright fluorescent spots under fluorescence imaging, which are then visualized. The corresponding nucleic acids are subsequently identified [177]. Despite evidence of the regulatory role of nucleic acids in viral enzymatic activity, the effect of nucleic acids on $nsP2^{pro}$ remains poorly understood, as does their relevance to CHIKV replication. Further research, potentially utilizing techniques like HiTS-FLIP, may help clarify how nucleic acids influence the catalytic activity of $nsP2^{pro}$ and contribute to the development of effective antiviral therapies.

2. Aim of the work

CHIKV is a re-emerging arbovirus with a dramatic increase in the number of infected cases and poses a major threat to public health [178]. Unfortunately, no approved treatment is currently available, and the development of an effective antiviral therapy is essential [179]. The protease activity of the non-structural protein 2 ($nsP2^{pro}$) is crucial for viral replication; due to its importance, $nsP2^{pro}$ is considered as a target in the development of antiviral agents [180].

The primary aim of this work was to identify peptide-based inhibitors targeting the CHIKV $nsP2^{pro}$, with the goal of reducing or completely inhibiting its enzymatic activity, thereby interfering with viral replication. To better understand their mechanism of action, the peptide candidates were subjected to further biochemical, biophysical, and *in silico* characterization. The combined results from these approaches aim to evaluate their potential as lead compounds for the development of peptide-based antiviral inhibitors.

In addition, this work aimed to gain a better understanding of the effect of different nucleic acids, including a specific DNA aptamer, random RNA, DNA, nucleotides, and double-stranded DNA, on protease activity. The goal was to investigate whether nucleic acid interactions with $nsP2^{pro}$ have an impact on the inhibitory effect of the peptide inhibitor, and whether this should be considered in antiviral development.

3. Results

3.1 Identification and characterization of potential peptidic inhibitors against CHIKV nsP2 protease

Title: Novel peptide inhibitor for the Chikungunya virus nsP2 protease: Identification and characterization

Authors: Mohammadamin Mastalipour, Ian Gering, Mônika Aparecida Coronado, Jorge Enrique Hernández González, Dieter Willbold, Raphael Josef Eberle

Journal: Current Research in Microbial Sciences

Published Date: March 2025

DOI: https://doi.org/10.1016/j.crmicr.2025.100376

Contribution: Conceptualization, Methodology, Investigation, Formal analysis, Data curation, Writing - original draft, Writing - review & editing

Current Research in Microbial Sciences 8 (2025) 100376

Contents lists available at ScienceDirect

Current Research in Microbial Sciences

journal homepage: www.sciencedirect.com/journal/current-research-in-microbial-sciences

Novel peptide inhibitor for the Chikungunya virus nsP2 protease: Identification and characterization

Mohammadamin Mastalipour [a], Ian Gering [b], Mônika Aparecida Coronado [a,b], Jorge Enrique Hernández González [c], Dieter Willbold [a,b], Raphael Josef Eberle [d,*]

[a] Institut für Physikalische Biologie, Heinrich-Heine-Universität Düsseldorf, Universitätsstraße 1, 40225 Düsseldorf, Germany
[b] Institut für Biologische Informationsprozesse, Strukturbiochemie (IBI-7), Forschungszentrum Jülich, 52425 Jülich, Germany
[c] São Paulo State University (UNESP), Institute of Biosciences, Humanities and Exact Sciences, São José do Rio Preto, Brazil
[d] Institut für Biochemische Pflanzenphysiologie, Heinrich-Heine-Universität Düsseldorf, Universitätsstraße 1, 40225 Düsseldorf, Germany

ARTICLE INFO

Keywords:
Chikungunya virus
nsP2 protease
Peptide inhibitor

ABSTRACT

Chikungunya virus (CHIKV) is an emerging pathogen affecting populations worldwide, with rapidly increasing infection rates. CHIKV, an arbovirus of the alphavirus genus, is predominantly found in tropical regions and transmitted by *Aedes* mosquitoes. Climate change has accelerated the global spread of these vectors, leading to outbreaks in non-tropical regions, including parts of Europe. The absence of antiviral therapies and the potential for co-infections with other viruses make CHIKV a significant public health concern. CHIKV replication relies on nsP2 cysteine protease activity to cleave its viral polyprotein into functional nonstructural and structural proteins. Targeting the nsP2 protease represents a promising strategy for antiviral therapy development. In this study, phage display was used to screen a library of peptides for potential binders of the target protease. Biophysical and biochemical analyses of the identified peptides assessed their inhibitory potential. Among the six identified peptides (named as P1–P6), four demonstrated inhibitory effects on the nsP2 protease ($nsP2^{pro}$). Peptide P1 exhibited the strongest inhibitory effect, with a half-maximal inhibitory concentration (IC_{50}) of 4.6 ± 1.9 μM, and a low cytotoxicity. The secondary structure analysis through CD spectroscopy and homology modelling revealed that P1 adopts an alpha-helical conformation. Finally, molecular dynamics simulations enabled us to investigate the dynamics of the $nsP2^{pro}$ active site and molecular docking was employed to predict the orthosteric binding mode of P1, providing insights into protein-peptide interaction. These findings underscore the potential of peptide P1 as a lead compound for further investigation in the context of CHIKV research.

1. Introduction

Changes in environmental, climatic, and ecological conditions create favorable environments for the proliferation of arthropod-borne viruses, affecting nations worldwide (El-Sayed and Kamel, 2020). The lack of awareness, combined with underinvestment in fragile health systems and scientific research, results in a scarcity of effective antiviral medications (Mayer et al., 2017), complicating disease control efforts. Chikungunya fever is a re-emerging disease that has spread across the globe (Mourad et al., 2022). The infection can cause in the acute phase a variety of clinical symptoms like fever, rash, muscle and joint pain, which can last for 7–10 days (Freppel et al., 2024; Rama et al., 2024). However, in the chronic phase, rheumatoid arthritis and chronic pain can occur (Marimoutou et al., 2015; Paixao et al., 2018; Zaid et al., 2018).

Chikungunya virus (CHIKV) is the causative agent of CHIKV fever (Peinado, et al., 2022) and it has been reported in diverse regions including Africa, Asia, and Central and South America, where it continues to cause new infections (Grabenstein and Tomar, 2023). From 2013 to 2023, approximately 3.7 million confirmed CHIKV cases were reported in the Americas, with the World Health Organization (WHO) estimating that 3–5 million new infections occur annually (de Souza et al., 2024; Sharif et al., 2021). Additionally, data from the European Center for Disease Prevention and Control (ECDC) indicate that by November 2024, Brazil, Argentina, Paraguay, and Bolivia accounted for approximately 480,000 new cases and 190 fatalities (European Centre for Disease Prevention and Control [ECDC], 2024).

CHIKV is an arthropod-borne human pathogenic virus (Arbovirus), which is transmitted to humans by mosquitoes of the genus *Aedes aegypti*

* Corresponding author.
E-mail address: eberler@uni-duesseldorf.de (R.J. Eberle).

https://doi.org/10.1016/j.crmicr.2025.100376

Available online 11 March 2025

(Delrieu et al., 2023; Simon et al., 2011). Besides CHIKV, other arboviruses, that belong to the flavivirus genus, such as Zika virus (ZIKV) and Dengue virus (DENV) share the same vector, potentially leading to co-infections that can result in complications like multi-organ dysfunction syndrome (Vikhe et al., 2023). Because these infections often present similar symptoms, misdiagnoses can occur and pose life-threatening risks; however, insufficient information is available to fully assess the outcomes of such co-infections (Ahmed et al., 2024; Khongwichit et al., 2022).

CHIKV belongs to the alphavirus genus and is a positive-sense single-stranded RNA virus whose genome encodes six structural proteins, including envelope proteins (E), capsid proteins, and four non-structural proteins (nsP1–4), which are vital for virus replication (Girard et al., 2024; Peinado et al., 2024; Solignat et al., 2009). The nsP2 protease (nsP2^{pro}), which is essential for viral proliferation, exhibits RNA triphosphatase and helicase activities in its N-terminus (Law et al., 2021). In contrast, its C-terminal region comprises two distinct functional domains: a cysteine protease domain and a methyltransferase-like domain. The cysteine protease domain plays a crucial role in cleaving the viral polyprotein P1234 into its functional proteins (Ghoshal et al., 2024; Merten et al., 2024; Silva and Dermody, 2017). The cysteine protease domain belongs to the papain superfamily, more precisely to the peptidase family C9 of clan CA (Rawlings et al., 2010). The alphavirus nsP2^{pro} structure uncovers a unique fold, distinct from other cysteine proteases. Nevertheless, the relative positioning of the catalytic Cys and His residues in the active site mirrors the catalytic arrangement seen in papain-like cysteine proteases (Narwal et al., 2018). The C-terminus methyltransferase-like domain of nsP2 is involved in suppressing interferon responses and disrupting MHC-I antigen presentation (Göertz et al., 2018; Ware et al., 2024).

For years, no vaccine was available for CHIKV, fortunately, a recently developed live-attenuated vaccine VLA1553 (IXCHIQ), has demonstrated safety and efficacy against CHIKV infections (Chen et al., 2024; Ly, 2024; Schneider et al., 2023). Although this vaccine represents a significant advance, its usefulness is limited for infected individuals. This factor highlights the ongoing need to develop antiviral drugs targeting CHIKV infections. Additionally, several studies described the usage of biologically active compounds, extracted from plants that possess an inhibitory effect against the virus protease including, hesperidin and thiazolidinone derivatives (Eberle et al., 2021; Jadav et al., 2015; Martins et al., 2024). However, no drug candidates or approved drugs targeting this protease have been reported to date.

Phage display is a widely used method for developing therapeutic drugs and diagnostics against various diseases, ranging from infectious diseases to neurodegenerative conditions like Alzheimer's. One promising drug, PRI-002, was originally identified through phage display screening and has shown significant potential in the treatment of Alzheimer's disease (Kutzsche et al., 2020; van Groen et al., 2017) . In 2020, it successfully passed its first phase of clinical trials. As mentioned, phage display can also be used to develop therapies against infectious diseases. Following the COVID-19 outbreak, researchers utilized phage display to identify peptides targeting the virus, e.g., targeting the main protease or the spike protein of SARS-CoV-2 (Sevenich et al., 2022; Eberle et al., 2023). Additionally, numerous studies have identified lead compounds and drug candidates through phage display, demonstrating its potential across various fields, including infectious diseases, neurodegenerative disorders, and cancer. Table 1 provides an overview of some of the different therapeutic agents identified using phage display, along with their respective target diseases. These findings highlight the effectiveness and versatility of phage display as a powerful tool for drug discovery and diagnostic development. In this manuscript, we employed phage display as an alternative strategy to identify peptide candidates targeting the CHIKV nsP2^{pro}. We successfully identified peptides that inhibit nsP2^{pro} activity in the micromolar range. Additionally, we demonstrated the low toxicity of the most promising peptide using the MTT assay, reinforcing its suitability as a lead compound for advancing CHIKV-related studies.

Table 1
Overview of therapeutic agents identified using phage display.

Agent(s)	Target	Reference
PRI-002	Aß-oligomeres (Alzheimer disease)	(Kutzsche et al., 2020; van Groen et al., 2017)
Peptide	Spike protein (SARS-CoV-2)	(Sevenich et al., 2022)
Peptide	Main protease (SARS-CoV-2)	(Eberle et al., 2023)
HER2, C5AR1	Breast cancer	(Yau et al., 2024)
Raxibacumab/ ABthrax®	Anthrax PA (*Bacillus anthracis*)	(Alfaleh et al., 2020)
V_HH (caplacizumab)	Blood clotting disorders	(Rossotti et al., 2023)

2. Materials and methods

2.1. Protein expression and purification

Protein expression and purification were carried out according to the method described in (Eberle et al., 2021) (Supplementary Fig. S1).

2.2. Phage display

The M13 bacteriophage library TriCo-16 (Creative Biolabs, Shirley, USA) was employed, offering a diversity of 2.6×10^{10} pIII-fused 16-mer peptide variants. The target protein was diluted in 10 mM sodium acetate buffer (pH 5.2) to 30 pM and added (100 µL) to a 96-well amino plate. Control wells received an immobilization buffer (10 mM sodium acetate, pH 5.2). The plate was incubated at room temperature (RT) for 30 min with shaking at 10 rpm. Binding was quenched by adding 200 µL of quenching buffer (1 M ethanolamine-HCl, pH 8.0) and incubating for 30 min, followed by the addition of 200 µL of blocking buffer (25 mM HEPES pH 7.4, 1 % (w/v) BSA) for another 30 min to block further binding. After washing the wells three times with wash buffer (25 mM HEPES, pH 7.4, 0.2 % BSA), 100 µL of the diluted phage library (1.66×10^{11} phages in 25 mM HEPES buffer) was added, and the mixture incubated for 20 min at RT. Unbound phages were removed by washing the wells five times.To elute bound phages, 100 µL of elution buffer (0.2 M glycine-HCl, pH 2.2) was added for 10 min at RT, and the eluted phages neutralized with 25 µL of neutralization buffer (1 M Tris-HCl, pH 9.1). To increase the specificity of the peptide binder, three rounds of selection were performed. After adding the phage in each round, Five-times washing step was carried out to remove nonspecific binders and those with low affinity.

2.2.1. Amplification and isolation of phages

120 µL of eluted phages were added to 20 mL of *E. coli* ER2738 culture ($OD_{600} = 0.1$) in LB medium with 50 µg/mL tetracycline. The culture was incubated at 37 °C for 4 h with shaking at 120 rpm. Afterwards, the culture was centrifuged at 5000 rpm for 1 hour at 4 °C. The pellet was resuspended in 1 mL of resuspension buffer (25 mM HEPES, pH 7.4) and centrifuged at 10,000 rpm for 5 min at 4 °C. The solution was then mixed with 200 µL of 20 % (w/v) PEG-8000, 2.5 M NaCl and incubated on ice for 1 hour, followed by a final centrifugation at 10,000 rpm for 45 min at 4 °C. The phage pellet was resuspended in 100 µL of resuspension buffer, and the concentration was measured at 269 nm. The phage solution was stored at 4 °C.

2.2.2. Plasmid isolation and sequencing

To isolate plasmid DNA, 10 µL of the phage solution was mixed with 90 µL of TBS buffer and 200 µL of a 20 % (w/v) PEG-8000, 2.5 M NaCl solution and incubated at RT for 20 min. The mixture was centrifuged at 14,000 rpm for 10 min at 4 °C, and the pellet was resuspended in 200 µL of Na-acetate: TE buffer (10:1). DNA was precipitated by adding 500 µL

of 99 % ethanol, incubated for 15 min, and centrifuged at 14,000 rpm for 10 min at 4 °C. The pellet was washed with 250 μL of 70 % ethanol, dried at 30 °C for 7 min, resuspended in 40 μL of ddH_2O, and the concentration was measured. DNA was amplified by PCR, sequenced at Heinrich Heine University Düsseldorf, and analyzed using the TSAT program (developed at IBI7 Institute at Research Center Jülich) (Altendorf et al., 2024) Sequences were ranked by enrichment and empty scores (Sevenich et al., 2022).

2.3. Peptides

All peptides were purchased from GenScript Biotech (Rijswijk, Netherlands) BV as lyophilized powder with >90 % purity. All peptides are all in the L-configuration and consist of 16 amino acids, except for P4, which contains 14 amino acids. All peptides are amidated at their C-terminus and acetylated at the N-terminus. Based on the P1 sequence, three scrambled peptides with randomly changed sequence were generated. The purity of each peptide was verified by an analysis certificate from GenScript Biotech (Rijswijk, Netherlands) BV (Supplementary Figs. S2-S4 and Table S1). The peptides were analyzed using high-performance liquid chromatography (HPLC) with an Inertsil ODS-3 column (4.6 × 250 mm). Mass spectrometry analysis was conducted using the Electrospray Ionization (ESI) technique.

2.4. Inhibition assay

An inhibition assay was performed using a fluorescence resonance energy transfer (FRET)-based assay with the synthesized fluorogenic substrate DABCYL-Arg-Ala-Gly-Gly-↓Tyr-Ile-Phe-Ser-EDANS (BACHEM, Bubendorf, Switzerland) (Eberle et al., 2021; Hu et al., 2016), which mimics the natural substrate sequence between the nsPs in the viral polyprotein. The assay was conducted in 96-well plates with a reaction solution of 20 mM Bis-Tris-Propane buffer at pH 7.5. The final reaction volume in each well was 100 μL, containing 10 μM $nsP2^{pro}$ and 9 μM substrate. The peptides were dissolved in 100 % dimethyl sulfoxide (DMSO) to a final stock concentration of 10 mM. A DMSO control with concentrations ranging from 0 % to 1 % was included to assess any potential effects of this substance on protease activity (Supplementary Fig. S5). The final concentration of the peptides in the reaction mixture was 50 μM. The Fluorescence intensities (excitation at 340 nm and emission at 490 nm) were measured at 30-second intervals over a 30-minute period at 37 °C using a CLARIOstar plate reader (BMGlabtech, Ortenberg, Germany) and the protease activity and inhibition were calculated using equation 1 (Eberle et al., 2021):

$$\textit{Protease activity}\ \% = \frac{\textit{Intensity of enzymatic activity after inhibiton}}{\textit{Intensity of enzymatic activity}} \times 100$$

To investigate the specificity of the identified peptides, a scrambled version of the P1 peptide, designated as SP1-SP3, was included in the assay at the same concentration as the experimental peptides. This control peptide served to evaluate any potential nonspecific binding or inhibition. All measurements were performed in triplicate, and data are presented as mean ± SD.

2.5. Determination of half maximal inhibitory concentration (IC_{50})

The protease was used at a concentration of 10 μM, while the substrate concentration was maintained at 9 μM. The inhibitory effects of the peptides at various concentrations (0–900 μM) were measured using excitation at 340 nm and emission at 490 nm. To minimize peptide aggregation, the buffer composition, experimental temperature, and duration of the experiment were optimized individually for each peptide (Table 2).

Table 2
Conditions for determination of the IC_{50} values of peptides against CHIKV $nsP2^{pro}$.

Peptides	Temp. [°C]	Cycle [sec]	Time [min]	Buffer
P1	37	30	10	20 mM Bis-Tris-Propane, pH 7.5, 0.1 Triton-X 100
P2, P4, P5	20	30	20	20 mM Bis-Tris-Propane, pH 7.5,

All measurements were performed in triplicate and data are presented as mean ± SD.

2.6. Determination of the inhibition mode of the peptide inhibitor

The mode of inhibition was investigated using the (FRET)-based assay described before. To evaluate the mode of inhibition of peptide P1, the enzymatic activity of $nsP2^{pro}$ was measured at varying concentrations of both the inhibitor and the substrate in 20 mM Bis-Tris-Propane pH 7.5, while maintaining a constant protease concentration of 10 μM (Table 3).

2.7. CD spectroscopy

Peptides were prepared in ddH_2O containing 5 % DMSO at a final concentration of 500 μM for secondary structure analysis. The spectra were recorded at 18 °C using a 0.1 mm pathlength cuvette across a wavelength range of 190–250 nm with a Jasco J-1100 spectropolarimeter (Jasco GmbH, Pfungstadt, Germany). Additionally, CD spectroscopy was performed to evaluate the folding quality of the purified $nsP2^{pro}$ after the purification process. The protease was diluted in 10 mM sodium phosphate buffer (2.39 mM NaH_2PO_4, 7.6 mM Na_2HPO_4, pH 7.5) to a final concentration of 5 μM, and measurements were conducted seven times using a 1 cm pathlength cuvette at 18 °C, covering a wavelength range of 190–260 nm (Supplementary Fig. S1). The baseline spectrum averaged from multiple measurements, was subtracted from the corresponding averaged sample spectrum to obtain corrected data. The results were expressed as molar ellipticity ([θ]) and calculated using the following equation 2:

$$[\theta]\lambda = \frac{\theta}{(c * l * n)}$$

Where θ is the ellipticity measured at the wavelength λ (deg), c is the protein concentration (mol/L), l is the cell path length (cm), and n is the number of amino acids. The secondary structure content was determined from CD results, and the K2D3 online tool (https://cbdm-01.zdv.uni-mainz.de/~andrade/k2d3/) was utilized to predict the secondary structure composition.

2.8. Secondary structure prediction of the selected peptides

The I-TASSER tool (https://zhanggroup.org/I-TASSER/) was used to predict the secondary structure of the selected peptides (P1-P6). Model confidence is evaluated using the C-score, which typically ranges from −5 to 2 with higher values indicating more reliable predictions. Additionally, I-TASSER calculates a TM-score (between 0 and 1) to measure the alignment quality between structural models. Higher TM-scores indicate greater structural agreement (Yang et al., 2015).

Table 3
Applied concentration of substrate and peptides in the inhibition mode assay.

Substrate conc. [μM]	0	3	6	9	12	15
Inhibitor conc. [μM]	0 0.75 1.5 3	0 0.75 1.5 3	0 0.75 1.5 3	0 0.75 1.5 3	0 0.75 1.5 3	0 0.75 1.5 3

2.9. Equilibrium dissociation constant determination using microscale thermophoresis (MST)

To determine the equilibrium dissociation constant (K_D), an MST (microscale thermophoresis) assay was conducted. The peptide was first labeled with CF™633 succinimidyl ester dye (Sigma-Aldrich, St. Louis, MO, USA). A total of 1 μmol of dye was warmed to room temperature and dissolved in DMSO to prepare a 10 mM stock solution. The peptide was diluted in 1 M sodium bicarbonate buffer (pH 8.3) to a final concentration of 0.12 mM in a volume of 50 μL. Following this, 50 μL of the dye solution was added to the peptide solution, and the mixture was incubated in the dark for one hour. Subsequently, the labeled peptide was purified using reversed-phase high-performance liquid chromatography (RP-HPLC) on an Agilent 1260 Infinity II system (Agilent Technologies, Santa Clara, CA, USA). A volume of 20 μL of the labeled peptide solution was injected into a Zorbax 300SB-C8 column (Agilent Technologies, Santa Clara, CA, USA) at 25 °C. The mobile phase consisted of buffer A (0.1 % trifluoroacetic acid, TFA) and buffer B (acetonitrile with 0.1 % TFA). The peptide was eluted using a linear gradient of 10 to 80 % of buffer B over 40 min. Chromatograms were recorded at three wavelengths: 214 nm, 280 nm, and 633 nm (Supplementary Fig. S6). Collected fractions were frozen using liquid nitrogen and lyophilized overnight. The lyophilized sample was reconstituted in 50 μL of 20 mM Bis-Tris-Propane buffer (pH 7.5). Absorbance measurements were taken at 280 nm and 630 nm using a UV–Vis spectrophotometer. The concentration of the labeled peptide was then calculated using the following equation 3:

$$labeled\ peptide\ mg \Big/ ml = \frac{(A280 - (AMax * CF))}{E} * df$$

The A280 and AMax represent the absorbance readings of the labeled peptide at 280 nm and the absorption maximum, respectively, while CF refers to the absorbance correction factor (0.48 for the CF™633 dye), and E is the extinction coefficient of the peptide. df indicates the dilution factor. The labeling process was carried out following the guidelines provided in the Sigma-Aldrich (St. Louis, MO, USA) technical bulletin. The equations were adapted to calculate the concentration of the labeled peptide. The labeling efficiency was determined separately and calculated to be approximately 54 %. To prepare the samples for the MST assay, a labeled peptide stock solution with a concentration of 2 μM was prepared. A 16-step, 1:2 serial dilution series of unlabeled CHIKV $nsP2^{pro}$ was created. Subsequently, 10 μL of the labeled peptide solution was added to each diluted protease solution, resulting in a final concentration of 1 μM and protease concentrations ranging from 2 nM to 74 μM. The samples were loaded into Monolith series premium capillaries (NanoTemper Technologies GmbH, Munich, Germany) and measured at 37 °C with 100 % LED power and 100 % MST power. The results were analyzed using the software provided by NanoTemper Technologies (Munich, Germany). To determine the best fit for calculating the equilibrium dissociation constant (K_D), the K_D model, based on the mass-action kinetics model, was used in the software. The program provided the fraction bound for each dose, and the K_D was determined by fitting the data to this model. Measurements were performed in triplicate, and the mean fraction bound per dose was calculated and analyzed using Prism software. The final K_D value was reported as the mean of the individual K_D values calculated for each measurement by the software.

2.10. Cell viability assay

Cell viability assay was performed using Vero cells, which are kidney epithelial cells derived from the African green monkey (*Chlorocebus aethiops*) and were generously provided by the group of Dr. Lisa Müller located at the Virology Institute, University Hospital Düsseldorf. The cells were cultured under standard conditions in a humidified incubator at 37 °C with 5 % CO_2. Peptide cytotoxicity was assessed by exposing cells to varying concentrations of peptides (dissolved in either water or DMSO and diluted in DMEM medium) ranging from 0 to 100 μM. The concentrations were selected based on the determined P1 IC_{50} value (4.7 μM). To assess the potential cytotoxic effects at different concentrations, peptide concentrations ranging from sub-IC_{50} values up to 100 μM were tested. The upper concentration limit (100 μM) was chosen to provide a broad evaluation of the peptide's effects on cell viability. This range allowed us to observe any potential cytotoxicity and to demonstrate the peptide's toxicity at higher concentrations. As a negative control, 0.1 % Triton X-100 was added to five wells to induce complete cell lysis. The plates were then incubated overnight under identical conditions to allow cytotoxic effects to develop. The following day, 10 μL of MTT labeling reagent from the Cell Viability Kit (Roche Diagnostics GmbH, Mannheim, Germany) was added to each well. Metabolically active cells converted MTT into formazan crystals, providing a measure of cell viability. After 4 h of incubation, 100 μL of solubilization buffer (Solution No. 2) was added to dissolve the crystals and the plates were incubated overnight to ensure complete solubilization. Absorbance was measured at 570 nm (signal) and 660 nm (reference) using a CLARIOstar plate reader (BMGlabtech, Ortenberg, Germany). The Cell viability percentages were calculated using the following formula equation 4:

$$\frac{(A570 - A660)of\ treated\ cells}{(A570 - A660)of\ control\ (not\ treated\ cells)} \times\ 100$$

2.11. Molecular docking

To predict the binding mode of peptide P1 to CHIKV $nsP2^{pro}$, we conducted protein-peptide blind docking at the web servers of three different docking programs: ClusPro (Jones et al., 2022), HDock (Yan et al., 2020) and Galaxy Tongdock (Park et al., 2019). The structure of CHIKV $nsP2^{pro}$ used for docking was obtained through clustering analysis of a concatenated 20 μs of the protein, as explained hereinafter. The peptide structure was modeled using the I-TASSER tool (Zhou et al., 2022). The top-ranked poses obtained with each docking program were subjected to subsequent analyses to assess the most likely binding mode.

2.12. Molecular dynamics simulations

The structure of CHIKV $nsP2^{pro}$ was retrieved from the PDB 3TRK. Protonation states of ionizable residues at pH 7.4 were predicted using propKa at the PDB2PQR web server (Dolinsky et al., 2004). The protein was then embedded in an octahedral box with edges spanning at least 10 Å from the solute surface. The box was filled with OPC water molecules (Izadi et al., 2014) and counterions to neutralize the protein net charge. The force field ff19SB (Tian et al., 2020) was employed to assign parameters for the protein atoms (Case et al., 2005)

The system was subjected to energy minimization (EM) to resolve steric clashes before advancing to the equilibration steps. A total of 5000 EM cycles were performed, with the first 3000 cycles using the steepest descent algorithm and the remaining 2000 cycles employing the conjugate gradient algorithm. Heating was subsequently carried out by linearly increasing the system's temperature from 10 K to 310 K under constant volume conditions over 500 ps. Initial atomic velocities were assigned from a Maxwell-Boltzmann distribution at 10 K. Following the heating phase, the pressure was equilibrated at 1 bar over an additional 500 ps while maintaining the temperature at 310 K. During both equilibration steps, harmonic position restraints ($k = 10$ kcal·Å^{-2}·mol^{-1}) were applied to the protein's heavy atoms. The harmonic restraints were gradually removed in 2 kcal·Å^{-2}·mol^{-1} strides during four consecutive 1 ns MD simulations conducted in the NPT ensemble. The temperature and pressure during equilibration were controlled using the Berendsen thermostat and barostat, respectively. A timestep of 2 fs was used to integrate the equations of motion in all these steps, employing the leapfrog algorithm (Case et al., 2005). A 2 μs productive MD simulation was subsequently performed in the NVT ensemble at 310 K, with frames

saved every 60,000 steps. The temperature during the removal of harmonic restraints and the productive simulations was controlled using the Langevin thermostat (Case et al., 2005). Hydrogen mass repartitioning was applied to increase the integration timestep to 4 fs during the 2 μs simulation (Hopkins et al., 2015). A cutoff of 10 Å was used for short-range interactions, while long-range electrostatic interactions were calculated with the Particle Mesh Ewald (PME) method. To enhance conformational sampling, 10 replicate MD simulations were performed by varying the initial random velocities assigned to atoms during the heating phase (Case et al., 2005).

A similar protocol was employed for the MD simulations carried out for CHIKV nsP2^{pro} in complex with peptide P1. The ACE and NME caps were added to the N- and C-termini of the peptide, respectively, and parameters for its atoms were derived for the ff19SB force field. 1 μs productive runs were conducted for the three top-ranked poses bound to the protease. Moreover, an extension of 2 μs was performed for the complex showing the largest affinity. No replicate MD simulations for the protein-peptide systems were conducted.

2.13. MM-GBSA free energy calculations

Molecular Mechanics Generalized-Born Surface Area (MM-GBSA) free energy calculations were carried out for the three top-ranked poses of peptide P1 in complex with CHIKV nsP2^{pro} using the program MMPBSA.py (Miller et al., 2012) of Amber22 (Case et al., 2005). The single trajectory approach, where frames from the free protein and the free ligand are extracted from the trajectory of the complex, was followed. Calculations were performed with 542 frames evenly collected from the last 0.5 μs of each analyzed trajectory. The GB-neck2 (igb = 8) implicit solvation model (Nguyen et al., 2013) was employed to estimate the polar solvation energy. Dielectric constants of 1 and 80 were assigned for the internal space of the solute and for the solvent, respectively, and a salt concentration of 0.1 M was set. A surface tension coefficient of 0.0072 kcal·Å^{-2}·mol^{-1} was used for the calculation of the surface free energy component (Case et al., 2005). Since the configurational entropy was neglected, the predicted free energies are referred to as effective binding free energies (ΔG_{eff}). To evaluate the contribution of interface residues to the binding free energy, the protocol of per-residue free energy decomposition implemented in MMPBSA.py was employed. This calculation was performed using the same implicit solvation model and conditions stated in the previous paragraph.

2.14. Trajectory analyses

Root-mean-square-deviations (RMSDs) and interatomic distances during the MD simulations were calculated with the *rmsd* and *distance* commands of *cpptraj* of Amber22. For trajectory clustering, the command *cluster* of the same program was employed. The RMSD of CHIKV nsP2^{pro} active site residues were set as a metric for clustering with the hierarchical agglomerative algorithm (Case et al., 2005). As a rule of thumb, five clusters were generated for each analyzed trajectory.

2.15. Statistical analysis

Statistical analysis, including the calculation of confidence intervals and significance levels (p-values), was performed using GraphPad Prism. Descriptive statistics were used to calculate confidence intervals, and one-way ANOVA followed by Tukey's post hoc test was conducted to assess differences between groups. Statistical significance was determined at $p < 0.05$ (*), $p < 0.01$ (**), and $p < 0.001$ (***).

3. Result

3.1. Phage display peptide selection

Phage display technology was utilized to identify specific peptide binders targeting the CHIKV nsP2^{pro} (Fig. 1). The selection process involved three rounds of phage display to isolate peptides with high affinity and specificity for the target protein. Subsequently, DNA was extracted from the phage and sequenced using next-generation sequencing (NGS). The NGS data were analyzed using the TSAT program (Altendorf et al., 2024), which ranked the sequences based on two metrics: the empty score and the enrichment score. Peptides with higher empty and enrichment scores were considered to have greater specificity for CHIKV nsP2^{pro}. Based on these criteria, six peptides were selected and named as P1, P2, P3, P4, P5, and P6 (Table 4).

3.2. Primary inhibition test of selected phage display peptides

A primary inhibition test, based on a FRET-based assay (Eberle et al., 2021; Hu et al., 2016) was conducted to evaluate the peptides' inhibitory potential on protease activity. The assay utilized peptides at a concentration of 50 μM, which were added to the nsP2^{pro}. Fluorescent intensity was recorded at 30-second intervals over 30 min at 37 °C. The results revealed that four out of the six peptides (P1, P2, P4 and P5) significantly inhibited the protease activity (Fig. 2A). Peptides P1 and P2 demonstrated the strongest inhibition, reducing protease activity by over 50 %, while peptides P4 and P5 exhibited moderate inhibition, reducing activity by approximately 50 %. In contrast, peptide P3 showed no detectable inhibitory effect, whereas peptide P6 reduced protease activity by approximately 30 %. A control experiment with three scrambled peptides (Sequence based on P1, Table S1) showed no significant effect on the nsP2^{pro} activity (Fig. 2B).

3.3. Determination of the half maximal inhibitory concentration (IC_{50}) of selected peptides

Based on the results of the primary test, the peptides with the strongest inhibition effect against CHIKV nsP2^{pro} (P1, P2, P4 and P5) were further investigated to evaluate their efficacy. The assay was performed as described before, with peptide concentrations ranging from 0 to 900 μM and 10 μM of nsP2^{pro}. Changes in the fluorescence intensity was recorded at 37 °C in 30-s intervals for 30 min. However, peptide aggregation occurred within 3–5 min, preventing accurate IC_{50} determination under these conditions. To address this issue, assay conditions were optimized to reduce peptide aggregation and extend measurement duration (Table 2). Fig. 3 illustrates IC_{50} of the peptides. Peptide P1 showed the strongest inhibition, with an IC_{50} value of 4.6 μM (Fig. 3A). Peptides P2 and P5 exhibited IC_{50} values of 194.7 μM (Fig. 3B) and 316.9 μM (Fig. 3C). Peptide P1 achieved complete inhibition of nsP2^{pro} activity at approximately 175 μM, while peptides P2 and P5 required up to 900 μM for significant inhibition (Supplementary Fig. S7).

3.4. Determination of the P1 inhibition mode

The IC_{50} results identified peptide P1 as the most potent inhibitor of CHIKV nsP2^{pro}, with an IC_{50} value of 4.6 μM. Based on this finding, P1 was selected for further investigation, including determination of its mode of inhibition. An FRET-based assay was performed by varying the concentrations of both the peptide (P1) and the substrate. The analysis revealed that increasing the concentration of P1 reduced substrate affinity, as indicated by an increase in the K_m constant. The data were subsequently analyzed using a Lineweaver-Burk plot. (Fig. 4A).

3.5. Determination of the equilibrium dissociation constant using microscale thermophoresis (MST)

Microscale thermophoresis (MST) measurements were used to determine the equilibrium dissociation constant (K_D) by analysing changes in molecular movement induced by a temperature gradient generated with an infrared laser. The peptide, labeled with CF™633 dye, was added to a series of dilutions of the protease ranging from 2 nM

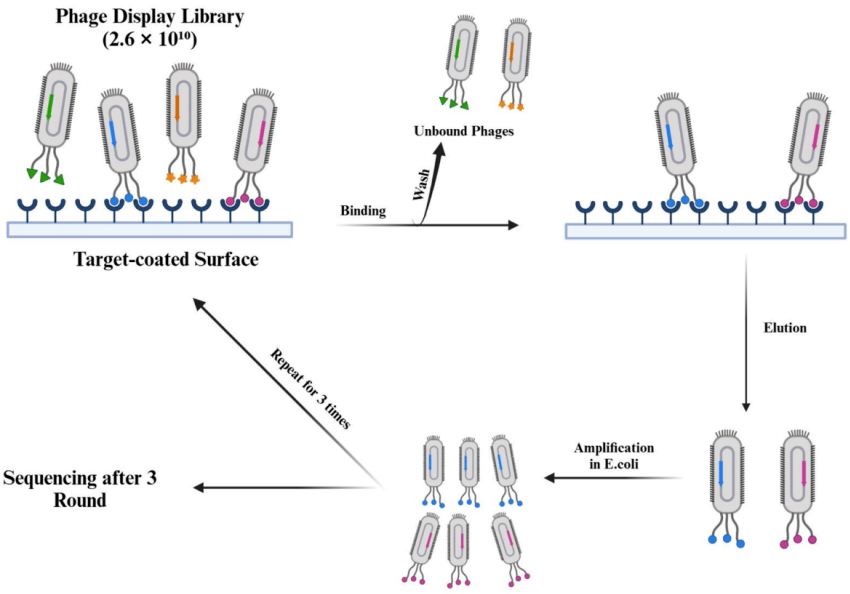

Fig. 1. Schematic representation of phage display technique and workflow. Modified figure from Eberle et al., 2023.

Table 4
Selected peptides from phage display.

Peptides	Sequence	Empty score	Enrichment score
P1	VMPWDEWLTKRKPELP	221	91
P2	HTSRIYIPSPIHAENI	61	38
P3	MEASGVNYQNMNKQTT	54	34
P4	FTMSPPLQMPSKNY	231	287
P5	NAMSHVMEGSHINWDA	220	136
P6	YISPQYYGETWVTTIG	167	104

to 74 μM. The motion of the peptide and protease complex was recorded at 37 °C with 100 % MST and LED power. The experiment was performed in triplicate. Based on the quantified data and analysis, a fraction-bound versus dose graph (Fig. 4B) was generated, yielding a K_D value of 1.39 ± 0.61 μM for peptide P1.

3.6. Cytotoxicity effects of peptide P1 on Vero cells

To assess the toxicity of peptide P1, Vero cells were used. These cells are a standard cell line widely employed in CHIKV infection research and other alphavirus studies due to their permissivity to these viruses (Ribeiro et al., 2018). To evaluate the toxicity of P1, Vero cells were exposed to varying concentrations of the peptide (0–100 μM), and cytotoxicity was assessed using the MTT assay. The results showed that peptide P1 dissolved in water exhibited low toxicity, with approximately 83 % cell viability observed at a concentration of 100 μM. In contrast,

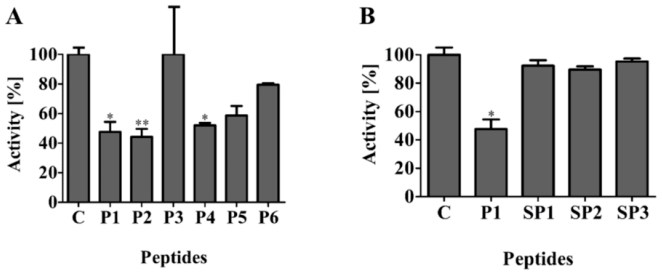

Fig. 2. Inhibition analysis of selected peptides (P1–P6) and scrambled peptide controls against CHIKV nsP2^{pro} activity. The inhibition analysis of CHIKV nsP2^{pro} by six identified peptides (P1–P6) and the specificity assessment of P1using scrambled peptides (SP1–SP3). **(A)** Primary inhibition assay, CHIKV nsP2^{pro} was tested at a 10 μM concentration, while peptides (P1–P6) were applied at 50 μM. The control (C) represents protease activity in the absence of peptides. **(B)** Specificity assessment of P1, The inhibitory activity of P1 was compared to three scrambled peptides (SP1–SP3) under the same conditions (10 μM protease, 50 μM peptides) to evaluate potential nonspecific inhibition effects. Statistical significance was determined using one-way ANOVA, followed by Tukey's test. Asterisks indicate significant differences from the control ((A): 0 μM inhibitor and (B): P1). Asterisks denote statistically significant differences from the control group as determined by one-way ANOVA and Tukey's test, where $p < 0.05$ (*), $p < 0.01$ (**). Data are presented as mean ± SD from three independent experiments ($n = 3$).

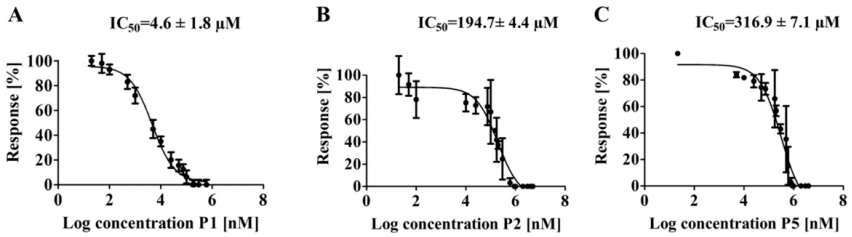

Fig. 3. Half maximal inhibitory concentration (IC_{50}) values, determined for the peptides P1, P2, and P5. Panels **A-C** present the dose-response curves for peptides (P1, P2, and P5) against CHIKV $nsP2^{pro}$.

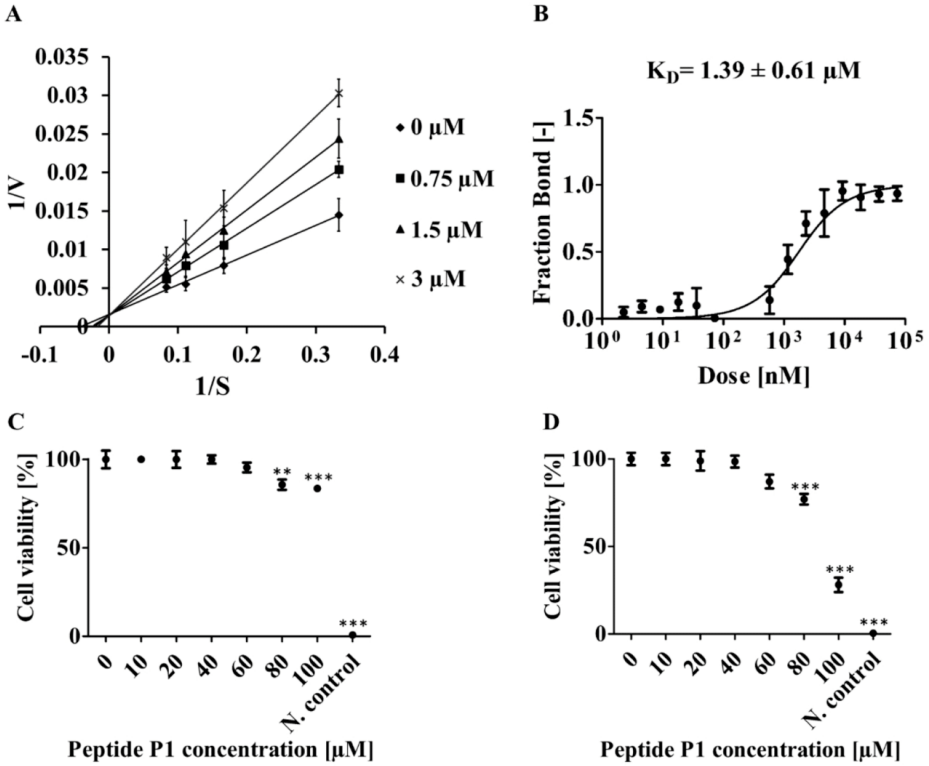

Fig. 4. Inhibition, binding, and toxicity assessment of peptide P1 against CHIKV $nsP2^{pro}$ (A) The inhibition mode of peptide P1 was determined using a Lineweaver-Burk plot. The intersection on the y-axis, characteristic of competitive inhibitors, indicates that peptide P1 acts as a competitive inhibitor. This suggests that peptide P1 competes with the substrate for binding to the enzyme's active site. As a result, the enzyme's affinity for the substrate decreases, leading to an increase in K_m. **(B)** Microscale thermophoresis (MST) assay demonstrating the binding affinity of peptide P1 to the CHIKV $nsP2^{pro}$, with a equilibrium dissociation constant (K_D) of 1.39 ± 0.61 µM. **(C)** MTT assay of peptide P1 dissolved in water, tested against Vero cells at concentrations ranging from 0 to 100 µM. The negative control used was 0.1 % Triton X-100. **(D)** MTT assay of peptide P1 dissolved in DMSO, tested against Vero cells at concentrations ranging from 0 to 100 µM. The negative control used was 0.1 % Triton X-100. Data from MTT assays are presented with 95 % confidence intervals for each group (see Supplementary Table S2). Significant differences between groups were determined by single-factor ANOVA. Asterisks indicate statistical significance, determined using one-way ANOVA, followed by Tukey's test. Asterisks indicate significant differences from the control (0 µM inhibitor). Asterisks denote statistically significant differences from the control group as determined by one-way ANOVA and Tukey's test, where $p < 0.01$ (**) and $p < 0.001$ (***).

when peptide P1 was dissolved in DMSO, cell viability was approximately 77 % at 80 μM but decreased significantly to 28 % at 100 μM (Fig. 4C,D).

3.7. Secondary structure prediction of the selected peptides

The peptide structure was predicted using the I-TASSER tool with each model assigned a confidence score (C-score) of [−5,2], indicating the reliability of the predictions. To validate these models, the secondary structure content, specifically the proportions of alpha-helices and beta-sheets, was experimentally determined through circular dichroism (CD) spectroscopy (Supplementary Table S3). The CD spectroscopy data were then compared to the predicted structures. Table S3 illustrates the predicted peptide structures alongside their corresponding CD spectroscopy analyses. These structures represent potential conformations within a structural ensemble in solution. The comparison between experimental and predicted data (Supplementary Table S3 and Fig. S8) demonstrated that most peptides exhibit a combination of random coil and alpha-helical structures, except for peptides P2, P4, and P6. Furthermore, the I-TASSER predictions aligned well with the secondary structure data obtained from CD spectroscopy.

3.8. Structural analysis and molecular modeling

MD simulations were performed to explore the dynamic properties of CHIKV nsP2^{pro}. Fig. 5A illustrates the flexibility of the protease's active site over a 20 μs timescale. Due to interdomain motion, a flap formed by residues A1080 to H1083 can adopt positions either close to or far from the C-terminal domain, leading to closed and open conformations of the active site, respectively. Interestingly, the crystal structure of CHIKV nsP2^{pro} (PDB 3TRK) exhibits a closed active site, which is not suitable for investigating the binding of orthosteric ligands. By measuring the distance between the flap and residue M1242 in the opposing domain, and defining a threshold of 19 Å based on visual inspection, we observed that the active site remains in a closed state approximately 87 % of the time, transitioning to an open state 13 % of the time (histogram in Fig. 5A).

Through clustering analysis, we identified five representative structures possessing distinct orientations of the catalytic domain relative to the C-terminal domain (Fig. 5B). As shown in the figure, the active site adopts a more open conformation as the flap moves farther away from a highlighted loop on the C-terminal domain (residues 1202–1206). Among the four central structures with open active sites, we selected the one closest (beige) to the central structure of the closed state (green) for subsequent peptide binding studies (Fig. 5B). This selection seeks to minimize the risk of the open conformation being a result of force-field artifacts, while ensuring the peptide can bind effectively within the open active site (the open cavity illustrated in Fig. 5C).

Subsequently, blind docking was performed using three different programs: ClusPro (Jones et al., 2022), HDock (Yan et al., 2020) and Galaxy Tongdock (Park et al., 2019) to predict the binding mode of peptide P1 to CHIKV nsP2^{pro}. The starting conformations of the peptide and the target protease employed for the docking studies are those depicted in supplementary Fig. 8A and Fig. 5C, respectively. Remarkably, P1 conformations interacting with the protein active site were consistently predicted as top-ranked solutions by all the three docking programs (Fig. 6A–C), in agreement with the experimental results. Each of the top-ranked docking poses was subjected to a 1 μs MD simulation to evaluate the stability of the predicted complex. The RMSD plots in Fig. 6D–F reveal that the peptides underwent moderate (<10 Å for Hdock and Galaxy Tondock poses) to significant (>10 Å for the ClusPro pose) changes in binding mode relative to the docking poses during the simulations. Despite these initial changes, relatively stable binding conformations were consistently observed throughout the second half of each trajectory.

The most favorable binding mode of P1 to CHIKV nsP2^{pro} was identified through MM-GBSA free energy calculations. Frames from the three MD trajectories, excluding the first 0.5 μs used for equilibration, were analyzed for this purpose. The resulting ΔG_{eff} values for the final segment of the analyzed MD simulations are summarized in Table S4. The binding mode sampled during the final segment of the MD simulation initiated from the Hdock docking pose exhibited the most negative ΔG_{eff} value (−62.56 kcal/mol), significantly outperforming the other two. Extending the MD simulation of the Hdock pose to 2.5 μs reinforced its stability. In fact, the ΔG_{eff} value calculated for the last 0.5 μs of the extended trajectory closely matched that of the 1 μs MD simulation (Supplementary Table S4). Additionally, the peptide RMSD plot for the extended trajectory (Supplementary Fig. S9) indicated no major conformational changes. Overall, the previous analyses suggest that the conformations sampled during the last 2 μs of the Hdock pose simulation are likely to be representative of the native binding mode of P1 at the CHIKV nsP2^{pro} active site.

Central structures for the 2.5 μs MD simulation of the CHIKV nsP2^{pro}:P1 complex were finally obtained through clustering analysis. The interface of the central structure from the largest cluster is shown in Fig. 7A. As observed, the peptide extends along the open active site, with most of its aromatic and hydrophobic residues buried at the interface, significantly contributing to binding. This is supported by the substantial free energy contributions (ΔG_{res}) of residues M2, W4, and W7 (Fig. 7B). Similarly, CHIKV nsP2^{pro} residues interacting with the peptide's key hotspots also display notable ΔG_{res} values, such as N1011, A1046, Y1079, L1205, M1238, and M1242 (Fig. 7B). These interactions contribute to the negative nonpolar free energy component, ultimately resulting in the favorable ΔG_{eff} value observed for the CHIKV nsP2^{pro}:P1 complex (Supplementary Table S4). Conversely, polar residues at the interface generally exhibited small energy contributions to complex formation, except for K10 and R11, which possess significantly favorable ΔG_{res} values (Fig. 7B). However, these polar residues compensate for the loss of favorable interactions with water upon binding by forming intermolecular hydrogen bonds (H-bonds), as depicted in Fig. 7A.

4. Discussion

Chikungunya virus (CHIKV) is an emerging virus with infections rising rapidly due to the global spread of its vector, posing a significant public health challenge. While several lead compounds such as 1,3-Thiazolbenzamide derivatives, Hesperetin (HST) have been identified as inhibitors of the CHIKV nsP2^{pro}, none has yet been approved as therapeutic agents for Chikungunya fever (Eberle et al., 2021; Ivanova et al., 2021). In this study, six different peptides were identified using phage display as specific binders against the nsP2^{pro} (Table 4). Among these, four peptides (P1, P2, P4, and P5) exhibited inhibitory effects on the protease in a primary inhibition test, with inhibition rates of ≤50 % (Fig. 2). The IC_{50} value of peptide P1 for the nsP2^{pro} was determined to be 4.6 μM (Fig. 3A), making it the most potent inhibitor identified in this study. Peptides P2 and P5 had IC_{50} values of 194.7 μM and 316.9 μM, respectively (Fig. 3B,C). However, the IC_{50} value of peptide P4 could not be determined due to aggregation occurring within 2–4 min under the assay conditions. These results highlight peptide P1 as the strongest inhibitor. The scrambled P1 peptides (SP1-SP3) (Supplementary Table S1 and Fig. 2B) showed a weak effect against the CHIKV nsP2^{pro} activity at the tested concentration of 50 μM. These results indicates that the inhibitory activity of P1 is sequence-dependent and highly specific. The inhibition mode assay revealed that peptide P1 increases the Michaelis-Menten constant (K_m), while the maximum velocity (V_{max}) remains unchanged (Fig. 4A) and this indicates a reduced affinity of the enzyme for its substrate, which is characteristic for a competitive inhibitor (Blat, 2010). Affinity measurements using MST (Jerabek-Willemsen et al., 2014) showed that peptide P1 has an equilibrium dissociation constant (K_D) of approximately 1.39 μM (Fig. 4B), demonstrating a binding affinity to its target in the low μM range. A comparison of P1 revealed a lower IC_{50} compared to other identified small molecules from various studies, such as the 1,3-thiazolbenzamide

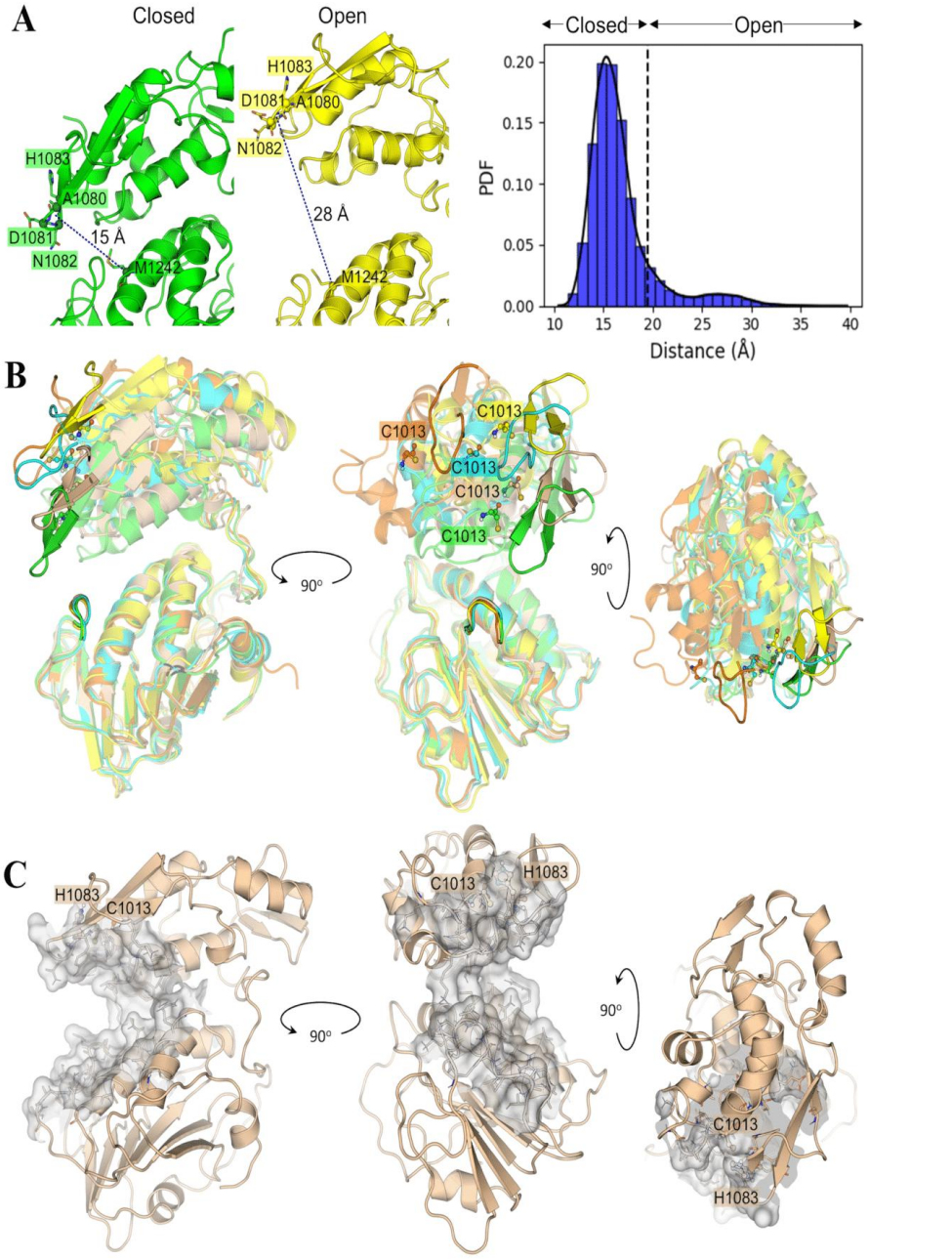

(caption on next page)

Fig. 5. Conformational dynamics of CHIKV nsP2^{pro}. (A) Structural representations of two snapshots of CHIKV nsP2^{pro}, illustrating closed and open conformations of the active site resulting from interdomain motion. To monitor these conformational changes throughout the MD simulations, the distance between the Cα atoms of residues A1080, D1081, N1082, and H1083 on the flap and the Cα of M1242 on a neighboring α-helix in the opposite domain was measured. The graph on the right shows the distribution of these distances along the 20 μs concatenated MD trajectory, with the dashed line indicating the threshold used to define open and closed states. **(B)** Structural representation of five central structures derived from clustering the 20 μs concatenated trajectory. The C-terminal domains (lower domain) were aligned to highlight the motion of the N-terminal catalytic domain (upper domain). The catalytic Cys residue (C1013) is depicted as spheres and sticks. Additionally, the flap of the catalytic domain and a loop interacting with it in the closed conformation are highlighted. **(C)** Surface representation of the open conformation of the active site, highlighting the catalytic residues C1013 and H1083. This snapshot was selected for the prediction of the CHIKV nsP2^{pro}: peptide complex structure.

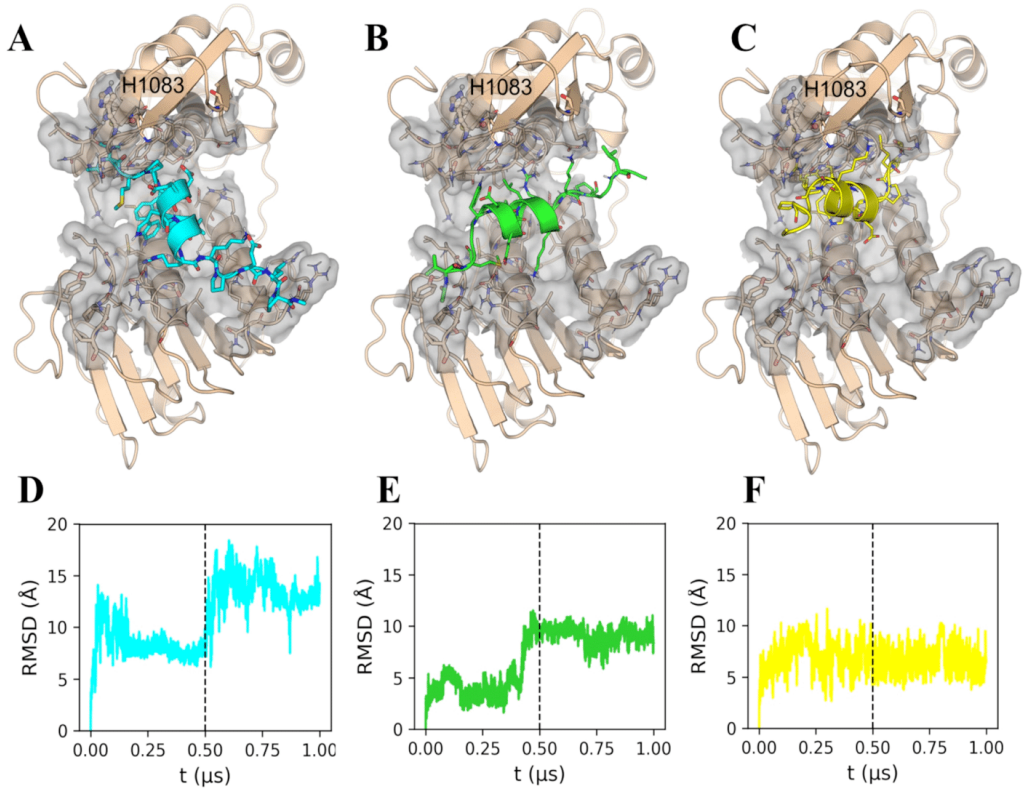

Fig. 6. Top-ranked docking poses of peptide P1 at the active site of CHIKV nsP2 protease obtained with three docking programs. (A) ClusPro, **(B)** Hdock and **(B)** Galaxy Tongdock. The peptide is colored in cyan, green or yellow depending on the program used for docking. The protein is depicted in beige, with the active site surface being colored in gray. **(D), (E)** and **(F)** show the peptide RMSD values along the MD simulations initiated with each of the docking poses shown on top. The colors of the RMSD plots match those of the peptide in the corresponding starting structure. RMSD values were calculated for the peptide's heavy atoms taking as reference the initial structure (docking pose). Prior to RMSD calculations, all trajectory frames were fitted onto the backbone atoms of the protein in the starting conformation. The dashed lines indicate that frames of the second half of each MD simulation were employed for subsequent MM-GBSA free energy calculations.

derivatives compound 10 (13.1 μM) and compound 10c (8.3 μM) (Ivanova et al., 2021). However, P1's inhibitory effect was weaker compared to RA-0,002,034 (Merten et al., 2024), which has an IC_{50} of 58 ± 17 nM. In comparison to peptide inhibitors like Pep-I (34 μM) and Pep-II (42 μM) (Singh et al., 2018) P1 demonstrated significantly greater potency, with IC_{50} values approximately tenfold lower Affinity measurements also underscore the favorable characteristics of peptide P1. The KD value of approximately 1.39 μM positions it among inhibitors with strong binding affinities. For example, P1's KD is markedly lower than that of flavonoids like hesperetin (HST) or hesperidin (HSD), further supporting its potential as an effective inhibitor of CHIKV nsP2^{pro} (Table 5).

Cytotoxicity is a crucial factor when evaluating the therapeutic potential of peptides. The MTT assay demonstrated that peptide P1, dissolved in water, exhibited low toxicity at concentrations up to 100 μM, with 77 % cell viability (Fig. 4C). However, when peptide P1 was dissolved in DMSO and subsequently diluted in DMEM medium, higher cytotoxicity was observed (Fig. 4D). Further analysis, including a DMSO titration test on Vero cells (Supplementary Fig. S10) revealed that the increased toxicity was not due to the peptide itself but rather the high concentration of DMSO. Specifically, DMSO concentrations up to 0.8 % were shown to have low toxicity. These findings are consistent with

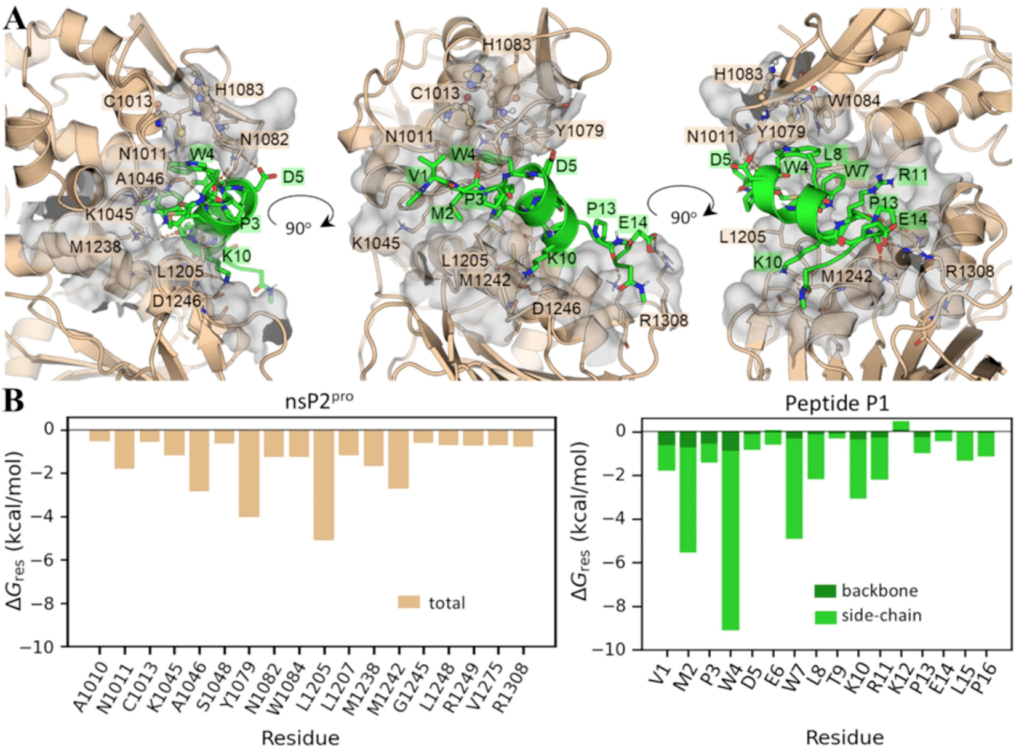

Fig. 7. Predicted binding mode of peptide P1 to CHIKV nsP2^{pro}. (A) Structural representation of the peptide P1 in complex with CHIKV nsP2^{pro}. Three views of the predicted complex are shown. Key interacting residues of the protein and the peptide are depicted as sticks and labeled. The active site cavity is displayed as a transparent gray surface. H-bonds at the complex interface observed during the MD simulations are represented as orange dashed lines. The central structure corresponding to the largest cluster of the 2.5 μs MD simulation was selected for representation. **(B)** Per-residue free energy (ΔG_{res}) values for warm- and hotspot residues of CHIKV nsP2^{pro} and for all residues of peptide P1. The free energy contributions of each residue side-chain and backbone are shown for the peptide.

Table 5
Inhibitors of CHIKV nsP2^{pro} reported in previous studies. The table provides an overview of the identified inhibitors, IC_{50} values, their mode of inhibition and binding affinities (if available).

Inhibitor	IC_{50} [μM]	Inhibition mode	K_D	Reference
RA-0,002,034(1)	0.058 ± 0.017	competitive	NA	(Merten et al., 2024)
1,3 Thiazolbenzamide derivatives	8.3–13.1	competitive	NA	(Ivanova et al., 2021)
Hesperetin (HST)	2.5 ± 0.4	noncompetitive	31.6 ± 2.5 μM	(Eberle et al., 2021)
Hesperidin (HSD)	7.1 ± 1.1	noncompetitive	40.7 ± 2.0 μM.	(Eberle et al., 2021)
Pep-I	34	noncompetitive	NA	(Singh et al., 2018)
Pep-II	42	competitive	NA	(Singh et al., 2018)
Novobiocin	2	NA	NA	(Tripathi et al., 2020)
Telmisarten	5	NA	NA	(Tripathi et al., 2020)

other studies, which indicate that DMSO becomes toxic at concentrations above 1 % (Aguilar et al., 2002). The differences between these studies could be attributed to variations in cell viability assessment methods. These results highlight the importance of optimizing solvent conditions to minimize toxicity in future applications. Cytotoxicity studies of other molecules, such as HST and HDT, showed that at approximately 150 μM, around 75 % of the cells remained viable (Eberle et al., 2021). A comparison suggests that P1 exhibits similar cytotoxicity, reinforcing the notion that P1 has low toxicity. Additionally, a comparison with other peptide inhibitors, such as Pep-I and Pep-II, revealed that P1 as a peptide inhibitor exhibited similar toxicity to Pep-I at 100 μM, but higher toxicity compared to Pep-II (Singh et al., 2018). To explore the structural properties of the peptides, we used I-TASSER to predict 3D structures and CD spectroscopy to determine secondary structures. Peptides P1, P3, and P5 were found to consist of a mixture of short α-helices and random coiled structures, as confirmed by their CD spectra. A typical minimum of the CD spectra between 200 and 220 nm and a maximum of around 190 nm were observed (Supplementary Fig. S8), indicative of characteristic features of α-helical structures (Haque et al., 2022). In contrast, peptides P2, P4, and P6 were determined to exhibit predominantly random coiled structures. Their CD spectra (Supplementary Fig. S8) displayed in the CD spectra a minimum of around 200 nm, which is characteristic of random coiled structures (Haque et al., 2022). The consistency between the 3D structural

predictions provided by I-TASSER and the results of CD spectroscopy, as illustrated in Table S3, was used to validate the reliability of the obtained structural data. Notably, the predominantly random coil structure of peptide P4, featuring charged amino acids and exposure of hydrophobic regions, may account for its tendency to aggregate during the IC_{50} assay. This structural tendency, along with sequence differences, may also contribute to the observed variation in IC_{50} values among peptides P1, P2, and P5. Specifically, peptide P1 exhibited a higher proportion of α-helices and a lower percentage of random coil structures compared to P2 and P5. According to literature and previous studies, α-helices stabilize the protein-protein interaction and this increased structural stability can enhance their binding affinity and inhibitory effects (Wang et al., 2021). These findings suggest that peptides with a higher α-helix content are more effective inhibitors of the protease. Our molecular docking and simulation studies demonstrated that at the simulated conditions ($T = 310$ K, with protonation at pH 7.4, and $t = 20$ μs) approximately 87 % of $nsP2^{pro}$ adopts a closed and inactive conformation. Exploring the open conformations of the active site is a crucial step to investigate the binding of orthostatic ligands, especially when these ligands are relatively large, as in the present study. Our computational results reinforce previous crystallographic evidence highlighting the flexibility of the active site flap among $nsP2^{pro}$s of alphaviruses and the occurrence of an open-closure dynamics (Narwal et al., 2018). Blind docking of peptide P1, using three different approaches, consistently positioned the peptide near the active site. The stability of the predicted binding modes was thoroughly assessed by subjecting the docking poses to MD simulations and MM-GBSA free energy calculations. The most likely binding conformations of P1 were sampled during the last 2 μs of an extended MD simulation initiated from a docking pose obtained with the program HDock. The representative structure of the complex shows the peptide stretching along the open active site cavity. Further structural analyses indicated that W4, and W7 of peptide P1 interact with the critical amino acids N1011 and Y1079 at the $nsP2^{pro}$ substrate-binding sites S2 and S4 (Narwal et al., 2018). These findings align with the results from the inhibition mode assay, indicating that P1 acts as a competitive inhibitor. Per-residue free energy calculations identified W4 as the primary hotspot residue in the peptide, with a side-chain ΔG_{res} values of −8.2 kcal/mol, followed by M2 (−4.8 kcal/mol) and W7 (−4.6 kcal/mol). These findings highlight the critical role of these three amino acid residues in the binding of peptide P1. Understanding the energy contribution of each residue is essential for optimizing and modifying the peptide to improve its binding affinity to the protease. Redesign strategies should prioritize mutations at these hotspot positions to explore potential improvements. Additionally, future studies also evaluate the specificity of peptide P1 against the CHIKV $nsP2^{pro}$.

5. Conclusion and future perspectives

In this study, six peptides were identified as potential binders of the CHIKV $nsP2^{pro}$ through phage display, with peptide P1 exhibiting the highest inhibitory activity. Peptide P1 showed a competitive inhibition mode, with an IC_{50} of 4.6 μM and K_D of approximately 1.39 μM, indicating strong binding affinity for its target. Structural and cytotoxicity analyses further emphasized P1′s therapeutic potential; however, solvent optimization is essential to mitigate DMSO-related toxicity. Molecular docking studies confirmed P1′s binding to essential substrate-binding sites of $nsP2^{pro}$, highlighting the importance of key residues in inhibitor-protease interactions.

Funding

MM thanks Jürgen Manchot Stiftung for providing financial assistance and resources. JEHG thanks the financial support of the National Council for Scientific and Technological Development (CNPq), Grant 153794/2024-0, and of the Sao Paulo Research Foundation (FAPESP), Grants 2022/03901-8, 2024/13327-2 and 2020/08615-8.

Declaration of generative AI and AI-assisted technologies in the writing process

ChatGPT was used to check grammar and spelling in order to improve readability. After using this tool, the authors reviewed and edited the content and take full responsibility for the content of the publication. Part of the figures were created by BioRender program.

CRediT authorship contribution statement

Mohammadamin Mastalipour: Conceptualization, Methodology, Formal analysis, Data curation, Writing – original draft, Writing – review & editing. **Ian Gering:** Methodology, Formal analysis, Writing – original draft, Writing – review & editing. **Mônika Aparecida Coronado:** Supervision, Formal analysis, Writing – original draft, Writing – review & editing. **Jorge Enrique Hernández González:** Methodology, Formal analysis, Data curation, Writing – original draft, Writing – review & editing. **Dieter Willbold:** Resources, Writing – original draft, Writing – review & editing. **Raphael Josef Eberle:** Conceptualization, Formal analysis, Supervision, Writing – original draft, Writing – review & editing.

Declaration of competing interest

The authors declare that they have no known competing financial interests or personal relationships that could have appeared to influence the work reported in this paper.

Acknowledgements

We would like to express our sincere gratitude to Jürgen Manchot Stiftung for providing financial assistance and resources that were critical to the success of this project. JEHG thanks the National Laboratory for Scientific Computing (LNCC/MCTI, Brazil) for providing HPC resources of the SDumont supercomputer, URL: http://sdumont.lncc.br.

Supplementary materials

Supplementary material associated with this article can be found, in the online version, at doi:10.1016/j.crmicr.2025.100376.

Data availability

All relevant data are included in this manuscript and its supporting information. Further inquiries or requests for materials can be directed to eberler@hhu.de.

References

Aguilar, J.S., Roy, D., Ghazal, P., Wagner, E.K., 2002. Dimethyl sulfoxide blocks herpes simplex virus-1 productive infection *in vitro* acting at different stages with positive cooperativity. Application of micro-array analysis. BMC Infect. Dis. 2. https://doi.org/10.1186/1471-2334-2-9.

Ahmed, S., Sultana, S., Kundu, S., Alam, S.S., Hossan, T., Islam, M.A., 2024. Global prevalence of Zika and Chikungunya coinfection: a systematic review and meta-analysis. Diseases 12 (2). https://doi.org/10.3390/diseases12020031.

Alfaleh, M.A., Alsaab, H.O., Mahmoud, A.B., Alkayyal, A.A., Jones, M.L., Mahler, S.M., & Hashem, A.M. (2020). Phage display derived monoclonal antibodies: from bench to bedside. https://doi.org/10.3389/fimmu.2020.01986.

Altendorf, T., Mohrlüder, J., Willbold, D., 2024. TSAT: efficient evaluation software for NGS data of phage/mirror-image phage display selections. Biophys. Rep. 4 (3). https://doi.org/10.1016/j.bpr.2024.100166 (N. Y).

Blat, Y., 2010. Non-competitive inhibition by active site binders. Chem. Biol. Drug Des. 75 (6), 535–540. https://doi.org/10.1111/j.1747-0285.2010.00972.x.

Case, D.A., Cheatham III, T.E., Darden, T., Gohlke, H., Luo, R., Merz Jr., K.M., Onufriev, A., Simmerling, C., Wang, B., Woods, R.J., 2005. The Amber biomolecular simulation programs. J. Comput. Chem. 26 (16), 1668–1688.

Chen, L.H., Fritzer, A., Hochreiter, R., Dubischar, K., Meyer, S., 2024. From bench to clinic: the development of VLA1553/IXCHIQ, a live-attenuated Chikungunya vaccine. J. Travel. Med. 31 (7). https://doi.org/10.1093/jtm/taae123.

Da Silva Ribeiro, A.C., de Carvalho, C.A.M., Casseb, S.M.M., Rodrigues, S.G., da Costa Vasconcelos, P.F., Carvalho, V.L, 2018. Infection profiles of Mayaro virus and Chikungunya virus in mammalian and mosquito cell lineages. Rev. Pan-Amaz. Saúde 9 (4), 11. http://doi.org/10.5123/s2176-62232018000400003.

Delrieu, M., Martinet, J.P., O'Connor, O., Viennet, E., Menkes, C., Burtet-Sarranmegna, V., Dupont-Rouzeyrol, M., 2023. Temperature and transmission of Chikungunya, dengue, and Zika viruses: a systematic review of experimental studies on Aedes aegypti and Aedes albopictus. Curr. Res. Parasitol. Vector-Borne Dis. 4. https://doi.org/10.1016/j.crpvbd.2023.100139.

De Souza, W.M., Ribeiro, G.S., de Lima, S.T.S., de Jesus, R., Moreira, F.R.R., Whittaker, C., Sallum, M.A.M., Carrington, C.V.F., Sabino, E.C., Kitron, U., Faria, N. R., Weaver, S.C., 2024. Chikungunya: a decade of burden in the Americas. Lancet Reg. Health Am. 30, 100673. https://doi.org/10.1016/j.lana.2023.100673 (Engl. ed).

Dolinsky, T.J., Nielsen, J.E., McCammon, J.A., Baker, N.A., 2004. PDB2PQR: an automated pipeline for the setup of Poisson–Boltzmann electrostatics calculations. Nucleic Acids Res. 32 (suppl_2), W665–W667. https://doi.org/10.1093/nar/gkh381.

Eberle, R.J., Olivier, D.S., Pacca, C.C., Avilla, C.M.S., Nogueira, M.L., Amaral, M.S., Coronado, M.A., 2021. study of Hesperetin and Hesperidin as inhibitors of Zika and Chikungunya virus proteases. PLoS One 16 (3). https://doi.org/10.1371/journal.pone.0246319.

Eberle, R.J., Sevenich, M., Gering, I., Scharbert, L., Strodel, B., Lakomek, N.A., Willbold, D., 2023. Discovery of all-D-peptide inhibitors of SARS-CoV-2 3C-like protease. ACS Chem. Biol. 18 (2), 315–330. https://doi.org/10.1021/acschembio.2c00735.

El-Sayed, A., Kamel, M., 2020. Climatic changes and their role in emergence and re-emergence of diseases. Environ. Sci. Pollut. Res. 27 (18), 22336–22352. https://doi.org/10.1007/s11356-020-08896-w.

European Centre for Disease Prevention and Control, 2024. Chikungunya Worldwide Overview. December 17. ECDC. https://www.ecdc.europa.eu/en/chikungunya-monthly.

Freppel, W., Silva, L.A., Stapleford, K.A., Herrero, L.J., 2024. Pathogenicity and virulence of Chikungunya virus. Virulence 15 (1). https://doi.org/10.1080/21505594.2024.2396484.

Ghoshal, A., Asressu, K.H., Hossain, M.A., Brown, P.J., Nandakumar, M., Vala, A., Willson, T.M., 2024. Structure activity of beta-amidomethyl vinyl sulfones as covalent inhibitors of Chikungunya nsP2 cysteine protease with antialphavirus activity. J. Med. Chem. 67 (18), 16505–16532. https://doi.org/10.1021/acs.jmedchem.4c01346.

Girard, J., Le Bihan, O., Lai-Kee-Him, J., Girleanu, M., Bernard, E., Castellarin, C., Bron, P., 2024. In situ fate of Chikungunya virus replication organelles. J. Virol. 98 (7), e0036824. https://doi.org/10.1128/jvi.00368-24.

Göertz, G.P., McNally, K.L., Robertson, S.J., Best, S.M., Pijlman, G.P., Fros, J.J., 2018. The methyltransferase-like domain of Chikungunya virus nsP2 inhibits the interferon response by promoting the nuclear export of STAT1. J. Virol. 92 (17). https://doi.org/10.1128/jvi.01008-18.

Grabenstein, J.D., Tomar, A.S., 2023. Global geotemporal distribution of Chikungunya disease, 2011-2022. Travel Med. Infect. Dis. 54. https://doi.org/10.1016/j.tmaid.2023.102603.

Haque, M.A., Kaur, P., Islam, A., Hassan, M.I., 2022. Chapter 14 - application of circular dichroism spectroscopy in studying protein folding, stability, and interaction (Eds.). In: Tripathi, T., Dubey, V.K. (Eds.), Advances in Protein Molecular and Structural Biology Methods. Academic Press, pp. 213–224. https://doi.org/10.1016/B978-0-323-90264-9.00014-3.

Hopkins, C.W., Le Grand, S., Walker, R.C., Roitberg, A.E., 2015. Long-time-step molecular dynamics through hydrogen mass repartitioning. J. Chem. Theory Comput. 11 (4), 1864. https://doi.org/10.1021/ct5010406.

Hu, X., Compton, J.R., Leary, D.H., Olson, M.A., Lee, M.S., Cheung, J., Legler, P.M., 2016. Kinetic, mutational, and structural studies of the Venezuelan Equine Encephalitis virus nonstructural protein 2 cysteine protease. Biochemistry 55 (21), 3007–3019. https://doi.org/10.1021/acs.biochem.5b00992.

Ivanova, L., Rausalu, K., Zusinaite, E., Tammiku-Taul, J., Merits, A., Karelson, M., 2021. 1,3-Thiazolbenzamide derivatives as Chikungunya virus nsP2 protease inhibitors. ACS Omega 6 (8), 5786–5794. https://doi.org/10.1021/acsomega.0c06191.

Izadi, S., Anandakrishnan, R., Onufriev, A.V., 2014. Building water models: a different approach. J. Phys. Chem. Lett. 5 (21), 3863–3871. https://doi.org/10.1021/jz501780a.

Jadav, S.S., Sinha, B.N., Hilgenfeld, R., Pastorino, B., de Lamballerie, X., Jayaprakash, V., 2015. Thiazolidone derivatives as inhibitors of Chikungunya virus. Eur. J. Med. Chem. 89, 172–178. https://doi.org/10.1016/j.ejmech.2014.10.042.

Jerabek-Willemsen, M., André, T., Wanner, R., Roth, H.M., Duhr, S., Baaske, P., Breitsprecher, D., 2014. MicroScale thermophoresis: interaction analysis and beyond. J. Mol. Struct. 1077, 101–113. https://doi.org/10.1016/j.molstruc.2014.03.009.

Jones, G., Jindal, A., Ghani, U., Kotelnikov, S., Egbert, M., Hashemi, N., Kozakov, D., 2022. Elucidation of protein function using computational docking and hotspot analysis by ClusPro and FTMap. Acta Crystallogr. D 78 (6), 690–697. https://doi.org/10.1107/S2059798322002741.

Khongwichit, S., Chuchaona, W., Vongpunsawad, S., Poovorawan, Y., 2022. Molecular surveillance of arboviruses circulation and co-infection during a large Chikungunya virus outbreak in Thailand, October 2018 to February 2020. Sci. Rep. 12 (1). https://doi.org/10.1038/s41598-022-27028-7.

Kutzsche, J., Jürgens, D., Willuweit, A., Adermann, K., Fuchs, C., Simons, S., Willbold, D., 2020. Safety and pharmacokinetics of the orally available antiprionic compound PRI-002: a single and multiple ascending dose phase I study. (New York, N. Y.) 6 (1), e12001. https://doi.org/10.1002/trc2.12001.

Law, Y.S., Wang, S., Tan, Y.B., Shih, O., Utt, A., Goh, W.Y., Lian, B.J., et al., 2021. Interdomain flexibility of chikungunya virus nsP2 helicase-protease differentially influences viral RNA replication and infectivity. J. Virol. 95 (6), 10–1128.

Ly, H., 2024. Ixchiq (VLA1553): the first FDA-approved vaccine to prevent disease caused by Chikungunya virus infection. Virulence 15 (1). https://doi.org/10.1080/21505594.2023.2301573.

Marimoutou, C., Ferraro, J., Javelle, E., Deparis, X., Simon, F., 2015. Chikungunya infection: self-reported rheumatic morbidity and impaired quality of life persist 6 years later. Clin. Microbiol. Infect. 21 (7), 688–693. https://doi.org/10.1016/j.cmi.2015.02.024.

Martins, D.O.S., Ruiz, U.E.A., Santos, I.A., Oliveira, I.S., Guevara-Vega, M., de Paiva, R.E. F., Jardim, A.C.G., 2024. Exploring the antiviral activities of the FDA-approved drug sulfadoxine and its derivatives against Chikungunya virus. Pharmacol. Rep. 76 (5), 1147–1159. https://doi.org/10.1007/s43440-024-00635-z.

Mayer, S.V., Tesh, R.B., Vasilakis, N., 2017. The emergence of arthropod-borne viral diseases: a global prospective on dengue, Chikungunya and Zika fevers. Acta Trop. 166, 155–163. https://doi.org/10.1016/j.actatropica.2016.11.020.

Merten, E.M., Sears, J.D., Leisner, T.M., Hardy, P.B., Ghoshal, A., Hossain, M.A., Pearce, K.H., 2024. Identification of a cell-active Chikungunya virus nsP2 protease inhibitor using a covalent fragment-based screening approach. Proc. Natl. Acad. Sci. U. S. A. 121 (42), e2409166121. https://doi.org/10.1073/pnas.2409166121.

Miller 3rd, B.R., McGee Jr., T.D., Swails, J.M., Homeyer, N., Gohlke, H., Roitberg, A.E., 2012. MMPBSA.py: an efficient program for end-state free energy calculations. J. Chem. Theory Comput. https://doi.org/10.1021/ct300418h.

Mourad, O., Makhani, L., Chen, L.H., 2022. Chikungunya: an emerging public health concern. Curr. Infect. Dis. Rep. 24 (12), 217–228. https://doi.org/10.1007/s11908-022-00789-y.

Narwal, M., Singh, H., Pratap, S., Malik, A., Kuhn, R.J., Kumar, P., Tomar, S., 2018. Crystal structure of Chikungunya virus nsP2 cysteine protease reveals a putative flexible loop blocking its active site. Int. J. Biol. Macromol. 116, 451–462. https://doi.org/10.1016/j.ijbiomac.2018.05.007.

Nguyen, H., Roe, D.R., Simmerling, C., 2013. Improved generalized born solvent model parameters for protein simulations. J. Chem. Theory Comput. 9 (4), 2020–2034. https://doi.org/10.1021/ct3010485.

Paixao, E.S., Rodrigues, L.C., Costa, M.D.N., Itaparica, M., Barreto, F., Gérardin, P., Teixeira, M.G., 2018. Chikungunya chronic disease: a systematic review and meta-analysis. Trans. R. Soc. Trop. Med. Hyg. 112 (7), 301–316. https://doi.org/10.1093/trstmh/try063.

Park, T., Baek, M., Lee, H., Seok, C., 2019. GalaxyTongDock: symmetric and asymmetric ab initio protein–protein docking web server with improved energy parameters. J. Comput. Chem. 40 (27), 2413–2417. https://doi.org/10.1002/jcc.25874.

Peinado, R.D.S., Eberle, R.J., Arni, R.K., Coronado, M.A., 2022. A review of omics studies on Arboviruses: Alphavirus, Orthobunyavirus and Phlebovirus. Viruses 14 (10), 2194. https://doi.org/10.3390/v14102194.

Peinado, R.D.S., Martins, L.G., Pacca, C.C., Saivish, M.V., Borsatto, K.C., Nogueira, M.L., Coronado, M.A., 2024. HR-MAS NMR metabolomics profile of vero cells under the influence of virus infection and nsP2 inhibitor: a Chikungunya case study. Int. J. Mol. Sci. 25 (3). https://doi.org/10.3390/ijms25031414.

Rama, K., de Roo, A.M., Louwsma, T., Hofstra, H.S., do Amaral, G.S.G., Vondeling, G.T., Freriks, R.D., 2024. Clinical outcomes of Chikungunya: a systematic literature review and meta-analysis. PLoS Negl. Trop. Dis. 18 (6). https://doi.org/10.1371/journal.pntd.0012254.

Rawlings, N.D., Barrett, A.J., Bateman, A., 2010. MEROPS: the peptidase database. Nucleic Acids Res. 38 (suppl_1), D227–D233.

Rossotti, M.A., Trempe, F., van Faassen, H., Hussack, G., Arbabi-Ghahroudi, M., 2023. Isolation and characterization of single-domain antibodies from immune phage display libraries. Methods Mol. Biol. 2702, 107–147. https://doi.org/10.1007/978-1-0716-3381-6_7 (Clifton, N.J.).

Schneider, M., Narciso-Abraham, M., Hadl, S., Mcmahon, R., Toepfer, S., Fuchs, U., Wressnigg, N., 2023. Safety and immunogenicity of a single-shot live-attenuated Chikungunya vaccine: a double-blind, multicentre, randomised, placebo-controlled, phase 3 trial. Lancet 401 (10394), 2138–2147. https://doi.org/10.1016/S0140-6736(23)00641-4.

Sevenich, M., Thul, E., Lakomek, N.A., Kluenemann, T., Schubert, M., Bertoglio, F., Willbold, D., 2022. Phage display-derived compounds displace hACE2 from its complex with SARS-CoV-2 spike protein. Biomedicines 10 (2). https://doi.org/10.3390/biomedicines10020441.

Sharif, N., Sarkar, M.K., Ferdous, R.N., Ahmed, S.N., Billah, M.B., Talukder, A.A., Dey, S. K., 2021. Molecular epidemiology, evolution and reemergence of Chikungunya virus in South Asia. Front. Microbiol. 12. https://doi.org/10.3389/fmicb.2021.689979.

Silva, L.A., Dermody, T.S., 2017. Chikungunya virus: epidemiology, replication, disease mechanisms, and prospective intervention strategies. J. Clin. Investig. 127 (3), 737–749. https://doi.org/10.1172/Jci84417.

Simon, F., Javelle, E., Oliver, M., Leparc-Goffart, I., Marimoutou, C., 2011. Chikungunya virus infection. Curr. Infect. Dis. Rep. 13 (3), 218–228. https://doi.org/10.1007/s11908-011-0180-1.

Singh, H., Mudgal, R., Narwal, M., Kaur, R., Singh, V.A., Malik, A., Tomar, S., 2018. Chikungunya virus inhibition by peptidomimetic inhibitors targeting virus-specific cysteine protease. Biochimie 149, 51–61. https://doi.org/10.1016/j.biochi.2018.04.004.

Solignat, M., Gay, B., Higgs, S., Briant, L., Devaux, C., 2009. Replication cycle of Chikungunya: a re-emerging arbovirus. Virology 393 (2), 183–197. https://doi.org/10.1016/j.virol.2009.07.024.

Tian, C., Kasavajhala, K., Belfon, K.A.A., Raguette, L., Huang, H., Migues, A.N., Simmerling, C., 2020. ff19SB: amino-acid-specific protein backbone parameters trained against quantum mechanics energy surfaces in solution. J. Chem. Theory Comput. 16 (1), 528–552. https://doi.org/10.1021/acs.jctc.9b00591.

Tripathi, P.K., Soni, A., Singh Yadav, S.P., Kumar, A., Gaurav, N., Raghavendhar, S., Patel, A.K., 2020. Evaluation of novobiocin and telmisartan for anti-CHIKV activity. Virology 548, 250–260. https://doi.org/10.1016/j.virol.2020.05.010.

van Groen, T.A.-O., Schemmert, S., Brener, O., Gremer, L., Ziehm, T., Tusche, M., Willbold, D.A.-O., 2017. The Aβ oligomer eliminating D-enantiomeric peptide RD2 improves cognition without changing plaque pathology. Sci. Rep. 7 (1), 16275. https://doi.org/10.1038/s41598-017-16565-1.

Vikhe, V.B., Faruqi, A.A., Reddy, A., Khandol, D., Lapsiwala, V.H., 2023. Dengue and Chikungunya Co-infection- associated multi-organ dysfunction syndrome: a case report. Cureus J. Med. Sci. 15 (12). https://doi.org/10.7759/cureus.50196.

Wang, H., Dawber, R.S., Zhang, P., Walko, M., Wilson, A.J., Wang, X., 2021. Peptide-based inhibitors of protein-protein interactions: biophysical, structural and cellular consequences of introducing a constraint. Chem. Sci. 12 (17), 5977–5993. https://doi.org/10.1039/d1sc00165e.

Ware, B.C., Parks, M.G., da Silva, M.O.L., Morrison, T.E., 2024. Chikungunya virus infection disrupts MHC-I antigen presentation via nonstructural protein 2. PLoS Pathog. 20 (3). https://doi.org/10.1371/journal.ppat.1011794.

Yan, Y., Tao, H., He, J., Huang, S.-Y., 2020. The HDOCK server for integrated protein–protein docking. Nat. Protoc. 15 (5), 1829–1852. https://doi.org/10.1038/s41596-020-0312-x.

Yang, J.Y., Yan, R.X., Roy, A., Xu, D., Poisson, J., Zhang, Y., 2015. The I-TASSER suite: protein structure and function prediction. Nat. Methods 12 (1), 7–8. https://doi.org/10.1038/nmeth.3213.

Yau, A.W.N., Chu, S.Y.C., Yap, W.H., Wong, C.L., Chia, A.Y.Y., Tang, Y.Q., 2024. Phage display screening in Breast Cancer: from peptide discovery to clinical applications. Life Sci. 357, 123077. https://doi.org/10.1016/j.lfs.2024.123077.

Zaid, A., Gérardin, P., Taylor, A., Mostafavi, H., Malvy, D., Mahalingam, S., 2018. Chikungunya arthritis implications of acute and chronic inflammation mechanisms on disease management. Arthritis Rheumatol. 70 (4), 484–495. https://doi.org/10.1002/art.40403.

Zhou, X., Zheng, W., Li, Y., Pearce, R., Zhang, C., Bell, E.W., Zhang, G., Zhang, Y., 2022. I-TASSER-MTD: a deep-learning-based platform for multi-domain protein structure and function prediction. Nat. Protoc. 17 (10), 2326–2353. https://doi.org/10.1038/s41596-022-00728-0.

Supplementary Material

Novel peptide inhibitor for the Chikungunya virus nsP2 protease: Identification and Characterization.

Mohammadamin Mastalipour[1], Ian Gering[2], Mônika Aparecida Coronado[1,2], Jorge Enrique Hernández González[3], Dieter Willbold[1,2], Raphael Josef Eberle[4]

[1] Institut für Physikalische Biologie, Heinrich-Heine-Universität Düsseldorf, Universitätsstraße 1, 40225 Düsseldorf, Germany

[2] Institut für Biologische Informationsprozesse, Strukturbiochemie (IBI-7), Forschungszentrum Jülich, 52425 Jülich, Germany

[3] São Paulo State University (UNESP), Institute of Biosciences, Humanities and Exact Sciences, São José do Rio Preto, Brazil

[4] Institut für Biochemische Pflanzenphysiologie, Heinrich-Heine-Universität Düsseldorf, Universitätsstraße 1, 40225 Düsseldorf, Germany

Table of content

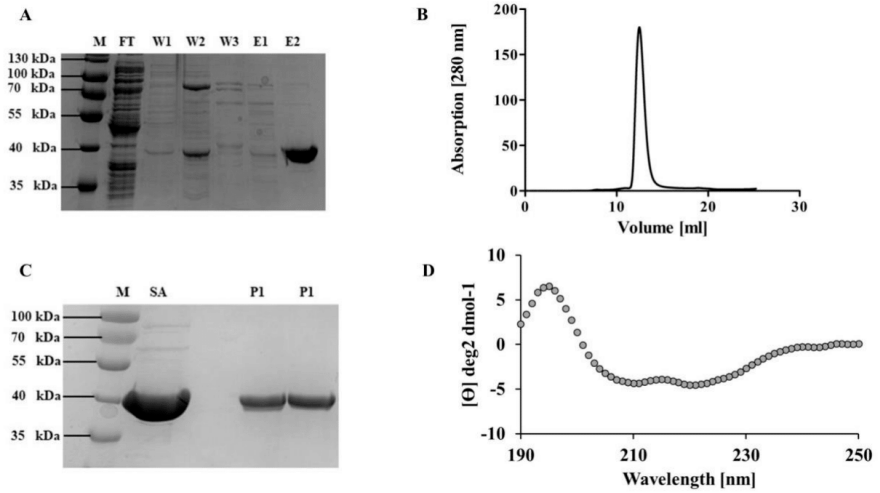

Fig. S1. Purification and CD spectroscopy of nsP2^{pro}. (A) SDS-PAGE gel showing the elution and purification of heterologous expressed CHIKV nsP2^{pro} in the second elution step. M: Marker (Protein ruler), FT: Flow-through, W1: Wash 1, W2: Wash 2, W3: Wash 3, E1: First elution with 100 mM Imidazole, E2: Second elution with 500 mM Imidazole. **(B)** SEC chromatogram displaying the elution profile of CHIKV nsP2^{pro} after approximately 12 ml of elution. **(C)** Representative SDS-PAGE gel of purified nsP2^{pro} after SEC purification. M: Marker, SA: Sample after Ni-NTA purification, P1: Peak 1. **(D)** CD spectroscopy of nsP2^{pro}. The spectrum was measured at 18°C, covering the wavelength range at 190-260 nm in a 1 mm cuvette. The nsP2^{pro} was diluted in phosphate buffer to a final concentration of 5 µM.

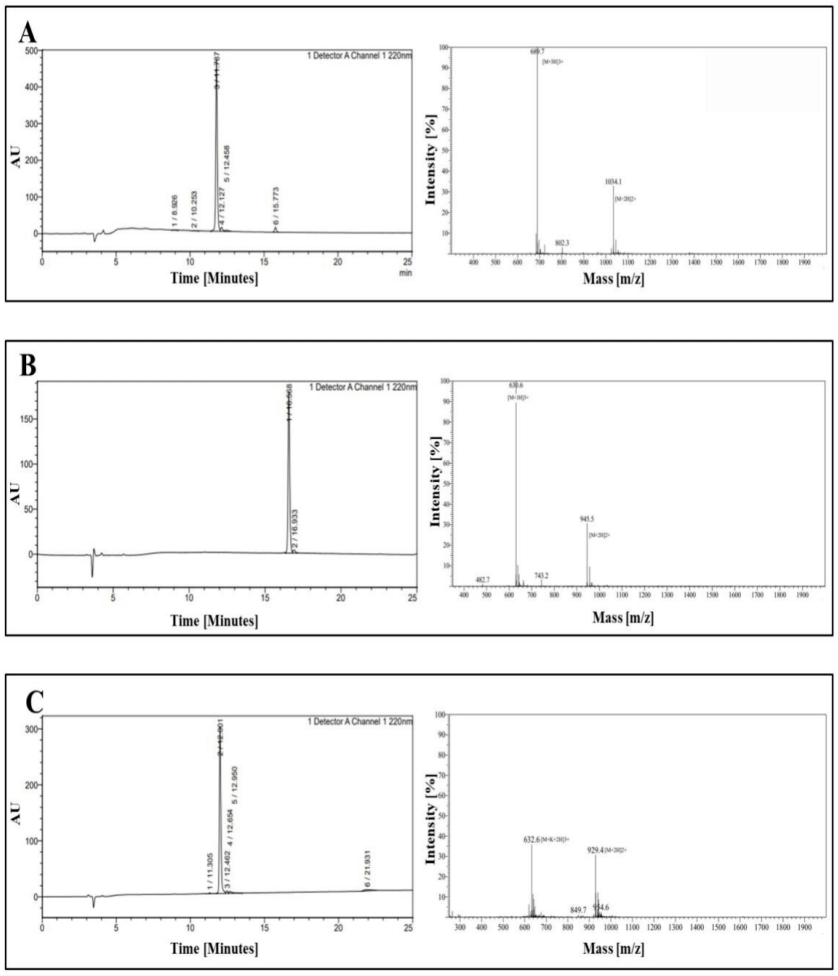

Fig. S2. HPLC chromatograms and mass spectrometry data for peptides P1–P3. The HPLC chromatograms and mass spectrometry were obtained from the certificates provided by GenScript Biotech (Netherlands). **(A)** P1, **(B)** P2, **(C)** P3

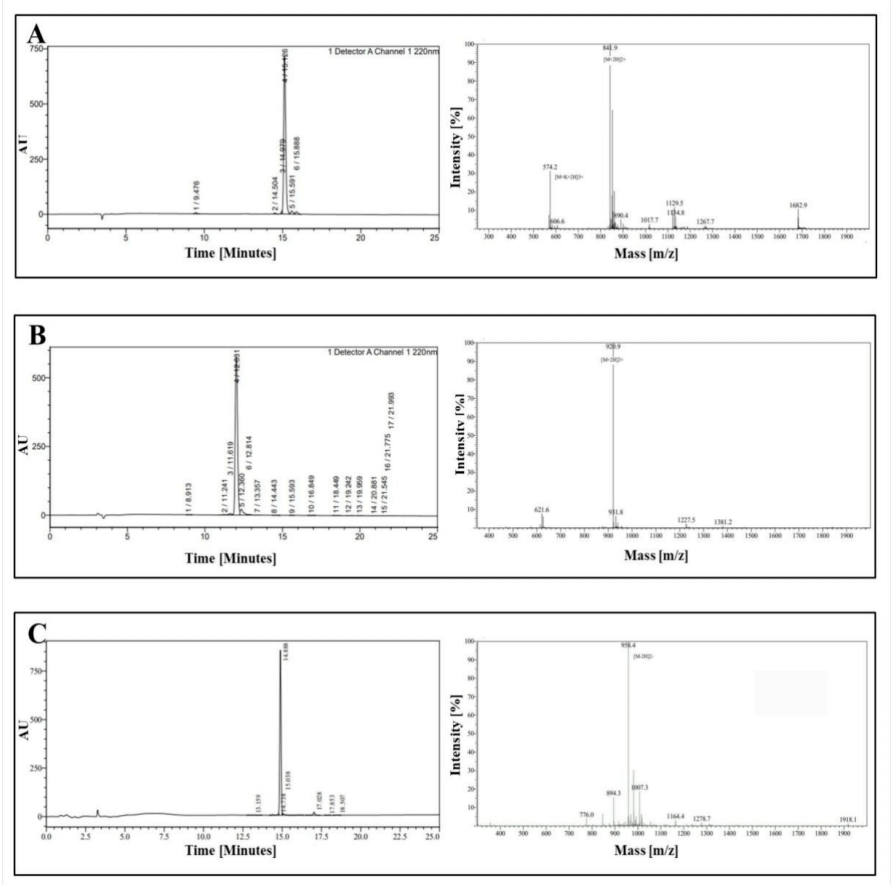

Fig. S3. HPLC chromatograms and mass spectrometry data for peptides P4–P6. The HPLC chromatograms and mass spectrometry were obtained from the certificates provided by GenScript Biotech (Netherlands). **(A)** P4, **(B)** P5, **(C)** P6.

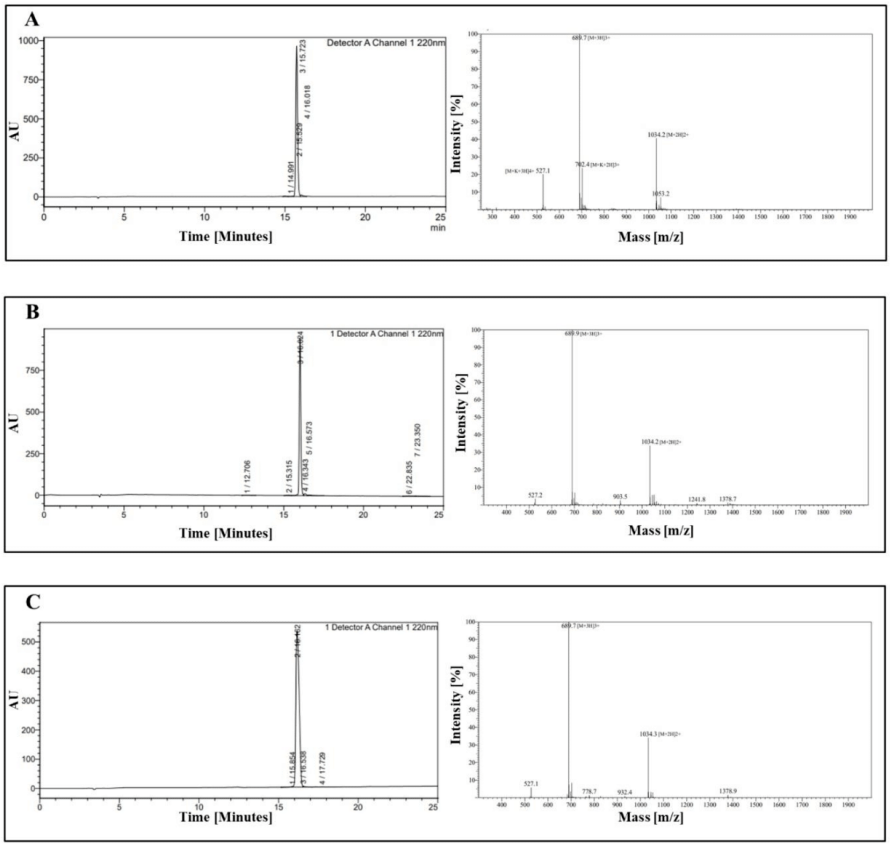

Fig. S4. HPLC chromatograms and mass spectrometry data for peptides SP1-SP3. The HPLC chromatograms and mass spectrometry were obtained from the certificates provided by GenScript Biotech (Netherlands). **(A)** SP1, **(B)** SP2, **(C)** SP3.

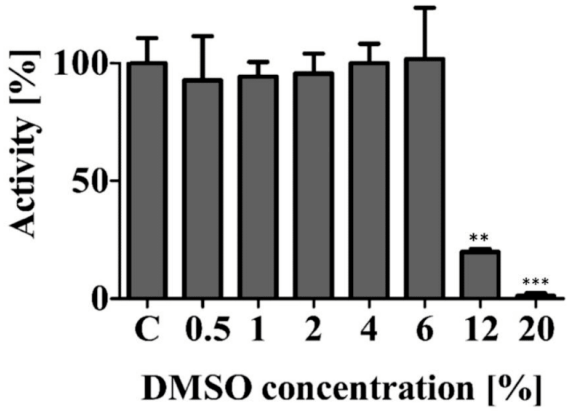

Fig. S5. Effect of DMSO on nsP2^{pro} activity. A control experiment was conducted to evaluate the impact of DMSO on protease activity at concentrations ranging up to 20%. No significant effect on protease activity was observed at concentrations up to 6%, confirming DMSO's suitability as a solvent within this range. Statistical significance was determined using one-way ANOVA, followed by Tukey's test. Asterisks indicate significant differences from the control (0 µM inhibitor). Asterisks denote statistically significant differences from the control group as determined by one-way ANOVA and Tukey's test, where $p < 0.01$ (**) and $p < 0.001$ (***). Data are presented as mean ± SD from three independent experiments (n = 3).

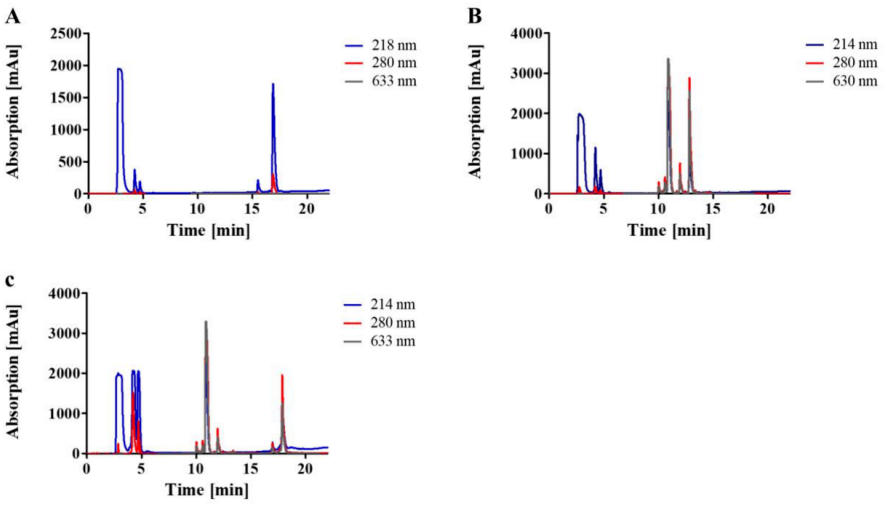

Fig. S6. R-HPLC chromatograms showing the separation profiles of the dye CF^{TM}633, peptide P1, and the labeled P1 conjugated with CF^{TM}633. (**A**) Chromatogram of peptide P1 used as a reference. **(B)** Chromatogram of the dye CF^{TM}633 used as a reference. **(C)** Chromatogram of labeled P1 conjugated with dye CF^{TM}633. The R-HPLC analysis was performed over 40 minutes, with absorption measured at three wavelengths: 214 nm, 280 nm, and 630 nm, at a temperature of 25°C.

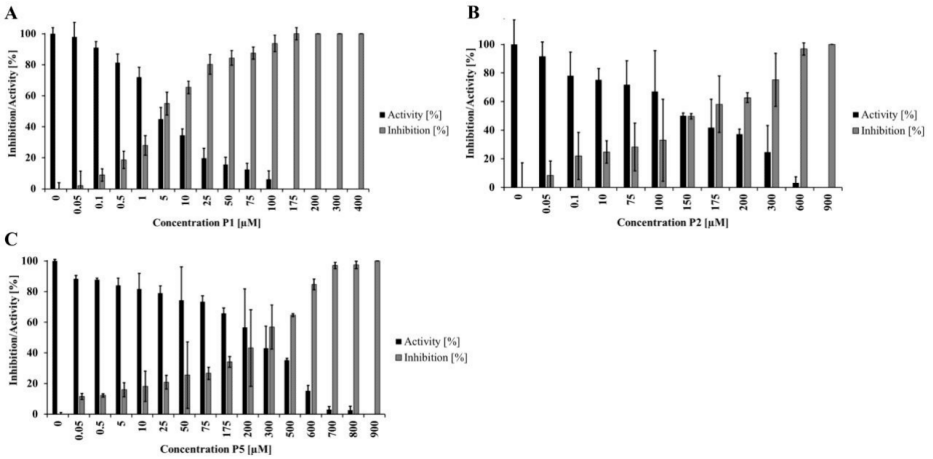

Fig. S7. Inhibitory effects of peptides (P1, P2, and P5) on CHIKV nsP2^{pro}. Panels **(A)** P1, **(B)** P2 and **(C)** P5 depict the normalized enzymatic activity and inhibition of nsP2^{pro} in the presence of L-peptides.

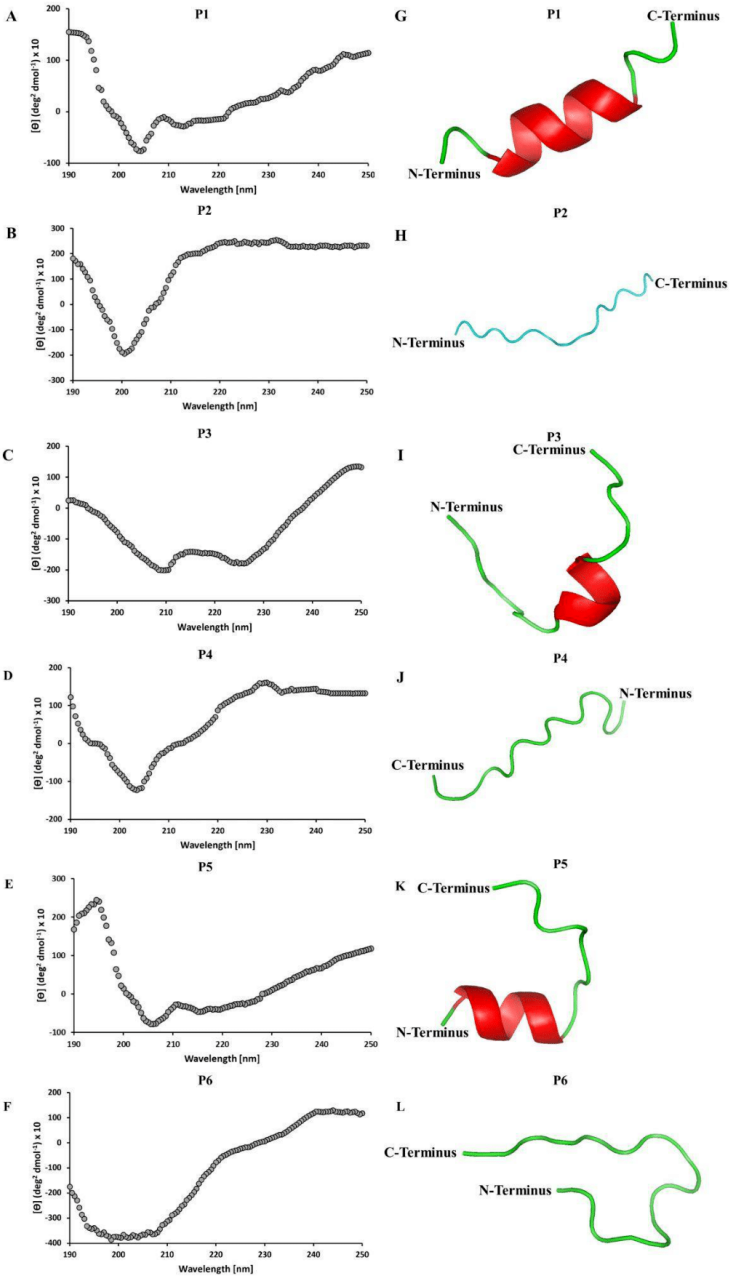

Fig. S8. Secondary structure in solution and predicted of peptides P1-P6. Panels (**A-F**) present the CD spectroscopy data for peptides P1-P6, measured at 18°C within the 190-260 nm range using a 0.1 mm pathlength cell. The peptide concentration was 500 µM in 5% DMSO. Panels **(G-L)** display the predicted structures of peptides P1-P6, generated using I-TASSER.

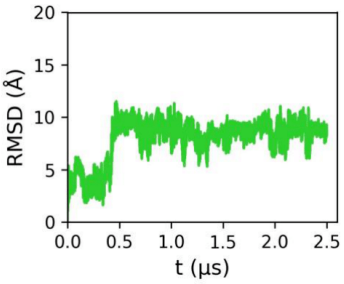

Fig. S9. Peptide RMSD plot for the extended MD simulation of CHIKV nsP2^{pro} in complex with peptide P1. The MD simulation was initiated from the Hdock docking pose and extended 1.5 μs after analysis of the 1 μs analysis of three trajectories started with different docking poses (Fig. S8). RMSD was calculated for the peptide's heavy atoms after fitting all trajectory frames onto the protein backbone in the initial structure.

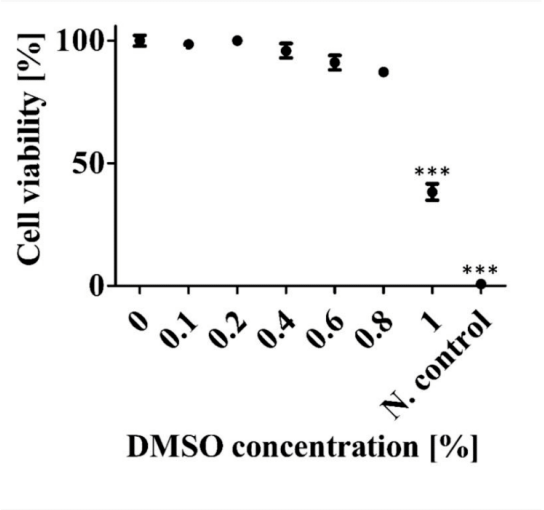

Fig. S10. Cytotoxicity effect of DMSO on Vero cells. The MTT assay was used to evaluate the effect of different concentrations of DMSO (0–1%) on cell viability. These concentrations correspond to those used in the MTT assay for peptide P1 dissolved in DMSO. The results demonstrated that DMSO exhibits cytotoxic effects at concentrations around 0.8–1%, with only approximately 38% of cells surviving at 1% DMSO. A negative control with 0.1% Triton X-100 was included in the assay. Data from MTT assays are presented with 95% confidence intervals for each group (see Supplementary Table S2). Statistical significance was determined using one-way ANOVA, followed by Tukey's test. Asterisks indicate significant differences from the control (0 µM inhibitor). Asterisks denote statistically significant differences from the control group as determined by one-way ANOVA and Tukey's test, where $p < 0.001$ (***).

Table S1. Selected peptides from phage display and scrambled peptide sequences.

Peptides	Sequence	Theoretical pI[1]	Solvent	Molecular weight (Da)
P1	VMPWDEWLTKRKPELP	6.15	DMSO	2025.40
P2	HTSRIYIPSPIHAENI	6.92	DMSO	1848.09
P3	MEASGVNYQNMNKQTT	5.75	DMSO	1815.99
P4	FTMSPPLQMPSKNY	8.59	DMSO	1640.93
P5	NAMSHVMEGSHINWDA	5.15	DMSO	1798.97
P6	YISPQYYGETWVTTIG	4.00	DMSO	1878.07
SP1	DEEVTKPLRLWPWMPK	6.18	DMSO	2025.40
SP2	TDKLEPVPLKPEWWRM	5.85	DMSO	2025.40
SP3	MEKEPVRKDTLWPPLW	5.94	DMSO	2025.40

[1] Based on Expasy ProtParam (https://web.expasy.org/protparam/)

Table S2. The **confidence intervals (CI) from the MTT assay** for three different experimental conditions: **P1 dissolved in water, P1 dissolved in DMSO, and DMSO control**

Peptides/chemical	Concentration	Lower 95% CI	Upper 95% CI
P1 dissolved in DMSO	0 [µM]	0.7966	0.8648
P1 dissolved in DMSO	10 [µM]	0.8188	0.8865
P1 dissolved in DMSO	20 [µM]	0.7684	0.8742
P1 dissolved in DMSO	40 [µM]	0.7855	0.8509
P1 dissolved in DMSO	60 [µM]	0.6626	0.8517
P1 dissolved in DMSO	80 [µM]	0.6153	0.7257
P1 dissolved in DMSO	100 [µM]	0.1889	0.4011
Negative control (Triton x 100)	0.1% [µM]	0.00004632	0.004954
P1 dissolved in Water	0 [µM]	0.7008	0.7861
P1 dissolved in Water	10 [µM]	0.7259	0.7917
P1 dissolved in Water	20 [µM]	0.7351	0.8058
P1 dissolved in Water	40 [µM]	0.7085	0.7897
P1 dissolved in Water	60 [µM]	0.6829	0.7986
P1 dissolved in Water	80 [µM]	0.6196	0.6870
P1 dissolved in Water	100 [µM]	0.5721	0.6614
Negative control (Triton x 100)	0.1 %	0.004728	0.006605313
DMSO	0 %	0.7444	0.7823
DMSO	0.1%	0.7312	0.7631
DMSO	0.2%	0.7585	0.8295
DMSO	0.4 %	0.7063	0.7581
DMSO	0.6 %	0.6410	0.7470
DMSO	0.8 %	0.6490	0.7247
DMSO	1 %	0.2436	0.5991
Negative control (Triton x 100)	0.1%	0.003463	0.007537

Table S3. Structural model generation of P1-P6 using the I-TASSER online server.

Model	C-score[1]	TM-score[2]	Secondary structure content based on Structural model	Secondary structure content based on CD-spectroscopy[3]
P1	-0.38	0.66 ± 0.13	α-Helix: 56% β-sheet: - Random coil: 44%	α-Helix: 47% β-sheet: - Random coil: 53%
P2	-1.32	0.55 ± 0.15	α-Helix: - β-sheet: - Random coil: 100%	α-Helix: 2% β-sheet: - Random coil: 98%
P3	-1.71	0.51 ± 0.15	α-Helix: 25% β-sheet: - Random coil: 75%	α-Helix: 21% β-sheet: - Random coil: 79%
P4	-1.32	0.55 ± 0.15	α-Helix: - β-sheet: - Random coil: 100%	α-Helix: 4% β-sheet: - Random coil: 96%
P5	-0.90	0.60 ± 0.14	α-Helix: 44% β-sheet: - Random coil: 56%	α-Helix: 35% β-sheet: - Random coil: 65%
P6	-1.46	0.53 ± 0.15	α-Helix: - β-sheet: - Random coil: 100%	α-Helix: 10% β-sheet: - Random coil: 90%

[1] C-score reflects the confidence level of the predicted structures. C-score is typically in the range of [-5, 2], where a C-score of higher value signifies a model with a high confidence.
[2] TM-score measures the similarity between the predicted structure and known structures from the PDB, with a score ranging from 0 to 1. A TM-score below 0.17 suggests no significant similarity, indicating that the structure was likely chosen at random.
[3] Secondary structure content was determined based on CD results. The K2D3 online tool (https://cbdm-01.zdv.uni-mainz.de/~andrade/k2d3/) was used to predict the secondary structure composition.

Table S4. MM-GBSA effective free energies calculated for the three top-ranked poses of P1 bound to CHIKV nsP2 protease.

Docking Program	ΔG_{pol}[b] (kcal/mol)	ΔG_{np}[c] (kcal/mol)	ΔG_{eff}[d] (kcal/mol)
ClusPro	34.40	-79.06	-44.66
Hdock	43.44	-106.00	-62.56
Galaxy Tongdock	35.48	-77.80	-42.32
Hdock (extended MD)	40.56	-104.53	-63.87

[a]Free energy calculations were conducted for frames collected after discarding the first 0.5 μs of each 1 μs MD simulation.
[b]Polar free energy component
[c]Nonpolar free energy component
[d]Effective free energy

3.2 Characterization of the inhibitory properties of the scorpion-derived peptide pantinin-1

Title: Inhibition of Chikungunya virus nsP2 protease *in vitro* by pantinin-1 isolated from scorpion venom

Authors: Mohammadamin Mastalipour, Mônika Aparecida Coronado, Jorge Enrique Hernández González, Dieter Willbold, Raphael Josef Eberle

Submission Date: Posted on June 29, 2025, on the bioRxiv preprint server

DOI: https://doi.org/10.1101/2025.06.29.662183

Contribution: Conceptualization, Methodology, Investigation, Formal analysis, Data curation, Writing - original draft, Writing - review & editing

Inhibition of Chikungunya virus nsP2 protease *in vitro* by pantinin-1 isolated from scorpion venom

Mohammadamin Mastalipour[1], Mônika Aparecida Coronado[1,2], Jorge Enrique Hernández González[3], Dieter Willbold[1,2], Raphael Josef Eberle[4]

[1] Institut für Physikalische Biologie, Heinrich-Heine-Universität Düsseldorf, Universitätsstraße 1, 40225 Düsseldorf, Germany

[2] Institut für Biologische Informationsprozesse, Strukturbiochemie (IBI-7), Forschungszentrum Jülich, 52425 Jülich, Germany

[3] São Paulo State University (UNESP), Institute of Biosciences, Humanities and Exact Sciences, São José do Rio Preto, Brazil

[4] Institut für Biochemische Pflanzenphysiologie, Heinrich-Heine-Universität Düsseldorf, Universitätsstraße 1, 40225 Düsseldorf, Germany

Abstract

Climate change has enhanced the spread of arboviruses such as Chikungunya virus (CHIKV). CHIKV is a re-emerging virus from the family *Togaviridae* that has spread globally, causing numerous outbreaks. The lack of antiviral therapy against CHIKV makes it a significant threat to public health. Cleavage of the viral polyprotein depends on the catalytic activity of nsP2, which is essential for viral replication. Due to this critical role, the nsP2 protease is a promising target for antiviral drug development. Animal venom-derived peptides have shown great potential against a variety of diseases, including infections, cancer, and neurodegenerative disorders. In this study, we evaluated the inhibitory effects and properties of pantinin-1, a peptide derived from the scorpion *Pandinus imperator* with broad antimicrobial activity, against CHIKV nsP2 protease. Pantinin-1 effectively inhibited CHIKV nsP2 protease, with a half-maximal inhibitory concentration (IC_{50}) of 6.4 ± 2.04 µM and complete inhibition at 175 µM. Further analysis revealed that pantinin-1 acts as a competitive inhibitor with low micromolar affinity and showed no toxicity up to 20 µM in cell culture. Lastly, using molecular docking with subsequent molecular dynamics, the protein–peptide interaction was analyzed, and the key residues involved in the interaction with the protease were predicted. These findings highlight the potential inhibitory effect of pantinin-1 as a lead candidate targeting nsP2 protease.

Keywords

Chikungunya virus nsP2 protease, Pantinin-1, Protease inhibitor

1. Introduction

Arthropod-borne viruses (arboviruses) are a significant global health threat due to their ability to cause severe illness and widespread outbreaks (Grace et al., 2022). These viruses are primarily transmitted by arthropods such as mosquitoes and ticks and include human pathogens such as dengue virus (DENV), Zika virus (ZIKV), and chikungunya virus (CHIKV), all of which are transmitted by *Aedes* mosquito species (Delrieu et al., 2023). Among these viruses, CHIKV stands out due to its rapid geographic expansion, with cases reported in more than 100 countries across Africa, Asia, the Americas, and Europe (Li et al., 2021; Vairo et al., 2019; Zhang et al., 2025). CHIKV infection causes chikungunya fever, which typically presents in two clinical phases. The acute phase is characterized by high fever, headache, rash, and severe joint pain (Imad et al., 2021). In some patients, symptoms persist into a chronic phase, characterized by ongoing arthralgia, sleep disturbances, and psychological conditions such as depression (Paixao et al., 2018; Silveira-Freitas et al., 2024). Additionally, CHIKV has been associated with neurological complications, including encephalitis and peripheral neuropathies, particularly in neonates (Das et al., 2010).

CHIKV is a single-stranded, positive-sense RNA virus belonging to the *Togaviridae* family, genus *Alphavirus* (Wang et al., 2024). Its genome encodes four non-structural proteins (nsP1–nsP4) and five structural proteins including the capsid (C), envelope protein (E1,E2) and three accessory proteins (E3, transframe protein and 6k) (Ahola & Merits, 2016; Metz & Pijlman, 2016). Among these, non-structural protein 2 (nsP2) plays a key role in viral replication. It contains an RNA helicase domain with nucleoside triphosphatase (NTPase) and RNA triphosphatase activities, as well as a C-terminal protease and methyltransferase domain (Das et al., 2014). The nsP2 protease ($nsP2^{pro}$) is a member of MEROPS clan CN, features a papain-like cysteine protease domain and is responsible for cleaving the viral polyprotein P1234 into individual functional units essential for replication (Ghoshal et al., 2024; Rausalu et al., 2016). Due to its essential enzymatic functions, $nsP2^{pro}$ is a promising target for antiviral drug development. Several studies have explored potential inhibitors of $nsP2^{pro}$ using *in silico*, *in vitro*, and biochemical approaches. These include peptide-based inhibitors such as P1 and natural products like hesperidin (Eberle et al., 2021; Mastalipour et al., 2025). However, none of these compounds have advanced beyond preclinical testing or received approval for human use. While two vaccines, VLA1553 (Schneider et al., 2023) and Vimkunya (Richardson et al., 2025), have recently been approved against CHIKV infection, vaccination is not effective for individuals who are already infected. This underscores the need for antiviral therapy.

In recent years, animal venoms from arthropods such as spiders and scorpions, as well as snakes and other venomous species have emerged as promising sources of bioactive compounds with pharmacological potential (Lyukmanova & Shenkarev, 2024). These venoms contain peptides and proteins with diverse mechanisms of action. They have been studied for applications including antimicrobial and antiviral therapies, as well as treatments for neurodegenerative diseases such as Alzheimer's and Parkinson's.(Alvarez-Fischer et al., 2013; Badari et al., 2020; Camargo et al., 2024; Zona Rubio et al., 2025). Besides the diversity and broad spectrum of venom-derived peptides, many of them exhibit advantages such as cell-penetrating properties, specificity, and resistance to enzymatic degradation (Lewis & Garcia, 2003; Rádis-Baptista, 2021). For example, a peptide from *Crotalus durissus terrificus* venom has demonstrated *in vitro* activity against amyloid-β_{42}, a key pathological hallmark of Alzheimer's disease (Camargo et al., 2024). In the context of infectious diseases, venom-derived peptides have shown broad-spectrum activity. Latarcins, derived from the spider *Lachesana tarabaevi*, have exhibited potent antibacterial and antiviral activity (Kozlov et al., 2006; Rothan et al., 2014). Likewise, the scorpion-derived peptide Mucroporin-M1 has shown virucidal activity against pathogens including SARS-CoV, measles virus, and influenza H5N1(Li et al., 2011). Additional venom-

derived compounds with antimicrobial or antiviral activity are summarized in Table 1. In addition to these known peptides, pantinin-1 has gained attention due to its potent and broad-spectrum antimicrobial properties (Zeng et al., 2013). Pantinin-1, a 14-amino acid peptide derived from the scorpion *Pandinus imperator* (Crusca et al., 2018; Zeng et al., 2013). Pantinin-1 possesses a characteristic α-helical, amphipathic structure believed to underlie its membrane-disrupting mechanism and hemolytic activity (Zeng et al., 2013) It has demonstrated antimicrobial activity against Gram-positive bacteria such as *Staphylococcus aureus* (AB 94004) and MRSA (16472), Gram-negative strains such as *Escherichia coli* (DH5α) and *Klebsiella oxytoca* (AB 2010143), as well as antifungal activity against *Candida tropicalis* (AY 91009), with a minimum inhibitory concentration (MIC) of 16 μM (Zeng et al., 2013).

Table 1. Representative proteins isolated from venom and venom-derived peptides with reported antimicrobial, antiviral, or therapeutic activity

Agent(s)	Species	Target	Reference
Captopril*	*Bothrops jararaca*	Hypertension	(Crow, 2012; Mohamed Abd El-Aziz et al., 2019)
Contortrostatin	*Agkistrodon contortrix*	Breast cancer	(Zhou et al., 2000)
Crotamine derivative peptides (CDP)	*Crotalus durissus terrificus*	amyloid-β42 (Alzheimer's disease), SARS-CoV2	(Camargo et al., 2024; Eberle et al., 2022)
Phospholipase A2		Dengue virus and Yellow fever virus	(Muller et al., 2014)
Echinhibin-1	*Echis coloratus*	Sendai virus	(Borkow & Ovadia, 1994)
Hemocoagulase*	*Bothrops atrox*	Blood coagulation	(Lodha et al., 2011)
Integrilin*	*Sistrurus miliarus barbourin*	Acute coronary syndrome	(Mohamed Abd El-Aziz et al., 2019)
Latarcin	*Lachesana tarabaevi*	Gram-positive and Gram-negative bacteria, antiviral activity against Dengue virus	(Kozlov et al., 2006; Rothan et al., 2014)
Mucroporin-M	*Lychas mucronatus*	SARS-CoV, influenza H5N1, Measles	(Li et al., 2011)

* FDA Approved

In this study, we investigated the inhibitory potential of pantinin-1 against the CHIKV nsP2 protease *in vitro*. Our findings revealed that pantinin-1 effectively inhibited $nsP2^{pro}$ activity, with an IC_{50} of 6.4 ± 2.04 μM. Further analysis showed that pantinin-1 binds at the active site as a competitive inhibitor with an equilibrium dissociation constant (K_D) of 9.29 μM. Cytotoxicity assessment using the MTT assay showed no detectable toxicity at concentrations up to 20 μM, while approximately 50% cell viability was observed at 40 μM. *In silico* studies predicted the most stable pose and interaction between the protease and pantinin-1, identifying key residues involved in binding. These results suggest that pantinin-1 has inhibitory effects within a concentration range that precedes the onset of cytotoxicity, supporting its potential as a lead compound for further development in CHIKV antiviral research.

2. Materials and methods

2.1 Protein expression and purification

Recombinant CHIKV nsP2 protease was expressed and isolated following a previously established and published protocol (Eberle et al., 2021; Mastalipour et al., 2025)

2.2 Peptide material

The peptide used in this study, pantinin-1, was supplied in solid, lyophilized form by GenScript Biotech (Rijswijk, Netherlands). It consists of 14 L-amino acids (GILGKLWEGFKSIV) and was chemically modified with an acetyl group at the N-terminus and an amide group at the C-terminus. Analytical documentation provided by the supplier confirmed that the peptide met a purity threshold exceeding 90%. Verification of peptide identity and purity was conducted by chromatographic and spectrometric methods. Reverse-phase HPLC was performed using an Inertsil ODS-0310 analytical column (dimensions: 4.6 mm × 250 mm), and molecular weight confirmation was achieved via electrospray ionization mass spectrometry (ESI-MS). The full analytical documentation supporting peptide purity and identity is shown in the Supplementary Information (Fig. S1).

2.3 Enzymatic inhibition assay of CHIKV nsP2^{pro}

The inhibitory effect of pantinin-1 on CHIKV nsP2^{pro} was assessed using a fluorescence-based enzymatic assay. This assay employed a synthetic peptide substrate labeled with DABCYL and EDANS fluorophores (DABCYL-Arg-Ala-Gly-Gly-↓Tyr-Ile-Phe-Ser-EDANS; BACHEM, Bubendorf, Switzerland), which reflects the native cleavage sequence of the CHIKV polyprotein (Eberle et al., 2021b; Hu et al., 2016). The assay was conducted in a 96-well microplate with a total volume of 100 µL per well. Each reaction mixture contained 20 mM Bis-Tris propane buffer (pH 7.5), 10 µM nsP2^{pro}, and 9 µM fluorogenic substrate. Pantinin-1 was prepared as a 10 mM stock solution in DMSO and diluted into the reaction mixture to achieve final concentrations ranging from 0 to 175 µM. Fluorescence emission, indicative of substrate cleavage, was monitored at 37 °C using a CLARIOstar plate reader (BMG Labtech, Ortenberg, Germany) with excitation and emission wavelengths set to 340 nm and 490 nm, respectively. Readings were taken at 30-second intervals for 30 minutes. Enzymatic activity in the presence of pantinin-1 was expressed as a percentage of the activity observed in untreated control samples, calculated using the equation (E1) (Eberle et al., 2021).

$$\text{Relative protease activity \%} = \frac{\text{Intensity of enzymatic activity after inhibiton}}{\text{Intensity of enzymatic activity}} \times 100$$

To determine the IC_{50} value, non-linear regression analysis was performed using GraphPad Prism (version 5). All experiments were performed as triplicates, and the results are presented as mean ± standard deviation (SD).

2.4 Inhibition mechanism analysis

To characterize how pantinin-1 interacts with the catalytic function of CHIKV nsP2^{pro}, an inhibition assay was performed using the same FRET-based platform described previously. The enzyme concentration was kept constant at 10 µM, while both substrate and inhibitor levels were systematically varied. All reactions were carried out in 20 mM Bis-Tris-Propane buffer, pH 7.5. The resulting data,

which include combinations of multiple substrate and inhibitor concentrations (Table 2), were used to evaluate the inhibition pattern using Lineweaver–Burk plot.

Table 2. Substrate and peptide concentrations used in the inhibition-mode assay.

Substrate conc. [µM]	**0**	**1**	**2.5**	**5**	**7.5**	**10**
Inhibitor conc. [µM]	0	0	0	0	0	0
	1	1	1	1	1	1
	2.5	2.5	2.5	2.5	2.5	2.5
	5	5	5	5	5	5

2.5 Biolayer interferometry (BLI)

Biolayer interferometry (BLI) was used to determine the equilibrium dissociation constant (K_D) of pantinin-1. Experiments were performed using an Octet RED96 system (Sartorius, Göttingen, Germany) with Octet AR2G biosensors (Sartorius, Göttingen, Germany). The biosensors were incubated in running buffer (20 mM Bis-Tris propane, 2% DMSO, pH 7.5) for 15 min before starting the experiment. The experiments were initiated with an equilibration step with running buffer for 600 s. Next, the sensor surface was activated with activation buffer containing 100 mM NHS and 50 mM MES, pH 5.2 (Xantec, Düsseldorf, Germany), for 420 s. The $nsP2^{pro}$ (10 µg/mL) was then immobilized onto the activated biosensor surface for 420 s in 20 mM sodium acetate, pH 5.0. The reaction was then quenched using 1 M ethanolamine-HCl, pH 8.5 (Xantec, Düsseldorf, Germany), for 300 s. Afterwards, sensors were re-equilibrated in running buffer for an additional 600 s. A six-step 1:3 serial dilution of pantinin-1 was prepared, ranging from 20 µM to 0 µM. Each sensor was exposed to pantinin-1 during an association step for 180 s, followed by a 600 s dissociation phase. After each cycle, sensors were regenerated with 20 mM glycine (pH 2.0) and equilibrated again in running buffer for 600 s. All experiments were performed in triplicate. To investigate the binding of pantinin-1 on sensors, a control experiment was performed same as described above without immobilizing the protease, with the highest concentrations of pantinin-1 at 20 µM and 6.66 µM. Data were analyzed using ForteBio Data Analysis Software 8.0 (Sartorius, Göttingen, Germany). Binding responses from three independent experiments were combined to construct a Scatchard plot, from which the dissociation constant (K_D) was determined (Kessler et al., 2008).

2.6 Cell viability assay

The cytotoxic potential of pantinin-1 was evaluated in Vero cells (African green monkey kidney epithelial cell line, *Chlorocebus aethiops*). Cells were cultured in Dulbecco's Modified Eagle Medium (DMEM) supplemented with 10% fetal calf serum (FCS) and 1% non-essential amino acids, and maintained at 37 °C in a humidified incubator with 5% CO_2. For the assay, cells were seeded in 96-well plates and treated with pantinin-1 at final concentrations ranging from 0 to 100 µM. The peptide was dissolved in DMSO with final concentration of 10 mM and subsequently diluted in complete culture medium. To establish a control for maximal cytotoxicity, 0.1% Triton X-100 was used as a positive control. After overnight incubation with the test compound, cell viability was assessed using the MTT assay (Roche Diagnostics GmbH, Mannheim, Germany). 10 µl of MTT reagent were added to each well, followed by a 4 h incubation to allow for formazan formation by metabolically active cells. Crystals were dissolved by the addition of 100 µL of solubilization solution, and the plates were incubated overnight to ensure complete dissolution. Absorbance was recorded at 570 nm and 660 nm

using a CLARIOstar plate reader (BMG Labtech, Ortenberg, Germany). Cell viability was calculated using the following equation:

$$\frac{(\text{A570} - \text{A660})\text{of treated cells}}{(\text{A570} - \text{A660})\text{of control (not treated cells)}} \times 100$$

2.7 Protein-peptide docking

An MD-derived nsP2^{pro} conformation with an open active site, reported in a previous work (Mastalipour et al., 2025), was employed here to dock the pantinin-1 peptide. The three-dimensional structure of pantinin-1 used for docking was predicted with AlphaFold3 (Abramson et al., 2024). Three docking programs, Galaxy TongDock (Park et al., 2019), ClusPro (Kozakov et al., 2017) and HDock (Yan et al., 2017), were used for this purpose with the default parameters established in their respective web servers. The best poses plus three poses exhibiting high conformational variation (i.e., large pair-wise peptide RMSD values) among the top-5 solutions determined with each docking program were selected for subsequent analyses to predict the most likely binding mode of pantinin-1 to nsP2^{pro}, as described below.

2.8 MD simulations

The selected nsP2^{pro}-pantinin-1 complexes were prepared for MD simulations with tleap of Amber22 (Case et al., 2022) as described in Mastalipour et al. (Mastalipour et al., 2025). Briefly, the peptide was capped at the N- and C-termini with ACE and NME moieties. The parameters for both the peptide and the protein were drawn from the ff19SB force field (Tian et al., 2020). Octahedral boxes were defined to simulate each system, with edges placed at least 10 Å away from the solute surface. The simulation boxes were then filled with OPC water molecules (Izadi et al., 2014) and 16 Cl- counterions were added to neutralize the solute net charge. Each system underwent energy minimization, followed by NVT heating and equilibration at the NPT ensemble to ensure a final temperature and pressure of 300 K and 1 bar, respectively. Then, the stepwise decrease of the harmonic restraints applied to the solute's heavy atoms during the equilibration phase was conducted during four NPT simulations. Finally, 1 μs productive runs were run for every complex. All the MD simulations were performed with pmemd.cuda of Amber22 (Case et al., 2022). More details on the MD simulation setup can be found elsewhere (Mastalipour et al., 2025).

2.9 MM-GBSA free energy calculations

Molecular Mechanics Generalized-Born Surface Area (MM-GBSA) calculations were performed for the three top-ranked poses of peptide P1 in complex with CHIKV nsP2^{pro} using the MMPBSA.py module of Amber22 (Case et al., 2022; Miller et al., 2012), following the protocol detailed in (Mastalipour et al., 2025). The single-trajectory approach was employed, extracting 542 frames from the final 0.5 μs of each MD trajectory. The GB-neck2 model (igb = 8) (Nguyen et al., 2013) was used to estimate polar solvation energies, with internal and external dielectric constants set to 1 and 80, respectively, and a salt concentration of 0.1 M. Per-residue free energy decomposition was also performed under the same conditions to identify key binding interface residues (Mastalipour et al., 2025).

2.10 Trajectory analyses

Trajectory analyses were conducted using the cpptraj module from Amber22 (Case et al., 20022). Root-mean-square deviation (RMSD) values were obtained via the rms command. Clustering analysis employed the cluster command with a hierarchical agglomerative algorithm, using RMSD of peptide heavy atoms as the distance metric. Typically, five clusters were generated, and the most populated cluster was selected for structural representation. Hydrogen bond analysis was performed with the hbond command, applying geometric criteria of a donor–hydrogen–acceptor angle greater than 120° and a hydrogen–acceptor distance of 3.2 Å or less to define intramolecular hydrogen bonds.

2.11 Statistical Analysis

All statistical analyses were conducted using GraphPad Prism version 5.0. Differences between treatment groups and the control were evaluated using one-way analysis of variance (ANOVA) followed by Tukey's post hoc test for multiple comparisons. Statistical significance was denoted as follows: $p < 0.05$ (*), $p < 0.01$ (**), and $p < 0.001$ (***).

3. Result

3.1. Inhibitory effect of pantinin-1 on CHIKV nsP2^{pro} activity

CHIKV nsP2^{pro} was expressed and purified as previously described (Eberle et al., 2021; Mastalipour et al., 2025). The pure protease was used to test the inhibitory potential of α-helical, amphipathic pantinin-1 (Fig. 1A) against the proteolytic activity of the CHIKV nsP2^{pro}, which was assessed using a FRET-based enzymatic assay. Enzymatic activity was determined by measuring fluorescence emission over a 30-min period at excitation and emission wavelengths of 340 and 490 nm, respectively. As shown in Fig. 1B, pantinin-1 exhibited a clear, concentration-dependent inhibitory effect on nsP2^{pro}. A reduction in enzymatic activity was observed at low micromolar concentrations, with approximately 50% inhibition at around 5 µM. This suggests that pantinin-1 is capable of efficiently interfering with nsP2^{pro} activity at relatively low concentrations. The inhibitory effect became progressively stronger with increasing peptide concentration, culminating in a complete loss of enzymatic activity at 175 µM, the highest concentration tested. To quantify the potency of pantinin-1, a dose–response curve was generated, and the IC_{50} value was calculated using non-linear regression analysis in GraphPad. As shown in Fig. 1C, the IC_{50} was determined to be 6.4 ± 2.04 µM, based on three independent replicates

3.2 Mode of inhibition of pantinin-1 toward CHIKV nsP2^{pro}

In Section 3.1, we demonstrated the inhibitory effect of pantinin-1 on the enzymatic activity of CHIKV nsP2^{pro}. To further characterize this interaction, it was essential to investigate the mechanism and mode of inhibition of pantinin-1. To this end, a FRET-based enzymatic assay was conducted using varying concentrations of both substrate and pantinin-1. The resulting data were analyzed using a Lineweaver–Burk plot, which allows assessment of how the inhibitor affects substrate binding. As shown in Fig. 1D, increasing the concentration of pantinin-1 at multiple fixed substrate concentrations led to a progressive increase in the apparent K_m constant. This pattern indicates that pantinin-1 decreasing the substrate's binding affinity to nsP2^{pro}.

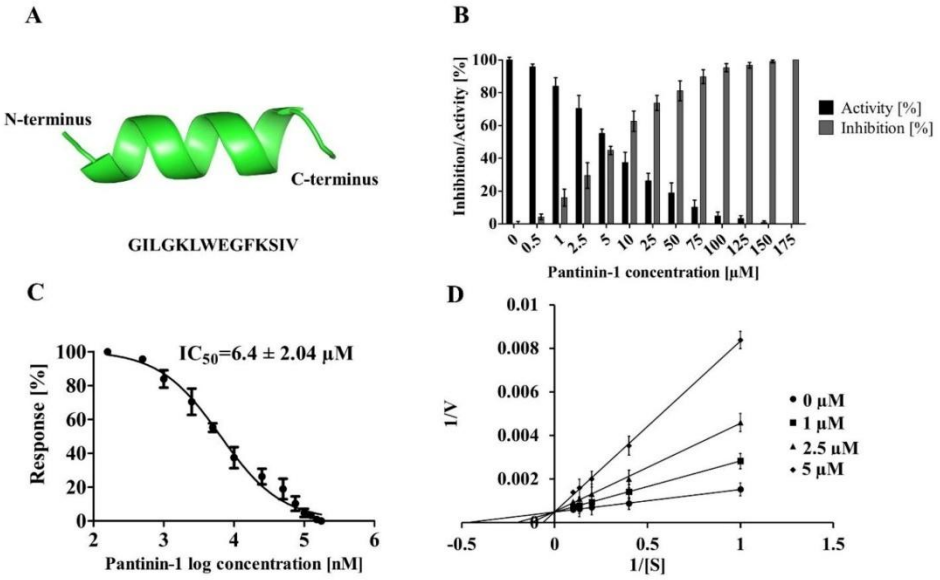

Fig. 1. Pantinin-1 structure prediction and its inhibitory activity and binding analysis of pantinin-1 toward CHIKV nsP2^{pro}. (A) The predicted structure of pantinin-1 generated by AlphaFold3 **(B)** Concentration-dependent inhibition of CHIKV nsP2^{pro} activity by pantinin-1, measured using a fluorescence-based enzymatic assay. Fluorescence was recorded over 30 min at 340/490 nm and 37 °C. Enzymatic activity was expressed as a percentage relative to the untreated control. **(C)** Dose–response curve of pantinin-1 inhibition, generated by non-linear regression analysis using GraphPad Prism. The calculated IC_{50} value was 6.4 ± 2.04 μM (mean ± SD; n = 3 technical replicates). **(D)** Kinetic evaluation of the inhibition mechanism of pantinin-1 using a Lineweaver–Burk plot. The intersection of the lines on the y-axis is characteristic of a competitive inhibition pattern, indicating that pantinin-1 competes with the substrate for binding to the enzyme's active site. This results in an apparent increase in the Michaelis constant (K_m).

3.3 Equilibrium dissociation constant measurement by biolayer interferometry (BLI)

To determine the equilibrium dissociation constant (K_D) for the interaction between pantinin-1 and CHIKV nsP2^{pro}, biolayer interferometry (BLI) was used. The experiment was performed using an Octet RED96 system (Sartorius, Göttingen, Germany) equipped with AR2G biosensors. Pantinin-1 was tested at six different concentrations, ranging from 20 μM to 0 μM. A sensor exposed only to the running buffer during the assay as the reference (0μM). All experiments were conducted at room temperature. The assay consisted of an association phase of 180 s followed by a dissociation phase of 600 s. A representative sensorgram is shown in Fig. S2A. All measurements were conducted in triplicate. From the BLI binding response data obtained across six concentrations of pantinin-1, a Scatchard plot was constructed using values extracted from ForteBio Data Analysis Software. This analysis yielded a dissociation constant (K_D) of 9.29 μM (Fig. S2B).To ensure that the observed binding was specifically between the protease and pantinin-1, a control experiment was performed in the absence of the protease using 20 μM and 6.66 μM pantinin-1. As shown in Fig. S3, no binding was observed between the sensor and the peptide, indicating that the interaction occurs specifically between the protease and pantinin-1.

3.4 Cytotoxicity assessment of pantinin-1 in Vero cells

To investigate the cytotoxic potential of pantinin-1, Vero cells were exposed to a concentration gradient (0–100 μM) of the peptide, which was initially dissolved in DMSO and subsequently diluted in cell culture medium. Cell viability was determined using the MTT assay. As illustrated in Fig. 2, pantinin-1 exhibited no detectable cytotoxicity at concentrations up to 20 μM, with viability levels comparable to untreated controls. A notable decrease in viability occurred at 40 μM, where approximately half of the cell population remained viable. Exposure to higher concentrations (60–100 μM) resulted in a progressive and substantial loss of cell viability, with near-complete cytotoxicity observed at 80 μM and above.

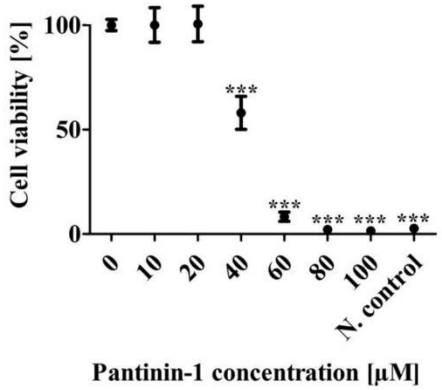

Fig. 2. Cytotoxicity of pantinin-1 in Vero cells assessed by MTT assay. Pantinin-1 was dissolved in DMSO and diluted in culture medium to final concentrations ranging from 0 to 100 μM. Vero cells were exposed to the peptide, and cell viability was assessed using the MTT assay. No cytotoxic effects were observed at concentrations up to 20 μM. At 40 μM, viability decreased to approximately 50%, and at higher concentrations, a further decline was observed, with most cells non-viable at 100 μM. 0.1% Triton X-100 was used as a negative control. Data are presented as mean ± SD from three independent experiments. Statistical significance was determined by one-way ANOVA, with $p < 0.001$ considered significant. Asterisks indicate statistically significant differences compared to untreated controls.

3.5 Prediction of the nsP2^{pro}-pantinin-1 complex structure

Protein-peptide docking was performed to predict the binding mode of pantinin-1 to nsP2^{pro}. The top-5 poses determined with the three docking algorithms chosen in this work are shown in Fig. 3. Most of the solutions point at the CHIKV nsP2^{pro} active site as the region preferentially targeted by pantinin-1. However, ClusPro and HDock also predicted alternative binding modes, with pantinin-1 interacting at the interdomain hinge region located opposite the active site (Figs. 3B-C).

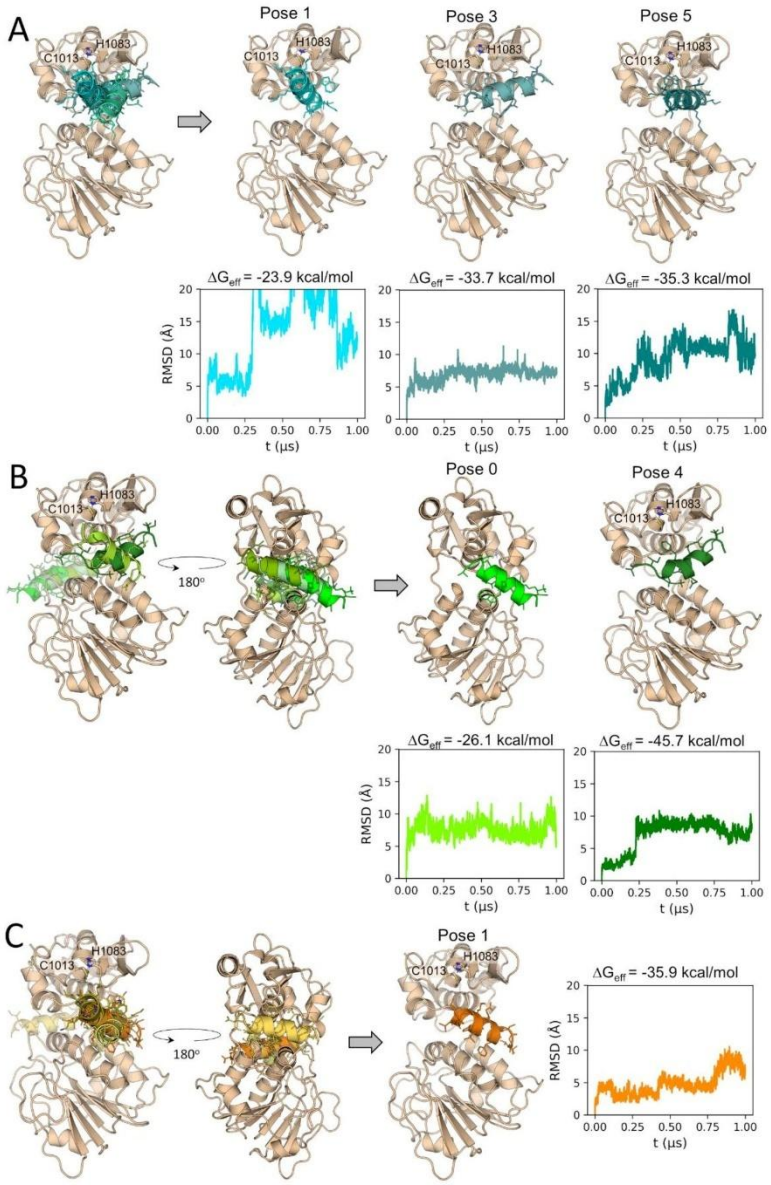

Fig. 3. Prediction of the CHIKV nsP2^{pro}-pantinin-1 complex through docking, MD simulations and free energy calculations. Superimposed five top-scoring docking poses of pantinin-1 predicted, determined with **(A)** Galaxy TongDock, **(B)** ClusPro and **(C)** HDock. Docking poses selected for MD simulations are depicted after the gray arrows. The RMSD time profiles of pantinin-1 from the simulated complexes are shown using the same colors as the corresponding peptide poses. The effective binding free energies (ΔG_{eff}) calculated from the MD simulations are shown above each RMSD graph. RMSD values were calculated for the peptide backbone atoms and with respect to the peptide's conformation in the docking pose. Prior to peptide RMSD calculations, all trajectory frames were superimposed on the nsP2^{pro} backbone in the initial conformation. The catalytic residues C1013 and H1083 are represented as sticks and labeled in the structural representation of the different CHIKV nsP2^{pro}-pantinin-1 docking poses.

As described in Materials and Methods, the best pose predicted by each docking algorithm, plus three poses selected among the top-5 poses generated by each algorithm, were chosen for subsequent analyses to determine their stability. The peptide RMSD values calculated during the MD simulations of the selected docking poses indicate that at least in three systems, i.e., Galaxy TongDock pose3, and ClusPro poses 0 and 4, that the peptide reached stable conformations, characterized by RMSD plateau regions (Fig. 3). Moreover, the calculated ΔG_{eff} values for all the simulated systems predict the conformation adopted during the second half of the MD simulation initiated from the ClusPro pose 4 as the most stable one.

The representative structure calculated for the trajectory of the most stable pose in complex with CHIKV nsP2^{pro} (ClusPro pose 4, Fig. 3B), is depicted in Fig. 4A. As can be observed, the final pantinin-1 binding mode diverges significantly from the docking pose, as also deduced by the peptide RMSD profile (Fig. 3B and 4A). At the new position, the peptide occupies an active site pocket at the interdomain region, while leaving the catalytic residues exposed. The free energy decomposition suggests a dominant contribution of hydrophobic interactions, as deduced from the nature of the most important residues at the interface (Fig. 4B). Residues L3, W7, F10, I13 and V14 of pantinin-1 are predicted as key residues for nsP2^{pro} binding. Their mutation to Ala can serve as a strategy to experimentally validate the conclusions derived from the *in silico* analyses presented here.

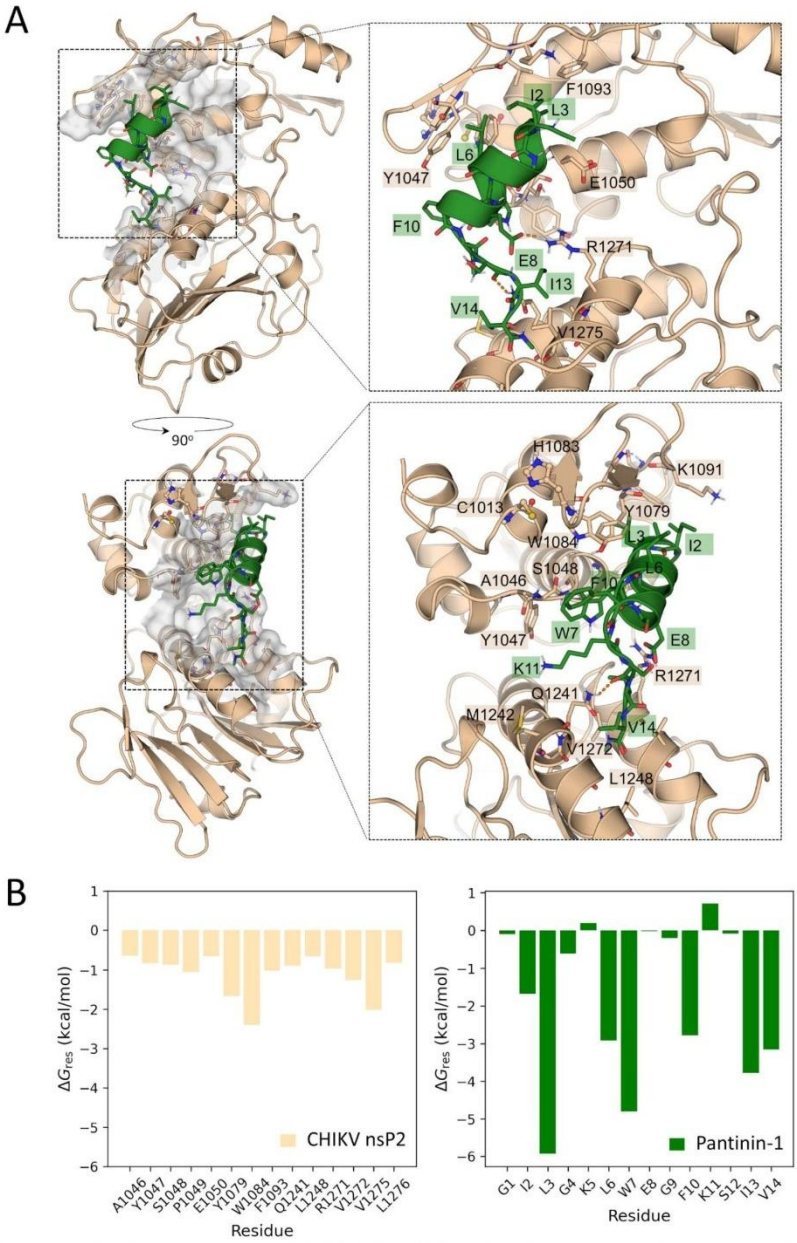

Fig. 4. Representative structure of the predicted CHIK nsP2^{pro}:pantinin-1 complex and the energy contribution of residues at the interface. (A) Two views of the CHIKV nsP2^{pro}:pantinin-1 complex. Interface residues are shown in sticks and are labeled. The active site residues C1013 and H1083 are represented as sticks and spheres. H-bonds are indicated as orange dashed lines. **(B)** Per-residue free energy contributions of the nsP2^{pro} interface residues (<0.6 kcal/mol) and of all pantinin-1 residues.

4. Discussion

Chikungunya virus (CHIKV), along with Dengue, Yellow Fever, and Zika viruses, is among the major emerging arboviruses transmitted by *Aedes* species mosquitoes and is responsible for outbreaks worldwide (Barreto-Vieira et al., 2021; Grace et al., 2022). CHIKV belongs to the genus *Alphavirus* (Delrieu et al., 2023), and its replication depends on the multifunctional non-structural protein 2 (nsP2). The C-terminal region of nsP2 contains a protease domain ($nsP2^{pro}$), which plays a crucial role in processing the viral polyprotein, an essential step in the viral life cycle (Rausalu et al., 2016). Over the years, various strategies have been explored to inhibit CHIKV $nsP2^{pro}$ as a potential antiviral target. Techniques such as phage display have been used to identify inhibitory compounds (Mastalipour et al., 2025). Although numerous candidates have been reported, none have advanced beyond the laboratory stage (Table 3).

Venom-derived peptides are new approach to develop a new therapeutic agent. These peptides have shown potential in treating a wide range of diseases, including bacterial and viral infections, cancer, and neurodegenerative disorders. For example, Phospholipase A2, isolated from the venom of *Crotalus durissus terrificus*, has shown antiviral activity against Dengue and Yellow Fever viruses (Muller et al., 2014). Ziconotide, a peptide from the marine snail *Conus magus*, is approved for chronic pain management (Deer et al., 2019; Rauck et al., 2009). Mastoparan and its synthetic analogs, derived from wasp venom, exhibit antiviral activity against Human *alphaherpesvirus 1* (HSV-1) (Vilas Boas et al., 2024). Similarly, Dermaseptins from hylid frogs have demonstrated broad-spectrum antimicrobial and anti-tumor properties (Bartels et al., 2019). Another venom-derived candidate is pantinin-1, a 14-amino-acid peptide isolated from the scorpion *Pandinus imperator*, known for its antibacterial activity (Zeng et al., 2013).

In this study, we evaluated pantinin-1 as a potential inhibitor of CHIKV $nsP2^{pro}$. A FRET-based assay was conducted using pantinin-1 at concentrations ranging from 0 to 175 µM to determine inhibition effect of the pantinin-1. As shown in Fig. 1B, increasing concentrations of pantinin-1 progressively inhibited protease activity, with complete inhibition observed at 175 µM. Dose–response analysis (Fig. 1C) revealed an IC_{50} of 6.4 ± 2.04 µM. This potency is comparable to that of other known inhibitors (Table 3) such as Peptide P1 (4.6 µM) (Mastalipour et al., 2025), Hesperetin (2.5 µM) (Eberle et al., 2021), and Hesperidin (7.1 µM) (Eberle et al., 2021), although it is higher than that of RA-0002034, which exhibited a much lower IC_{50} of 58 ± 17 nM (Merten et al., 2024).

To understand the mechanism of inhibition, we performed Lineweaver–Burk analysis using varying concentrations of both substrate and pantinin-1. The resulting plot (Fig. 1D) showed all lines intersecting at the y-axis, with increased K_m and unchanged V_{max} indicating that pantinin-1 acts as a competitive inhibitor (Kenakin, 2017). This mode of inhibition is consistent with what we previously observed for peptide P1 (Mastalipour et al., 2025). Notably, both pantinin-1 and peptide P1 share a high content of α-helical secondary structure, which we have previously suggested may play a key role in peptide binding to the $nsP2^{pro}$ active site. Next, we evaluated the binding affinity of pantinin-1 to CHIKV $nsP2^{pro}$ using biolayer interferometry (BLI). Binding responses were measured across a concentration range of 0–20 µM, and values extracted from three independent experiments were used to construct a Scatchard plot. As shown in Fig. S2B, this analysis yielded a dissociation constant (K_D) of 9.29 µM. While the binding affinity of pantinin-1) is slightly weaker than that of peptide P1 (1.39 µM) (Mastalipour et al., 2025), it is significantly stronger than that of Hesperetin (31.6 ± 2.5µM) and Hesperidin (40.7 ± 2.0 µM), as reported by Eberle et al. (Eberle et al., 2021). This difference does not necessarily indicate that pantinin-1 has superior binding, as various methods were used to determine the K_D of the inhibitors. For example, in the case of peptide P1, microscale thermophoresis was used, which underscores that this difference in affinity may lie in the different methods used.

We also assessed the cytotoxicity of pantinin-1 on Vero cells across a concentration range of 0–100 µM. Fig. 2 shows that pantinin-1 had no detectable cytotoxic effect up to 20 µM. At 40 µM, cell viability decreased to around 50%, and at 80-100 µM, most cells were non-viable. As mentioned before, pantinin-1 is an α-helical, amphipathic peptide (Zeng et al., 2013). It exhibits both antimicrobial and hemolytic activity by interacting with and disrupting cell membranes (Zeng et al., 2013). This property explains the toxicity observed in the MTT assay, where cell death occurred at higher concentrations of pantinin-1. In addition, Zeng et al. reported that the hemolytic activity of pantinin-1 begins at concentrations above 32 µM, which is consistent with the cytotoxic effects observed in this study (Zeng et al., 2013). Although cytotoxicity occurs only at concentrations above 20 µM, this still represents more than three times of the IC_{50}.

Table 3. Summary of characterized CHIKV $nsP2^{pro}$ inhibitors from prior research.

Compound	Type	IC_{50}	K_D (µM)	Inhibition Mode	Reference
Peptide P1	Peptide	4.6 ± 1.9 µM	1.39 ± 0.61	Competitive	(Mastalipour et al., 2025)
RA-0002034	Small molecule	58 ± 17 nM	N/A	Covalent (Cys binding)	(Merten et al., 2024)
Withaferin A (WFA)	Natural compund	0.51 µM (In BHK-21 cells)	64	N/A	(Sharma et al., 2024)
Hesperetin (HST)	Natural flavonoid	2.5 ± 0.4 µM	31.6 ± 2.5	Noncompetitive	(Eberle et al., 2021)
Hesperidin (HSD)	Natural flavonoid	7.1 ± 1.1 µM	40.7 ± 2.0	Noncompetitive	(Eberle et al., 2021)
Pep-I	peptidomimetic	34 µM	N/A	Noncompetitive	(Singh et al., 2018)
Pep-II	peptidomimetic	42 µM	N/A	Competitive	(Singh et al., 2018)
MBZM-N-IBT	Small Molecule	31.96	6.14 ± 0.58	Competitive	(De et al., 2022)

During the molecular docking studies with three different programs (ClusPro (Kozakov et al., 2017) HDock (Yan et al., 2017) and Galaxy TongDock (Park et al., 2019)), we were able to predict likely conformations for the protease/pantinin-1 complexes. Most of these complexes showed binding at the active site of the protease (Fig. 3A). However, two of the programs exhibited conformations among the top-5 poses in which pantinin-1 binds to a region opposite to the active site (Fig. 3B–C). Further analysis, consisting in MD simulations followed by MM-GBSA free energy calculations, led to the identification of the most stable binding mode of pantinin-1 to CHIKV $nsP2^{pro}$ (Pose 4; Fig. 3B). In the identified conformation, pantinin-1 interacts with active site residues located in both domains of the protease (Fig. 4A). The proposed binding mode is consistent with the competitive inhibition mechanism determined for this peptide.

Free energy decomposition analysis demonstrated that hydrophobic interactions are the dominant force between pantinin-1and CHIKV $nsP2^{pro}$. The lowest per-residue free energies (ΔG_{res}) correspond to L3, W7, F10, I13, and V14, indicating their important role in the interaction. However, this result needs to be confirmed, for example, by alanine substitution. Moreover, as shown in Fig. 4B, residues Y1079,

Y1047, and W1084 are involved in the interaction with Pantinin-1. These amino acids are part of the substrate-binding site subunits S2, S3, and S4, suggesting possible binding at the substrate-binding site (Narwal et al., 2018). Overall, we demonstrated that pantinin-1, in addition to its antimicrobial activity, exhibits an inhibitory effect against CHIKV nsP2^{pro} *in vitro*, with binding affinity and an IC_{50} in the low micromolar range. This makes pantinin-1 a promising candidate for antiviral therapy development

5. Conclusion and outlook

In this study, it was demonstrated that pantinin-1, a peptide derived from scorpion, has the potential to inhibit CHIKV nsP2^{pro} with an IC_{50} of 6.4 ± 2.04 μM and a binding affinity in the low micromolar range. Molecular docking analysis revealed that, in its most stable state, pantinin-1 likely binds to the substrate binding site. The inhibition mode analysis confirmed this result by showing that pantinin-1 acts as a competitive inhibitor. In addition, the cytotoxicity assay demonstrated that pantinin-1 has no toxic effect on Vero cells at concentrations up to 20 μM. However, the potential of pantinin-1 still needs to be tested in a virus cell culture model. Overall, we demonstrated that pantinin-1 could be a promising candidate for the development of antiviral therapy.

Funding

MM thanks Jürgen Manchot Stiftung for providing financial assistance and resources. JEHG thanks the Brazilian Council for Scientific and Technological Development (CNPq, 309940/2019-2 and 403193/2022-2) and the Sao Paulo Research Foundation (FAPESP, grants 2024/13327-2, 2020/08615-8 and 2024/01956-5) for providing financial support. J.E.H.G. also thanks the National Laboratory for Scientific Computing (LNCC/MCTI, Brazil) for providing HPC resources of the SDumont supercomputer, URL: http://sdumont.lncc.br.

Declaration of generative AI and AI-assisted technologies in the writing process

ChatGPT was used to check grammar and spelling in order to improve readability. After using this tool, the authors reviewed and edited the content and take full responsibility for the content of the publication. Part of the figures were created by BioRender program.

CRediT authorship contribution statement

Mohammadamin Mastalipour: Conceptualization, Methodology, Investigating, Formal analysis, Data curation, Writing – original draft, Writing – review & editing. **Mônika Aparecida Coronado:** Formal analysis, Writing – original draft, Writing – review & editing. **Jorge Enrique Hernández González:** Methodology, Formal analysis, Data curation, Writing – original draft, Writing – review & editing. **Dieter Willbold:** Resources, Writing – original draft, Writing – review & editing. **Raphael Josef Eberle:** Conceptualization, Formal analysis, Supervision, Writing – original draft, Writing – review & editing.

Declaration of competing interest

The authors declare that they have no known competing financial interests or personal relationships that could have appeared to influence the work reported in this paper.

Acknowledgements

We would like to express our sincere gratitude to Jürgen Manchot Stiftung for providing financial assistance and resources that were critical to the success of this project.

Reference

Abramson, J., Adler, J., Dunger, J., Evans, R., Green, T., Pritzel, A., Ronneberger, O., Willmore, L., Ballard, A. J., Bambrick, J., Bodenstein, S. W., Evans, D. A., Hung, C.-C., O'Neill, M., Reiman, D., Tunyasuvunakool, K., Wu, Z., Žemgulytė, A., Arvaniti, E., Jumper, J. M. (2024). Accurate structure prediction of biomolecular interactions with AlphaFold 3. *Nature*, *630*(8016), 493-500. https://doi.org/10.1038/s41586-024-07487-w

Ahola, T., & Merits, A. (2016). Functions of Chikungunya Virus Nonstructural Proteins. In C. M. Okeoma (Ed.), *Chikungunya Virus: Advances in Biology, Pathogenesis, and Treatment* (pp. 75-98). Springer International Publishing. https://doi.org/10.1007/978-3-319-42958-8_6

Alvarez-Fischer, D., Noelker, C., Vulinović, F., Grünewald, A., Chevarin, C., Klein, C., Oertel, W. H., Hirsch, E. C., Michel, P. P., & Hartmann, A. (2013). Bee Venom and Its Component Apamin as Neuroprotective Agents in a Parkinson Disease Mouse Model. *PLOS ONE*, *8*(4), e61700. https://doi.org/10.1371/journal.pone.0061700

Badari, J. C., Díaz-Roa, A., Teixeira Rocha, M. M., Mendonça, R. Z., & da Silva Junior, P. I. (2020). Patagonin-CRISP: Antimicrobial Activity and Source of Antimicrobial Molecules in Duvernoy's Gland Secretion (Philodryas patagoniensis Snake). *Front Pharmacol*, *11*, 586705. https://doi.org/10.3389/fphar.2020.586705

Barreto-Vieira, D. F., Couto-Lima, D., Jácome, F. C., Caldas, G. C., & Barth, O. M. (2021). Dengue, Yellow Fever, Zika and Chikungunya epidemic arboviruses in Brazil: ultrastructural aspects. *Mem Inst Oswaldo Cruz*, *115*, e200278. https://doi.org/10.1590/0074-02760200278

Bartels, E. J. H., Dekker, D., & Amiche, M. (2019). Dermaseptins, Multifunctional Antimicrobial Peptides: A Review of Their Pharmacology, Effectivity, Mechanism of Action, and Possible Future Directions. *Front Pharmacol*, *10*, 1421. https://doi.org/10.3389/fphar.2019.01421

Borkow, G., & Ovadia, M. (1994). Echinhibin-1--an inhibitor of Sendai virus isolated from the venom of the snake Echis coloratus. *Antiviral Res*, *23*(2), 161-176. https://doi.org/10.1016/0166-3542(94)90042-6

Camargo, L. C., Gering, I., Mastalipour, M., Kraemer-Schulien, V., Bujnicki, T., Willbold, D., Coronado, M. A., & Eberle, R. J. (2024). A Snake Venom Peptide and Its Derivatives Prevent Abeta(42) Aggregation and Eliminate Toxic Abeta(42) Aggregates In Vitro. *ACS Chem Neurosci*, *15*(14), 2600-2611. https://doi.org/10.1021/acschemneuro.4c00089

Case, D. A., Aktulga, H. M., Belfon, K., Ben-Shalom, I. Y., Berryman, J. T., Brozell, S. R., Cerutti, D. S., Cheatham, T. E., III, Cisneros, G. A., Cruzeiro, V. W. D., Darden, T. A., Duke, R. E., Giambasu, G., Gilson, M. K., Gohlke, H., Goetz, A. W., Harris, R., Izadi, S., Izmailov, S. A.,

Kasavajhala, K., & Kollman, P. A. (2022). *Amber 2022* (Amber22). University of California, San Francisco.

Crow, J. M. (2012). Venomous drugs: Captopril. *New Scientist*, *214*(2863), 35. https://doi.org/10.1016/S0262-4079(12)61171-3

Crusca, E., Basso, L. G. M., Altei, W. F., & Marchetto, R. (2018). Biophysical characterization and antitumor activity of synthetic Pantinin peptides from scorpion's venom. *Biochimica et Biophysica Acta (BBA) - Biomembranes*, *1860*(11), 2155-2165. https://doi.org/10.1016/j.bbamem.2018.08.012

Das, P. K., Merits, A., & Lulla, A. (2014). Functional Cross-talk between Distant Domains of Chikungunya Virus Non-structural Protein 2 Is Decisive for Its RNA-modulating Activity*. *Journal of Biological Chemistry*, *289*(9), 5635-5653. https://doi.org/10.1074/jbc.M113.503433

Das, T., Jaffar-Bandjee, M. C., Hoarau, J. J., Krejbich Trotot, P., Denizot, M., Lee-Pat-Yuen, G., Sahoo, R., Guiraud, P., Ramful, D., Robin, S., Alessandri, J. L., Gauzere, B. A., & Gasque, P. (2010). Chikungunya fever: CNS infection and pathologies of a re-emerging arbovirus. *Progress in Neurobiology*, *91*(2), 121-129. https://doi.org/10.1016/j.pneurobio.2009.12.006

De, S., Ghosh, S., Keshry, S. S., Mahish, C., Mohapatra, C., Guru, A., Mamidi, P., Datey, A., Pani, S. S., Vasudevan, D., Beuria, T. K., Chattopadhyay, S., Subudhi, B. B., & Chattopadhyay, S. (2022). MBZM-N-IBT, a Novel Small Molecule, Restricts Chikungunya Virus Infection by Targeting nsP2 Protease Activity In Vitro, In Vivo, and Ex Vivo. *Antimicrobial Agents and Chemotherapy*, *66*(7), e00463-00422. https://doi.org/doi:10.1128/aac.00463-22

Deer, T. R., Pope, J. E., Hanes, M. C., & McDowell, G. C. (2019). Intrathecal Therapy for Chronic Pain: A Review of Morphine and Ziconotide as Firstline Options. *Pain Med*, *20*(4), 784-798. https://doi.org/10.1093/pm/pny132

Delrieu, M., Martinet, J.-P., O'Connor, O., Viennet, E., Menkes, C., Burtet-Sarramegna, V., D. Frentiu, F., & Dupont-Rouzeyrol, M. (2023). Temperature and transmission of chikungunya, dengue, and Zika viruses: A systematic review of experimental studies on Aedes aegypti and Aedes albopictus. *Current Research in Parasitology & Vector-Borne Diseases*, *4*, 100139. https://doi.org/10.1016/j.crpvbd.2023.100139

Eberle, R. J., Gering, I., Tusche, M., Ostermann, P. N., Müller, L., Adams, O., Schaal, H., Olivier, D. S., Amaral, M. S., Arni, R. K., Willbold, D., & Coronado, M. A. (2022). Design of D-Amino Acids SARS-CoV-2 Main Protease Inhibitors Using the Cationic Peptide from Rattlesnake Venom as a Scaffold. *Pharmaceuticals (Basel)*, *15*(5). https://doi.org/10.3390/ph15050540

Eberle, R. J., Olivier, D. S., Pacca, C. C., Avilla, C. M. S., Nogueira, M. L., Amaral, M. S., Willbold, D., Arni, R. K., & Coronado, M. A. (2021). In vitro study of Hesperetin and Hesperidin as inhibitors of zika and chikungunya virus proteases. *PLoS One*, *16*(3), e0246319. https://doi.org/10.1371/journal.pone.0246319

Ghoshal, A., Asressu, K. H., Hossain, M. A., Brown, P. J., Nandakumar, M., Vala, A., Merten, E. M., Sears, J. D., Law, I., Burdick, J. E., Morales, N. L., Perveen, S., Pearce, K. H., Popov, K. I., Moorman, N. J., Heise, M. T., & Willson, T. M. (2024). Structure Activity of beta-Amidomethyl Vinyl Sulfones as Covalent Inhibitors of Chikungunya nsP2 Cysteine Protease with Antialphavirus Activity. *J Med Chem*, *67*(18), 16505-16532. https://doi.org/10.1021/acs.jmedchem.4c01346

Grace, M. P., Aisling, M. V., Luxi, Q., Nuria Sanchez, C., Julia, M. P., Enny, S. P., Ludmila, L., Amber, I. R., André Portela, S., Mauricio Lima, B., & Elizabeth, B. B. (2022). Socioeconomic risk

markers of arthropod-borne virus (arbovirus) infections: a systematic literature review and meta-analysis. *BMJ Global Health*, *7*(4), e007735. https://doi.org/10.1136/bmjgh-2021-007735

Hu, X., Compton, J. R., Leary, D. H., Olson, M. A., Lee, M. S., Cheung, J., Ye, W., Ferrer, M., Southall, N., Jadhav, A., Morazzani, E. M., Glass, P. J., Marugan, J., & Legler, P. M. (2016). Kinetic, Mutational, and Structural Studies of the Venezuelan Equine Encephalitis Virus Nonstructural Protein 2 Cysteine Protease. *Biochemistry*, *55*(21), 3007-3019. https://doi.org/10.1021/acs.biochem.5b00992

Imad, H. A., Phadungsombat, J., Nakayama, E. E., Suzuki, K., Ibrahim, A. M., Afaa, A., Azeema, A., Nazfa, A., Yazfa, A., Ahmed, A., Saeed, A., Waheed, A., Shareef, F., Islam, M. M., Anees, S. M., Saleem, S., Aroosha, A., Afzal, I., Leaungwutiwong, P., & Shioda, T. (2021). Clinical Features of Acute Chikungunya Virus Infection in Children and Adults during an Outbreak in the Maldives. *The American Journal of Tropical Medicine and Hygiene*, *105*(4), 946-954. https://doi.org/10.4269/ajtmh.21-0189

Izadi, S., Anandakrishnan, R., & Onufriev, A. V. (2014). Building Water Models: A Different Approach. *The Journal of Physical Chemistry Letters*, *5*(21), 3863-3871. https://doi.org/10.1021/jz501780a

Kenakin, T. P. (2017). Chapter 6 - Enzymes as Drug Targets. In T. P. Kenakin (Ed.), *Pharmacology in Drug Discovery and Development (Second Edition)* (pp. 131-156). Academic Press. https://doi.org/10.1016/B978-0-12-803752-2.00006-5

Kessler, M., Suzuki, E., Montgomery, K., & Arai, A. C. (2008). Physiological significance of high- and low-affinity agonist binding to neuronal and recombinant AMPA receptors. *Neurochem Int*, *52*(8), 1383-1393. https://doi.org/10.1016/j.neuint.2008.02.009

Kozakov, D., Hall, D. R., Xia, B., Porter, K. A., Padhorny, D., Yueh, C., Beglov, D., & Vajda, S. (2017). The ClusPro web server for protein-protein docking. *Nat Protoc*, *12*(2), 255-278. https://doi.org/10.1038/nprot.2016.169

Kozlov, S. A., Vassilevski, A. A., Feofanov, A. V., Surovoy, A. Y., Karpunin, D. V., & Grishin, E. V. (2006). Latarcins, Antimicrobial and Cytolytic Peptides from the Venom of the Spider Lachesana tarabaevi (Zodariidae) That Exemplify Biomolecular Diversity*. *Journal of Biological Chemistry*, *281*(30), 20983-20992. https://doi.org/https://doi.org/10.1074/jbc.M602168200

Lewis, R. J., & Garcia, M. L. (2003). Therapeutic potential of venom peptides. *Nature Reviews Drug Discovery*, *2*(10), 790-802. https://doi.org/10.1038/nrd1197

Li, Q., Zhao, Z., Zhou, D., Chen, Y., Hong, W., Cao, L., Yang, J., Zhang, Y., Shi, W., Cao, Z., Wu, Y., Yan, H., & Li, W. (2011). Virucidal activity of a scorpion venom peptide variant mucroporin-M1 against measles, SARS-CoV and influenza H5N1 viruses. *Peptides*, *32*(7), 1518-1525. https://doi.org/10.1016/j.peptides.2011.05.015

Li, Z., Wang, J., Cheng, X., Hu, H., Guo, C., Huang, J., Chen, Z., & Lu, J. (2021). The worldwide seroprevalence of DENV, CHIKV and ZIKV infection: A systematic review and meta-analysis. *PLOS Neglected Tropical Diseases*, *15*(4), e0009337. https://doi.org/10.1371/journal.pntd.0009337

Lodha, A., Kamaluddeen, M., Akierman, A., & Amin, H. (2011). Role of Hemocoagulase in Pulmonary Hemorrhage in Preterm Infants: A Systematic Review. *The Indian Journal of Pediatrics*, *78*(7), 838-844. https://doi.org/10.1007/s12098-010-0326-4

Lyukmanova, E. N., & Shenkarev, Z. O. (2024). Toxins from Animal Venom—A Rich Source of Active Compounds with High Pharmacological Potential. *Toxins*, *16*(12), 512. https://doi.org/10.3390/toxins16120512

Mastalipour, M., Gering, I., Coronado, M. A., González, J. E. H., Willbold, D., & Eberle, R. J. (2025). Novel peptide inhibitor for the Chikungunya virus nsP2 protease: Identification and characterization. *Current Research in Microbial Sciences*, *8*, 100376. https://doi.org/10.1016/j.crmicr.2025.100376

Merten, E. M., Sears, J. D., Leisner, T. M., Hardy, P. B., Ghoshal, A., Hossain, M. A., Asressu, K. H., Brown, P. J., Tse, E. G., Stashko, M. A., Li, K., Norris-Drouin, J. L., Herring, L. E., Mordant, A. L., Webb, T. S., Mills, C. A., Barker, N. K., Streblow, Z. J., Perveen, S., & Pearce, K. H. (2024). Identification of a cell-active chikungunya virus nsP2 protease inhibitor using a covalent fragment-based screening approach. *Proc Natl Acad Sci U S A*, *121*(42), e2409166121. https://doi.org/10.1073/pnas.2409166121

Metz, S. W., & Pijlman, G. P. (2016). Function of Chikungunya Virus Structural Proteins. In C. M. Okeoma (Ed.), *Chikungunya Virus: Advances in Biology, Pathogenesis, and Treatment* (pp. 63-74). Springer International Publishing. https://doi.org/10.1007/978-3-319-42958-8_5

Miller, B. R., III, McGee, T. D., Jr., Swails, J. M., Homeyer, N., Gohlke, H., & Roitberg, A. E. (2012). MMPBSA.py: An Efficient Program for End-State Free Energy Calculations. *Journal of Chemical Theory and Computation*, *8*(9), 3314-3321. https://doi.org/10.1021/ct300418h

Mohamed Abd El-Aziz, T., Garcia Soares, A., & Stockand, J. D. (2019). Snake Venoms in Drug Discovery: Valuable Therapeutic Tools for Life Saving. *Toxins (Basel)*, *11*(10). https://doi.org/10.3390/toxins11100564

Muller, V. D., Soares, R. O., dos Santos-Junior, N. N., Trabuco, A. C., Cintra, A. C., Figueiredo, L. T., Caliri, A., Sampaio, S. V., & Aquino, V. H. (2014). Phospholipase A2 Isolated from the Venom of Crotalus durissus terrificus Inactivates Dengue virus and Other Enveloped Viruses by Disrupting the Viral Envelope. *PLOS ONE*, *9*(11), e112351. https://doi.org/10.1371/journal.pone.0112351

Narwal, M., Singh, H., Pratap, S., Malik, A., Kuhn, R. J., Kumar, P., & Tomar, S. (2018). Crystal structure of chikungunya virus nsP2 cysteine protease reveals a putative flexible loop blocking its active site. *International Journal of Biological Macromolecules*, *116*, 451-462. https://doi.org/10.1016/j.ijbiomac.2018.05.007

Nguyen, H., Roe, D. R., & Simmerling, C. (2013). Improved Generalized Born Solvent Model Parameters for Protein Simulations. *J Chem Theory Comput*, *9*(4), 2020-2034. https://doi.org/10.1021/ct3010485

Paixao, E. S., Rodrigues, L. C., Costa, M. D. N., Itaparica, M., Barreto, F., Gérardin, P., & Teixeira, M. G. (2018). Chikungunya chronic disease: a systematic review and meta-analysis. *Transactions of the Royal Society of Tropical Medicine and Hygiene*, *112*(7), 301-316. https://doi.org/10.1093/trstmh/try063

Park, T., Baek, M., Lee, H., & Seok, C. (2019). GalaxyTongDock: Symmetric and asymmetric ab initio protein-protein docking web server with improved energy parameters. *J Comput Chem*, *40*(27), 2413-2417. https://doi.org/10.1002/jcc.25874

Rádis-Baptista, G. (2021). Cell-Penetrating Peptides Derived from Animal Venoms and Toxins. *Toxins (Basel)*, *13*(2). https://doi.org/10.3390/toxins13020147

Rauck, R. L., Wallace, M. S., Burton, A. W., Kapural, L., & North, J. M. (2009). Intrathecal Ziconotide for Neuropathic Pain: A Review. *Pain Practice*, *9*(5), 327-337. https://doi.org/10.1111/j.1533-2500.2009.00303.x

Rausalu, K., Utt, A., Quirin, T., Varghese, F. S., Žusinaite, E., Das, P. K., Ahola, T., & Merits, A. (2016). Chikungunya virus infectivity, RNA replication and non-structural polyprotein processing depend on the nsP2 protease's active site cysteine residue. *Scientific Reports*, *6*(1), 37124. https://doi.org/10.1038/srep37124

Richardson, J. S., Anderson, D. M., Mendy, J., Tindale, L. C., Muhammad, S., Loreth, T., Tredo, S. R., Warfield, K. L., Ramanathan, R., Caso, J. T., Jenkins, V. A., Ajiboye, P., & Bedell, L. (2025). Chikungunya virus virus-like particle vaccine safety and immunogenicity in adolescents and adults in the USA: a phase 3, randomised, double-blind, placebo-controlled trial. *The Lancet*, *405*(10487), 1343-1352. https://doi.org/10.1016/S0140-6736(25)00345-9

Rothan, H. A., Bahrani, H., Rahman, N. A., & Yusof, R. (2014). Identification of natural antimicrobial agents to treat dengue infection: In vitro analysis of latarcin peptide activity against dengue virus. *BMC Microbiology*, *14*(1), 140. https://doi.org/10.1186/1471-2180-14-140

Schneider, M., Narciso-Abraham, M., Hadl, S., McMahon, R., Toepfer, S., Fuchs, U., Hochreiter, R., Bitzer, A., Kosulin, K., Larcher-Senn, J., Mader, R., Dubischar, K., Zoihsl, O., Jaramillo, J. C., Eder-Lingelbach, S., Buerger, V., & Wressnigg, N. (2023). Safety and immunogenicity of a single-shot live-attenuated chikungunya vaccine: a double-blind, multicentre, randomised, placebo-controlled, phase 3 trial. *Lancet*, *401*(10394), 2138-2147. https://doi.org/10.1016/s0140-6736(23)00641-4

Sharma, K. B., Subramani, C., Ganesh, K., Sharma, A., Basu, B., Balyan, S., Sharma, G., Ka, S., Deb, A., Srivastava, M., Chugh, S., Sehrawat, S., Bharadwaj, K., Rout, A., Sahoo, P. K., Saurav, S., Motiani, R. K., Singh, R., Jain, D., & Vrati, S. (2024). Withaferin A inhibits Chikungunya virus nsP2 protease and shows antiviral activity in the cell culture and mouse model of virus infection. *PLoS Pathog*, *20*(12), e1012816. https://doi.org/10.1371/journal.ppat.1012816

Silveira-Freitas, J. E. P., Campagnolo, M. L., Dos Santos Cortez, M., de Melo, F. F., Zarpelon-Schutz, A. C., & Teixeira, K. N. (2024). Long chikungunya? An overview to immunopathology of persistent arthralgia. (2220-3249 (Print)). https://doi.org/10.5501/wjv.v13.i2.89985

Singh, H., Mudgal, R., Narwal, M., Kaur, R., Singh, V. A., Malik, A., Chaudhary, M., & Tomar, S. (2018). Chikungunya virus inhibition by peptidomimetic inhibitors targeting virus-specific cysteine protease. *Biochimie*, *149*, 51-61. https://doi.org/10.1016/j.biochi.2018.04.004

Tian, C., Kasavajhala, K., Belfon, K. A. A., Raguette, L., Huang, H., Migues, A. N., Bickel, J., Wang, Y., Pincay, J., Wu, Q., & Simmerling, C. (2020). ff19SB: Amino-Acid-Specific Protein Backbone Parameters Trained against Quantum Mechanics Energy Surfaces in Solution. *J Chem Theory Comput*, *16*(1), 528-552. https://doi.org/10.1021/acs.jctc.9b00591

Vairo, F., Haider, N., Kock, R., Ntoumi, F., Ippolito, G., & Zumla, A. (2019). Chikungunya: Epidemiology, Pathogenesis, Clinical Features, Management, and Prevention. *Infectious Disease Clinics of North America*, *33*(4), 1003-1025. https://doi.org/10.1016/j.idc.2019.08.006

Vilas Boas, L. C. P., Buccini, D. F., Berlanda, R. L. A., Santos, B. P. O., Maximiano, M. R., Lião, L. M., Gonçalves, S., Santos, N. C., & Franco, O. L. (2024). Antiviral Activities of Mastoparan-L-Derived Peptides against Human Alphaherpesvirus 1. *Viruses*, *16*(6). https://doi.org/10.3390/v16060948

Wang, M., Wang, L., Leng, P., Guo, J., & Zhou, H. (2024). Drugs targeting structural and nonstructural proteins of the chikungunya virus: A review. *International Journal of Biological Macromolecules*, *262*, 129949. https://doi.org/10.1016/j.ijbiomac.2024.129949

Yan, Y., Zhang, D., Zhou, P., Li, B., & Huang, S. Y. (2017). HDOCK: a web server for protein-protein and protein-DNA/RNA docking based on a hybrid strategy. *Nucleic Acids Res*, *45*(W1), W365-w373. https://doi.org/10.1093/nar/gkx407

Zeng, X.-C., Zhou, L., Shi, W., Luo, X., Zhang, L., Nie, Y., Wang, J., Wu, S., Cao, B., & Cao, H. (2013). Three new antimicrobial peptides from the scorpion Pandinus imperator. *Peptides*, *45*, 28-34. https://doi.org/10.1016/j.peptides.2013.03.026

Zhang, D., Qiu, Z., Hao, Y., Yuan, Y., Ma, W., Li, N., & Xiao, P. (2025). Progress in the molecular epidemiology of chikungunya virus. *Animals and Zoonoses*. https://doi.org/10.1016/j.azn.2025.01.003

Zhou, Q., Sherwin, R. P., Parrish, C., Richters, V., Groshen, S. G., Tsao-Wei, D., & Markland, F. S. (2000). Contortrostatin, a dimeric disintegrin from Agkistrodon contortrix contortrix, inhibits breast cancer progression. *Breast Cancer Res Treat*, *61*(3), 249-260. https://doi.org/10.1023/a:1006457903545

Zona Rubio, D. C., Aragón, D. M., & Almeida Alves, I. (2025). Innovations in Snake Venom-Derived Therapeutics: A Systematic Review of Global Patents and Their Pharmacological Applications. *Toxins*, *17*(3), 136. https://doi.org/10.3390/toxins17030136

Inhibition of Chikungunya virus nsP2 protease *in vitro* by pantinin-1 isolated from scorpion venom

Mohammadamin Mastalipour[1], Mônika Aparecida Coronado[1,2], Jorge Enrique Hernández González[3], Dieter Willbold[1,2], Raphael Josef Eberle[4]

[1] Institut für Physikalische Biologie, Heinrich-Heine-Universität Düsseldorf, Universitätsstraße 1, 40225 Düsseldorf, Germany

[2] Institut für Biologische Informationsprozesse, Strukturbiochemie (IBI-7), Forschungszentrum Jülich, 52425 Jülich, Germany

[3] São Paulo State University (UNESP), Institute of Biosciences, Humanities and Exact Sciences, São José do Rio Preto, Brazil

[4] Institut für Biochemische Pflanzenphysiologie, Heinrich-Heine-Universität Düsseldorf, Universitätsstraße 1, 40225 Düsseldorf, Germany

Table of content

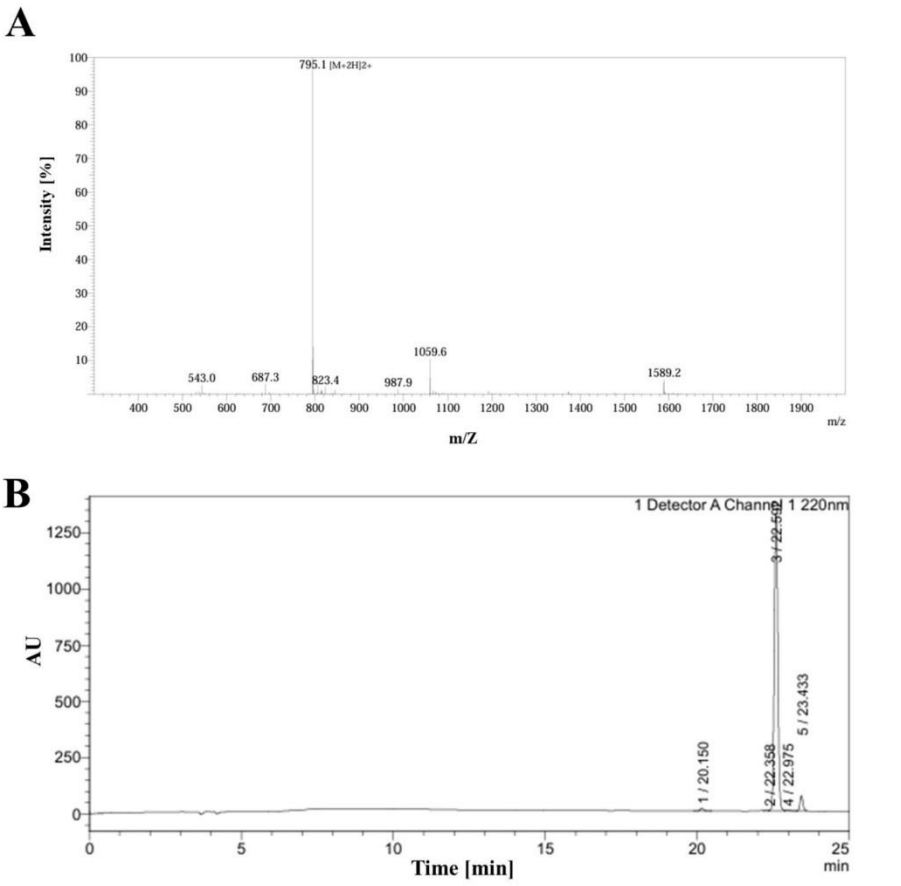

Fig. S1. HPLC chromatograms and mass spectrometry data of pantinin-1. (A) Mass spectrometry data provided by GenScript Biotech (Netherlands) confirming the molecular weight and purity of the synthesized Pantinin-1 peptide. **(B)** HPLC chromatogram showing the retention time and purity profile of pantinin-1.

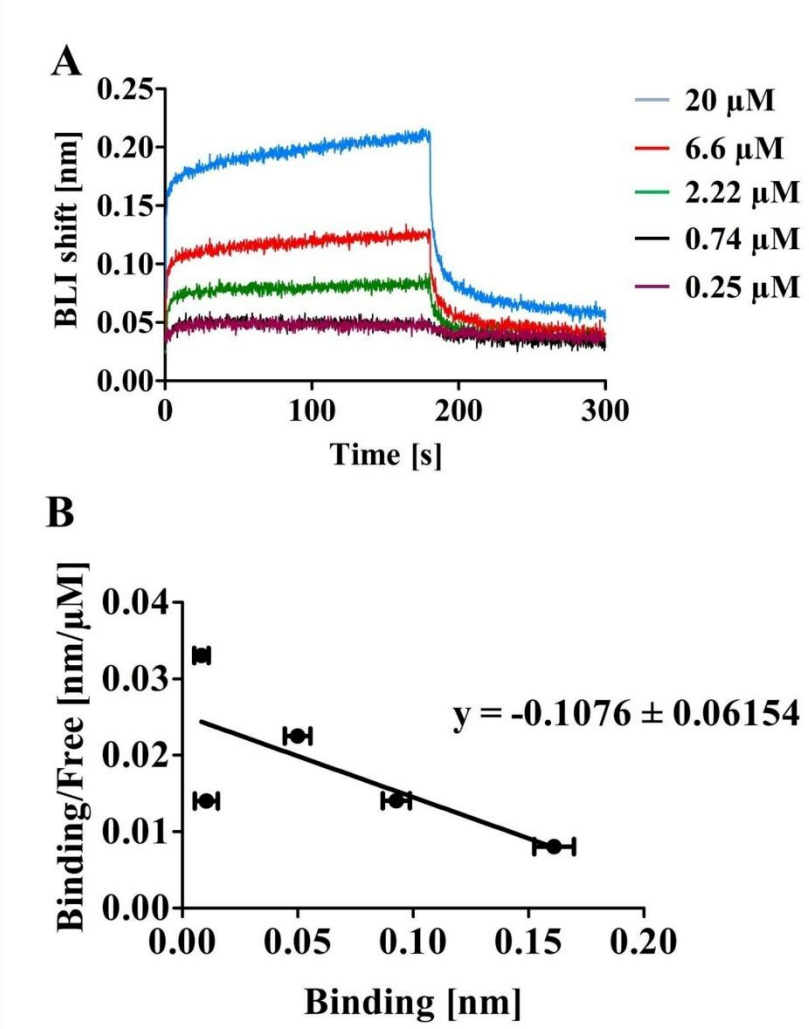

Fig. S2. Fig. S2. Representative BLI sensorgram and Scatchard plot analysis of pantinin-1 binding to immobilized CHIKV nsP2^{pro}. (A) Measurement performed using Octet AR2G biosensors. Pantinin-1 was tested at six concentrations (0–20 µM). The sensorgram includes a 180-second association phase followed by a 600-second dissociation phase at room temperature.**(B)** Scatchard plot of pantinin-1 binding to CHIKV nsP2^{pro} based on BLI response data. Binding values at five concentrations were extracted from sensorgrams and plotted as Bound/Free versus Bound. The dissociation constant (K_D) was calculated from the slope of the linear regression using the equation (K_D) = –1/slope (Kessler et al., 2008), yielding a (K_D) of 9.29 µM.

Kessler, M., Suzuki, E., Montgomery, K., & Arai, A. C. (2008). Physiological significance of high- and low-affinity agonist binding to neuronal and recombinant AMPA receptors. *Neurochem Int*, 52(8), 1383-1393. https://doi.org/10.1016/j.neuint.2008.02.00

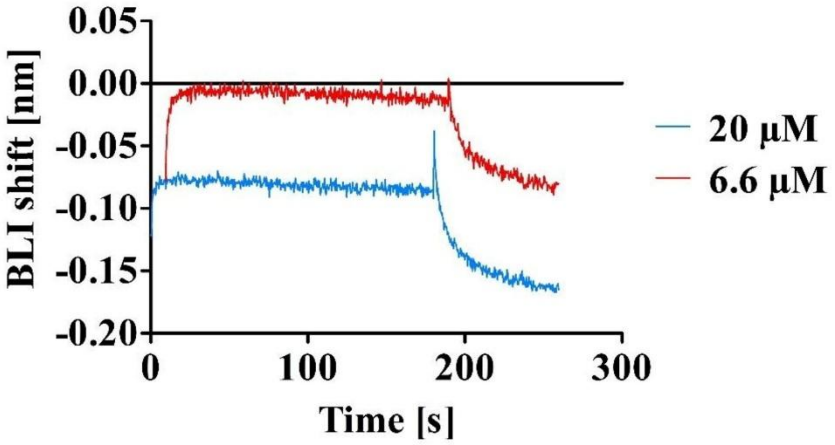

Fig. S3. Representative BLI sensorgram showing the control experiment for nonspecific binding of pantinin-1. Measurements were performed using Octet AR2G biosensors without immobilized CHIKV nsP2^{pro} to assess non-specific interaction with the sensor surface. Pantinin-1 was tested at two concentrations (20 µM and 6.66 µM). Each sensorgram includes a 180-second association phase and a 600-second dissociation phase at room temperature. No measurable binding response was detected at either concentration, indicating that pantinin-1 does not interact with the biosensor surface in the absence of the target protein.

3.3 Effect of nucleic acids on CHIKV nsP2 protease activity

Title: Single-Stranded nucleic acid binding enhances the *in vitro* catalytic activity of Chikungunya virus nsP2 protease

Authors: Mohammadamin Mastalipour, Mônika Aparecida Coronado, Ruth Anasthasia Siahaan, Alissa Drees, Christian Ahlers, Markus Fischer, Dieter Willbold, Raphael Josef Eberle

Submission Date: Posted on May 13, 2025, on the bioRxiv preprint server. Submitted to *PLOS ONE* on May 22, 2025.

DOI: https://doi.org/10.1101/2025.05.13.653680

Contribution: Conceptualization, Methodology, Investigation, Formal analysis, Data curation, Writing - original draft, Writing - review & editing

Single-Stranded nucleic acid binding enhances the *in vitro* catalytic activity of Chikungunya virus nsP2 protease

Mohammadamin Mastalipour[1], Mônika Aparecida Coronado[1,2], Ruth Anasthasia Siahaan[3], Alissa Drees[4], Christian Ahlers[4], Markus Fischer[4], Dieter Willbold[1,2], Raphael Josef Eberle[5]

[1] Institut für Physikalische Biologie, Heinrich-Heine-Universität Düsseldorf, Universitätsstraße 1, 40225 Düsseldorf, Germany

[2] Institut für Biologische Informationsprozesse, Strukturbiochemie (IBI-7), Forschungszentrum Jülich, 52425 Jülich, Germany

[3] Faculty of Chemistry and Biotechnology, FH Aachen, Campus Jülich, 52428 Jülich, Germany

[4]Hamburg School of Food Science, Institute of Food Chemistry, University of Hamburg, Grindelallee 117, 20146 Hamburg, Germany

[5] Institut für Biochemische Pflanzenphysiologie, Heinrich-Heine-Universität Düsseldorf, Universitätsstraße 1, 40225 Düsseldorf, Germany

Abstract

Chikungunya virus (CHIKV) is an emerging arbovirus whose replication relies on the multifunctional nonstructural protein 2 (nsP2), particularly its viral protease (nsP2^{pro}), which is essential for polyprotein processing. In this study, we investigated how interactions with nucleic acids influence nsP2^{pro} activity. Using high-throughput sequencing–fluorescent ligand interaction profiling, we identified specific single-stranded DNA aptamers that enhanced nsP2^{pro} activity. Additionally, both random single-stranded DNA and single-stranded RNA were found to stimulate protease activity, whereas double-stranded DNA showed no such effect. Circular dichroism spectroscopy and secondary structure predictions confirmed that the identified aptamers adopt stable folded conformations. Similarly, structured RNA sequences were also capable of promoting protease activity. The observed stimulatory effect depended on the nucleic acid strand type, length, and buffer conditions, suggesting the involvement of electrostatic interactions. Molecular docking analyses further let us assume that these nucleic acids interact specifically with the nsP2^{pro} methyltransferase domain. Our findings provide novel insights into the regulation of nsP2^{pro}, enhancing our understanding of CHIKV replication mechanisms, and may guide future antiviral development strategies.

Keywords

Chikungunya virus; nsP2 protease (nsP2^{pro}); single-stranded nucleic acid; protein–nucleic acid interaction; aptamers; viral replication

1. Introduction

Changes in climate and environmental conditions, including rising temperatures, create favorable environments for the proliferation and spread of vectors such as mosquitoes (Pavia et al., 2025). This, in turn, facilitates the transmission of arthropod-borne viruses to areas where they were previously not endemic, including Chikungunya virus (CHIKV), Dengue virus (DENV), and other tropical infections (Chitre et al., 2024). Chikungunya, a member of the *Alphavirus* genus within the *Togaviridae* family (Alissa, Alsuwat, & Alzahrani, 2024; C. K. Martin et al., 2025), has caused outbreaks across Asia, and South and Central Africa, infected over 3 million people worldwide (Zhang et al., 2025). Approximately 39% of the world's population lives in endemic regions and remains at risk of infection. (Maneerattanasak et al., 2024). CHIKV can cause a variety of clinical symptoms, including high fever, joint pain, skin rash, and arthralgia, as well as complications such as cardiac and neurological issues (de Souza et al., 2024; Sagar et al., 2024). The infection can progress to a chronic phase characterized by persistent pain and joint inflammation (Silveira-Freitas et al., 2024). Patients in this phase may also experience depression, memory loss, and sleep disturbances (Silveira-Freitas et al., 2024; van Aalst, Nelen, Goorhuis, Stijnis, & Grobusch, 2017), which contribute to disability and significantly reduce quality of life (Resck et al., 2024).

CHIKV is a positive-sense, single-stranded RNA virus whose genome encodes five structural proteins, including envelope (E) and capsid proteins, along with four non-structural proteins (nsP1-nsP4) (Sreekumar et al., 2010; Noranate et al., 2014). Among these, nsP2 is a multifunctional protein essential for viral infection. It contains an N-terminal RNA helicase with both nucleotide triphosphatase (NTPase) and RNA triphosphatase activities, and a C-terminal papain-like cysteine protease domain ($nsp2^{pro}$) responsible for polyprotein processing, followed by a Ftsj methyltransferase (MTase)-like domain (Aher, & Lole, 2011; Das, Merits, & Lulla, 2014). Law et al. 2019 provided a structural analysis of the CHIKV nsP2 helicase domain bound to RNA (Law et al., 2019)

Besides its proteolytic activity, $nsP2^{pro}$ interacts with host proteins, further facilitating viral replication. Notably, studies have demonstrated that $nsP2^{pro}$ migrates to the cell nucleus, although the precise biological significance of this localization remains unclear (Saisawang et al., 2017). The interferon response is a critical first-line defense mechanism of the innate immune system against viral infections, but it can be suppressed by viral factors (Göertz et al., 2018; tenOever, 2016). Specifically, the methyltransferase domain of CHIKV $nsP2^{pro}$ is known to downregulate the interferon response by inhibiting the JAK/STAT signaling pathway, which is essential for interferon activation. Furthermore, this domain disrupts MHC-I antigen presentation, enabling the virus to evade detection by $CD8^+$ T cells (Ware et al., 2024). Given that many virus proteases are activated upon interaction with cofactor proteins, these proteases interact with virus and host nucleic acids (DNA or RNA) in several ways, primarily to process viral polyproteins and regulate host cell functions. These interactions are crucial for viral replication, pathogenesis, and immune evasion. Table 1 summarizes reported virus protease-nucleic acid interactions.

Table 1. Summary of virus proteases interacting with nucleic acids**.**

Virus	Virus protease	Nucleic acid	Binding/Activation/ Inhibition	Reference
Coxsackievirus	$3C^{pro}$	Virus RNA	Binding	(Dias-Solange, Le, Gottipati, & Choi, 2025)
Foamy virus	Foamy virus protease	Virus RNA	Activation	(Hartl et al., 2011)
Hepatitis A virus	$3C^{pro}$	Synthetic DNA	Inhibition	(Blaum et al., 2011)
Hepatitis C virus	NS3 protease	Virus RNA	Binding	(Beran, Serebrov, & Pyle, 2007)
Hepatitis C virus	NS3 protease	RNA aptamer	Inhibition	(Urvil et al., 1997)
Human immunodeficiency virus type 1	HIV-1 PR	Virus RNA	Activation	(Potempa et al., 2015)
Human immunodeficiency virus type 1	HIV-1 PR	RNA aptamer	Inhibition	(Duclair, Gautam, Ellington, & Prasad, 2015)
Poliovirus	$3C^{pro}$	Virus RNA	Activation	(Campagnola & Peersen, 2023)
Seneca Valley virus	$3C^{pro}$	Host DNA	Activation	(L. Wu et al., 2025)

In this study, we explore how nucleic acids influence the catalytic activity of $nsP2^{pro}$ to better understand the regulation of its enzymatic function. Through Throughput Sequencing–Fluorescent Ligand Interaction Profiling (HiTS-FLIP), we identified specific DNA aptamers that bind to $nsP2^{pro}$ and evaluated their effects on its proteolytic activity. Additionally, we demonstrated that random single-stranded RNA (ssRNA) and single-stranded DNA (ssDNA) also modulate $nsP2^{pro}$ function. Finally, *in silico* analyses and molecular docking were conducted to predict the potential binding sites of these nucleic acids on $nsP2^{pro}$.

2. Materials and Methods

2.1 Expression and purification of nsP2^{pro}

The protein was expressed and purified as previously described (Eberle et al., 2021; Mastalipour et al., 2025).

2.2 High-Throughput Sequencing–Fluorescent Ligand Interaction Profiling (HiTS-FLIP)

The aptamer selection was performed by HiTS-FLIP as described previously (Drees et al., 2024). In specific, we sequenced a random library (5′-TCGCACATTCCGCTTCTACC-N_{50}-CGTAAGTCCGTGTGTGCGAA-3′, acquired PAGE-purified and hand-mixed from Integrated DNA Technologies Inc., Coralville, IA, USA) using a v2 Nano 300 cycle MiSeq kit (Illumina Inc., San Diego, CA, USA) after spiking in 12% phiX (Illumina Inc., San Diego, CA, USA) and 1.25% fiducial mark oligo (acquired from Integrated DNA Technologies Inc., Coralville, IA, USA). Of the 1,682,200 clusters, 84.5% passed filters. For the aptamer selection via HiTS-FLIP, CHIKV nsP2^{pro} was labelled using AF647-NHS-ester (Lumiprobe GmbH, Hannover, Germany), which primarily binds to lysine side chains and the α-amino group at the N-terminus of the protein, with a labelling efficiency of approximately 1 dye molecule per protein. Subsequent to sequencing, the labeled protein was introduced to the flow cell of a modified MiSeq sequencer (Illumina Inc.) at concentrations of 29.8 pM, 149 pM, 745 pM, 3.73 nM, 18.7 nM, 93.2 nM, and 466 nM in 1x PBS + 0.1% Tween20 (pH 7.4, Sigma-Aldrich Corp., St. Louis, MO, USA) via an external valve (C25Z-31812EUHB, Valco Instruments Co. Inc., Houston, TX, USA; VICI). On the flow cell, each protein concentration was incubated for 30 min at 37 °C. For each DNA cluster, fluorescence signals were measured and normalized to reflect the amount of AF647-NHS-ester labelled CHIKV nsP2^{pro} bound at each concentration. Binding curves for each cluster were generated by plotting fluorescence intensity against protein concentration, and K_D values were determined using a one-site binding model with Hill-fit analysis in MATLAB R2022b (The MathWorks Inc., Natick, MA, USA). The resulting apparent K_D values represent the equilibrium binding affinities under the specific conditions of the flow cell assay (Drees et al., 2024). Out of the 910,150 distinct aptamer library sequences displayed on the flow cell, after filtering the data as described previously (Drees et al., 2024) the ten aptamer candidates with the highest affinity were chosen for further analysis.

2.3 Nucleic acids

All DNA aptamers and RNA oligonucleotides were purchased in lyophilized form from Integrated DNA Technologies, Inc. (Coralville, Iowa, USA). DNA aptamers were purified by standard desalting, while RNA oligonucleotides were purified by RNase-free high-performance liquid chromatography (HPLC). Two RNA oligonucleotides a 5-mer and a 10-mer sequences, randomly derived from the CHIKV genome and were used in the study (Supplementary Table S1). Additionally, a single-stranded DNA oligonucleotide (5′-CGTCGCTATA-3′) with the same sequence as RAC2 was purchased from Integrated DNA Technologies (Coralville, Iowa, USA) and included in the experiments. Double-stranded DNA was isolated from brain tissue of TgM83$^{+/-}$ mice (Giasson et al., 2002) using the DNeasy Blood & Tissue Kit (Qiagen GmbH, Hilden Germany), which is optimized for genomic DNA extraction. The double-stranded DNA (dsDNA) was provided by Sara Reithoffer at the Institut für Physikalische Biologie, Heinrich-Heine-Universität Düsseldorf. A random single-stranded DNA (5′-TGACCATGGAGCCTGCCGTCTACTTCAAG-3′) was obtained from Sigma-Aldrich (St. Louis, MO, USA) and kindly provided by Dr. Jeannine Mohrlüder, from the Institut für Biologische Informationsprozesse, Strukturbiochemie (IBI-7), Forschungszentrum Jülich.

2.4 Enzymatic assay

To assess the activity of CHIKV nsP2^{pro} and the effects of nucleic acids, a FRET-based assay was performed using a synthesized fluorogenic peptide substrate, DABCYL-Arg-Ala-Gly-Gly-↓Tyr-Ile-Phe-Ser-EDANS (BACHEM, Bubendorf, Switzerland) (Eberle et al., 2021). The enzymatic assay was conducted in a 96-well plate with a final reaction volume of 100 µL per well. Unless otherwise stated, 1× PBS (pH 7.5) was used as the standard assay buffer condition.

Each well contained 10 µM nsP2^{pro}, 9 µM fluorogenic substrate, and nucleic acids at a protease-to-nucleic acid molar ratio of either 1:1 (10 µM) or 1:3 (30 µM). Fluorescence intensities were measured (excitation at 340 nm, emission at 490 nm) every 30 seconds for 30 minutes at 37 °C.

To assess the influence of buffer conditions on nsP2^{pro} activity, a separate experiment was conducted using three different buffer environments: 20mM Phosphate buffer (pH 7.5), 20 mM Bis-Tris propane (pH 7.5), and 400 mM NaCl in Bis-Tris propane buffer (pH 7.5).

The activity and effects of nucleic acids on the protease were calculated using Eq. 1 (Eberle et al., 2021)

$$\text{Protease activity \%} = \frac{\text{Fluorescence intensity with nucleic acid}}{\text{Fluorescence intensity without nucleic acid}} \times 100$$

All assays were carried out in technical triplicates, and the resulting data were analyzed and presented as mean ± standard deviation (SD).

2.5 Structure predication of DNA aptamers

The secondary structures of DNA aptamers were predicted using the DINAMelt Server – Quikfold (https://www.unafold.org/quikfold.php) (Markham & Zuker, 2005). The Fast Folding – Energies & Structures algorithm was used to determine the most thermodynamically stable conformations. Predictions were carried out at 18 °C with two different Na^+ concentrations: 137 mM and 10 mM. The sequence type was set to linear, and all other parameters were kept at their default values as provided by the server, including 5% suboptimality, a default window size, a maximum of 50 suboptimal foldings, and no limit on the distance between base-paired nucleotides.

2.6 CD spectroscopy

DNA and RNA samples were separately prepared in ddH_2O and 1x PBS, respectively, to final concentrations of 30 µM for DNA aptamers and 50 µM for RNAs, enabling subsequent secondary structure analysis Circular Dichroism (CD) spectra were recorded at 18 °C using a 0.1 mm pathlength cuvette (Hellma GmbH & Co.KG, Muellheim, Germany), with a step size of 0.5 nm, over a wavelength range of 200–350 nm on a Jasco J-1100 spectropolarimeter (Jasco GmbH, Pfungstadt, Germany). Additionally, CD spectroscopy was employed to assess the conformational integrity of the purified nsP2^{pro} enzyme post-purification. The protease was diluted to a final concentration of 5 µM in a 10 mM sodium phosphate buffer (2.39 mM NaH_2PO_4, 7.6 mM Na_2HPO_4, pH 7.5). Measurements were conducted at 18°C using a 1 cm pathlength cuvette across the wavelength range of 190–260 nm, with seven replicate scans to ensure data reliability. For data processing, baseline spectra, averaged from multiple measurements, were subtracted from the corresponding sample spectra to yield corrected readings. The resulting data were expressed as molar ellipticity ([θ]), calculated using the Eq.2:

$$[\theta]\lambda = \theta/(c * l * n)$$

Where θ represents the ellipticity measured at the wavelength λ (in degrees), c is the protein concentration (mol/L), l is the cell path length (cm), and n is the number of residues in the protein.

2.7 *In silico* analysis

Models of CHIKV nsP2^{pro} and in complex with nucleic acids were generated using the AlphaFold 3 web server (Abramson et al., 2024). The structure of CHIKV nsP2^{pro} was retrieved from the PDB (code: 3TRK) and compared with the AlphaFold model (Supplementary Fig. S1).
To predict amino acids with the potential to interact with nucleic acids, the nsP2^{pro} alpha fold model was investigated with the PROBind webserver (https://www.csuligroup.com/PROBind/home) (Wu C. et al., 2025). A possible binding mode of different nucleic acids with CHIKV nsP2^{pro} was predicted by protein-nucleic acid blind docking at the web server HDOCK (Yan, Tao, He, & Huang, 2020), the results were compared with the models generated by the AlphaFold 3 web server (Abramson et al., 2024). Therefore, the AlphaFold modelled structures of CHIKV nsP2^{pro} and respective nucleic acids (ssDNA, DAC1, RAC1 and RAC2) were used for docking. The best HDOCK clusters were chosen based on the HDOCK score (Supplementary Fig. S2 and Table 2).

Table 2. Summary of chosen clusters after protein-nucleic acid blind docking using HDOCK.

	ssDNA	DAC1	RAC2	RAC1
HDOCK score[1]	-101.6 ± 7.3	-109.2 ± 3.3	-78.8 ± 3.9	-71.5 ± 4.0
Cluster	2	1	1	7
Cluster size	17	96	20	13
RMSD[2]	1.0 ± 0.7	14.9 ± 0.4	0.6 ± 0.2	2.3 ± 0.1
VWD[3] energy	-54.9 ± -5.3	-45.5 ± 6.0	-52.7 ± 1.4	-36.9 ± 5.6
Electrostatic energy	-323.8 ± 46.4	-403.8 ± 35.7	-222.4 ± 15.0	-244.8 ± 30.2
Desolvation energy[4]	12.5 ± 0.8	14.8 ± 1.1	14.9 ± 1.1	13.4 ± 0.9
Restraints violation energy[5]	55.0 ± 18.7	22.7 ± 9.8	34.8 ± 23.1	19.5 ± 7.5
Z-score[6]	-2.1	-1.0	-2.2	-1.3

[1] Weighted sum of various energy terms, including van der Waals, electrostatic, and desolvation energies.
[2] RMSD from the overall lowest-energy structure.
[3] Van der Waals
[4] Energy penalty associated with bringing molecules into contact.
[5] Energy penalty assigned when a defined restraint (distance or dihedral angle), is not perfectly satisfied in a generated model.
[6] Indicates how many standard deviations a cluster's HADDOCK score deviates from the mean HADDOCK score of all clusters. A lower z-score (more negative) generally indicates a better, more favorable cluster.

All figures were created using the PyMOL Molecular Graphics System, Version 1.3, Schrödinger, LLC.

2.8 Statistical analysis

To assess the significance level (p-value), statistical analyses were performed using GraphPad Prism (version 5.0). One-way ANOVA followed by Tukey's post hoc test was used to evaluate the differences between the groups and the control. Significance levels are indicated as follows: $p < 0.05$ (*), $p < 0.01$ (**), and $p < 0.001$ (***).

3. Results

3.1 DNA aptamer selection

Aptamers are short, single-stranded DNA or RNA molecules that fold into defined secondary and tertiary structures, allowing them to bind selectively and with high affinity to specific target molecules (Khan et al., 2022; Xu et al., 2023). To isolate DNA aptamers capable of binding the CHIKV nsP2^{pro}, a High-Throughput Sequencing–Fluorescent Ligand Interaction Profiling (HiTS-FLIP) approach incorporating a primer-blocking strategy was employed. This method facilitated the direct selection of high-affinity aptamers from a large pool of randomized DNA sequences. Based on their strong binding affinity to the nsP2^{pro}, ten candidate aptamers were selected for further analysis. The sequences and corresponding K_D values of the top ten aptamers, named DAC1–DAC10 (DNA against Chikungunya), are listed in Table 3, while the K_D fitting data are shown in Supplementary Fig. S3.

Table 3. Sequences and properties of the selected DNA aptamers (DAC1–DAC10).

Aptamer	Sequence (5'-3')	K_D [nM][1]	Tm [°C][2]
DAC1	CTTTTATCAACTCACACTTTTCGTAAGTTTCTTCTTAA ATCGCCGCACTT	37 ± 19	64.4
DAC2	CCGAACTTTTCTCTTTTAGATTGGAATCTAGGTCAAT GTTGTATTTAATC	1 ± 0.7	61.6
DAC3	CAAACATTTCTGCGAATATTTCTCCCGATACCTGTTGT GTTAAACCAGCC	3 ± 1.5	66.1
DAC4	TTTTAGACCACAGTAACATCCTGAACATGGCACTCGG CGCGATTTTCCTT	8 ± 2	68.9
DAC5	ATATAGCAGTTGGGCTCATTTGTCCACCACTGAAAGC CCGAAAACCCGTT	8 ± 2	69.9
DAC6	ACACTGTACCAGCGTTTATTTTCTATCCGTATTTTTAG GTTCTTTATTTC	14 ± 6	62.4
DAC7	ATCTCCTACCCGACGTGACTATACTATCTGTCGTATTC CGTCTTCTGATT	0.5 ± 0.4	66.1
DAC8	GGCCTCAAGCACGCCTTCATAACTTCTGCTTACCTAG ATTGGATATTAGT	1 ± 0.6	66.7
DAC9	CATTGATTTATCACTTTATAGTATTAATCACTGGGATC AATCGCTCCTGA	3 ± 1	62.6
DAC10	AATTCACCCGGTCCCGCGTGAGGTTCTATCTAACTTA GCGACAGAGACCT	9 ± 4	70.1

[1] Apparent dissociation constants (K_D) for DNA aptamers were calculated based on fluorescence intensities obtained from HiTS-FLIP experiments by Hill-fits.

[2] Melting temperatures (T_m) of DNA aptamers were calculated using the OligoAnalyzer Tool from Integrated DNA Technologies, Inc.

3.2 Secondary structure prediction of the nucleic acids

To evaluate the secondary structure of the selected DNA aptamers targeting CHIKV nsP2^{pro}, the DINAMelt Server – Quikfold web tool was utilized (Markham & Zuker, 2005). This tool predicts folding conformations based on thermodynamic parameters (Supplementary Figs. S4-S5). The structural predictions revealed that all DNA aptamers could adopt secondary structures characterized by hairpin formations, although the lengths of the stems and sizes of the loops varied among the different sequences. To experimentally validate these computational predictions, CD spectroscopy was performed to assess the secondary structure content of the aptamers (Supplementary Figs. S6-S8). CD spectroscopy results showed similar structural features under both ddH_2O and 1× PBS buffer conditions, with two positive peaks around 280 nm and 220 nm, and a negative peak near 245 nm. In addition to the DNA aptamers, two single-stranded RNA molecules RAC1 (5 nucleotides) and RAC2 (10 nucleotides), where "RAC" denotes RNA Against Chikungunya (see Supplementary Table S1), were analyzed by CD spectroscopy to evaluate their secondary structure characteristics. RAC1 exhibited a broad spectrum with low ellipticity, showing a weak positive peak around 270–280 nm, suggesting minimal or disordered secondary structure. In contrast, RAC2 displayed a more defined CD spectrum, with a clear positive peak at 270–280 nm and a distinct negative peak at around 240 nm, indicating the formation of a more ordered secondary structure (Supplementary Fig. S8).

3.3 Impact of DNA aptamers on CHIKV nsP2^{pro} enzymatic activity

To investigate the impact of nucleic acids on the enzymatic activity of nsP2^{pro}, a primary activity assay was conducted in 1x PBS buffer using DNA aptamers targeting CHIKV nsP2^{pro} (DAC1–DAC10). The aptamers were mixed with 10 µM nsP2^{pro} at two molar ratios: 1:1 (10 µM) and 1:3 (30 µM). Fluorescence intensities (excitation at 340 nm, emission at 490 nm) were recorded every 30 seconds over a 30-minute. As shown in Fig. 1, all tested DNA aptamers significantly enhanced nsP2^{pro} activity. Among the ten aptamers variants, DAC1 exhibited the most pronounced effect, increasing enzymatic activity by approximately 600%. DAC2, DAC6, DAC8, and DAC9 induced up to 500% enhancement, while DAC3, DAC4, and DAC5 demonstrated moderate levels of activation (approximately 300-400%), suggesting differences in their ability to promote protease activity. The results also revealed that nsP2^{pro} activity was influenced by the aptamer-to-protease molar ratio. For most DAC variants, increasing the aptamer concentration from 10 µM to 30 µM did not further enhance activity. In fact, for DAC1, DAC2, DAC3, DAC4, and DAC6, higher concentrations led to a reduction in enzymatic activity, suggesting that higher aptamer concentrations do not lead to the higher activity rate in these cases. In contrast,

DAC7, DAC8, DAC9, and DAC10 showed a slight increase in activity at the 1:3 ratio compared to 1:1, indicating only minimal additional enhancement.

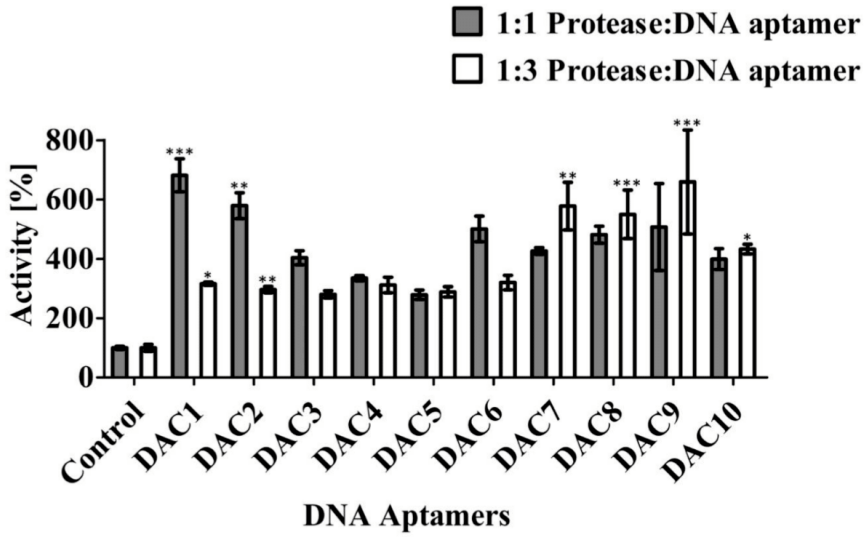

Fig. 1. Enzymatic activity of nsP2^{pro} in the presence of DNA aptamers (DAC1–DAC10) at different molar ratios. A primary activity assay of DNA aptamers was performed in 1× PBS at two different molar ratios: 1:1 and 1:3. The protease concentration was 10 µM, and the substrate concentration was maintained at 9 µM. The protease was mixed with DNA aptamers at 1:1 (10 µM, gray bars) and 1:3 (30 µM, white bars) molar ratios. Data from three independent experiments (n = 3) are presented as mean ± standard deviation (SD). Statistical significance was evaluated using one-way ANOVA followed by Tukey's post hoc test. Asterisks indicate values that differ significantly from the respective control group. The significance levels are defined as follows: $p < 0.05$ (*), $p < 0.01$ (**) and $p < 0.01$ (***). If no asterisk is shown, the difference was not statistically significant ($p > 0.05$).

3.4 Impact of random ssDNA and dsDNA on the enzymatic activity of CHIKV nsP2^{pro}

In Section 3.3, the impact of specific DNA aptamers on nsP2^{pro} activity was assessed. To determine the specificity of this effect, random single-stranded DNA (ssDNA) was used as a control. It was found that random ssDNA, at a 1:1 molar ratio with the protease, also enhanced protease activity, increasing it by up to 600% (Fig. 2A). To further investigate the effect of random DNA on nsP2^{pro} activity, the potential of random dsDNA, isolated from TgM83$^{+/-}$ mice, was also examined. In contrast to ssDNA, dsDNA did not induce any detectable increase in nsP2^{pro} activity (Fig. 2A), indicating that the stimulatory effect is likely dependent on the single-stranded conformation of the nucleic acid.

3.5 Impact of single-stranded RNA on CHIKV nsP2^{pro} enzymatic activity

Since CHIKV is an RNA virus that replicates in the host cell cytoplasm, it is of interest to evaluate whether RNA can influence the activity of nsP2^{pro}. To investigate this, two ssRNA oligonucleotides, 5-mer and 10-mer sequences, randomly derived from the CHIKV genome were tested. These were designated RAC1 (5 nucleotides) and RAC2 (10 nucleotides) (Supplementary Table S1). The primary activity assay, conducted in 1x PBS buffer, showed that the shorter ssRNA, RAC1, did not enhance nsP2^{pro} enzymatic activity at either the 1:1 or 1:3 molar ratios (Fig. 2B) However, RAC2 significantly increased protease activity. At 10 µM, activity increased to around 300%, and at 30 µM, it rose to approximately 500% compared to the control (Fig. 2B). In addition, we tested a ssDNA oligonucleotide with the same sequence as RAC2. Interestingly, this ssDNA also enhanced nsP2^{pro} enzymatic activity, increasing it by approximately 260% at the 1:1 molar ratio and around 500% at the 1:3 molar ratio, similar to the effect observed with RAC2 (Fig. 2B).

3.6 Impact of nucleotides on the activity of CHIKV nsP2^{pro}

To investigate whether individual nucleotides could enhance nsP2^{pro} activity, a primary activity assay was conducted under the same experimental conditions. Nucleotides were tested at concentrations of 10 µM and 30 µM. At the lower concentration (10 µM), no significant increase in protease activity was observed. However, at 30 µM, a modest increase in protease activity was detected (Fig. 2C). Specifically, dATP at 30 µM induced a modest increase of approximately 38%, which is substantially lower than the activity observed in presence of the ssDNA or ssRNA.

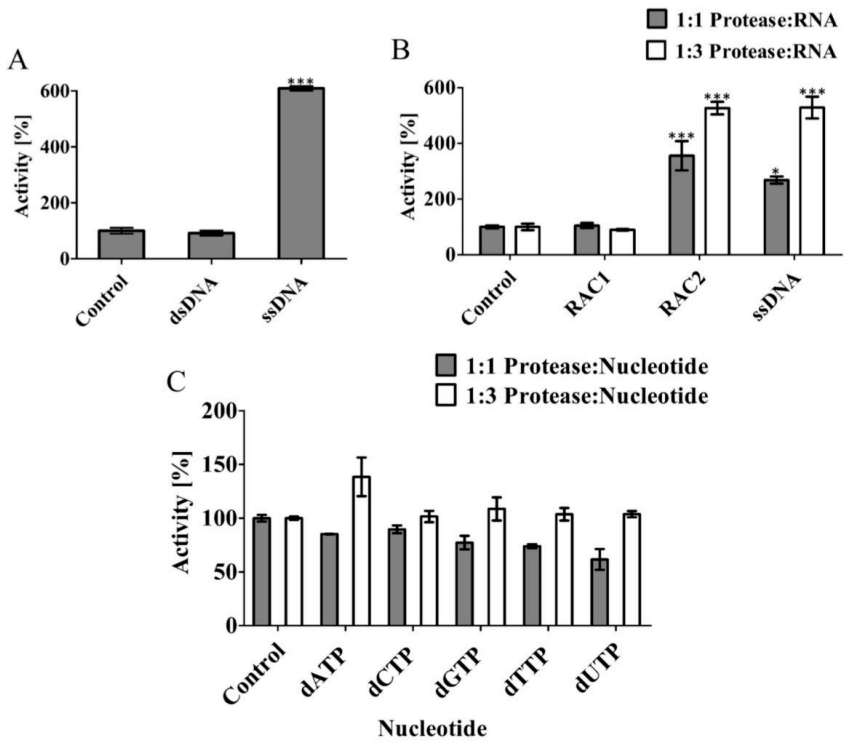

Fig. 2. Influence of nucleic acids and nucleotides on nsP2^{pro} enzymatic activity. (A) Effect of random ssDNA and dsDNA on nsP2^{pro} activity. **(A)** Primary assay was conducted to assess the influence of random ssDNA (5′-TGACCATGGAGCCTGCCGTCTACTTCAAG-3′) and dsDNA on the enzymatic activity of nsP2^{pro}. **(B)** Enzymatic activity of nsP2^{pro} in the presence of ssRNAs (RAC1–2) and ssDNA (5'-CGTCGCTATA-3') corresponding to RAC2, tested at 1:1 (10 µM, gray bars) and 1:3 (30 µM, white bars) molar ratios. **(C)** Enzymatic activity of nsP2^{pro} in the presence of single nucleotides. Assays were performed in 1× PBS at two molar ratios: 1:1 (10 µM, gray bars) and 1:3 (30 µM, white bars). In all experiments, the protease concentration was 10 µM and the substrate concentration was maintained at 9 µM. Data are shown as mean ± standard deviation (SD) from three independent experiments (n = 3). Statistical significance was evaluated using one-way ANOVA followed by Tukey's post hoc test. Asterisks indicate significant differences compared to the control group, with thresholds defined as: $p < 0.05$ (*), $p < 0.01$ (**), and $p < 0.001$ (***). If no asterisk is shown, the difference was not statistically significant ($p > 0.05$).

3.7 Impact of buffer composition on the activity of CHIKV nsP2^{pro} by DNA aptamer and ssRNA

To assess the effect of different buffers on nsP2^{pro} activity in the presence of nucleic acids, the ability of DAC8 (a representative DNA aptamer) and RAC2 (a 10-mer ssRNA) to enhance protease activity was evaluated under various buffer conditions. Assays were conducted using 10 µM nsP2^{pro} and two molar ratios of protease-to-nucleic acids: 1:1 and 1:3. Three buffer systems were tested: 20 mM Bis-Tris propane (pH 7.5), 20 mM phosphate buffer (pH 7.5), and 20 mM Bis-Tris propane supplemented with 400 mM NaCl (pH 7.5). As shown in Fig. 3A–B, both DAC8 and RAC2 enhanced protease activity in Bis-Tris propane and phosphate buffers at both molar ratios. Notably, DAC8 induced a more pronounced increase in activity than RAC2 at the 1:1 ratio. However, at the 1:3 ratio, RAC2 exhibited greater

activation than DAC8 in Bis-Tris propane buffer, while in phosphate buffer, both nucleic acids produced similar effects. In contrast, under high-salt conditions (400 mM NaCl), neither DAC8 nor RAC2 was able to stimulate nsP2^{pro} activity at either molar ratio. These findings suggest that elevated ionic strength inhibits nucleic acid-mediated enhancement of protease activity and underscore the critical role of buffer composition in modulating nsP2^{pro} enzymatic function.

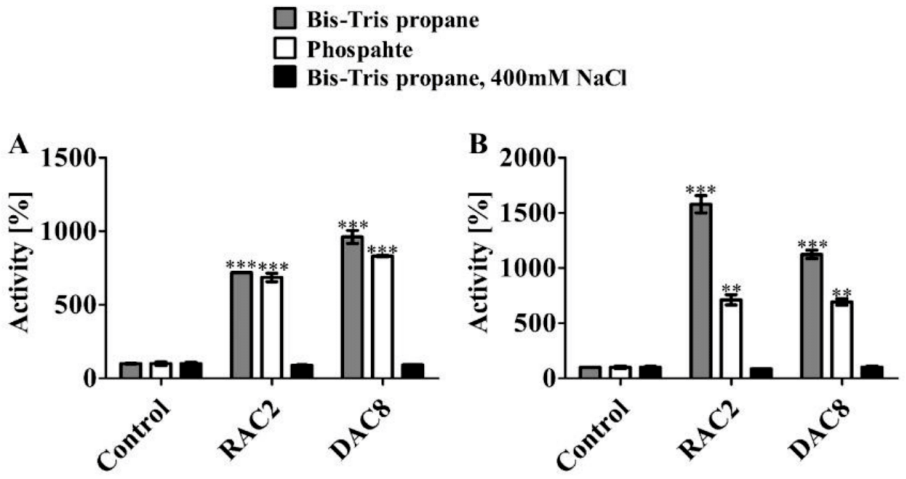

Fig. 3. Effect of buffer composition on the activity of nsP2^{pro} by nucleic acids. The activity of nsP2^{pro} by DAC8 (a DNA aptamer) and RAC2 (ssRNA) was assessed in the presence of three different buffer conditions: (1) 20 mM Bis-Tris propane, pH 7.5, (2) 20 mM phosphate buffer, pH 7.5, and (3) 20 mM Bis-Tris propane, 400 mM NaCl, pH 7.5. Nucleic acids were tested at molar ratios of 1:1 **(A)** and 1:3 **(B)** with nsP2^{pro} (10 µM). The substrate concentration was kept at 9 µM. Data are presented as the mean ± SD from three independent experiments (n = 3). Statistical significance was evaluated using one-way ANOVA followed by Tukey's post hoc test. Asterisks indicate significant differences compared to the control group, with thresholds defined as: $p < 0.05$ (*), $p < 0.01$ (**), and $p < 0.001$ (***). If no asterisk is shown, the difference was not statistically significant ($p > 0.05$).

3.8 Possible binding mode of nucleic acids with CHIKV nsP2^{pro}

CHIKV nsP2^{pro} consists of an N-terminal papain-like protease domain, directly followed by a Ftsj MTase-like domain (Fig. 4A). The surface of the MTase-like domain possesses clusters of positive charges, located near the protease active site loop carrying His1083 (Fig. 4B), which may propagate the binding of the negative charged phosphate backbone of nucleic acids.

The online tool PROBind was used to predict amino acids that are involved in DNA and RNA binding (Fig. 4C-D). Thereby, 14 residues were predicted to interact with DNA, located mainly at a surface cluster in the MTase domain (Fig. 4C). 23 residues were predicted to interact with RNA, where 16 residues are located at the MTase domain and 7 residues at the active site loop carrying His1083 on the protease domain. Some areas seem to overlap regarding the DNA and RNA interaction, the predicted amino acids are shown in the nsP2^{pro} sequence at supplementary Fig. S9.

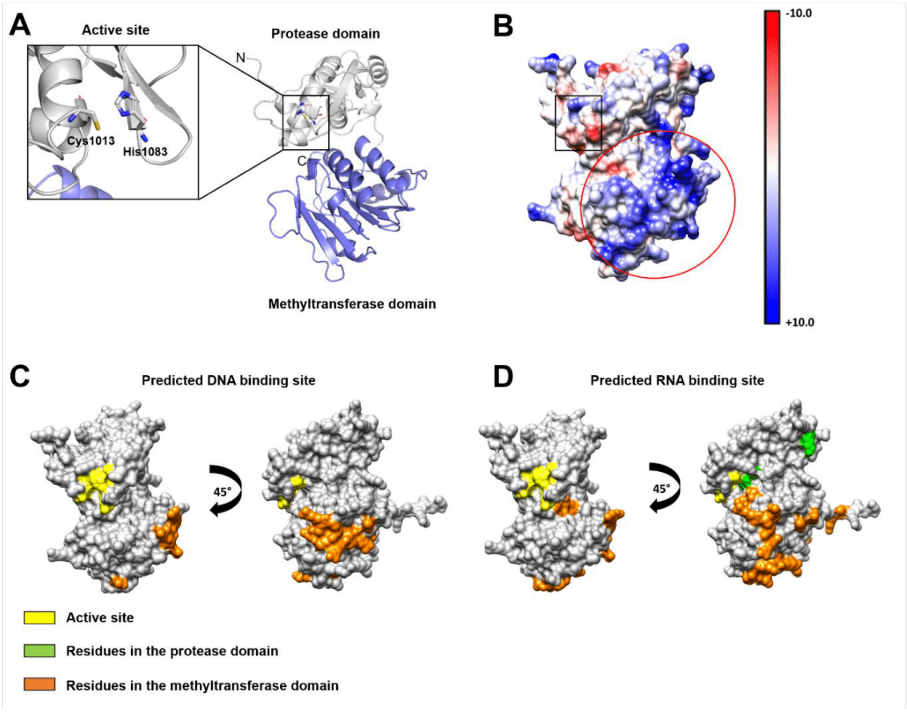

Fig. 4. Investigation of the nsP2^{pro} AlphaFold model with regard to possible nucleic acid binding regions. A structural comparison between the crystal structure of the protein (PDB code: 3TRK) and the generated AlphaFold model is shown in supplementary Fig. S1. **(A)** nsP2^{pro} is shown in ribbon view, the papain-like cysteine protease is colored in grey and the Ftsj methyltransferase (MTase)-like domain in blue. The black box labels the position of the active site residues Cys1013 and His1083. **(B)** Coulombic surface of nsP2^{pro}, the red circle labels a strongly positively charged area at the MTase domain, the black box labels the position of the active site residues. The online tool PROBind was used to predict amino acids that can take part in interactions with DNA and RNA. The protein is shown in surface view and the predicted amino acids are labeled in orange (MTase domain) and green (Protease domain). The position of the active site is labeled in yellow. **(C)** Predicted DNA binding site. **(D)** Predicted RNA binding site.

To predict a possible binding area, models of complexes between CHIKV nsP2^{pro} and different nucleic acids were generated using AlphaFold 3. The tested nucleic acids included ssDNA (5′-CGTCGCTATA-3’), DAC1 (5′-CTTTTATCAACTCACACTTTTCGTAAGTTTCTTCTTAAATCGCCGCACTT-3`), RAC1 (5′-CGUCG-3′) and RAC2 (5′-CGUCGCUAUA-3′). Additionally, blind docking was performed using HDOCK (Yan et al., 2020). The positions of the nucleic acids in the complexes with the protein were compared between both approaches, as shown in Fig. 5. To demonstrate a stable pose within the different clusters, an overlay of all predicted docking poses is shown in supplementary Fig S10. The results of both approaches demonstrated that the tested nucleic acids were docked without exception to the MTase domain. Interestingly, RAC2 showed almost the same pose between both approaches (Fig. 4D). These observations let us assume that the nucleic acids mainly interact with the MTase domain.

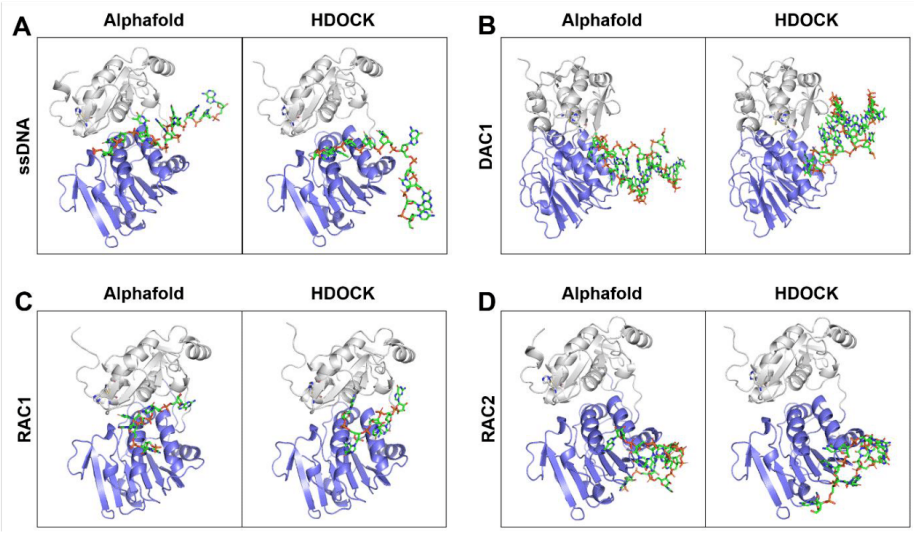

Fig. 5. Binding pose of the different nucleic acids with nsP2^{pro} after complex generation using AlphaFold and docking using HDOCK. The target protein is shown in ribbon view, the papain-like cysteine protease is colored in grey and the Ftsj methyltransferase (MTase)-like domain in blue. The nucleic acids are shown as green sticks. One representative AlphaFold model is shown, the overlay of the five generated models is presented in supplementary Fig. S10 and show especially in the binding region a stable pose. A representative structure of the best-scoring cluster following protein-nucleic acid blind docking using HDOCK is also shown.

4. Discussion

The Chikungunya virus (CHIKV) is a rapidly emerging arthropod-borne pathogen whose increasing global distribution is related to climate and environmental changes. Central to CHIKV replication is its nonstructural protein 2 (nsP2), a multifunctional enzyme that plays an important role as a viral protease (nsP2^{pro}) by mediating the cleavage of the viral polyprotein. Several studies have reported that interactions between viral proteins and nucleic acids are pivotal for mediating key aspects of the viral life cycle. For example, the Rep protein of adeno-associated virus type 2 binds single-stranded DNA (ssDNA), a process that facilitates viral replication (Stracker et al., 2004) and HIV-1 protease has been shown to bind viral RNA, potentially augmenting its catalytic activity (Potempa et al., 2015). In other cases, the binding of viral RNA to proteases such as those of the Foamy virus (Hartl et al., 2011) and the 3C^{pro} protease of poliovirus (Campagnola & Peersen, 2023) has been reported to activate protease function. Not only RNA but also DNA can mediate protease activation. For instance, host DNA has been shown to activate the 3C^{pro} of Seneca Valley virus (L. Wu et al., 2025), highlighting the potential role of host nucleic acids in modulating viral protein activity. Interestingly, nucleic acid interactions do not always facilitate viral replication; in some cases, they can inhibit it. For example, RNA aptamers have been identified that bind to the NS3 protease of hepatitis C virus, inhibiting its function in polyprotein processing (Urvil et al., 1997). Similarly, RNA aptamers targeting HIV-1 PR have been reported to block its enzymatic activity (Duclair et al., 2015). In light of these findings, this study focused on CHIKV nsP2^{pro} to assess the impact of nucleic acid interactions on its protease activity. HiTS-FLIP was employed to identify ssDNA aptamers that bind to nsP2^{pro}. Ten aptamers (designated DAC1–DAC10) were selected based on their binding affinity (Table 3) and were subsequently tested for their effect on protease activity. To evaluate the effect of these aptamers on nsP2^{pro} activity, primary activity assays were conducted. The results showed that all ssDNA aptamers had the potential to enhance the

activity of the target protease (Fig. 1). Among the ten DAC variants, DAC1 exhibited the most pronounced effect, increasing enzymatic activity by 600% (Fig. 1). DAC2, DAC6, DAC8, and DAC9 also induced substantial increases, reaching up to 500%. In contrast, DAC3, DAC4, and DAC5 showed moderate enhancement at a 1:1 ratio relative to the protease concentration (10 µM). However, when the DNA concentration was increased to a 1:3 ratio, a reduction in protease activity was observed, with DAC1-induced activity decreasing to approximately 300% compared to the 1:1 condition. This reduction may be attributed to the elevated ssDNA concentration, which could promote protein precipitation and aggregation-a phenomenon reported for proteins such as tau and α-synuclein, where nucleic acids have been shown to induce aggregation (Yin, Chen, & Liu, 2009). To ensure that the observed activity increase was due to protease–nucleic acid interactions and not simply optical interference from the aptamers themselves, control experiments were conducted in the absence of substrate. Reactions were prepared with buffer alone, protease plus buffer, and protease with buffer and DNA aptamers, excluding the fluorogenic substrate. No detectable absorbance was observed in the lack of substrate, confirming that the increased signal in the complete assays was attributable to enzymatic activity, not background fluorescence or absorbance changes caused by the aptamers (Supplementary Fig. S11). To determine whether the observed increase in $nsP2^{pro}$ activity was due to specific binding by the selected ssDNA aptamers or could also result from non-specific interactions, a random ssDNA sequence was tested. Interestingly, as shown in Fig. 2A, the random ssDNA also enhanced protease activity, suggesting that the effect is not sequence-specific. To further explore this phenomenon, the effect of a random dsDNA, isolated from $TgM83^{+/-}$ mice, was examined. In contrast to ssDNA, the random dsDNA did not cause any enhancement in protease activity compared to the control (Fig. 2A), suggesting that the stimulatory effect is dependent on the single-stranded nature of the nucleic acid. Since CHIKV is a ssRNA virus that replicates in the cytoplasm, it is likely that $nsP2^{pro}$ naturally encounters ssRNA during infection. To evaluate whether ssRNA could similarly influence protease activity, two random ssRNA oligonucleotides were tested: a 5-mer (RAC1) and a 10-mer (RAC2), both derived from the CHIKV genome (Table S1). Activity assays revealed that RAC1 did not enhance $nsP2^{pro}$ activity, whereas RAC2 significantly increased activity, reaching approximately 600% (Fig. 2B). These findings suggest that ssRNA, like ssDNA, can enhance protease activity, but the effect is length-dependent and requires a minimum RNA length. To confirm the length dependency, an additional assay was performed using single nucleotides. At a 1:1 molar ratio with the protease, no change in activity was observed; however, at a 1:3 ratio, a slight increase was detected (Fig. 2C). This result aligns with the ssRNA experiments and further supports the conclusion that enhancement of $nsP2^{pro}$ activity by nucleic acids requires a minimal oligonucleotide length.

The influence of buffer composition on nucleic acid-mediated activation of $nsP2^{pro}$ was systematically evaluated using two representative oligonucleotides: DAC8 (ssDNA aptamer) and RAC2 (ssRNA). Three buffer systems were tested: 20 mM Bis-Tris propane (pH 7.5), 20 mM phosphate buffer (pH 7.5), and 20 mM Bis-Tris propane supplemented with 400 mM NaCl (pH 7.5). As shown in Fig. 3A–B, both DAC8 and RAC2 significantly enhanced protease activity in Bis-Tris propane and phosphate buffers without added salt. At the 1:1 ratio, DAC8 induced a stronger activation compared to RAC2, while at the 1:3 ratio, RAC2 exhibited greater enhancement in Bis-Tris propane. In phosphate buffer, both oligonucleotides led to similar effects. However, in the presence of high salt (400 mM NaCl), the activation was completely abolished for both DAC8 and RAC2, irrespective of the molar ratio. These results indicate that the stimulatory interaction between nucleic acids and $nsP2^{pro}$ is highly sensitive to ionic strength. The loss of activity in high-salt conditions suggests that electrostatic interactions play a critical role in facilitating protease activity. This observation aligns with findings from other studies, such as those involving the hsRosR protein, demonstrated that high salt concentrations can disrupt protein-nucleic acid binding by altering solvent properties or changing the electrostatic environment of the protein and DNA and the correlation in between aptamer affinity and pI value of target proteins

(Kutnowski et al., 2019; Drees et al., 2023). Therefore, the effect of high salt on nsP2^{pro} activity likely stems from the disruption of protein- nucleic acids interactions, emphasizing the importance of buffer conditions for nucleic acid-mediated protease activation. To gain a better understanding of the structural basis of the DNA aptamers, the secondary structures of the selected DNA aptamers were predicted using the DINAMelt Server – Quikfold web tool. (Markham & Zuker, 2005). The predictions revealed that all sequences adopted secondary structures characterized by hairpin formations, although the lengths of the stems and the sizes of the loops varied among the different aptamers (Supplementary Figs. S4–S5). CD spectroscopy further confirmed the presence of these structured forms in both ddH_2O and 1× PBS conditions. The spectra of all DNA aptamers exhibited two distinct positive peaks around 280 nm and 220 nm, along with a strong negative peak near 245 nm. A pattern consistent with the B-form DNA conformation (Kypr, Kejnovská, Renčiuk, & Vorlíčková, 2009) (Supplementary Figs. S6–S8). These spectral features corroborate the computational predictions and indicate that all DNA aptamers retain stable secondary structures in solution. Furthermore, comparative CD analysis of these DNA aptamers with two ssRNA molecules (RAC1 and RAC2) revealed marked structural differences. RAC2 exhibited a spectral profile characteristic of the A-form RNA helix, including a moderate positive band near 270 nm, reflecting a well-structured RNA fold (Sosnick, Fang, & Shelton, 2000). In contrast, RAC1 showed significantly diminished ellipticity across the spectrum, consistent with an unfolded or denatured state. This interpretation is in agreement with previous findings, where unfolded RNAs lack the defined CD spectral features associated with stable secondary structures (Sosnick et al., 2000) (Supplementary Fig. S8). These findings suggest that the secondary structure of nucleic acids may influence their binding capacity to nsP2^{pro} and contribute to their ability to enhance enzymatic activity.

Finally, nsP2^{pro} was investigated to specify possible nucleic acid binding regions at the protein surface, using the PROBind webserver (Wu C. et al., 2025). Predicted residues involved in DNA and RNA interaction differ in quantity and the localization in the protein. 14 amino acid residues were predicted to interact with DNA and 23 residues with RNA. DNA binding regions are exclusively localized at the MTase domain, also the majority of the RNA binding residues, but the protease domain carries five amino acids with the potential to interact with RNA. The proposed residues involved in DNA interaction included two main regions $_{1281}$RSSR$_{1284}$ and $_{1305}$DNGRR$_{1309}$. Contrary, predicted regions for RNA interaction included $_{1308}$RRN$_{1310}$, $_{1241}$QML$_{1243}$, $_{1183}$TKR$_{1185}$, $_{1165}$K(I)NGH$_{1169}$ (predicted without the I) and five residues in the protease domain, $_{1054}$NE$_{1055}$, $_{1050}$E and $_{47}$YS$_{48}$ (Supplementary Fig. S9).
Viral proteins utilize various nucleic acid binding motifs, including the RNA recognition motif (RRM) and the zinc finger motif (Frequently involved in DNA binding), to interact with viral and host nucleic acids. Moreover, arginine plays an important role in several RNA binding motifs in virus proteins, e.g. arginine rich motif (ARM) (Casu, Duggan, & Hennig, 2013), HR motif (Ogino & Banerjee, 2010), RG/RGG motif (Iacovides, O'Shea, Oses-Prieto, Burlingame, & McCormick, 2007), SR/RS motif (Nikolakaki & Giannakouros, 2020). Arginine has a high occurrence in the predicted nucleic acid interaction regions of nsP2^{pro}, these regions differ slightly to the typical motifs mentioned above. Viral proteins often exhibit significant variation in their RNA and DNA binding motifs. This variation arises from evolutionary pressures and the need for viruses to efficiently interact with the host cell's RNA machinery and evade the host's immune system (Garcia-Moreno et al., 2019). However, arginine plays a crucial role in nucleic acid interactions, particularly in RNA, due to its unique ability to form strong, multivalent interactions. Arginine can interact with the phosphate backbone and base pairs in RNA, forming salt bridges and hydrogen bonds that are essential for recognition and binding (B. Martin et al., 2022).

To predict a possible nucleic acid binding region on nsP2^{pro}, molecular docking of four different nucleic acids, ssDNA, DAC1, RAC1 and RAC2 with the protein was performed using AlphaFold 3 and HDOCK. During the docking experiments no amino acids or regions were predefined, where the nucleic

acids supposed to bind, we performed blind docking, with two different approaches, AlphaFold 3 and HDOCK. The results indicated that the different nucleic acids interact in the regions predicted by PROBind. Comparison of the nucleic acid positions between the Alphafold 3 models demonstrated that there were small differences between the binding poses of the tested nucleic acids between the AlphaFold 3 and HDOCK approach. However, our results let us assume, that the nucleic acids interact with the nsP2^{pro} MTase domain, but to generate valid information about the nucleic acid binding region of nsP2^{pro} further experiments are necessary.

Interestingly, a previous study from our group demonstrated an interdomain motion leading to closed and open conformations of the nsP2^{pro} active site. Thereby, a flap formed by residues A1080 to H1083 can adopt positions either close to or far from the residues $_{1202}$NLELGL$_{1207}$ in the MTase domain. When the active site adopts a more open conformation, the flap moves farther away from the loop on the C-terminal domain. (Mastalipour et al. 2025). Nearby the MTase $_{1202}$NLELGL$_{1207}$ loop are predicted nucleic binding regions are located. Especially, $_{1241}$QML$_{1243}$ is in direct neighborhood of this loop, 1242M and L1243 have a distance of 3.4 to 3.5 Å to the $_{1202}$NLELGL$_{1207}$ loop, which makes the formation of van der waals (VDW) interactions between both regions highly possible (Supplementary Figs S12 and S13). VDW interactions occur at distances typically between 2.5 and 4.6 angstroms (Å), averaging around 3.6 Å (Qi, Wang, & Ren, 2016). We assume that nucleic acids may interact with $_{1241}$QML$_{1243}$ and disturb the interaction to $_{1202}$NLELGL$_{1207}$, with the result that the active site exists in the open conformation. Moreover, the residues $_{1054}$NE$_{1055}$, $_{1050}$E and $_{47}$YS$_{48}$ are located at a helix beside the active site. Nucleic acid binding in this region may also induce a conformational change that results in the open conformation of the protease active site.

Conclusion and Future Perspectives

In this study, it was demonstrated that single-stranded nucleic acids-including both DNA aptamers and structured RNA fragments-can significantly enhance the catalytic activity of the Chikungunya virus nsP2^{pro}. This enhancement appears to be influenced by several factors: the single-stranded nature of the nucleic acid, a minimum oligonucleotide length, the presence of stable secondary structures, and sensitivity to ionic strength. Molecular docking analyses predicted that these nucleic acids interact with the methyltransferase domain of nsP2^{pro}; however, this binding site remains to be experimentally validated. Further studies are needed to confirm the precise binding interface and determine whether this interaction occurs under physiological conditions. Future investigations should focus on assessing the *in vivo* relevance of these interactions during CHIKV infection and replication, as well as on high-resolution structural studies to define the molecular details of the nucleic acid–nsP2^{pro} complex.

Funding

M.M. thanks Jürgen Manchot Stiftung for providing financial assistance and resources. A.D. was supported by the Joachim Herz Foundation.

CRediT authorship contribution statement

Mohammadamin Mastalipour: Conceptualization, Methodology, Formal analysis, Data curation, Writing – original draft, Writing – review & editing. **Mônika Aparecida Coronado:** Formal analysis, Writing – review & editing. **Ruth Anasthasia Siahaan:** Investigation. **Alissa Drees:** Methodology, Investigation, Data curation, Writing – review & editing**. Christian Ahlers:** Software, Investigation, Analysis, Writing – review & editing**. Markus Fischer:** Resources, Supervision, Writing – review & editing**. Dieter Willbold:** Resources, Writing – review & editing. **Raphael Josef Eberle:** Conceptualization, Supervision, Writing – review & editing. All authors have read and agreed to the published version of the manuscript.

Declaration of generative AI and AI-assisted technologies in the writing process

ChatGPT (OpenAI) was utilized to assist with grammar and spelling checks to enhance the readability of the manuscript. All content was subsequently reviewed and edited by the authors, who take full responsibility for the final version of the text. In addition, selected figures were created using the BioRender platform.

Declaration of competing interest

The authors declare that they have no known competing financial interests or personal relationships that could have appeared to influence the work reported in this paper.

Acknowledgements

This work was supported by funding and resources from the Jürgen Manchot Stiftung, whose contribution was essential to the advancement of this research

References

Abramson, J., Adler, J., Dunger, J., Evans, R., Green, T., Pritzel, A., & Jumper, J. M. (2024). Accurate structure prediction of biomolecular interactions with AlphaFold 3. *Nature, 630*(8016), 493-500. https://doi.org/10.1038/s41586-024-07487-w

Alissa, M., Alsuwat, M. A., & Alzahrani, K. J. (2024). Neurological manifestations of Flaviviridae, Togaviridae, and Peribunyaviridae as vector-borne viruses. *Reviews in Medical Virology, 34*(4), e2571. https://doi.org/10.1002/rmv.2571

Beran, R. K. F., Serebrov, V., & Pyle, A. M. (2007). The Serine Protease Domain of Hepatitis C Viral NS3 Activates RNA Helicase Activity by Promoting the Binding of RNA Substrate. *Journal of Biological Chemistry, 282*(48), 34913-34920. https://doi.org/10.1074/jbc.M707165200

Blaum, B. S., Wünsche, W., Benie, A. J., Kusov, Y., Peters, H., Gauss-Müller, V., & Sczakiel, G. (2011). Functional binding of hexanucleotides to 3C protease of hepatitis A virus. *Nucleic Acids Research, 40*(7), 3042-3055. https://doi.org/10.1093/nar/gkr1152

Campagnola, G., & Peersen, O. (2023). Co-folding and RNA activation of poliovirus 3Cpro polyprotein precursors. *Journal of Biological Chemistry, 299*(11), 105258. https://doi.org/10.1016/j.jbc.2023.105258

Casu, F., Duggan, Brendan M., & Hennig, M. (2013). The Arginine-Rich RNA-Binding Motif of HIV-1 Rev Is Intrinsically Disordered and Folds upon RRE Binding. *Biophysical Journal, 105*(4), 1004-1017. https://doi.org/10.1016/j.bpj.2013.07.022

Chitre, S. D., Crews, C. M., Tessema, M. T., Plėštytė-Būtienė, I., Coffee, M., & Richardson, E. T. (2024). The impact of anthropogenic climate change on pediatric viral diseases. *Pediatric research, 95*(2), 496-507. https://doi.org/10.1038/s41390-023-02929-z

Das, P. K., Merits, A., & Lulla, A. (2014). Functional Cross-talk between Distant Domains of Chikungunya Virus Non-structural Protein 2 Is Decisive for Its RNA-modulating Activity*. *Journal of Biological Chemistry, 289*(9), 5635-5653. https://doi.org/10.1074/jbc.M113.503433

de Souza, W. M., Fumagalli, M. J., de Lima, S. T. S., Parise, P. L., Carvalho, D. C. M., Hernandez, C., & Weaver, S. C. (2024). Pathophysiology of chikungunya virus infection associated with fatal outcomes. *Cell Host & Microbe, 32*(4), 606-622.e608. https://doi.org/10.1016/j.chom.2024.02.011

Dias-Solange, D., Le, M. T., Gottipati, K., & Choi, K. H. (2025). Structure of coxsackievirus cloverleaf RNA and $3C^{pro}$ dimer establishes the RNA-binding mechanism of enterovirus protease $3C^{pro}$. *Science Advances, 11*(11), eads6862. https://doi.org/10.1126/sciadv.ads6862

Drees, A., Ahlers, C., Kehrer, T., Ehmke, N., Grün, A. F. R., Uetrecht, C., & Fischer, M. (2024). Automated high-throughput selection of DNA aptamers using a common optical next-generation sequencer. *bioRxiv*, 2024-2006. https://doi.org/10.1101/2024.06.24.600375

Drees, A., Trinh, T. L., & Fischer, M. (2023). The Influence of Protein Charge and Molecular Weight on the Affinity of Aptamers. *Pharmaceuticals*, *16*(3), 457. https://doi.org/10.3390/ph16030457

Duclair, S., Gautam, A., Ellington, A., & Prasad, V. R. (2015). High-affinity RNA Aptamers Against the HIV-1 Protease Inhibit Both In Vitro Protease Activity and Late Events of Viral Replication. *Molecular Therapy - Nucleic Acids, 4*, e228. https://doi.org/10.1038/mtna.2015.1

Eberle, R. J., Olivier, D. S., Pacca, C. C., Avilla, C. M. S., Nogueira, M. L., Amaral, M. S., & Coronado, M. A. (2021). In vitro study of Hesperetin and Hesperidin as inhibitors of zika and chikungunya virus proteases. *Plos One, 16*(3) , e0246319. https://doi.org/10.1371/journal.pone.0246319

Garcia-Moreno, M., Noerenberg, M., Ni, S., Järvelin, A. I., González-Almela, E., Lenz, C. E., & Davis, T. (2019). System-wide profiling of RNA-binding proteins uncovers key regulators of virus infection. *Molecular cell, 74*(1), 196-211. e111. https://doi.org/10.1016/j.molcel.2019.01.017

Ghoshal, A., Asressu, K. H., Hossain, M. A., Brown, P. J., Nandakumar, M., Vala, A., & Willson, T. M. (2024). Structure Activity of beta-Amidomethyl Vinyl Sulfones as Covalent Inhibitors of Chikungunya nsP2 Cysteine Protease with Antialphavirus Activity. *J Med Chem, 67*(18), 16505-16532. https://doi.org/10.1021/acs.jmedchem.4c01346

Giasson, B. I., Duda, J. E., Quinn, S. M., Zhang, B., Trojanowski, J. Q., & Lee, V. M. Y. (2002). Neuronal α-Synucleinopathy with Severe Movement Disorder in Mice Expressing A53T Human α-Synuclein. *Neuron, 34*(4), 521-533. https://doi.org/10.1016/S0896-6273(02)00682-7

Göertz, G. P., McNally, K. L., Robertson, S. J., Best, S. M., Pijlman, G. P., & Fros, J. J. (2018). The Methyltransferase-Like Domain of Chikungunya Virus nsP2 Inhibits the Interferon Response by Promoting the Nuclear Export of STAT1. *Journal of Virology, 92*(17). e01008-18. https://doi.org/10.1128/JVI.01008-18

Hartl, M. J., Bodem, J., Jochheim, F., Rethwilm, A., Rösch, P., & Wöhrl, B. M. (2011). Regulation of Foamy Virus Protease Activity by Viral RNA: a Novel and Unique Mechanism among Retroviruses. *Journal of Virology, 85*(9), 4462-4469. https://doi.org/10.1128/JVI.02211-10

Iacovides, D. C., O'Shea, C. C., Oses-Prieto, J., Burlingame, A., & McCormick, F. (2007). Critical role for arginine methylation in adenovirus-infected cells. *Journal of Virology, 81*(23), 13209-13217. https://doi.org/10.1128/jvi.01415-06

Karpe, Y. A., Aher, P. P., & Lole, K. S. (2011). NTPase and 5′-RNA Triphosphatase Activities of Chikungunya Virus nsP2 Protein. *PLOS ONE, 6*(7), e22336. https://doi.org/10.1371/journal.pone.0022336

Khan, S., Hussain, A., Fahimi, H., Aliakbari, F., Haj Bloukh, S., Edis, Z., & Falahati, M. (2022). A review on the therapeutic applications of aptamers and aptamer-conjugated nanoparticles in cancer, inflammatory and viral diseases. *Arabian Journal of Chemistry, 15*(2), 103626. https://doi.org/10.1016/j.arabjc.2021.103626

Kutnowski, N., Shmulevich, F., Davidov, G., Shahar, A., Bar-Zvi, D., Eichler, J., & Shaanan, B. (2019). Specificity of protein–DNA interactions in hypersaline environment: structural studies on complexes of Halobacterium salinarum oxidative stress-dependent protein hsRosR. *Nucleic Acids Research, 47*(16), 8860-8873. https://doi.org/10.1093/nar/gkz604

Kypr, J., Kejnovská, I., Renčiuk, D., & Vorlíčková, M. (2009). Circular dichroism and conformational polymorphism of DNA. *Nucleic Acids Research, 37*(6), 1713-1725. https://doi.org/10.1093/nar/gkp026

Law, Y.-S., Utt, A., Tan, Y. B., Zheng, J., Wang, S., Chen, M. W., & Luo, D. (2019). Structural insights into RNA recognition by the Chikungunya virus nsP2 helicase. *Proceedings of the National Academy of Sciences, 116*(19), 9558-9567. https://doi.org/10.1073/pnas.1900656116

Maneerattanasak, S., Ngamprasertchai, T., Tun, Y. M., Ruenroengbun, N., Auewarakul, P., & Boonnak, K. (2024). Prevalence of dengue, Zika, and chikungunya virus infections among mosquitoes in Asia: A systematic review and meta-analysis. *International Journal of Infectious Diseases, 148*, 107226. https://doi.org/10.1016/j.ijid.2024.107226

Markham, N. R., & Zuker, M. (2005). DINAMelt web server for nucleic acid melting prediction. *Nucleic acids research*, *33*(Web Server issue), W577–W581. https://doi.org/10.1093/nar/gki591

Martin, B., Dans, P. D., Wieczor, M., Villegas, N., Brun-Heath, I., Battistini, F., & Orozco, M. (2022). Molecular basis of Arginine and Lysine DNA sequence-dependent thermo-stability modulation. *PLOS Computational Biology, 18*(1), e1009749. https://doi.org/10.1371/journal.pcbi.1009749

Martin, C. K., Wan, J. J., Yin, P., Morrison, T. E., Messer, W. B., Rivera-Amill, V., & Kielian, M. (2025). The alphavirus determinants of intercellular long extension formation. *mBio, 16*(2), e01986-01924. https://doi.org/10.1128/mbio.01986-24

Mastalipour, M., Gering, I., Coronado, M. A., González, J. E. H., Willbold, D., & Eberle, R. J. (2025). Novel peptide inhibitor for the Chikungunya virus nsP2 protease: Identification and characterization. *Current Research in Microbial Sciences, 8*, 100376. https://doi.org/10.1016/j.crmicr.2025.100376

Nikolakaki, E., & Giannakouros, T. (2020). SR/RS motifs as critical determinants of coronavirus life cycle. *Frontiers in molecular biosciences, 7*, 219. https://doi.org/10.3389/fmolb.2020.00219

Noranate, N., Takeda, N., Chetanachan, P., Sittisaman, P., A-Nuegoonpipat, A., & Anantapreecha, S. (2014). Characterization of chikungunya virus-like particles. *PloS one*, *9*(9), e108169. https://doi.org/10.1371/journal.pone.0108169

Ogino, T., & Banerjee, A. K. (2010). The HR motif in the RNA-dependent RNA polymerase L protein of Chandipura virus is required for unconventional mRNA-capping activity. *Journal of General Virology, 91*(5), 1311-1314. https://doi.org/10.1099/vir.0.019307-0

Pavia, G., Branda, F., Ciccozzi, A., Romano, C., Locci, C., Azzena, I., & Scarpa, F. (2025). The issue of climate change and the spread of tropical diseases in Europe and Italy: vector biology, disease transmission, genome-based monitoring and public health implications. *Infectious Diseases, 57*(2), 121-136. https://doi.org/10.1080/23744235.2024.2437027

Potempa, M., Nalivaika, E., Ragland, D., Lee, S.-K., Schiffer, C. A., & Swanstrom, R. (2015). A Direct Interaction with RNA Dramatically Enhances the Catalytic Activity of the HIV-1 Protease In Vitro. *Journal of Molecular Biology, 427*(14), 2360-2378. https://doi.org/10.1016/j.jmb.2015.05.007

Qi, R., Wang, Q., & Ren, P. (2016). General van der Waals potential for common organic molecules. *Bioorganic & medicinal chemistry, 24*(20), 4911-4919. https://doi.org/10.1016/j.bmc.2016.07.062

Rausalu, K., Utt, A., Quirin, T., Varghese, F. S., Žusinaite, E., Das, P. K., & Merits, A. (2016). Chikungunya virus infectivity, RNA replication and non-structural polyprotein processing depend on the nsP2 protease's active site cysteine residue. *Scientific Reports, 6*(1), 37124. https://doi.org/10.1038/srep37124

Resck, M. E. B., Câmara, D. C. P., Dos Santos, F. B., Dos Santos, J. P. C., Alto, B. W., & Honório, N. A. (2024). Spatial–temporal distribution of chikungunya virus in Brazil: a review on the

circulating viral genotypes and Aedes (Stegomyia) albopictus as a potential vector. *Frontiers in Public Health, 12*, 1496021. https://doi.org/10.3389/fpubh.2024.1496021

Sagar, R., Raghavendhar, S., Jain, V., Khan, N., Chandele, A., Patel, A. K., & Kapoor, N. (2024). Viremia and clinical manifestations in acute febrile patients of Chikungunya infection during the 2016 CHIKV outbreak in Delhi, India. *Infectious Medicine, 3*(1), 100088. https://doi.org/10.1016/j.imj.2024.100088

Saisawang, C., Kuadkitkan, A., Smith, D. R., Ubol, S., & Ketterman, A. J. (2017). Glutathionylation of chikungunya nsP2 protein affects protease activity. *Biochimica et Biophysica Acta (BBA) - General Subjects, 1861*(2), 106-111. https://doi.org/10.1016/j.bbagen.2016.10.024

Silva, L. A., & Dermody, T. S. (2017). Chikungunya virus: epidemiology, replication, disease mechanisms, and prospective intervention strategies. *Journal of Clinical Investigation, 127*(3), 737-749. https://doi.org/10.1172/JCI84417

Silveira-Freitas, J. E. P., Campagnolo, M. L., Dos Santos Cortez, M., de Melo, F. F., Zarpelon-Schutz, A. C., & Teixeira, K. N. (2024). Long chikungunya? An overview to immunopathology of persistent arthralgia. *World journal of virology*, *13*(2), 89985. https://doi.org/10.5501/wjv.v13.i2.89985

Sosnick, T. R., Fang, X., & Shelton, V. M. (2000). Application of circular dichroism to study RNA folding transitions. In *Methods in Enzymology* (Vol. 317, pp. 393-409): Academic Press. https://doi.org/10.1016/s0076-6879(00)17026-0

Sreekumar, E., Issac, A., Nair, S., Hariharan, R., Janki, M. B., Arathy, D. S., & Pillai, M. R. (2010). Genetic characterization of 2006–2008 isolates of Chikungunya virus from Kerala, South India, by whole genome sequence analysis. *Virus Genes, 40*(1), 14-27. https://doi.org/10.1007/s11262-009-0411-9

Stracker, T. H., Cassell, G. D., Ward, P., Loo, Y.-M., Breukelen, B. v., Carrington-Lawrence, S. D., & Weitzman, M. D. (2004). The Rep Protein of Adeno-Associated Virus Type 2 Interacts with Single-Stranded DNA-Binding Proteins That Enhance Viral Replication. *Journal of Virology, 78*(1), 441-453. https://doi.org/10.1128/jvi.78.1.441-453.2004

tenOever, B. R. (2016). The Evolution of Antiviral Defense Systems. *Cell host & microbe*, *19*(2), 142–149. https://doi.org/10.1016/j.chom.2016.01.006

Urvil, P. T., Kakiuchi, N., Zhou, D.-M., Shimotohno, K., Kumar, P. K. R., & Nishikawa, S. (1997). Selection of RNA Aptamers that Bind Specifically to the NS3 Protease of Hepatitis C Virus. *European Journal of Biochemistry, 248*(1), 130-138. https://doi.org/10.1111/j.1432-1033.1997.t01-1-00130.x

van Aalst, M., Nelen, C. M., Goorhuis, A., Stijnis, C., & Grobusch, M. P. (2017). Long-term sequelae of chikungunya virus disease: A systematic review. *Travel Medicine and Infectious Disease, 15*, 8-22. https://doi.org/10.1016/j.tmaid.2017.01.004

Ware, B. C., Parks, M. G., da Silva, M. O. L., & Morrison, T. E. (2024). Chikungunya virus infection disrupts MHC-I antigen presentation via nonstructural protein 2. *PLOS Pathogens, 20*(3), e1011794. https://doi.org/10.1371/journal.ppat.1011794

Weber, W. C., Streblow, D. N., & Coffey, L. L. (2024). Chikungunya Virus Vaccines: A Review of IXCHIQ and PXVX0317 from Pre-Clinical Evaluation to Licensure. *BioDrugs, 38*(6), 727-742. https://doi.org/10.1007/s40259-024-00677-y

Wu, C., Zhang, F., Jia, P., Zhu, J., Zeng, M., Hu, G., & Li, M. (2025). PROBind: A Web Server for Prediction, Analysis and Visualization of Protein-Protein and Protein-Nucleic Acid Binding Residues. *bioRxiv*, 2025.2002.2008.637237. https://doi.org/10.1101/2025.02.08.637237

Wu, L., Yan, Y., Yuan, Y., Zhao, Z., Qu, W., Huang, X., & Li, X. (2025). Viral protease binds to nucleosomal DNA and cleaves nuclear cGAS that attenuates type I interferon. *mBio, 16*(4), e03395-03324. https://doi.org/10.1128/mbio.03395-24

Xu, G., Wang, C., Yu, H., Li, Y., Zhao, Q., Zhou, X., & Liu, M. (2023). Structural basis for high-affinity recognition of aflatoxin B1 by a DNA aptamer. *Nucleic Acids Research, 51*(14), 7666-7674. https://doi.org/10.1093/nar/gkad541

Yan, Y., Tao, H., He, J., & Huang, S.-Y. (2020). The HDOCK server for integrated protein–protein docking. *Nature Protocols, 15*(5), 1829-1852. https://doi.org/10.1038/s41596-020-0312-x

Yin, J., Chen, R., & Liu, C. (2009). Nucleic acid induced protein aggregation and its role in biology and pathology. *Front Biosci (Landmark Ed), 14*, 5084-5106. https://doi.org/10.2741/3588

Zhang, D., Qiu, Z., Hao, Y., Yuan, Y., Ma, W., Li, N., & Xiao, P. (2025). Progress in the molecular epidemiology of Chikungunya Virus. *Animals and Zoonoses*. https://doi.org/10.1016/j.azn.2025.01.003

Single-Stranded nucleic acid binding enhances the in vitro catalytic activity of Chikungunya virus nsP2 protease

Mohammadamin Mastalipour[1], Mônika Aparecida Coronado[1,2], Ruth Anasthasia Siahaan[3], Alissa Drees[4], Christian Ahlers[4], Markus Fischer[4], Dieter Willbold[1,2], Raphael Josef Eberle[5]

[1] Institut für Physikalische Biologie, Heinrich-Heine-Universität Düsseldorf, Universitätsstraße 1, 40225 Düsseldorf, Germany

[2] Institut für Biologische Informationsprozesse, Strukturbiochemie (IBI-7), Forschungszentrum Jülich, 52425 Jülich, Germany

[3] Faculty of Chemistry and Biotechnology, FH Aachen, Campus Jülich, 52428 Jülich, Germany

[4] Hamburg School of Food Science, Institute of Food Chemistry, University of Hamburg, Grindelallee 117, 20146 Hamburg, Germany

[5] Institut für Biochemische Pflanzenphysiologie, Heinrich-Heine-Universität Düsseldorf, Universitätsstraße 1, 40225 Düsseldorf, Germany

Table of content

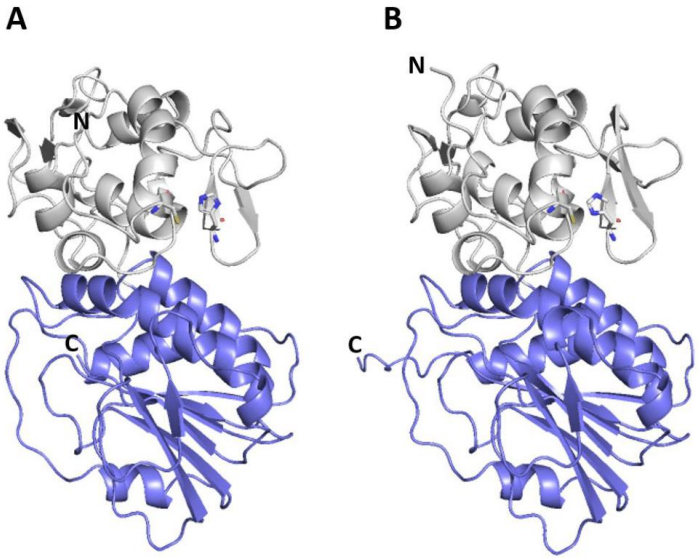

Fig. S1. Structural comparison of the nsP2^{pro} structure and the generated nsP2^{pro} AlphaFold model. Both structures are shown in ribbon view, the papain-like cysteine protease is colored in grey and the Ftsj methyltransferase (MTase)-like domain in blue. An overlay of both structures indicated a RMSD value of 0.435 (2165 to 2165 atoms). **(A)** nsP2^{pro} crystal structure (PDB code: 3TRK) and **(B)** nsP2^{pro} AlphaFold 3 model.

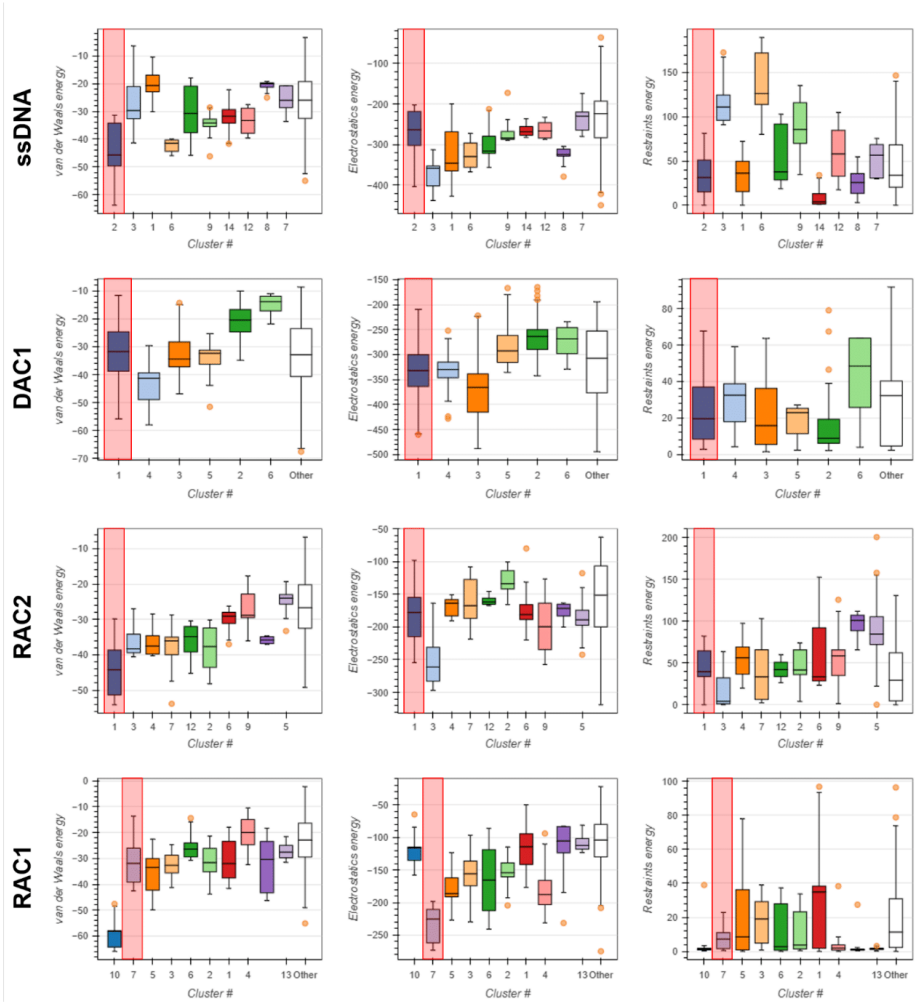

Fig. S2. Van der Waals energy, electrostatic energy and restraints energy of the generated clusters after protein-nucleic acid blind docking using HDOCK. Red boxes label the representative cluster for each nucleic acid.

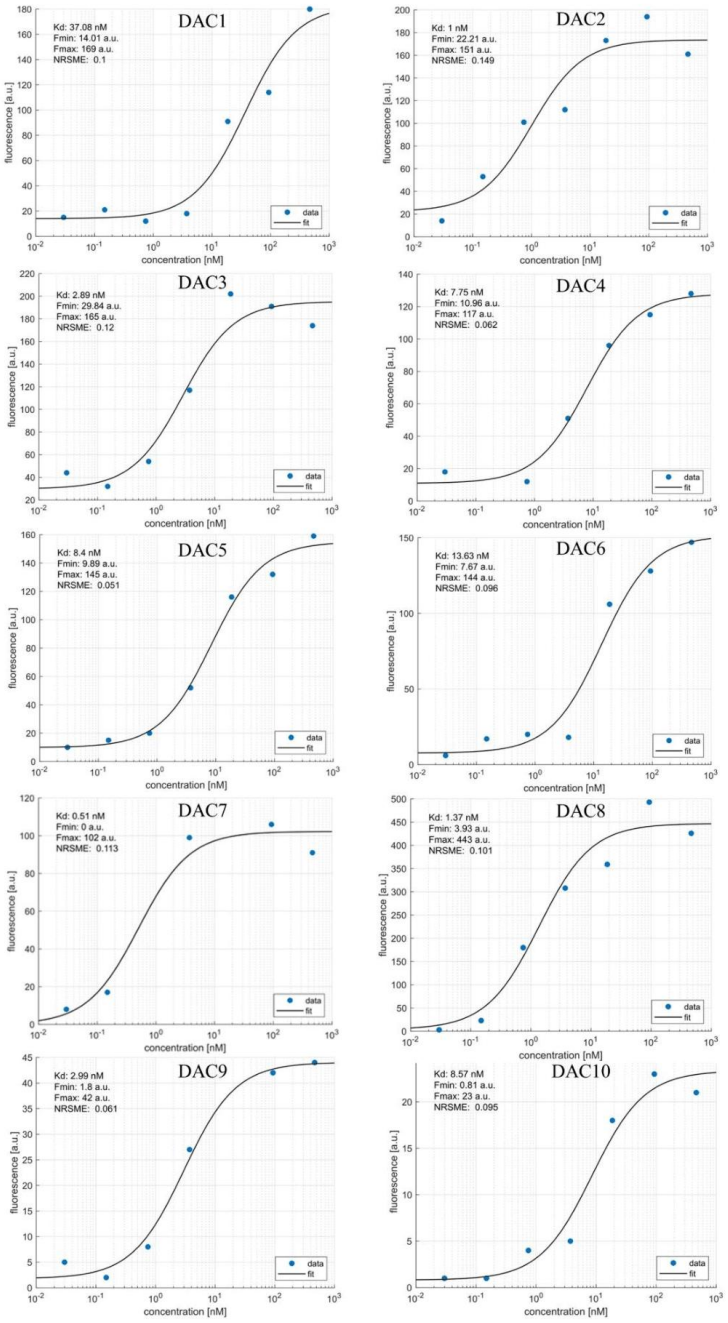

Fig. S3. K_D fitting of DNA aptamers DAC1–DAC10. Binding affinities for DAC1–DAC10 were determined using HiTS-FLIP, and the data were fitted using a nonlinear Hill-fit.

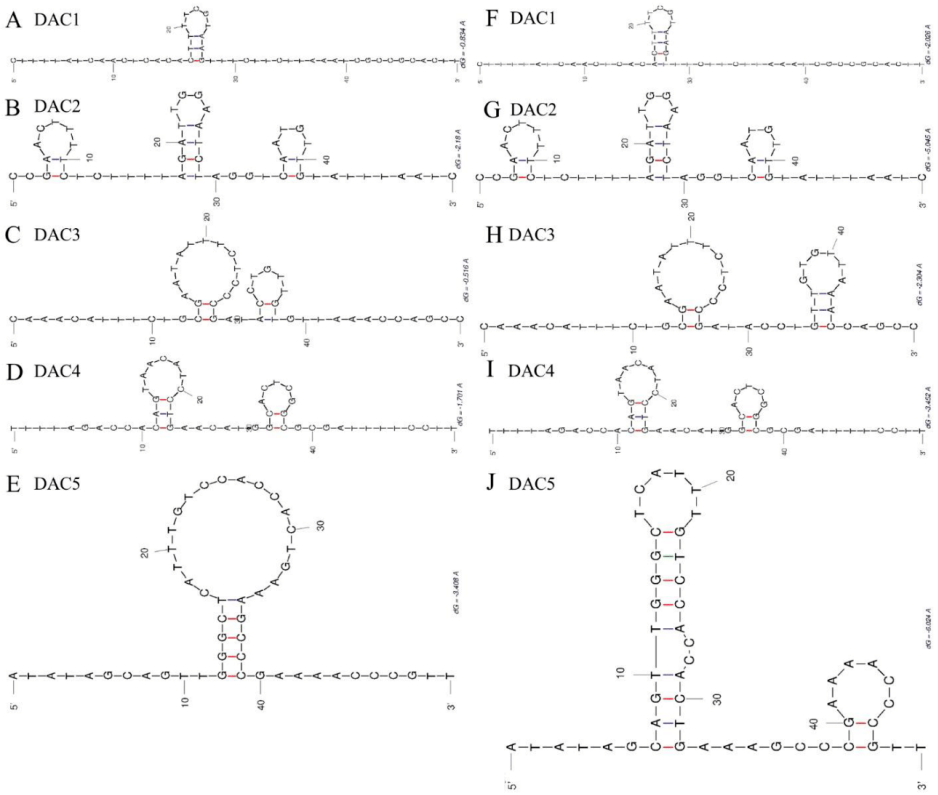

Fig. S4. Predicted secondary structures of DAC1–DAC5. Panels (A–E) show the predicted secondary structures of DAC1–DAC5 in water at 18°C, and panels (F–J) display the corresponding structures in 1×PBS at 18°C. Predictions were generated using the DINAMelt Server – Quikfold web tool, and only the structure with the lowest ΔG (Gibbs free energy) was presented.

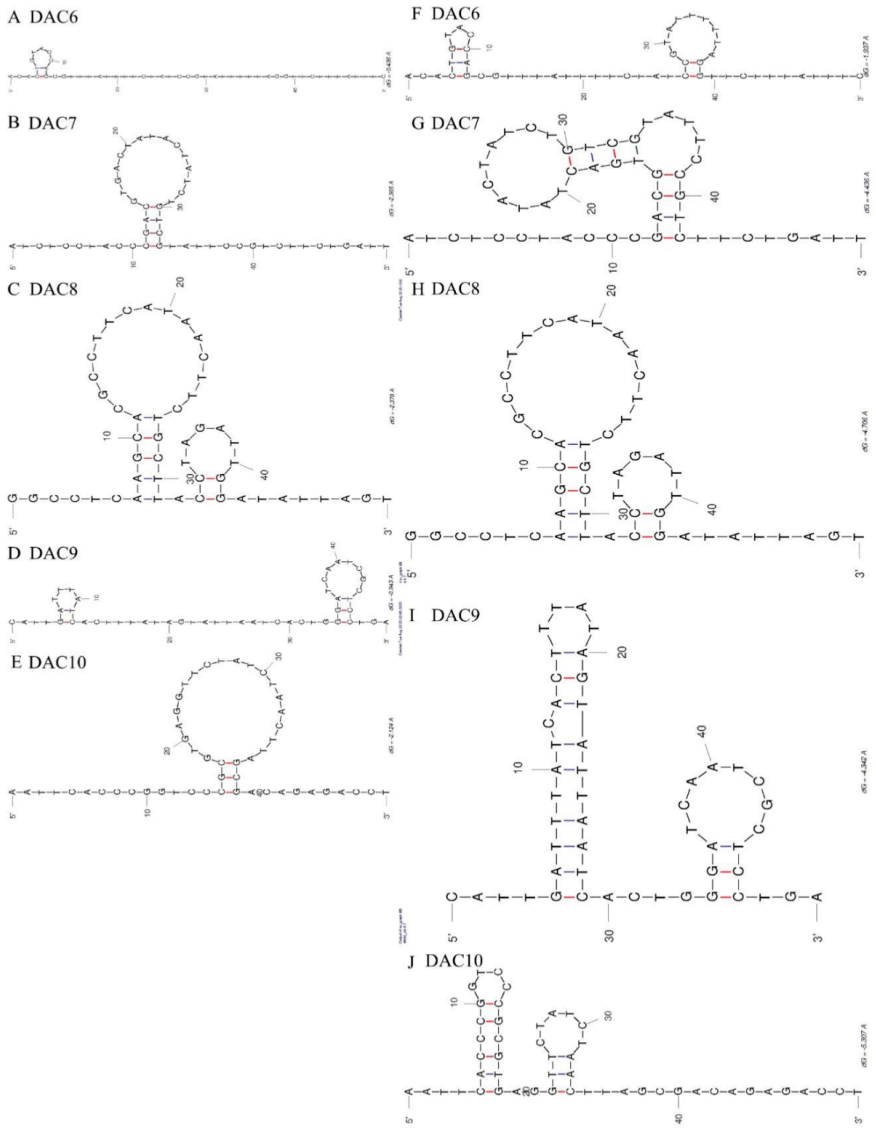

Fig. S5. Predicted secondary structures of DAC6–DAC10. Panels (A–E) show the predicted secondary structures of DAC6–DAC10 in water at 18°C, and panels (F–J) display the corresponding structures in 1×PBS at 18°C. Predictions were generated using the DINAMelt Server – Quikfold web tool, and only the structure with the lowest ΔG (Gibbs free energy) was presented.

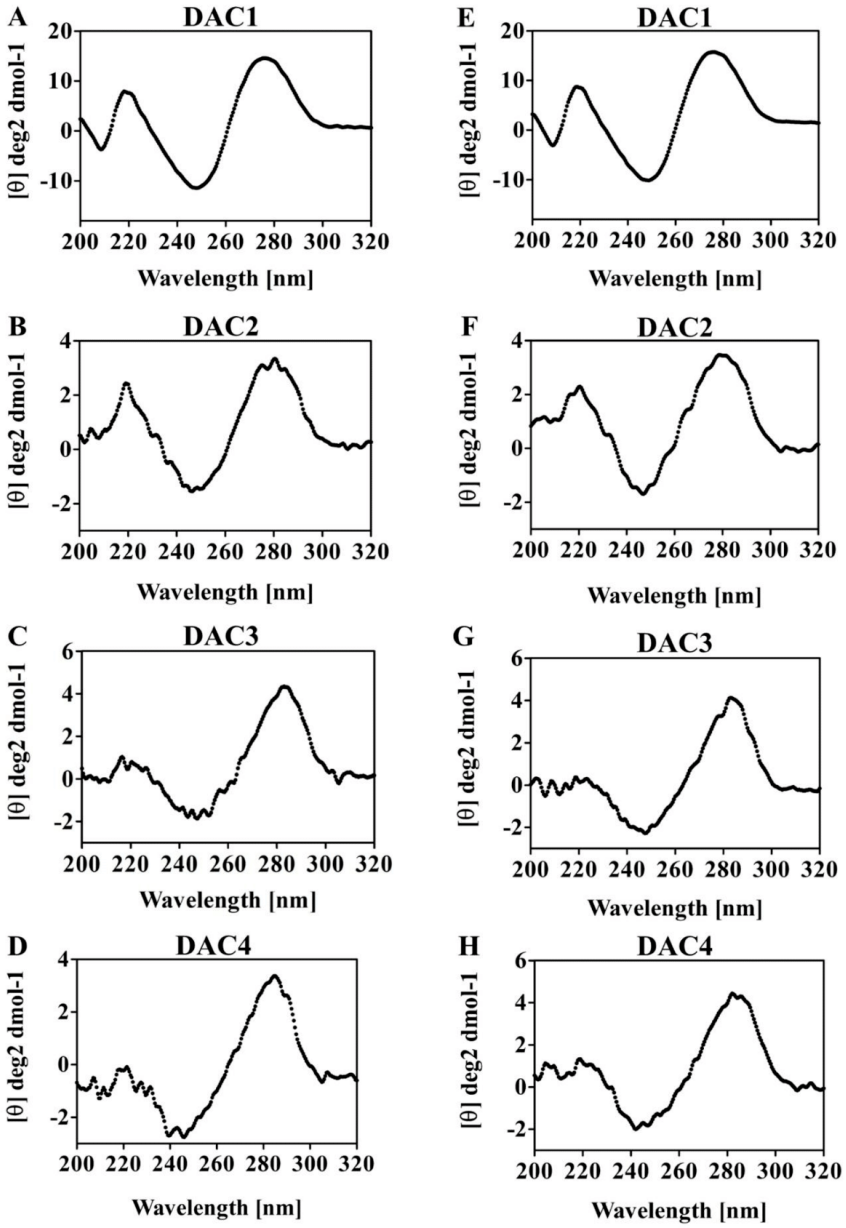

Fig. S6. **Secondary structure of DAC1–DAC4.** Panels (A–D) show the CD spectra of DAC1–DAC4 in water at 18°C, while panels (E–H) present the corresponding spectra in 1×PBS at 18°C. All spectra were recorded over the wavelength range of 320–200 nm

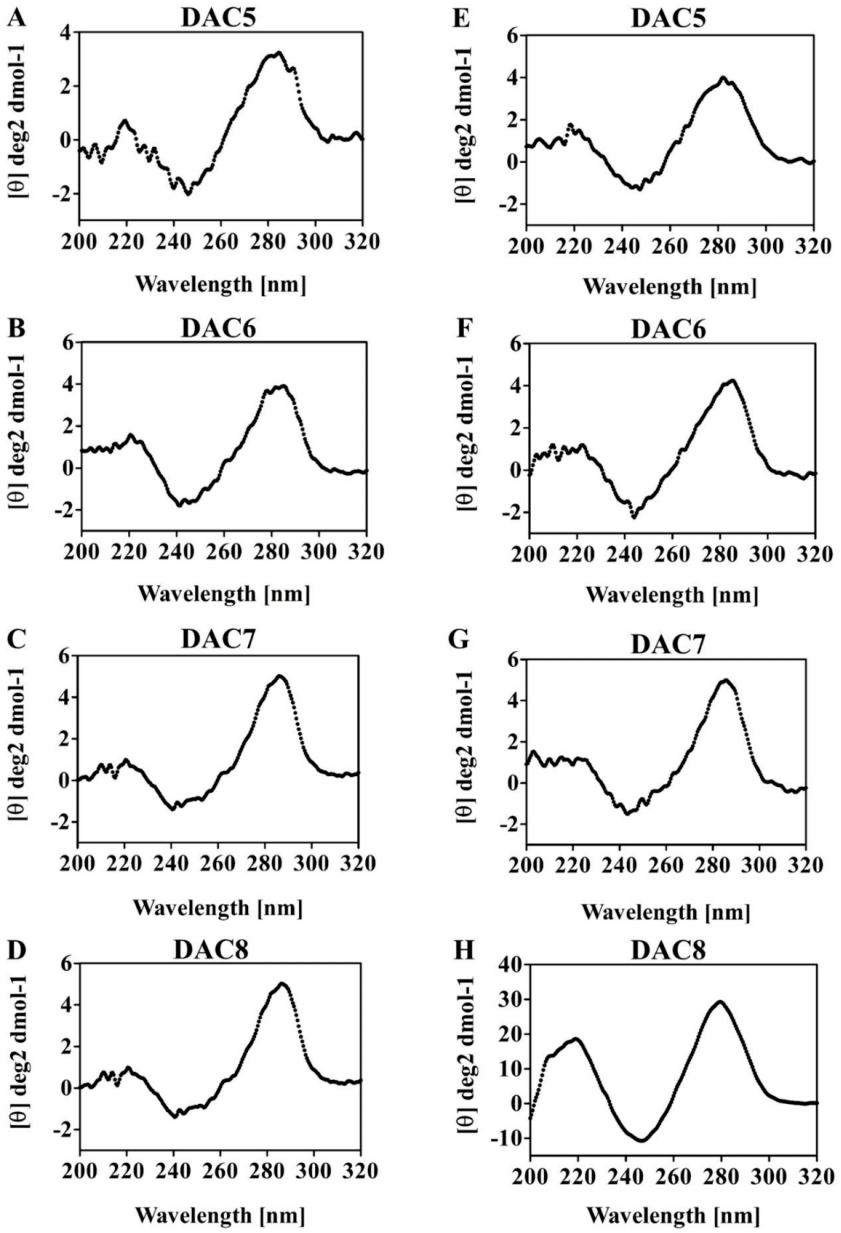

Fig. S7. **Secondary structure of DAC5–DAC8.** Panels (A–D) show the CD spectra of DAC5–DAC8 in water at 18°C, while panels (E–H) present the corresponding spectra in 1×PBS at 18°C. All spectra were recorded over the wavelength range of 320–200 nm

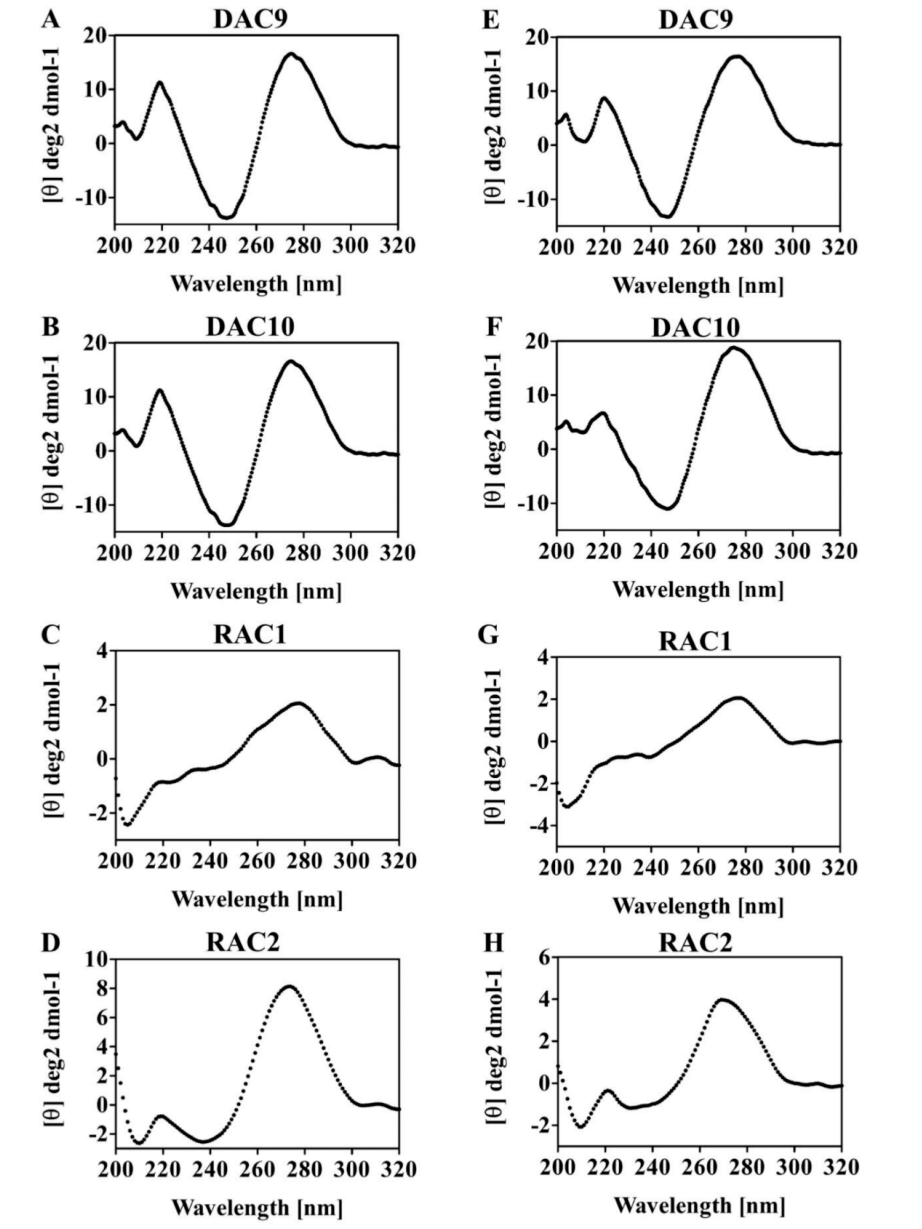

Fig. S8. **Secondary structure of DAC9–DAC10 and RAC1-RAC2.** Panels (A–D) show the CD spectra of DAC9–DAC10 and RAC1-RAC2 in water at 18°C, while panels (E–H) present the corresponding spectra in 1×PBS at 18°C. All spectra were recorded over the wavelength range of 320–200 nm

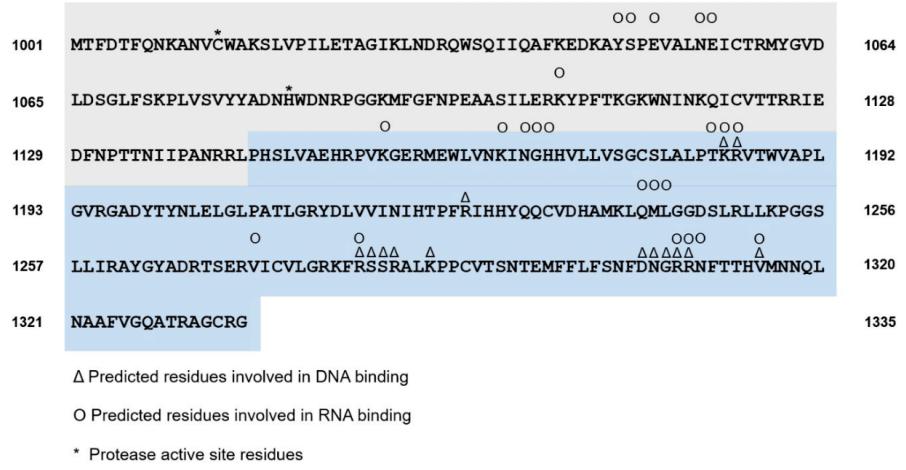

Fig. S9. Predicted nucleic acid binding regions in the nsP2^{pro} sequence. The papain-like cysteine protease sequence is displayed with a grey background and the Ftsj methyltransferase (MTase)-like domain is highlighted in blue. The sequence numbering based on the CHIKV polyprotein. Predicted amino acids involved in DNA binding are labeled by a triangle and those predicted to be involved in RNA binding are labeled by a circle. The catalytically active residues of the cysteine protease are labeled by asterisks.

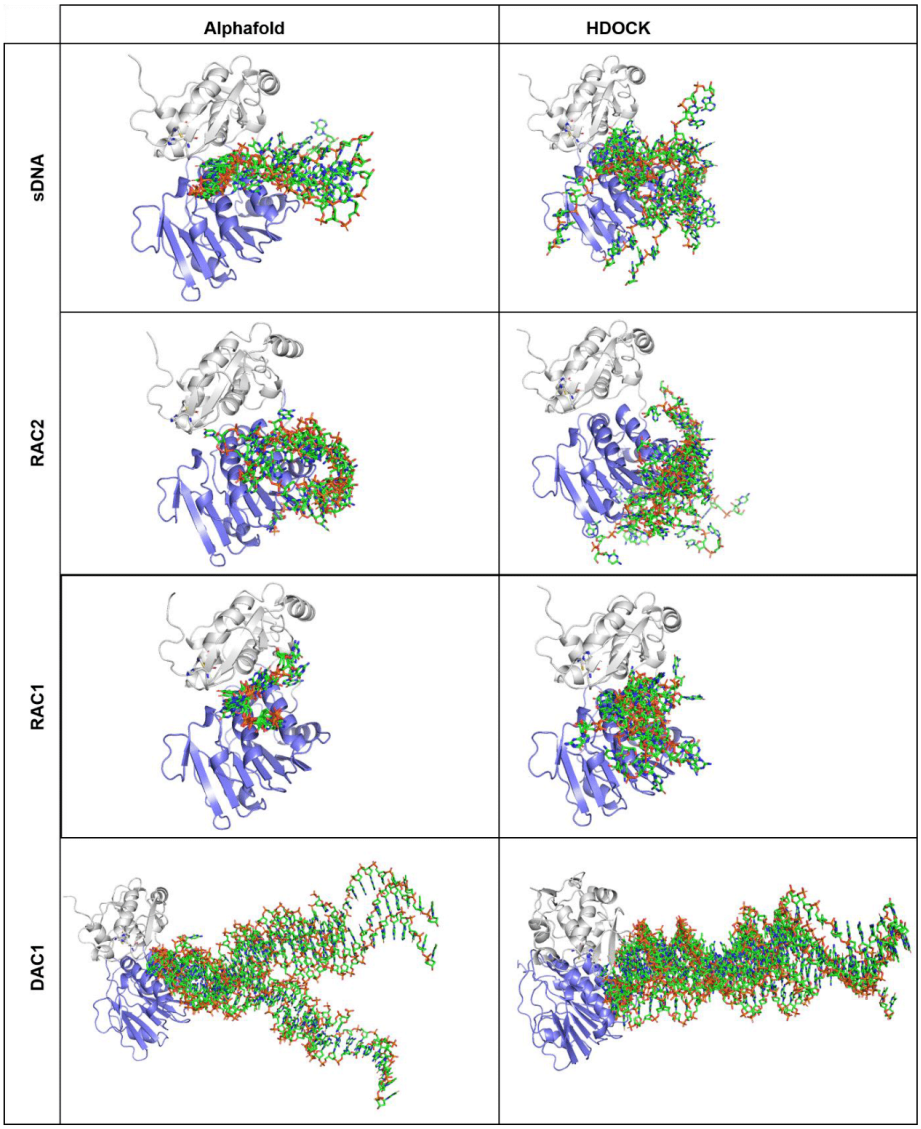

Fig. S10. Overlay of the predicted nucleic acid positions for AlphaFold models and HDOCK results. The nsp2^{pro} structures are shown in ribbon view, the papain-like cysteine protease is colored in grey and the Ftsj methyltransferase (MTase)-like domain in blue. The nucleic acids are shown as sticks and in green color. AlphaFold, generated five structures per complex and the overlay of these five structures are shown. The docking with HDOCK generated clusters and the best results of each cluster (depending on the HDOCK score) was used for the overlay.

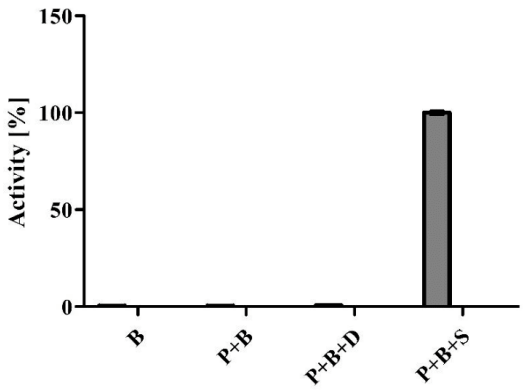

Fig. S11. Control experiments confirm substrate-specific fluorescence signal in the nsP2^{pro} activity assay. Fluorescence intensity was measured under four conditions to evaluate potential background signal in the absence of the fluorogenic substrate: (1) buffer alone (B), (2) buffer with CHIKV nsP2^{pro} (P), and (3) buffer with both protease and DNA aptamer DAC8 (D). A positive control containing buffer, protease, and the fluorogenic substrate (Control) was included to represent true enzymatic activity. No significant fluorescence was detected in the absence of the substrate, confirming that background signal from buffer components, protease, or DNA aptamer was negligible.

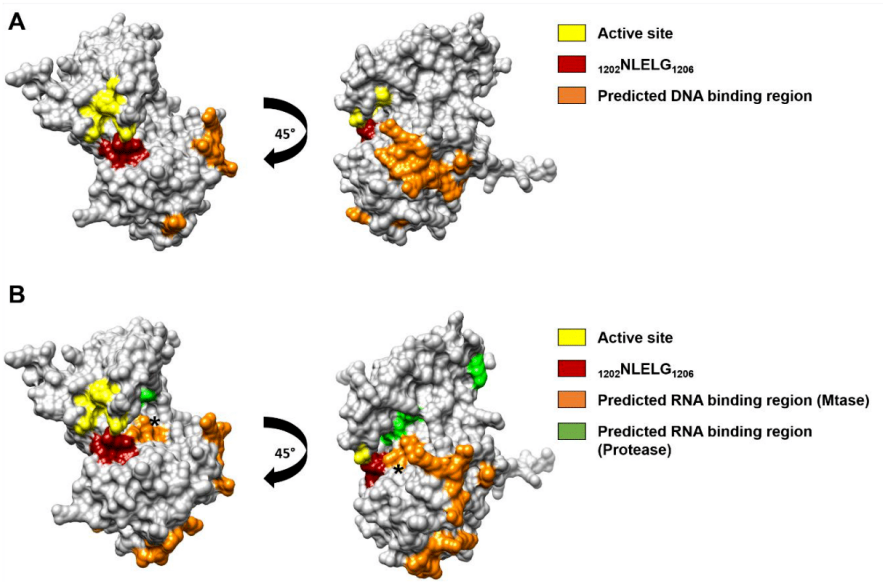

Fig. S12. Surface view of nsP2^{pro} with labeled predicted nucleic acid binding areas, protease active site and MTase loop $_{1202}$NLELG$_{1206}$. The nsP2^{pro} active site is shown in close conformation were the protease active site residues Cys1013 and His1083 and the Mtase loop $_{1202}$NLELG$_{1206}$ are nearby. A: Predicted DNA binding region. B: Predicted RNA binding region. Asterisk label the position of $_{1241}$QML$_{1243}$.

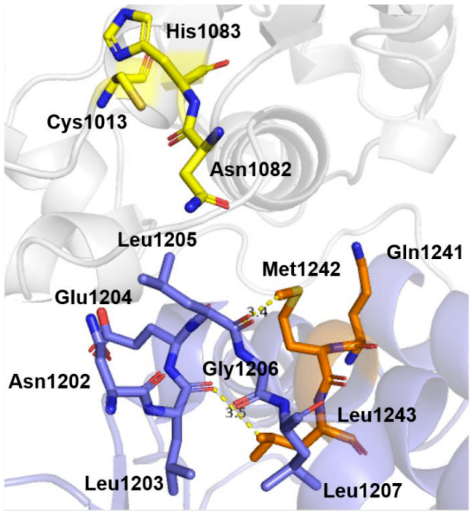

Fig. S13. Closed conformation of the nsP2^{pro} active site with $_{1202}$NLELG$_{1206}$ and possible $_{1241}$QML$_{1243}$ interactions. The nsP2^{pro} active site residues are colored in yellow. The Mtase loop $_{1202}$NLELG$_{1206}$ is colored in blue and the Mtase region $_{1241}$QML$_{1243}$ is colored in orange.

Table S1. Sequences and properties of the RNAs used in this study. The RNA sequences were derived from the Chikungunya virus (CHIKV) genome (associated GenBank accession: KM673291).

RNA	Sequence (5'-3')	Origin	Tm [°C]	Manufacturer
RAC1	CGTUCG	CHIKV genome	0.0	Integrated DNA Technologies (IDT)
RAC2	CGUCGCUAUA	CHIKV genome	21.1	Integrated DNA Technologies (IDT)

3.4 Additional results (not published): Effect of nucleic acid on inhibitory potential of the peptide P1

To evaluate the influence of nucleic acids on the inhibitory effect of peptide P1, a FRET-based assay (as described in section 3.1) was performed. The assay was conducted in 20 mM Bis-Tris propane buffer (pH 7.5) at 37 °C, using 10 µM protease. The assay included a control, 50 µM peptide P1 alone, 10 µM DAC 8 as a representative nucleic acid (see section 3.3), and a mixture of 50 µM peptide P1 with 10 µM DAC 8. The enzymatic assay revealed, as shown in section 3.1, that peptide P1 is able to inhibit the protease and reduce its catalytic activity, while DAC8, as described in section 3.3, increased the activity by more than 10-fold compared to the control. In the case of the mixture of P1 and DAC8, the activity dropped to below 2-fold compared to DAC8 alone, but remained significantly higher than both the control and P1 alone (Fig. 9).

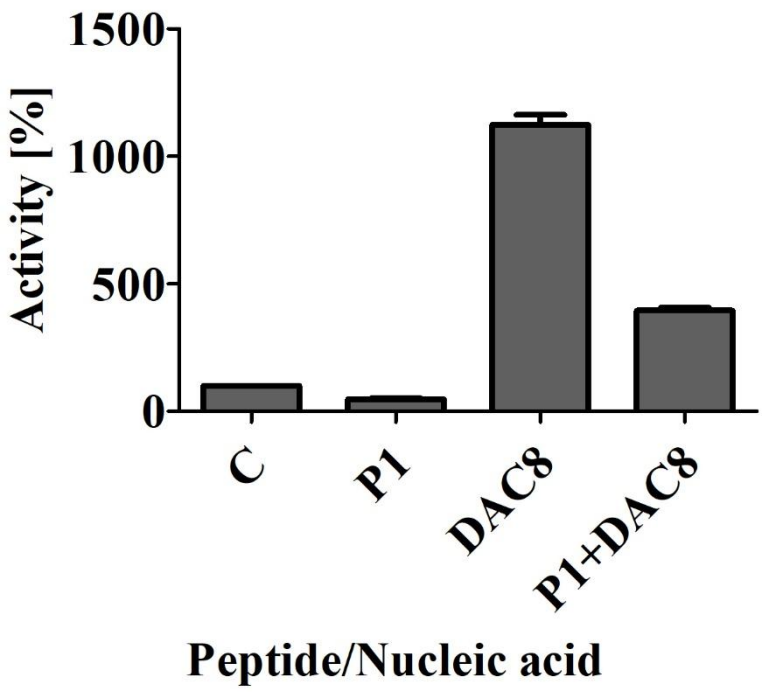

Fig. 9. Effect of peptide P1, DAC8, and their combination on the catalytic activity of CHIKV nsP2^{pro}. The assay was performed in 20 mM Bis-Tris propane buffer (pH 7.5) at 37 °C, using 10 µM protease and 9 µM fluorogenic substrate. Peptide P1 was used at a concentration of 50 µM and DAC8 at 10 µM. The assay was performed in triplicate, and the results are shown as mean ± standard deviation (SD).

4. Discussion

Chikungunya fever is caused by the chikungunya virus (CHIKV), an arthropod-borne virus (Arbovirus) that belongs to the family *Togaviridae* [18, 181] . CHIKV is mainly transmitted by mosquito bites (*Aedes* spp.), and it has spread globally due to environmental changes, posing a growing public health concern [1-3]. CHIKV replication depends on its non-structural protein 2 protease activity (nsP2^{pro}), which is responsible for the cleavage of the viral polyprotein 1234 [73]. Owing to the significance of this role in viral replication, nsp2^{pro} was chosen as a target for the development of antiviral therapy. There have been many attempts to identify inhibitors against nsP2^{pro}, and numerous agents ranging from small molecules to peptide inhibitors have been discovered. However, none of them have been approved for therapeutic use [124]. In addition the regulation of the protease activity of nsP2 is poorly studied, although it may play an important role in antiviral research. In this work, two approaches, phage display and a peptide derived from animal venom, were used to identify potential inhibitors against CHIKV nsP2^{pro}. In addition, the inhibitory properties and protein-peptide interactions were characterized using biophysical and biochemical methods. Finally, to further explore the catalytic activity of nsP2^{pro} in the presence of nucleic acids, the influence of different nucleic acids on nsP2^{pro} was evaluated, including their effect on peptide inhibition.

4.1 Biochemical properties of phage display selected peptides and pantinin-1

Two approaches were used to identify peptide-based inhibitors against CHIKV nsP2^{pro}. First, phage display were performed, and six different peptides (named P1 to P6) with the highest enrichment and empty scores were selected (Section 3.1, Table 4). As a second approach, a venom-derived peptide was evaluated as a potential inhibitor. Pantinin-1, an α-helical, amphipathic peptide derived from scorpion venom with known antimicrobial properties [156-157], was selected as a candidate inhibitor of nsP2^{pro}.

To assess and validate whether the selected peptides from both approaches were functionally active and capable of inhibiting protease activity, a FRET-based inhibition assay (referred to as the primary inhibition assay) was performed. This assay revealed that four of the six phage display selected peptides inhibited nsP2^{pro} activity and reduced protease catalytic activity by up to 50% (Section 3.1, Fig. 2A). The IC_{50} values indicated that peptide P1, with an IC_{50} of 4.6 ± 1.8 µM and complete inhibition at approximately 175 µM, exhibited the strongest inhibitory effect compared to P2 (IC_{50} = 194.7 ± 4.4 µM) and P5 (IC_{50} = 316.9 ± 7.1 µM) (Section 3.1, Fig. 3A-C; Fig. S7). Due to peptide aggregation under experimental conditions, the IC_{50} of P4 could not be determined.

To confirm sequence specificity, three scrambled versions of peptide P1 were tested and showed low inhibitory effects on protease activity (Section 3.1, Fig. 2B), indicating that the inhibitory activity is sequence-dependent. These results underscore the strength of peptide diversity generated by phage display, while also highlighting its limitation, namely, that not all binders have functional inhibition.

Additionally, the primary inhibition assay demonstrated that pantinin-1 is also capable of inhibiting protease activity, with an IC_{50} of 6.4 ± 2.04 µM. Increasing the concentration to 175 µM resulted in complete inhibition of $nsP2^{pro}$ (Section 3.2, Fig. 1B-C).

Various other inhibitors against CHIKV $nsP2^{pro}$ have been reported in the literature (Section 3.1, Table 5). For example, Singh et al. identified two peptidomimetics, Pep-I (IC_{50} = 34 µM) and Pep-II (IC_{50} = 42 µM) [138], with inhibitory effects against $nsP2^{pro}$. Compared to these, peptide P1 exhibits approximately ninefold lower IC_{50}, indicating stronger inhibition. Pantinin-1 also showed higher inhibition, with an IC_{50} approximately 6 times lower than those of Pep-I and Pep-II. A comparison with small molecules such as 1,3-thiazolbenzamide derivatives, including compound 10 (IC_{50} = 13.1 µM) and compound 10c (IC_{50} = 8.3 µM) [139], as well as Hesperetin (IC_{50} = 2.5 ± 0.4 µM), Hesperidin (IC_{50} = 7.1 ± 1.1 µM) [129], Telmisartan (IC_{50} = 5 µM) [130], shows that pantinin-1 and peptide P1 possess comparable inhibitory effects in the low micromolar range. In contrast, the small molecule RA-0002034 exhibits a significantly higher inhibitory effect, with an IC_{50} of 0.058 ± 0.017 µM, likely due to its covalent binding to the enzyme's active site [125].

Understanding the mechanism of inhibition is essential for developing lead compounds. To investigate the mode of inhibition for both peptide P1 and pantinin-1, inhibition mode assays were performed and analyzed using Lineweaver-Burk plots. The results showed an increase in the Michaelis-Menten constant (K_m) and an interception point on the y-axis, indicating that the maximum reaction velocity (V_{max}) remained unchanged (Section 3.1, Fig. 4A; Section 3.2, Fig. 1D). This indicates that both peptides act as competitive inhibitors [182, 183]. Competitive inhibitors bind to the active site of an enzyme, directly competing with the substrate [184]. A highlight of this inhibition type is its high specificity by binding to the active site and being used in the development of drugs with high specificity against the target, which reduces the probability of off-target effects. However, the efficiency of competitive inhibitors can be limited under conditions of high substrate concentration [185] such as in the case of the CHIKV p1234 polyprotein, which may be abundant in infected host cells. In contrast, non-competitive and uncompetitive inhibitors bind to allosteric sites. Their highlight is that their efficacy is independent of substrate concentration [185]. Non-competitive inhibitors are usually used in development of drugs with multiple binding sites (lower specificity compared to competitive inhibitors) [185]. Uncompetitive inhibitors are often less utilized due to the requirement for an enzyme-substrate complex [185].

The equilibrium dissociation constant (K_D) is another critical parameter for drug development. It reflects binding affinity, or the strength of interaction between two molecules, and provides insight into concentration-dependent interactions [186]. Methods for determining K_D include surface plasmon resonance (SPR), microscale thermophoresis (MST), and biolayer interferometry (BLI) [187, 188].The K_D of peptide P1, determined using MST, was 1.39 ± 0.61 µM, indicating low micromolar affinity (Section 3.1, Fig. 4B). For pantinin-1, BLI analysis combined with Scatchard plot evaluation revealed a K_D of 9.29 µM (Section 3.2, Fig. S2A-B). While both peptides have K_D values in the micromolar range, peptide P1 exhibits approximately ninefold stronger binding affinity compare to the pantinin-1. In comparison to small molecules such as Hesperetin (K_D = 31.6 ± 2.5 µM) [129], Hesperidin (K_D = 40.7 ± 2.0 µM) [129], and MBZM-N-IBT (K_D = 6.14 ± 0.58 µM) [140], both peptides display considerably lower or similar K_D values. However, it should be noted that the K_D values of these molecules were determined using different methods, which may account for the variation in the constants and reduce the reliability of direct comparison.

4.2 Cytotoxicity effects of peptide P1 and pantinin-1

One of the critical aspects in drug development, especially before entering the late stages, is the evaluation of cytotoxicity [189]. Cytotoxicity testing provides essential information about the concentration at which a molecule induces cell death and helps assess potential off-target effects on healthy cells [189, 190]. One commonly used method to evaluate cytotoxicity is the MTT assay. This assay relies on the mitochondrial activity of viable cells to convert MTT (3-[4,5-dimethylthiazol-2-yl]-2,5-diphenyl tetrazolium bromide) into formazan crystals, which correlates with the number of viable cells [190]. To evaluate the cytotoxicity of peptide P1, two distinct MTT assays were performed: one with P1 dissolved in water and one with P1 dissolved in DMSO. The MTT assay with P1 dissolved in water revealed that peptide P1 exhibited low toxicity up to a concentration of 100 µM, with approximately 77% cell viability (Section 3.1, Fig. 4C). In contrast, the MTT assay with P1 dissolved in DMSO showed significantly higher toxicity, with cell viability dropping below 50% at a concentration of 100 µM (Section 3.1, Fig. 4D). Other studies have reported that solvents such as DMSO can influence cell viability; specifically, DMSO has a toxic effect at concentrations above 1% [191]. To determine whether the observed toxicity in the DMSO-based assay was caused by the peptide or the solvent, a control MTT assay using different concentrations of DMSO was performed. The results revealed that DMSO alone reduced cell viability to below 50% at a concentration of 1% (Section 3.1, Fig. S10), which is comparable to the results observed in the P1 dissolved in DMSO assay. In other words, the observed toxicity was due to the solvent (DMSO), not peptide P1. The cytotoxicity effect of peptide P1 is comparable to peptidomimetics such as Pep-I, which showed low toxicity up to 100 µM in BHK-21 cells. In contrast, Pep-II showed no toxicity

up to 1 mM in BHK-21 cells [138]. However, it should be noted that, in addition to differences between peptides, different cell lines were used in this study and in the studies of Pep-I and Pep-II. This variation in cell lines can influence the outcomes of cytotoxicity evaluation and may affect the comparison between peptides. For example, Campoccia et al. reported that the antimicrobial peptide KSL showed different cytotoxic effects across three different cell lines [192]. Eberle et al. reported that two small molecules, Hesperetin and Hesperidin, exhibited low cytotoxicity, with over 70% cell viability at relevant concentrations [129]. Overall, comparison of the reported cytotoxicity data for Pep-I, Pep-II, Hesperetin, and Hesperidin suggests that peptide P1 exhibits low toxicity up to 100 µM, which is more than 20 times higher than its IC_{50} value, supporting its potential as a low-toxicity lead candidate.

In comparison, cytotoxicity assays demonstrated that pantinin-1 has a higher cytotoxic effect compared to peptide P1 and other known inhibitors. Pantinin-1 exhibited cytotoxicity above 20 µM; at 40 µM, cell viability dropped to approximately 50%, and at 60 µM and above, most cells were no longer viable. In contrast, peptide P1 showed only slight cytotoxicity beginning at 80 µM. The cytotoxicity of pantinin-1 may be attributed to its nature as an antimicrobial and hemolytic agent. As demonstrated by Zeng et al., pantinin-1 exhibited no hemolytic activity below 32 µM [157], which is consistent with the findings of this study. In comparison to the molecules mentioned above, pantinin-1 exhibits a higher cytotoxic effect.

Overall, these results highlight that both peptides exhibit low cytotoxicity at concentrations well above their IC_{50} values (approximately 20 times higher in the case of P1 and around 4 times higher for pantinin-1), which suggests a safe margin for further development and supports their potential as inhibitory candidates.

4.3 Structural analysis and molecular docking of phage display selected peptides and pantinin-1

To gain better insight into the structure of the selected peptides (P1-P6), the I-TASSER online tool (https://zhanggroup.org/I-TASSER/) was used to predict their 3D structures [193]. The predicted models for peptides P1, P3, and P5 exhibited a mixture of α-helical and random coil structures (Section 3.1, Fig. S8). In contrast, peptides P2, P4, and P6 consisted primarily of random coil structures. CD spectrometry analysis confirmed that peptides P1, P3, and P5 displayed characteristic spectra of α-helical structures, with a minimum between 200 and 220 nm and a maximum near 190 nm, aligning with the predicted models (Section 3.1, Fig. S8) [194]. The CD spectra of peptides P2, P4, and P6 showed a distinct minimum near 200 nm, indicating that these peptides primarily adopt a random coil structure, consistent with the predictions (Section 3.1, Fig. S8) [194]. The calculated secondary structure content from CD spectrometry and predicted models (Section 3.1, Table S3) showed that peptide P1 had the highest percentage of α-helical content compared to the other peptides. As Wang et al. described, α-helical structures play an important role in protein-protein interactions by stabilizing the complex [195] . In addition, a study on antimicrobial peptides has shown that a higher content of α-helical structure and hydrophobicity increases specificity and improves interaction with membranes (at least in prokaryotic membranes), leading to enhanced antimicrobial activity [196]. Furthermore, the α-helical structure can enhance hydrophobic interactions between non-polar amino acids on the amphipathic face of the helix and the lipid membrane [197]. This may explain the stronger inhibitory potential of peptide P1, in addition to its sequence specificity, and suggests that α-helical content contributes to the effectiveness of inhibition.

In this study, molecular docking simulations under conditions (T = 310 K, pH 7.4, t = 20 μs) demonstrated that 13% of the protease adopts an open (active) conformation, while 87% remains in a closed state (Section 3.1, Fig. 5), which supports the crystallographic findings by Narwal et al., indicating that nsP2^{pro} has a flexible active site flap that can lead to open or closed conformations of the active site [116]. Finally, blind docking was then performed using three different programs to predict the binding site of peptide P1 to nsP2^{pro}. Notably, all programs predicted interactions near the active site, as shown in the most stable binding pose (Section 3.1, Fig. 6). The predominant binding conformations of P1 were obtained from an extended molecular dynamics simulation (Section 3.1, Fig. 6B). Per-residue free energy decomposition of peptide P1(VMPWDEWLTKRKPELP) revealed that W4 (−8.2 kcal/mol), M2 (−4.8 kcal/mol), and W7 (−4.6 kcal/mol) significantly contributed to the binding of the peptide to the protease (Section 3.1, Fig. 7B). These residues are involved in hydrophobic interactions. Furthermore, residues W4 and W7 formed interactions with N1011 and Y1079 at the nsP2^{pro}

substrate-binding site [116]. In addition, residues K10 and R11 are involved in intermolecular hydrogen bonding. These results are in agreement with the inhibition mode assay, which indicated that the peptide acts as a competitive inhibitor.

Finally, to complement this analysis, molecular docking of nsP2^{pro} with the peptide pantinin-1 was performed using the same setup. The docking results showed that most predicted poses indicated binding at the active site (Section 3.2, Fig. 3A). However, ClusPro [198] and HDock [199] also predicted alternative binding sites located on the opposite side of the active site (Section 3.2, Fig. 3B-C). A comparison of these results with the inhibition mode assay revealed a discrepancy, as the *in vitro* assay showed that pantinin-1 acts as a competitive inhibitor of CHIKV nsP2^{pro}. Therefore, the most stable model (Section 3.2, Fig. 3B; Pose 4), selected based on RMSD values and effective binding free energies (ΔG_{eff}), was used for further analysis. This model showed that pantinin-1 binds at the active site region of the protease (Section 3.2, Fig. 4A), without directly interacting with the catalytic residues.

Free energy decomposition revealed that amino acids L3, W7, F10, I13, and V14 in pantinin-1 engage in hydrophobic interactions with nsP2^{pro} and have the lowest per-residue binding free energies, highlighting their key role in the interaction. The per-residue free energy contribution of nsP2^{pro} (Section 3.2, Fig. 4B) showed that residues Y1079, Y1047, and W1084 had the most favorable ΔG_{eff} values. These residues are part of the substrate-binding subunits S2, S3, and S4, suggesting that pantinin-1 likely binds at or near the substrate-binding site [116].

A comparison between the molecular docking results of pantinin-1 (GILGKLWEGFKSIV) and peptide P1 (VMPWDEWLTKRKPELP) shows that in both peptides, hydrophobic amino acids (particularly the conserved tryptophan residues) play a crucial role in the interaction, due to hydrophobic contacts between the peptide and the protease. Interestingly, both peptides also adopt an α-helical structure. As mentioned above, peptide P1 showed the highest α-helical content among the tested peptides. Previous studies suggest that α-helices can enhance hydrophobic interactions with lipid membranes [197] and, possibly in this case, with the protease substrate-binding site. A comparison with the synthetic nsP2^{pro} substrate (ABCYL-RAGG↓YIFS-EDANS) [129, 200], derived from the polyprotein sequence shows that all three sequences contain hydrophobic residues, although the specific amino acids differ. Overall, these results may support future efforts to design or optimize peptide-based inhibitors targeting CHIKV nsP2^{pro}.

4.4 Nucleic acids effect on catalytic activity of nsP2^{pro}

Numerous studies have shown that nucleic acids can influence the activity of viral proteases, such as the foamy virus protease [170], 3C^{pro} of poliovirus [172], or Seneca Valley virus protease [201]. As summarized in section 3.3, Table 1, the binding of nucleic acids to viral proteases can either enhance or inhibit their enzymatic activity. To investigate the influence of nucleic acids on the protease activity of CHIKV nsP2^{pro}, a HiTS-FLIP screen was performed to select single-stranded DNA (ssDNA) aptamer binders against nsP2^{pro} (Section 3.3, Table 3). The ten best-binding aptamers were selected and named DAC1-DAC10 (DNA against CHIKV). A primary activity assay revealed that all ten selected aptamers had the potential to enhance CHIKV nsP2^{pro} activity (Section 3.3, Fig. 1). The most substantial enhancement was observed with DAC1, which increased protease activity by 6-fold compared to the control. DAC2, DAC6, DAC8, and DAC9 also showed strong enhancement, with increases of around 5-fold. The lowest levels of enhancement were observed with DAC3, DAC4, and DAC5. To evaluate concentration dependency, the same assay was repeated using a 1:3 ratio of protease to DAC. Interestingly, this condition resulted in a reduction of activity compared to the 1:1 ratio. For example, in the presence of DAC1 and DAC2, enhancement dropped to around 3-fold compare to 1:1 ratio. Previous work by Yin et al. demonstrated that nucleic acids can induce protein aggregation in proteins such as tau and α-synuclein [202]. Based on this, the observed reduction in activity at higher DAC concentrations may be due to protein aggregation induced by the nucleic acids. To evaluate the sequence dependency of DAC-induced activity enhancement, a random non-specific ssDNA oligonucleotide was tested. As shown in section 3.3, Fig. 2A, the non-specific ssDNA also increased protease activity by up to 6-fold, similar to DAC1. Further analysis revealed that activity enhancement occurred in the presence of ssDNA, while double-stranded DNA (dsDNA) did not increase protease activity (Section 3.3, Fig. 2A).

In addition to ssDNA, single-stranded RNA (ssRNA) was tested to determine its effect on activity. Two ssRNA oligonucleotides, RAC1 (5-mer) and RAC2 (10-mer), were designed based on CHIKV genome sequences (Section 3.3, Table S1) and subsequently tested. The assay showed that RAC2 enhanced activity approximately 6 times (Section 3.3, Fig. 2B) compare to the control, whereas the shorter ssRNA (RAC1) did not show any enhancement. Single nucleotides were also tested at two different protease:nucleotide ratios (1:1 and 1:3). At a 1:1 ratio, there was no effect on catalytic activity, and only a slight, non-significant increase was observed at the 1:3 ratio (Section 3.3, Fig. 2C). These results indicate that both ssRNA and ssDNA can enhance protease activity, and that this enhancement is length-dependent, requiring a minimum oligonucleotide length for a measurable effect.

4.5 Buffer composition alters nucleic acid-mediated activation of nsP2^{pro}

To evaluate the impact of buffer composition on nucleic acid-mediated activation, DAC8 (ssDNA aptamer) and RAC2 (ssRNA) were chosen as representative oligonucleotides. Their enhancement potential was tested in three different buffers: 20 mM Bis-Tris propane (pH 7.5), 20 mM phosphate buffer (pH 7.5), and 20 mM Bis-Tris propane supplemented with 400 mM NaCl (pH 7.5). At a 1:1 molar ratio, DAC8 in both Bis-Tris propane and phosphate buffer showed a higher enhancement effect compared to RAC2 (Section 3.3, Fig. 3A). However, at a 1:3 molar ratio in Bis-Tris propane, the activity enhancement of RAC2 reached 15 times the activity of the control, which was significantly higher than that of DAC8 in the same buffer (Section 3.3, Fig. 3B). Experiments conducted in Bis-Tris propane supplemented with 400 mM NaCl showed that both oligonucleotides were unable to increase protease activity at both molar ratios. These results suggest a possible electrostatic interaction between nucleic acids and the protease. As shown in other protein such as HIV-1 NCp7, which also exhibits electrostatic interactions with nucleic acids similar to this study [203]. It is also possible that other interactions, such as hydrogen bonds (like DNA binding to zinc finger proteins) [204] or cation–π interactions (like the binding of the stair motif to DNA) [205], are involved. However, more research is needed to confirm and fully understand the types of interactions involved in CHIKV nsP2^{pro}-nucleic acid binding. Previous studies have shown that high salt concentrations can interfere with protein-nucleic acid binding, such as observed with the hsRosR protein, by altering solvent properties or changing the electrostatic environment [206, 207]. This may explain the lack of enhancement observed in the presence of high salt concentrations. In other words, ions can act as shields and may even cause conformational changes in nucleic acids or proteins, interfering with the electrostatic attraction between negatively charged nucleic acids and positively charged amino acid residues of the protein, thus weakening the free energy of binding [206]. In addition, it has been shown that changes in pH can affect the binding of nucleic acids to proteins by altering the net charge and, consequently, the complex formation [208]. For example, the Sp1 protein (a member from the zinc finger family) showed a 7-fold increase in binding when the pH decreased from 8.0 to 6.0 [208]. Another example is the methionine repressor transcription factor, whose binding to DNA decreased when the pH increased [208]. This is another point that should be investigated further in the context of nucleic acid-CHIKV nsP2^{pro} interactions.

4.6 Structural characterization and *in silico* study of nucleic acids and nsp2^{pro}

The structures of the DNA aptamers were investigated using the DINAMelt Server-Quikfold web tool [209] and CD spectrometry. The predicted structures indicated that all aptamers adopted secondary structures containing hairpin formations of varying lengths and sizes (Section 3.3, Figs. S4-S5). CD spectrometry revealed that all aptamers exhibited positive peaks at approximately 280 nm and 220 nm, and a negative peak near 245 nm (Section 3.3, Figs. S6-S8). These results are characteristic of B-form DNA and align with the predicted structures [210]. In addition, the structure of the RAC1 and RAC2 were analysed by CD spectrometry. In addition, the structures of RAC1 and RAC2 (ssRNA oligonucleotides) were analyzed using CD spectrometry. The CD spectrum of RAC1 showed reduced ellipticity across the wavelength range (Section 3.3, Fig. S8), indicating that RAC1 exists in an unfolded state. In contrast, the CD spectrum of RAC2 exhibited a positive peak around 270 nm (Section 3.3, Fig. S8), suggesting that RAC2 contains an A-form RNA helical structure [211]. As shown in section 3.3, Figs. 1 and 2B, RAC2 and all DNA aptamers enhanced protease activity, while RAC1 did not. As discussed in section 4.4, increased protease activity requires a minimum nucleic acid length. Structural analysis further demonstrated that well-structured nucleic acids can enhance catalytic activity, unlike unfolded ones such as RAC1. Together, these findings suggest that, in addition to length, the secondary structure of the nucleic acids may also play a critical role in nsP2^{pro} activation. To gain deeper insight into nucleic acid binding to nsP2^{pro}, potential binding sites were predicted using the PROBind webserver. The results showed that 14 amino acid residues are involved in DNA binding and 23 residues in RNA binding. Further analysis revealed that both DNA and RNA bind predominantly to the methyltransferase domain. However, five amino acids ($_{1054}$NE$_{1055}$, $_{1050}$E and $_{47}$YS$_{48}$) in the protease domain were also predicted to interact with RNA. Although the prediction indicated that most nucleic acid interactions occur within the methyltransferase domain, the binding residues for DNA and RNA differed. The predicted DNA-binding regions included $_{1281}$RSSR$_{1284}$ and $_{1305}$DNGRR$_{1309}$, while RNA-binding regions included $_{1308}$RRN1310, $_{1241}$QML$_{1243}$, $_{1183}$TKR$_{1185}$, $_{1165}$K(I)NGH$_{1169}$ (except I) (Section 3.3, Fig. S9). To compare these predictions with experimental aptamers used in this study (DAC1, RAC1, and RAC2), blind molecular docking was performed using AlphaFold 3 and HDOCK. The docking results showed that nucleic acids bind to regions consistent with PROBind predictions. Comparison between AlphaFold and HDOCK results showed slight differences in binding poses, but both pointed to interactions with the methyltransferase domain. These findings suggest that nucleic acids bind primarily to the methyltransferase domain of nsP2^{pro} (Section 3.3, Fig. 4-5). However, further experimental validation and evidence is necessary to confirm these interactions.

4.7 Nucleic acids decrease the inhibitory potential of peptide P1

In sections 4.1 and 4.4, the individual effects of peptide P1 and nucleic acids on CHIKV nsP2^{pro} were discussed. To investigate whether the presence of nucleic acids could alter the inhibitory potential of peptide P1, an assay was performed using a mixture of P1 and DAC8 (a representative nucleic acid). As shown in section 3.4, peptide P1 alone reduced protease activity to below 50%, while DAC8 significantly increased activity. However, the combination of P1 and DAC8 resulted in a decrease in protease activity of approximately 5-fold compared to DAC8 alone, but the activity was still about 10 times higher than that observed with peptide P1 alone. These findings highlight the important role of nucleic acids in modulating protease activity and suggest that their influence may may need to be taken into account in future efforts to develop therapeutic inhibitors targeting CHIKV nsP2^{pro}.

4.8 Phage display selected peptides or natural peptides? A comparative assessment for future research and development

To provide an overview of the strengths and limitations of the two inhibitors, peptide P1 (the peptide selected from phage display with the strongest inhibitory effect) and pantinin-1 (a naturally occurring peptide derived from scorpion venom) are compared in Table 6. Both peptides demonstrated inhibitory activity in the micromolar range; however, peptide P1 exhibited a lower IC_{50} value, indicating higher potency. Interestingly, molecular docking and structural analysis of the two peptides revealed that both utilize hydrophobic interactions to bind to the protease and display a high α-helical content compared to the other phage display selected peptides. This suggests that the loss or absence of α-helical structure may reduce inhibitory efficiency, making it a critical factor in protease inhibition. Additionally, the presence of hydrophobic amino acids such as tryptophan, which is conserved in both peptide P1 and pantinin-1, should be considered in future optimization steps. One key difference between the peptides is cytotoxicity. Peptide P1 exhibited significantly lower cytotoxicity compared to pantinin-1, causing minimal cell death even at concentrations up to 100 µM, which is well above its IC_{50}.

Taken together, these findings suggest that peptide P1 may represent a more favourable starting point and could serve as a lead candidate for future optimization and antiviral development.

Table 6. Comparative overview of peptide P1 and pantinin-1

Peptide	Peptide P1	Pantinin-1
Origin	Artificial, selected via phage display	Natural, derived from scorpion venom
Structure	α-helical, high α-helical content	α-helical, amphipathic
Cytotoxicity	Low-toxic up to 100 μM	Toxic above 20 μM
Inhibition type	Competitive	Competitive
Binding site	Substrate-binding region near active site	Substrate-binding region, different subunit compared to P1
Key residues	Hydrophobic amino acids (Trp)	Hydrophobic amino acids (Trp)
Interactions	Hydrophobic + H-bonds	Hydrophobic interactions
IC_{50}	4.6 ± 1.8 μM	6.4 ± 2.04 μM
Affinity (K_D)	1.39 ± 0.61	9.29 μM
Potential advantages	Low toxicity, specificity, synthetic flexibility	Natural activity, membrane permeability
Limitations	Requires synthesis/optimization	Higher cytotoxicity, less specific,

5. Conclusion and outlook

In the wake of accelerating climate change and increased global mobility, arboviruses such as chikungunya virus (CHIKV) are expanding into new regions, presenting a growing threat to global public health. As vector-borne diseases continue to spread, the development of targeted antiviral strategies becomes increasingly urgent. CHIKV replication depends on the protease activity of the non-structural protein 2 ($nsP2^{pro}$), which is responsible for cleaving the viral polyprotein p1234. This essential function makes $nsP2^{pro}$ a promising target for antiviral drug development. In this study, two distinct approaches were used to identify inhibitors against CHIKV $nsP2^{pro}$. In the first approach, phage display was employed to identify six peptides, whose inhibitory potential was evaluated. Peptide P1 was found to be the most potent, with an IC_{50} of 4.6 ± 1.8 µM and a binding affinity in the low micromolar range. Biochemical and biophysical analyses demonstrated that P1 adopts an α-helical structure and acts as a competitive inhibitor by binding to the substrate-binding site. Molecular docking predicted its binding site and identified key residues involved in the interaction with $nsP2^{pro}$. In the second approach, a peptide derived from animal venom, pantinin-1, was investigated as a potential inhibitor. Pantinin-1 is a small α-helical, amphipathic peptide from scorpion venom with known antimicrobial activity. This study revealed that pantinin-1 can inhibit the catalytic activity of $nsP2^{pro}$, with an IC_{50} of 6.4 ± 2.04 µM and a dissociation constant (K_D) of 9.29 µM. Similar to P1, both *in vitro* and *in silico* studies confirmed that pantinin-1 acts as a competitive inhibitor and binds to the substrate-binding site, but at a different subunit. Interestingly, both peptides were found to have α-helical structures, indicating a potentially important role for this structural motif in protease binding. Further studies, such as *in silico* alanine scanning and biophysical methods (e.g., NMR or X-ray crystallography), are needed to confirm the predicted binding models and further characterize critical interaction residues. In addition, molecular dynamics simulations may support the optimization of these peptides to improve binding affinity and inhibitory potential. Cytotoxicity assays in Vero cells showed that peptide P1 was non-toxic up to 100 µM, while pantinin-1 exhibited higher toxicity, with approximately 50% cell viability observed at 40 µM. However, this concentration is still more than three times higher than the IC_{50} of pantinin-1. Future studies should evaluate cytotoxicity in human cell lines such as HEK293 to better understand potential side effects in therapeutic applications. Most importantly, antiviral activity assays in infected cell cultures are required to assess the peptides' ability to inhibit viral replication and determine their EC_{50} values. In addition to peptide screening, the effect of nucleic acids on $nsP2^{pro}$ activity was explored. *In vitro* studies revealed that protease activity can be enhanced by single-stranded nucleic acids. This enhancement may not sequence-specific but appeared to depend on oligonucleotide length and structure. Folded nucleic acids, such as DAC1 and RAC2, were able to increase activity,

whereas unfolded or short strands like RAC1 showed no effect. Structural analysis and molecular docking suggested that nucleic acids bind primarily to the methyltransferase domain of nsP2^{pro}, with a few potential RNA interaction residues also located within the protease domain. However, these predictions require confirmation by structural studies and cell-based validation. A molecular investigation of P1 revealed that a flexible interdomain loop contributes to open and closed conformations of the active site. Specifically, the flap formed by residues A_{1080}-H_{1083} can shift in proximity to or away from residues N_{1202}-$L1_{207}$ (NLELGL) in the methyltransferase domain. Based on this, we hypothesize that nucleic acid binding to the methyltransferase domain could promote the open conformation of nsP2^{pro}. Nonetheless, further experimental validation is required to support this model. Finally, it was shown that in the presence of nucleic acids, the inhibitory potential of peptide P1 was significantly reduced compared to its effect in isolation. This suggests that nucleic acids play a crucial modulatory role and should be considered when designing and developing antiviral inhibitors targeting CHIKV nsP2^{pro}.

Publication list

Published:

- **Mastalipour, M.**, Gering, I., Coronado, M. A., González, J. E. H., Willbold, D., & Eberle, R. J. (2025). Novel peptide inhibitor for the Chikungunya virus nsP2 protease: Identification and characterization. *Current research in microbial sciences*, *8*, 100376. https://doi.org/10.1016/j.crmicr.2025.100376
- Coronado, M. A., Gering, I., Sevenich, M., Olivier, D. S., **Mastalipour, M.**, Amaral, M. S., Willbold, D., & Eberle, R. J. (2023). The Importance of Epigallocatechin as a Scaffold for Drug Development against Flaviviruses. *Pharmaceutics*, *15*(3), 803. https://doi.org/10.3390/pharmaceutics15030803
- Camargo, L. C., Gering, I., **Mastalipour, M.**, Kraemer-Schulien, V., Bujnicki, T., Willbold, D., Coronado, M. A., & Eberle, R. J. (2024). A Snake Venom Peptide and Its Derivatives Prevent $A\beta_{42}$ Aggregation and Eliminate Toxic $A\beta_{42}$ Aggregates *In Vitro*. *ACS chemical neuroscience*, *15*(14), 2600-2611. https://doi.org/10.1021/acschemneuro.4c00089

Submitted/ Preprint:

- **Mastalipour, M.**, Coronado, M. A., González, J. E. H., Willbold, D., & Eberle, R. J. (2025). Inhibition of Chikungunya virus nsP2 protease in vitro by pantinin-1 isolated from scorpion venom. bioRxiv 2025.06.29.662183; doi: https://doi.org/10.1101/2025.06.29.662183
- **Mastalipour, M.**, Coronado, M. A., Siahaan, R.A., Drees, A., Ahlers. C., Fischer, M., Willbold, D., & Eberle, R. J. (2025). Single-Stranded nucleic acid binding enhances the *in vitro* catalytic activity of Chikungunya virus nsP2 protease bioRxiv 2025.05.13.653680; doi: https://doi.org/10.1101/2025.05.13.653680. Submitted to PLOS ONE, under peer review.

Reference

1. Carlson CJ, Albery GF, Merow C, Trisos CH, Zipfel CM, Eskew EA, et al. Climate change increases cross-species viral transmission risk. *Nature*. 2022;607(7919):555-62. https://doi.org/10.1038/s41586-022-04788-w

2. Mora C, McKenzie T, Gaw IM, Dean JM, von Hammerstein H, Knudson TA, et al. Over half of known human pathogenic diseases can be aggravated by climate change. *Nature Climate Change*. 2022;12(9):869-75. https://doi.org/10.1038/s41558-022-01426-1

3. Ali A, Shaikh A, Sethi I, Surani S. Climate change and the emergence and exacerbation of infectious diseases: A review. *World J Virol*. 2024;13(4):96476. https://doi.org/10.5501/wjv.v13.i4.96476

4. Ryan SJ, Carlson CJ, Mordecai EA, Johnson LR. Global expansion and redistribution of Aedes-borne virus transmission risk with climate change. *PLOS Neglected Tropical Diseases*. 2019;13(3):e0007213. https://doi.org/10.1371/journal.pntd.0007213

5. Bartlow AW, Manore C, Xu C, Kaufeld KA, Del Valle S, Ziemann A, et al. Forecasting Zoonotic Infectious Disease Response to Climate Change: Mosquito Vectors and a Changing Environment. *Veterinary Sciences*. 2019;6(2):40. https://doi.org/10.3390/vetsci6020040

6. Gubler DJ. The global resurgence of arboviral diseases. Transactions of The Royal Society of Tropical Medicine and Hygiene. 1996;90(5):449-51. https://doi.org/10.1016/s0035-9203(96)90286-2

7. Centers for Disease Control and Prevention. Arbovirus Catalog [Internet]. Atlanta (GA): CDC; [cited 2025 May 29]. Available from: https://wwwn.cdc.gov/arbocat/#:~:text=The%20Centers%20for%20Disease%20Control%20and%20Prevention%20%28CDC%29,or%20potentially%20infectious%20for%20humans%20or%20domestic%20animals

8. Labeaud AD, Bashir F, King CH. Measuring the burden of arboviral diseases: the spectrum of morbidity and mortality from four prevalent infections. *Popul Health Metr*. 2011;9(1):1. https://doi.org/10.1186/1478-7954-9-1

9. Eldridge BF, Scott TW, Day JF, Tabachnick WJ. Arbovirus Diseases. In: Eldridge BF, Edman JD, editors. *Medical Entomology: A Textbook on Public Health and Veterinary Problems Caused by Arthropods*. Dordrecht: Springer Netherlands; 2004. p. 415-60. https://doi.org/10.1007/978-94-007-1009-2_11

10. Go YY, Balasuriya UBR, Lee C-k. Zoonotic encephalitides caused by arboviruses: transmission and epidemiology of alphaviruses and flaviviruses. *Clin Exp Vaccine Res*. 2014;3(1):58-77. https://doi.org/10.7774/cevr.2014.3.1.58

11. Ciota AT, Kramer LD. Insights into arbovirus evolution and adaptation from experimental studies. *Viruses*. 2010;2(12):2594-617. https://doi.org/10.3390/v2122594

12. Weaver, S., Barrett, A. Transmission cycles, host range, evolution and emergence of arboviral disease. *Nat Rev Microbiol* **2**. 2004; 789–801. https://doi.org/10.1038/nrmicro1006

13. Windhaber S, Xin Q, Lozach PY. Orthobunyaviruses: From Virus Binding to Penetration into Mammalian Host Cells. *Viruses*. 2021;13(5). https://doi.org/10.3390/v13050872

14. Roy P. Bluetongue virus assembly and exit pathways. *Adv Virus Res*. 2020;108:249-73. https://doi.org/10.1016/bs.aivir.2020.08.002

15. Harris EK, Foy BD, Ebel GD. Colorado tick fever virus: a review of historical literature and research emphasis for a modern era. Journal of Medical Entomology. 2023;60(6):1214-20. https://doi.org/10.1093/jme/tjad094

16. Briolant S, Garin D, Scaramozzino N, Jouan A, Crance JM. In vitro inhibition of Chikungunya and Semliki Forest viruses replication by antiviral compounds: synergistic effect of interferon-α and ribavirin combination. *Antiviral Research*. 2004;61(2):111-7. https://doi.org/10.1016/j.antiviral.2003.09.005

17. Lumsden WHR. An epidemic of virus disease in Southern Province, Tanganyika territory, in 1952–1953 II. General description and epidemiology. *Transactions of the Royal Society of Tropical Medicine and Hygiene.* 1955;49(1):33-57. https://doi.org/10.1016/0035-9203(55)90081-x

18. Ross RW. The Newala epidemic: III. The virus: isolation, pathogenic properties and relationship to the epidemic. *Journal of Hygiene*. 1956;54(2):177-91. https://doi.org/10.1017/s0022172400044442

19. Pan American Health Organization. Chikungunya: data and analysis 2025 [Internet]. Washington (DC): PAHO; [cited 2025 May 30]. Available from: https://www.paho.org/en/arbo-portal/chikungunya-data-and-analysis.

20. European Centre for Disease Prevention and Control. Countries/territories reporting Chikungunya cases since February 2023 and as of January 2024 [Internet]. Stockholm: ECDC; 2024 [cited 2025 May 30]. Available from: https://www.ecdc.europa.eu/en/publications-data/countriesterritories-reporting-chikungunya-cases-february-2023-and-january-2024.

21. European Centre for Disease Prevention and Control. Chikungunya worldwide overview 2025 [Internet]. Stockholm: ECDC; 2025 [cited 2025 May 30]. Available from: https://www.ecdc.europa.eu/en/chikungunya-monthly#:~:text=Since%20the%20beginning%20of%202025%2C%20and%20as%20of,CHIKVD-related%20deaths%20have%20been%20reported%20in%2014%20countries%2Fterritories.

22. Caputo B, Russo G, Manica M, Vairo F, Poletti P, Guzzetta G, et al. A comparative analysis of the 2007 and 2017 Italian chikungunya outbreaks and implication for public health response. *PLoS Negl Trop Dis*. 2020;14(6):e0008159. https://doi.org/10.1371/journal.pntd.0008159

23. Bordi L, Carletti F, Lalle E, Colavita F, Meschi S, Di Caro A, et al. Molecular Characterization of Autochthonous Chikungunya Cluster in Latium Region, Italy. Emerg Infect Dis. 2018;24(1):178-80. https://doi.org/10.3201/eid2401.171605

24. World Health Organization. Disease Outbreak News, Chikungunya – La Réunion and Mayotte [Internet]. Geneva: WHO; 2025 May 12 [cited 2025 May 29]. Available from: https://www.who.int/emergencies/disease-outbreak-news/item/2025-DON567

25. World Health Organization. Global distribution of Chikungunya virus 2020 [Internet]. Geneva: WHO; 2020 [cited 2025 May 30]. Available from: https://www.who.int/multi-media/details/global-distribution-of-chikungunya-virus

26. Zeller H, Van Bortel W, Sudre B. Chikungunya: Its History in Africa and Asia and Its Spread to New Regions in 2013–2014. *The Journal of Infectious Diseases*. 2016;214(suppl_5):S436-S40. https://doi.org/10.1093/infdis/jiw391

27. Hammon WM, Rundnick A, Sather GE. Viruses Associated with Epidemic Hemorrhagic Fevers of the Philippines and Thailand. *Science*. 1960;131(3407):1102-3. https://doi.org/10.1126/science.131.3407.1102

28. Kalantri SP, Joshi R, Riley LW. Chikungunya epidemic: an Indian perspective. *Natl Med J India*. 2006;19(6):315-22

29. Sergon K, Njuguna C, Kalani R, Ofula V, Onyango C, Konongoi LS, et al. Seroprevalence of Chikungunya Virus (CHIKV) Infection on Lamu Island, Kenya, October 2004. *The American Journal of Tropical Medicine and Hygiene Am J Trop Med Hyg*. 2008;78(2):333-7. https://doi.org/10.4269/ajtmh.2008.78.333

30. Gérardin P, Guernier V, Perrau J, Fianu A, Le Roux K, Grivard P, et al. Estimating Chikungunya prevalence in La Réunion Island outbreak by serosurveys: two methods for two critical times of the epidemic. *BMC Infect Dis*. 2008;8:99. https://doi.org/10.1186/1471-2334-8-99

31. World Health Organization. Disease Outbreak News, India [Internet]. Geneva: WHO; 2006 Oct 17 [cited 2025 May 30]. Available from: https://www.who.int/emergencies/disease-outbreak-news/item/2006_10_17-en

32. Rezza G, Nicoletti L, Angelini R, Romi R, Finarelli AC, Panning M, et al. Infection with chikungunya virus in Italy: an outbreak in a temperate region. *The Lancet*. 2007;370(9602):1840-6.doi:10.1016/S0140-6736(07)61779-6

33. World Health Organization. Disease Outbreak News, Chikungunya – Congo [Internet]. Geneva: WHO; 2019 May 1 [cited 2025 May 30]. Available from: https://web.archive.org/web/20190504212703/https://www.who.int/csr/don/01-may-2019-chikungunya-congo/en/

34. Vega-Rúa A, Zouache K, Girod R, Failloux A-B, Lourenço-de-Oliveira R. High Level of Vector Competence of Aedes aegypti and Aedes albopictus from Ten American Countries as a Crucial Factor in the Spread of Chikungunya Virus. *Journal of Virology*. 2014;88(11):6294-306. https://doi.org/10.1128/JVI.00370-14

35. Gérardin P, Sampériz S, Ramful D, Boumahni B, Bintner M, Alessandri JL, et al. Neurocognitive outcome of children exposed to perinatal mother-to-child Chikungunya virus infection: the CHIMERE cohort study on Reunion Island. *PLoS Negl Trop Dis*. 2014;8(7):e2996. https://doi.org/10.1371/journal.pntd.0002996

36. Silva LA, Dermody TS. Chikungunya virus: epidemiology, replication, disease mechanisms, and prospective intervention strategies. *J Clin Invest*. 2017;127(3):737-49. https://doi.org/10.1172/JCI84417

37. Diallo D, Sall AA, Buenemann M, Chen R, Faye O, Diagne CT, et al. Landscape ecology of sylvatic chikungunya virus and mosquito vectors in southeastern Senegal. *PLoS Negl Trop Dis*. 2012;6(6):e1649. https://doi.org/10.1371/journal.pntd.0001649

38. Weaver SC. Evolutionary influences in arboviral disease. *Curr Top Microbiol Immunol*. 2006;299:285-314. https://doi.org/10.1007/3-540-26397-7_10

39. Powers AM. Chikungunya. *Clinics in Laboratory Medicine*. 2010;30(1):209-19. https://doi.org/10.1016/j.cll.2009.10.003

40. Kawada H, Honda S, Takagi M. Comparative Laboratory Study on the Reaction of Aedes aegypti and Aedes albopictus to Different Attractive Cues in a Mosquito Trap. *Journal of Medical Entomology*.2007;44(3):427-32. https://doi.org/10.1093/jmedent/44.3.427

41. Mbaika S, Lutomiah J, Chepkorir E, Mulwa F, Khayeka-Wandabwa C, Tigoi C, et al. Vector competence of Aedes aegypti in transmitting Chikungunya virus: effects and implications of extrinsic incubation temperature on dissemination and infection rates. *Virol J*. 2016;13:114. https://doi.org/10.1186/s12985-016-0566-7

42. Ali Ou Alla S, Combe B. Arthritis after infection with Chikungunya virus. *Best Practice & Research Clinical Rheumatology*. 2011;25(3):337-46. https://doi.org/10.1016/j.berh.2011.03.005

43. Cunha RVD, Trinta KS. Chikungunya virus: clinical aspects and treatment - A Review. *Mem Inst Oswaldo Cruz*. 2017;112(8):523-31. https://doi.org/10.1590/0074-02760170044

44. Khongwichit S, Chansaenroj J, Chirathaworn C, Poovorawan Y. Chikungunya virus infection: molecular biology, clinical characteristics, and epidemiology in Asian countries. *J Biomed Sci*. 2021;28(1):84. https://doi.org/10.1186/s12929-021-00778-8

45. Venturi G, Fabiani M, Amendola A, Marsili G, Benedetti E, Fiorentini C, et al. Lack of Evidence of Chikungunya Virus Infection among Blood Donors during the Chikungunya Outbreak in Lazio Region, Italy, 2017. *Viruses*. 2022;14(3). https://doi.org/10.3390/v14030619

46. Hua C, Combe B. Chikungunya Virus-Associated Disease. *Current Rheumatology Reports*. 2017;19(11):69. https://doi.org/10.1007/s11926-017-0694-0

47. Santiago RA, Bavaresco SPP, Citrangulo SG, Medronho RdA, Sampaio V, Costa AJL. Clinical manifestations associated with the chronic phase of Chikungunya Fever: A systematic review of prevalence. *PLOS Neglected Tropical Diseases*. 2025;19(2):e0012810. https://doi.org/10.1371/journal.pntd.0012810

48. Silveira-Freitas JEP, Campagnolo ML, Dos Santos Cortez M, de Melo FF, Zarpelon-Schutz AC, Teixeira KN. Long chikungunya? An overview to immunopathology of persistent arthralgia. *World J Virol*. 2024;13(2):89985. https://doi.org/10.5501/wjv.v13.i2.89985

49. Bertolotti A, Thioune M, Abel S, Belrose G, Calmont I, Césaire R, et al. Prevalence of chronic chikungunya and associated risks factors in the French West Indies (La Martinique): A prospective cohort study. *PLOS Neglected Tropical Diseases*. 2020;14(3):e0007327. https://doi.org/10.1371/journal.pntd.0007327

50. Heath CJ, Lowther J, Noël TP, Mark-George I, Boothroyd DB, Mitchell G, et al. The Identification of Risk Factors for Chronic Chikungunya Arthralgia in Grenada, West Indies: A Cross-Sectional Cohort Study. *Open Forum Infect Dis*. 2018;5(1):ofx234. https://doi.org/10.1093/ofid/ofx234

51. Traverse EM, Millsapps EM, Underwood EC, Hopkins HK, Young M, Barr KL. Chikungunya Immunopathology as It Presents in Different Organ Systems. *Viruses*. 2022;14(8). https://doi.org/10.3390/v14081786

52. Brito Ferreira ML, Militão de Albuquerque MFP, de Brito CAA, de Oliveira França RF, Porto Moreira Á J, de Morais Machado M, et al. Neurological disease in adults with Zika and chikungunya virus infection in Northeast Brazil: a prospective observational study. *Lancet Neurol*. 2020;19(10):826-39. https://doi.org/10.1016/S1474-4422(20)30232-5

53. Economopoulou A, Dominguez M, Helynck B, Sissoko D, Wichmann O, Quenel P, et al. Atypical Chikungunya virus infections: clinical manifestations, mortality and risk factors for severe disease during the 2005–2006 outbreak on Réunion. *Epidemiology and Infection*. 2009;137(4):534-41. https://doi.org/10.1017/S0950268808001167

54. Mehta R, Gerardin P, de Brito CAA, Soares CN, Ferreira MLB, Solomon T. The neurological complications of chikungunya virus: A systematic review. *Rev Med Virol*. 2018;28(3):e1978. https://doi.org/10.1002/rmv.1978

55. Puntasecca CJ, King CH, LaBeaud AD. Measuring the global burden of chikungunya and Zika viruses: A systematic review. *PLoS Negl Trop Dis*. 2021;15(3):e0009055. https://doi.org/10.1371/journal.pntd.0009055

56. Gulati S, Duggu SR, Chawla K, Dessai R, Jain S. A Study of Neurological Involvement in Dengue and Chikungunya Infection. *Annals of African Medicine*. 2024;23(4):563-6. https://doi.org/10.4103/aam.aam_131_23

57. Khan AH, Morita K, Parquet MDC, Hasebe F, Mathenge EGM, Igarashi A. Complete nucleotide sequence of chikungunya virus and evidence for an internal polyadenylation site. *J Gen Virol*. 2002;83(Pt 12):3075-84. https://doi.org/10.1099/0022-1317-83-12-3075

58. Pfeffer M, Kinney RM, Kaaden O-R. The Alphavirus 3′-Nontranslated Region: Size Heterogeneity and Arrangement of Repeated Sequence Elements. *Virology*. 1998;240(1):100-8. https://doi.org/10.1006/viro.1997.8907

59. Solignat M, Gay B, Higgs S, Briant L, Devaux C. Replication cycle of chikungunya: a re-emerging arbovirus. *Virology*. 2009;393(2):183-97. https://doi.org/doi:10.1016/j.virol.2009.07.024

60. Singh SK, Unni SK. Chikungunya virus: host pathogen interaction. *Reviews in Medical Virology*. 2011;21(2):78-88. https://doi.org/10.1002/rmv.681

61. Snyder JE, Kulcsar KA, Schultz KL, Riley CP, Neary JT, Marr S, et al. Functional characterization of the alphavirus TF protein. *J Virol*. 2013;87(15):8511-23. https://doi.org/10.1128/jvi.00449-13

62. Varikkodan MM, Kunnathodi F, Azmi S, Wu T-Y. An Overview of Indian Biomedical Research on the Chikungunya Virus with Particular Reference to Its Vaccine, an Unmet Medical Need. *Vaccines*. 2023;11(6):1102. https://doi.org/10.3390/vaccines11061102

63. Sharma R, Kesari P, Kumar P, Tomar S. Structure-function insights into chikungunya virus capsid protein: Small molecules targeting capsid hydrophobic pocket. *Virology*. 2018;515:223-34. https://doi.org/10.1016/j.virol.2017.12.020

64. Hahn CS, Strauss EG, Strauss JH. Sequence analysis of three Sindbis virus mutants temperature-sensitive in the capsid protein autoprotease. *Proceedings of the National Academy of Sciences*. 1985;82(14):4648-52. http://www.jstor.org/stable/26101

65. Hahn CS, Strauss JH. Site-directed mutagenesis of the proposed catalytic amino acids of the Sindbis virus capsid protein autoprotease. *Journal of virology*. 1990;64(6):3069-73. https://doi.org/10.1128/JVI.64.6.3069-3073.1990

66. van Duijl-Richter MK, Hoornweg TE, Rodenhuis-Zybert IA, Smit JM. Early Events in Chikungunya Virus Infection-From Virus Cell Binding to Membrane Fusion. *Viruses*. 2015;7(7):3647-74. https://doi.org/10.3390/v7072792

67. Voss JE, Vaney M-C, Duquerroy S, Vonrhein C, Girard-Blanc C, Crublet E, et al. Glycoprotein organization of Chikungunya virus particles revealed by X-ray crystallography. *Nature*. 2010;468(7324):709-12. https://doi.org/10.1038/nature09555

68. Singh A, Kumar A, Uversky Vladimir N, Giri R. Understanding the interactability of chikungunya virus proteins via molecular recognition feature analysis. *RSC Advances*. 2018;8(48):27293-303. https://doi.org/10.1039/C8RA04760J

69. Dey D, Siddiqui SI, Mamidi P, Ghosh S, Kumar CS, Chattopadhyay S, et al. The effect of amantadine on an ion channel protein from Chikungunya virus. *PLOS Neglected Tropical Diseases*. 2019;13(7):e0007548. https://doi.org/10.1371/journal.pntd.0007548

70. Melton JV, Ewart GD, Weir RC, Board PG, Lee E, Gage PW. Alphavirus 6K Proteins Form Ion Channels *. *Journal of Biological Chemistry*. 2002;277(49):46923-31. https://doi.org/10.1074/jbc.M207847200

71. Ahola T, Kääriäinen L. Reaction in alphavirus mRNA capping: formation of a covalent complex of nonstructural protein nsP1 with 7-methyl-GMP. *Proc Natl Acad Sci U S A*. 1995;92(2):507-11. https://doi.org/10.1073/pnas.92.2.507

72. Ahola T, Laakkonen P, Vihinen H, Kääriäinen L. Critical residues of Semliki Forest virus RNA capping enzyme involved in methyltransferase and guanylyltransferase-like activities. *J Virol*. 1997;71(1):392-7. https://doi.org/10.1128/jvi.71.1.392-397.1997

73. Saisawang C, Sillapee P, Sinsirimongkol K, Ubol S, Smith DR, Ketterman AJ. Full length and protease domain activity of chikungunya virus nsP2 differ from other alphavirus nsP2 proteases in recognition of small peptide substrates. *Biosci Rep*. 2015;35(3). https://doi.org/10.1042/bsr20150086

74. Ghoshal A, Asressu KH, Hossain MA, Brown PJ, Nandakumar M, Vala A, et al. Structure Activity of β-Amidomethyl Vinyl Sulfones as Covalent Inhibitors of Chikungunya nsP2 Cysteine Protease with Antialphavirus Activity. *J Med Chem*. 2024;67(18):16505-32. https://doi.org/10.1021/acs.jmedchem.4c01346

75. Abu Bakar F, Ng LFP. Nonstructural Proteins of Alphavirus-Potential Targets for Drug Development. *Viruses*. 2018;10(2). https://doi.org/10.3390/v10020071

76. Gao Y, Goonawardane N, Ward J, Tuplin A, Harris M. Multiple roles of the non-structural protein 3 (nsP3) alphavirus unique domain (AUD) during Chikungunya virus genome replication and transcription. *PLOS Pathogens*. 2019;15(1):e1007239. https://doi.org/10.1371/journal.ppat.1007239

77. Chen MW, Tan YB, Zheng J, Zhao Y, Lim BT, Cornvik T, et al. Chikungunya virus nsP4 RNA-dependent RNA polymerase core domain displays detergent-sensitive primer extension and terminal adenylyltransferase activities. *Antiviral Research*. 2017;143:38-47. https://doi.org/10.1016/j.antiviral.2017.04.001

78. Silva LA, Khomandiak S, Ashbrook AW, Weller R, Heise MT, Morrison TE, et al. A single-amino-acid polymorphism in Chikungunya virus E2 glycoprotein influences glycosaminoglycan utilization. *J Virol*. 2014;88(5):2385-97. https://doi.org/10.1128/jvi.03116-13

79. McAllister N, Liu Y, Silva LM, Lentscher AJ, Chai W, Wu N, et al. Chikungunya Virus Strains from Each Genetic Clade Bind Sulfated Glycosaminoglycans as Attachment Factors. *J Virol*. 2020;94(24). https://doi.org/10.1128/jvi.01500-20

80. Zhang R, Kim AS, Fox JM, Nair S, Basore K, Klimstra WB, et al. Mxra8 is a receptor for multiple arthritogenic alphaviruses. *Nature*. 2018;557(7706):570-4. https://doi.org/10.1038/s41586-018-0121-3

81. Vaney M-C, Duquerroy S, Rey FA. Alphavirus structure: activation for entry at the target cell surface. *Current Opinion in Virology*. 2013;3(2):151-8. https://doi.org/10.1016/j.coviro.2013.04.003

82. Sahoo B, Gudigamolla NK, Chowdary TK. Acidic pH-Induced Conformational Changes in Chikungunya Virus Fusion Protein E1: a Spring-Twisted Region in the Domain I-III Linker Acts as a Hinge Point for Swiveling Motion of Domains. *Journal of Virology*. 2020;94(23):10.1128/jvi.01561-20. https://doi.org/10.1128/jvi.01561-20

83. Strauss JH, Strauss EG. The alphaviruses: gene expression, replication, and evolution. *Microbiol Rev*. 1994;58(3):491-562. https://doi.org/10.1128/mr.58.3.491-562.1994

84. Kril V, Aïqui-Reboul-Paviet O, Briant L, Amara A. New Insights into Chikungunya Virus Infection and Pathogenesis. *Annual Review of Virology*. 2021;8(Volume 8, 2021):327-47. https://doi.org/10.1146/annurev-virology-091919-102021

85. Elmasri Z, Nasal BL, Jose J. Alphavirus-Induced Membrane Rearrangements during Replication, Assembly, and Budding. *Pathogens (Basel, Switzerland)*. 2021;10(8):984. https://doi.org/10.3390/pathogens10080984

86. Ahmed S, Sultana S, Kundu S, Alam SS, Hossan T, Islam MA. Global Prevalence of Zika and Chikungunya Coinfection: A Systematic Review and Meta-Analysis. *Diseases*. 2024;12(2). https://doi.org/10.3390/diseases12020031

87. Furuya-Kanamori L, Liang S, Milinovich G, Soares Magalhaes RJ, Clements AC, Hu W, et al. Co-distribution and co-infection of chikungunya and dengue viruses. *BMC Infect Dis*. 2016;16:84. https://doi.org/10.1186/s12879-016-1417-2

88. Näslund J, Ahlm C, Islam K, Evander M, Bucht G, Lwande OW. Emerging Mosquito-Borne Viruses Linked to Aedes aegypti and Aedes albopictus: Global Status and Preventive Strategies. *Vector-Borne and Zoonotic Diseases*. 2021;21(10):731-46. https://doi.org/10.1089/vbz.2020.2762

89. Liu T, Gao C, Wang J, Song J, Chen X, Chen H, et al. Peptide aptamer-based time-resolved fluoroimmunoassay for CHIKV diagnosis. *Virol J*. 2023;20(1):166. https://doi.org/10.1186/s12985-023-02132-w

90. Sethi KS, Aryan AK, Ganeshan PK. Magnetic Resonance Imaging Brain Findings in Chikungunya Virus (CHIKV) Infection with Neurological Complication during Epidemic Outbreak. *Neurology India*. 2023;71(3):467-70. https://doi.org/10.4103/0028-3886.378660

91. Blettery M, Brunier L, Banydeen R, Derancourt C, de Bandt M. Management of acute-stage chikungunya disease: Contribution of ultrasonographic joint examination. *International Journal of Infectious Diseases*. 2019;84:1-4. https://doi.org/10.1016/j.ijid.2019.03.031

92. Patramool S, Bernard E, Hamel R, Natthanej L, Chazal N, Surasombatpattana P, et al. Isolation of infectious chikungunya virus and dengue virus using anionic polymer-coated magnetic beads. *Journal of Virological Methods*. 2013;193(1):55-61. https://doi.org/10.1016/j.jviromet.2013.04.016

93. Suryavanshi KT, Chakraborty A. Investigation of Chikungunya virus genotype at tertiary care center in Western Maharashtra, India. *Journal of Vector Borne Diseases*. 2023;60(1):106-10. https://doi.org/10.4103/0972-9062.353231

94. Gupta N, Augustine S, Narayan T, O'Riordan A, Das A, Kumar D, et al. Point-of-Care PCR Assays for COVID-19 Detection. *Biosensors (Basel).* 2021;11(5). https://doi.org/10.3390/bios11050141

95. da Silva SJR, Pardee K, Balasuriya UBR, Pena L. Development and validation of a one-step reverse transcription loop-mediated isothermal amplification (RT-LAMP) for rapid detection of ZIKV in patient samples from Brazil. *Scientific Reports*. 2021;11(1):4111. https://doi.org/10.1038/s41598-021-83371-1

96. Simo FBN, Burt FJ, Makoah NA. Chikungunya Virus Diagnosis: A Review of Current Antigen Detection Methods. *Tropical Medicine and Infectious Disease*. 2023;8(7):365. https://doi.org/10.3390/tropicalmed8070365

97. Moreira J, Barros J, Fernandez-Carballo BL, Escadafal C, Ribeiro GS, Dittrich S, et al. Evaluating the Performance of the DPP® ZDC IgM/IgG Rapid Test for Chikungunya Virus Diagnosis in Febrile Outpatients: A Prospective, Diagnostic Accuracy Study. *medRxiv*. 2023:2023.04.27.23289217. https://doi.org/10.1101/2023.04.27.23289217

98. World Health Organization. Chikungunya [Internet]. Geneva: WHO; 2025 Apr 14 [cited 2025 Jun 1]. Available from: https://www.who.int/news-room/fact-sheets/detail/chikungunya

99. Schneider M, Narciso-Abraham M, Hadl S, McMahon R, Toepfer S, Fuchs U, et al. Safety and immunogenicity of a single-shot live-attenuated chikungunya vaccine: a double-blind, multicentre, randomised, placebo-controlled, phase 3 trial. *Lancet*. 2023;401(10394):2138-47. https://doi.org/10.1016/s0140-6736(23)00641-4

100. Weber WC, Streblow ZJ, Kreklywich CN, Denton M, Sulgey G, Streblow MM, et al. The Approved Live-Attenuated Chikungunya Virus Vaccine (IXCHIQ(®)) Elicits Cross-Neutralizing Antibody Breadth Extending to Multiple Arthritogenic Alphaviruses Similar to the Antibody Breadth Following Natural Infection. *Vaccines (Basel).* 2024;12(8). https://doi.org/10.3390/vaccines12080893

101. Valneva Austria GmbH, IXCHIQ (Chikungunya Vaccine, Live) Solution for Intramuscular Injection 2023 [Available from: https://ixchiqhcp.com/PI.]

102. Hallengärd D, Kakoulidou M, Lulla A, Kümmerer BM, Johansson DX, Mutso M, et al. Novel attenuated Chikungunya vaccine candidates elicit protective immunity in C57BL/6 mice. *J Virol*. 2014;88(5):2858-66. https://doi.org/10.1128/jvi.03453-13

103. Ly H. Ixchiq (VLA1553): The first FDA-approved vaccine to prevent disease caused by Chikungunya virus infection. *Virulence*. 2024;15(1):2301573. https://doi.org/10.1080/21505594.2023.2301573

104. Roongaraya P, Boonyasuppayakorn S. Chikungunya vaccines: An update in 2023. *Asian Pac J Allergy Immunol*. 2023;41(1):1-11. https://doi.org/10.12932/ap-271222-1520

105. Richardson JS, Anderson DM, Mendy J, Tindale LC, Muhammad S, Loreth T, et al. Chikungunya virus virus-like particle vaccine safety and immunogenicity in adolescents and adults in the USA: a phase 3, randomised, double-blind, placebo-controlled trial. *The Lancet*. 2025;405(10487):1343-52. https://doi.org/10.1016/S0140-6736(25)00345-9

106. Shaw CA, August A, Bart S, Booth P-GJ, Knightly C, Brasel T, et al. A phase 1, randomized, placebo-controlled, dose-ranging study to evaluate the safety and immunogenicity of an mRNA-based chikungunya virus vaccine in healthy adults. *Vaccine*. 2023;41(26):3898-906. https://doi.org/10.1016/j.vaccine.2023.04.064

107. Flandes X, Hansen CA, Palani S, Abbas K, Bennett C, Caro WP, et al. Vaccine value profile for Chikungunya. *Vaccine*. 2024;42(19, Supplement 1):S9-S24. https://doi.org/10.1016/j.vaccine.2023.07.069

108. Folegatti PM, Harrison K, Preciado-Llanes L, Lopez FR, Bittaye M, Kim YC, et al. A single dose of ChAdOx1 Chik vaccine induces neutralizing antibodies against four chikungunya virus lineages in a phase 1 clinical trial. *Nat Commun*. 2021;12(1):4636. https://doi.org/10.1038/s41467-021-24906-y

109. Law YS, Wang S, Tan YB, Shih O, Utt A, Goh WY, et al. Interdomain Flexibility of Chikungunya Virus nsP2 Helicase-Protease Differentially Influences Viral RNA Replication and Infectivity. *J Virol*. 2021;95(6). https://doi.org/10.1128/jvi.01470-20

110. Karpe YA, Aher PP, Lole KS. NTPase and 5'-RNA triphosphatase activities of Chikungunya virus nsP2 protein. *PLoS One*. 2011;6(7):e22336. https://doi.org/10.1371/journal.pone.0022336

111. Jones R, Hons M, Rabah N, Zamarreño N, Arranz R, Reguera J. Structural basis and dynamics of Chikungunya alphavirus RNA capping by nsP1 capping pores. *Proceedings of the National Academy of Sciences*. 2023;120(12):e2213934120. https://doi.org/10.1073/pnas.2213934120

112. Rausalu K, Utt A, Quirin T, Varghese FS, Žusinaite E, Das PK, et al. Chikungunya virus infectivity, RNA replication and non-structural polyprotein processing depend on the nsP2 protease's active site cysteine residue. *Sci Rep*. 2016;6:37124. https://doi.org/10.1038/srep37124

113. Rawlings ND, Barrett AJ, Bateman A. MEROPS: the peptidase database. *Nucleic acids research*. 2010;38(suppl_1):D227-D33. https://doi.org/10.1093/nar/gkm954

114. Lemm JA, Rice CM. Roles of nonstructural polyproteins and cleavage products in regulating Sindbis virus RNA replication and transcription. J Virol. 1993;67(4):1916-26. https://doi.org/10.1128/jvi.67.4.1916-1926.1993

115. Vasiljeva L, Merits A, Golubtsov A, Sizemskaja V, Kääriäinen L, Ahola T. Regulation of the Sequential Processing of Semliki Forest Virus Replicase Polyprotein*. *Journal of Biological Chemistry*. 2003;278(43):41636-45. https://doi.org/10.1074/jbc.M307481200

116. Narwal M, Singh H, Pratap S, Malik A, Kuhn RJ, Kumar P, et al. Crystal structure of chikungunya virus nsP2 cysteine protease reveals a putative flexible loop blocking its active site. *International Journal of Biological Macromolecules*. 2018;116:451-62. https://doi.org/10.1016/j.ijbiomac.2018.05.007

117. Wang S, Mahalingam S, Merits A. Alphavirus nsP2: A Multifunctional Regulator of Viral Replication and Promising Target for Anti-Alphavirus Therapies. *Rev Med Virol*. 2025;35(2):e70030. https://doi.org/10.1002/rmv.70030

118. Akhrymuk I, Kulemzin SV, Frolova EI. Evasion of the innate immune response: the Old World alphavirus nsP2 protein induces rapid degradation of Rpb1, a catalytic subunit of RNA polymerase II. *J Virol*. 2012;86(13):7180-91. https://doi.org/10.1128/jvi.00541-12

119. Bae S, Lee JY, Myoung J. Chikungunya Virus nsP2 Impairs MDA5/RIG-I-Mediated Induction of NF-κB Promoter Activation: A Potential Target for Virus-Specific Therapeutics. *J Microbiol Biotechnol*. 2020;30(12):1801-9. https://doi.org/10.4014/jmb.2012.12005

120. Göertz GP, McNally KL, Robertson SJ, Best SM, Pijlman GP, Fros JJ. The Methyltransferase-Like Domain of Chikungunya Virus nsP2 Inhibits the Interferon Response by Promoting the Nuclear Export of STAT1. *J Virol*. 2018;92(17). https://doi.org/10.1128/jvi.01008-18

121. Ware BC, Parks MG, da Silva MOL, Morrison TE. Chikungunya virus infection disrupts MHC-I antigen presentation via nonstructural protein 2. *PLoS Pathog*. 2024;20(3):e1011794. https://doi.org/10.1371/journal.ppat.1011794

122. Ahola T, Merits A. Functions of Chikungunya Virus Nonstructural Proteins. In: Okeoma CM, editor. Chikungunya Virus: Advances in Biology, Pathogenesis, and Treatment. Cham: Springer International Publishing; 2016. p. 75-98. https://doi.org/10.1007/978-3-319-42958-8_6

123. Battisti V, Urban E, Langer T. Antivirals against the Chikungunya Virus. *Viruses*. 2021;13(7):1307. https://doi.org/10.3390/v13071307

124. Mastalipour M, Gering I, Coronado MA, González JEH, Willbold D, Eberle RJ. Novel peptide inhibitor for the Chikungunya virus nsP2 protease: Identification and characterization. *Curr Res Microb Sci*. 2025;8:100376. https://doi.org/10.1016/j.crmicr.2025.100376

125. Merten EM, Sears JD, Leisner TM, Hardy PB, Ghoshal A, Hossain MA, et al. Identification of a cell-active chikungunya virus nsP2 protease inhibitor using a covalent fragment-based screening approach. *Proceedings of the National Academy of Sciences*. 2024;121(42):e2409166121. https://doi.org/10.1073/pnas.2409166121

126. Boike L, Henning NJ, Nomura DK. Advances in covalent drug discovery. *Nat Rev Drug Discov*. 2022;21(12):881-98. https://doi.org/10.1038/s41573-022-00542-z

127. Kim DH, Jung EA, Sohng IS, Han JA, Kim TH, Han MJ. Intestinal bacterial metabolism of flavonoids and its relation to some biological activities. *Arch Pharm Res*. 1998;21(1):17-23. https://doi.org/10.1007/bf03216747

128. Middleton Jr E, Kandaswami C, Theoharides TC. The effects of plant flavonoids on mammalian cells: implications for inflammation, heart disease, and cancer. *Pharmacological reviews*. 2000;52(4):673-751. https://doi.org/10.1016/S0031-6997(24)01472-8

129. Eberle RJ, Olivier DS, Pacca CC, Avilla CMS, Nogueira ML, Amaral MS, et al. In vitro study of Hesperetin and Hesperidin as inhibitors of zika and chikungunya virus proteases. *PLoS One*. 2021;16(3):e0246319. https://doi.org/10.1371/journal.pone.0246319

130. Tripathi PK, Soni A, Singh Yadav SP, Kumar A, Gaurav N, Raghavendhar S, et al. Evaluation of novobiocin and telmisartan for anti-CHIKV activity. *Virology*. 2020;548:250-60. https://doi.org/10.1016/j.virol.2020.05.010

131. Sen S, Samat R, Jash M, Ghosh S, Roy R, Mukherjee N, et al. Potential Broad-Spectrum Antimicrobial, Wound Healing, and Disinfectant Cationic Peptide Crafted from Snake Venom. *J Med Chem*. 2023;66(16):11555-72. https://doi.org/10.1021/acs.jmedchem.3c01150

132. Yau AWN, Chu SYC, Yap WH, Wong CL, Chia AYY, Tang YQ. Phage display screening in breast cancer: From peptide discovery to clinical applications. *Life Sci*. 2024;357:123077. https://doi.org/10.1016/j.lfs.2024.123077

133. Wang L, Wang N, Zhang W, Cheng X, Yan Z, Shao G, et al. Therapeutic peptides: current applications and future directions. *Signal Transduction and Targeted Therapy*. 2022;7(1):48. https://doi.org/10.1038/s41392-022-00904-4

134. van Groen T, Schemmert S, Brener O, Gremer L, Ziehm T, Tusche M, et al. The Aβ oligomer eliminating D-enantiomeric peptide RD2 improves cognition without changing plaque pathology. *Sci Rep*. 2017;7(1):16275. https://doi.org/10.1038/s41598-017-16565-1

135. Rossino G, Marchese E, Galli G, Verde F, Finizio M, Serra M, et al. Peptides as Therapeutic Agents: Challenges and Opportunities in the Green Transition Era. *Molecules*. 2023;28(20):7165. https://doi.org/10.3390/molecules28207165

136. Barman P, Joshi S, Sharma S, Preet S, Sharma S, Saini A. Strategic Approaches to Improvise Peptide Drugs as Next Generation Therapeutics. International Journal of Peptide Research and Therapeutics. 2023;29(4):61. https://doi.org/10.1007/s10989-023-10524-3

137. Dhindwal S, Pooja K, Harvijay S, Pravindra K, and Tomar S. Conformer and pharmacophore based identification of peptidomimetic inhibitors of chikungunya virus nsP2 protease. *Journal of Biomolecular Structure and Dynamics*. 2017;35(16):3522-39. https://doi.org/10.1080/07391102.2016.1261046

138. Singh H, Mudgal R, Narwal M, Kaur R, Singh VA, Malik A, et al. Chikungunya virus inhibition by peptidomimetic inhibitors targeting virus-specific cysteine protease. *Biochimie*. 2018;149:51-61. https://doi.org/10.1016/j.biochi.2018.04.004

139. Ivanova L, Rausalu K, Žusinaite E, Tammiku-Taul J, Merits A, Karelson M. 1,3-Thiazolbenzamide Derivatives as Chikungunya Virus nsP2 Protease Inhibitors. *ACS Omega*. 2021;6(8):5786-94. https://doi.org/10.1021/acsomega.0c06191

140. De S, Ghosh S, Keshry SS, Mahish C, Mohapatra C, Guru A, et al. MBZM-N-IBT, a Novel Small Molecule, Restricts Chikungunya Virus Infection by Targeting nsP2 Protease Activity *In Vitro, In Vivo,* and *Ex Vivo. Antimicrobial Agents and Chemotherapy*. 2022;66(7):e00463-22. https://doi.org/10.1128/aac.00463-22

141. Barderas R, Benito-Peña E. The 2018 Nobel Prize in Chemistry: phage display of peptides and antibodies. *Analytical and Bioanalytical Chemistry*. 2019;411(12):2475-9. https://doi.org/10.1007/s00216-019-01714-4

142. Boder ET, Wittrup KD. Yeast surface display for screening combinatorial polypeptide libraries. *Nature Biotechnology*. 1997;15(6):553-7. https://doi.org/10.1038/nbt0697-553

143. Gai SA, Wittrup KD. Yeast surface display for protein engineering and characterization. *Current Opinion in Structural Biology*. 2007;17(4):467-73. https://doi.org/10.1016/j.sbi.2007.08.012

144. Lewis RJ, Garcia ML. Therapeutic potential of venom peptides. *Nature Reviews Drug Discovery*. 2003;2(10):790-802. https://doi.org/10.1038/nrd1197

145. Maia EHB, Assis LC, de Oliveira TA, da Silva AM, Taranto AG. Structure-Based Virtual Screening: From Classical to Artificial Intelligence. Frontiers in Chemistry. 2020;Volume 8 - 2020. https://doi.org/10.3389/fchem.2020.00343

146. Bozovičar K, Bratkovič T. Evolving a Peptide: Library Platforms and Diversification Strategies. International Journal of Molecular Sciences. 2019;21:215. https://doi.org/10.3390/ijms21010215

147. Smith GP. Filamentous Fusion Phage: Novel Expression Vectors That Display Cloned Antigens on the Virion Surface. *Science*. 1985;228(4705):1315-7. https://doi.org/10.1126/science.4001944

148. Wu C-H, Liu IJ, Lu R-M, Wu H-C. Advancement and applications of peptide phage display technology in biomedical science. *Journal of Biomedical Science*. 2016;23(1):8. https://doi.org/10.1186/s12929-016-0223-x

149. Christiansen A, Kringelum JV, Hansen CS, Bøgh KL, Sullivan E, Patel J, et al. High-throughput sequencing enhanced phage display enables the identification of patient-specific epitope motifs in serum. *Scientific Reports*. 2015;5(1):12913. https://doi.org/10.1038/srep12913

150. Kutzsche J, Cosma NC, Kauselmann G, Fenski F, Bieniek C, Bujnicki T, et al. Oral PRI-002 treatment in patients with MCI or mild AD: a randomized, double-blind phase 1b trial. *Nat Commun*. 2025;16(1):4180. https://doi.org/10.1038/s41467-025-59295-z

151. Eberle RJ, Sevenich M, Gering I, Scharbert L, Strodel B, Lakomek NA, et al. Discovery of All-d-Peptide Inhibitors of SARS-CoV-2 3C-like Protease. *ACS Chemical Biology*. 2023;18(2):315-30.https://doi.org/10.1021/acschembio.2c00735

152. Pennington MW, Czerwinski A, Norton RS. Peptide therapeutics from venom: Current status and potential. *Bioorganic & Medicinal Chemistry*. 2018;26(10):2738-58. https://doi.org/10.1016/j.bmc.2017.09.029

153. Freuville L, Matthys C, Quinton L, Gillet J-P. Venom-derived peptides for breaking through the glass ceiling of drug development. *Frontiers in Chemistry*. 2024;12:1465459. https://doi.org/10.3389/fchem.2024.1465459

154. Hemajha L, Singh S, Biji CA, Balde A, Benjakul S, Nazeer RA. A review on inflammation modulating venom proteins/peptide therapeutics and their delivery strategies: A review. *International Immunopharmacology*. 2024;142:113130. https://doi.org/10.1016/j.intimp.2024.113130

155. Rabea EY, Mahmoud ED, Mohamed NK, Ansary ER, Alrouby MR, Shehata RR, et al. Potential of Venom-Derived Compounds for the Development of New Antimicrobial Agents. Toxins. 2025;17(5):238. https://doi.org/10.3390/toxins17050238

156. Crusca E, Basso LGM, Altei WF, Marchetto R. Biophysical characterization and antitumor activity of synthetic Pantinin peptides from scorpion's venom. *Biochimica et Biophysica Acta (BBA) - Biomembranes*. 2018;1860(11):2155-65. https://doi.org/10.1016/j.bbamem.2018.08.012

157. Zeng X-C, Zhou L, Shi W, Luo X, Zhang L, Nie Y, et al. Three new antimicrobial peptides from the scorpion Pandinus imperator. *Peptides*. 2013;45:28-34. https://doi.org/10.1016/j.peptides.2013.03.026

158. Bordon KCF, Cologna CT, Fornari-Baldo EC, Pinheiro-Júnior EL, Cerni FA, Amorim FG, et al. From Animal Poisons and Venoms to Medicines: Achievements, Challenges and Perspectives in Drug Discovery. *Front Pharmacol*. 2020;11:1132. https://doi.org/10.3389/fphar.2020.01132

159. Soroceanu L, Gillespie Y, Khazaeli MB, Sontheimer H. Use of Chlorotoxin for Targeting of Primary Brain Tumors1. *Cancer Research*. 1998;58(21):4871-9

160. Eberle RJ, Gering I, Tusche M, Ostermann PN, Müller L, Adams O, et al. Design of D-Amino Acids SARS-CoV-2 Main Protease Inhibitors Using the Cationic Peptide from Rattlesnake Venom as a Scaffold. *Pharmaceuticals (Basel)*. 2022;15(5). https://doi.org/10.3390/ph15050540

161. Borkow G, Ovadia M. Echinhibin-1--an inhibitor of Sendai virus isolated from the venom of the snake Echis coloratus. *Antiviral Res*. 1994;23(2):161-76. https://doi.org/10.1016/0166-3542(94)90042-6

162. Cvetković RS, Plosker GL. Exenatide. *Drugs*. 2007;67(6):935-54. https://doi.org/10.2165/00003495-200767060-00008

163. Furman BL. The development of Byetta (exenatide) from the venom of the Gila monster as an anti-diabetic agent. *Toxicon*. 2012;59(4):464-71. https://doi.org/10.1016/j.toxicon.2010.12.016

164. Wachinger M, Kleinschmidt A, Winder D, von Pechmann N, Ludvigsen A, Neumann M, et al. Antimicrobial peptides melittin and cecropin inhibit replication of human immunodeficiency virus 1 by suppressing viral gene expression. *J Gen Virol*. 1998;79 (Pt 4):731-40. https://doi.org/10.1099/0022-1317-79-4-731

165. Zhang HQ, Sun C, Xu N, Liu W. The current landscape of the antimicrobial peptide melittin and its therapeutic potential. *Front Immunol*. 2024;15:1326033. https://doi.org/10.3389/fimmu.2024.1326033

166. Vetterli SU, Zerbe K, Müller M, Urfer M, Mondal M, Wang S-Y, et al. Thanatin targets the intermembrane protein complex required for lipopolysaccharide transport in *Escherichia coli*. *Science Advances*. 2018;4(11):eaau2634. https://doi.org/10.1126/sciadv.aau2634

167. Deer TR, Pope JE, Hanes MC, McDowell GC. Intrathecal Therapy for Chronic Pain: A Review of Morphine and Ziconotide as Firstline Options. *Pain Med*. 2019;20(4):784-98. https://doi.org/10.1093/pm/pny132

168. Safavi-Hemami H, Brogan SE, Olivera BM. Pain therapeutics from cone snail venoms: From Ziconotide to novel non-opioid pathways. *J Proteomics*. 2019;190:12-20. https://doi.org/10.1016/j.jprot.2018.05.009

169. Mangel WF, McGrath WJ, Toledo DL, Anderson CW. Viral DNA and a viral peptide can act as cofactors of adenovirus virion proteinase activity. *Nature*. 1993;361(6409):274-5. https://doi.org/10.1038/361274a0

170. Hartl MJ, Bodem J, Jochheim F, Rethwilm A, Rösch P, Wöhrl BM. Regulation of Foamy Virus Protease Activity by Viral RNA: a Novel and Unique Mechanism among Retroviruses. *Journal of Virology*. 2011;85(9):4462-9. https://doi.org/10.1128/jvi.02211-10

171. Potempa M, Nalivaika E, Ragland D, Lee S-K, Schiffer CA, Swanstrom R. A Direct Interaction with RNA Dramatically Enhances the Catalytic Activity of the HIV-1 Protease *In Vitro*. *Journal of Molecular Biology*. 2015;427(14):2360-78. https://doi.org/10.1016/j.jmb.2015.05.007

172. Campagnola G, Peersen O. Co-folding and RNA activation of poliovirus $3C^{pro}$ polyprotein precursors. *Journal of Biological Chemistry*. 2023;299(11). https://doi.org/10.1016/j.jbc.2023.105258

173. Xu G, Wang C, Yu H, Li Y, Zhao Q, Zhou X, et al. Structural basis for high-affinity recognition of aflatoxin B1 by a DNA aptamer. *Nucleic Acids Research*. 2023;51(14):7666-74. https://doi.org/10.1093/nar/gkad541

174. Keefe AD, Pai S, Ellington A. Aptamers as therapeutics. *Nature Reviews Drug Discovery*. 2010;9(7):537-50. https://doi.org/10.1038/nrd3141

175. Fukuda K, Vishnuvardhan D, Sekiya S, Hwang J, Kakiuchi N, Taira K, et al. Isolation and characterization of RNA aptamers specific for the hepatitis C virus nonstructural protein 3 protease. *Eur J Biochem*. 2000;267(12):3685-94. https://doi.org/10.1046/j.1432-1327.2000.01400.x

176. Yang D, Meng X, Yu Q, Xu L, Long Y, Liu B, et al. Inhibition of Hepatitis C Virus Infection by DNA Aptamer against Envelope Protein. *Antimicrobial Agents and Chemotherapy*. 2013;57(10):4937-44. https://doi.org/10.1128/aac.00897-13

177. Drees A, Fischer M. High-Throughput Selection and Characterisation of Aptamers on Optical Next-Generation Sequencers. *Int J Mol Sci*. 2021;22(17). https://doi.org/10.3390/ijms22179202

178. Burt FJ, Rolph MS, Rulli NE, Mahalingam S, Heise MT. Chikungunya: a re-emerging virus. *The Lancet*. 2012;379(9816):662-71. https://doi.org/10.1016/S0140-6736(11)60281-X

179. Hucke FIL, Bugert JJ. Current and Promising Antivirals Against Chikungunya Virus. *Front Public Health*. 2020;8:618624. https://doi.org/10.3389/fpubh.2020.618624

180. Saha A, Acharya BN, Priya R, Tripathi NK, Shrivastava A, Rao MK, et al. Development of nsP2 protease based cell free high throughput screening assay for evaluation of inhibitors against emerging Chikungunya virus. *Scientific Reports*. 2018;8(1):10831. https://doi.org/10.1038/s41598-018-29024-2

181. Horwood PF, Buchy P. Chikungunya. *Rev Sci Tech*. 2015;34(2):479-89. https://doi.org/10.20506/rst.34.2.2373

182. Waldrop GL. A qualitative approach to enzyme inhibition. *Biochemistry and Molecular Biology Education*. 2009;37(1):11-5. https://doi.org/10.1002/bmb.20243

183. Blat Y. Non-competitive inhibition by active site binders. *Chem Biol Drug Des*. 2010;75(6):535-40. https://doi.org/10.1111/j.1747-0285.2010.00972.x

184. Pelley JW. 4 - Enzymes and Energetics. In: Pelley JW, editor. Elsevier's Integrated Review Biochemistry (Second Edition). Philadelphia: W.B. Saunders; 2012. p. 29-37. https://doi.org/10.1016/B978-0-323-07446-9.00004-0

185. Singh K, Bhushan B, Mittal N, Kushwaha A, Raikwar C, Sharma A, et al. Recent Advances in Enzyme Inhibition: A Pharmacological Review. *Current Enzyme Inhibition*. 2024;20:2-19. https://doi.org/10.2174/0115734080271639231030093152

186. Lee D, Kim J, Lee G. Simple methods to determine the dissociation constant, Kd. *Molecules and Cells*. 2024;47(10):100112. https://doi.org/10.1016/j.mocell.2024.100112

187. Ma W, Yang L, He L. Overview of the detection methods for equilibrium dissociation constant K(D) of drug-receptor interaction. *J Pharm Anal*. 2018;8(3):147-52. https://doi.org/10.1016/j.jpha.2018.05.001

188. Matsunaga R, Ujiie K, Inagaki M, Fernández Pérez J, Yasuda Y, Mimasu S, et al. High-throughput analysis system of interaction kinetics for data-driven antibody design. *Scientific Reports*. 2023;13(1):19417. https://doi.org/10.1038/s41598-023-46756-y

189. Sun H, Wang Y, Cheff DM, Hall MD, Shen M. Predictive models for estimating cytotoxicity on the basis of chemical structures. *Bioorg Med Chem*. 2020;28(10):115422. https://doi.org/10.1016/j.bmc.2020.115422

190. van Meerloo J, Kaspers GJL, Cloos J. Cell Sensitivity Assays: The MTT Assay. In: Cree IA, editor. *Methods in molecular biology (Clifton, N.J.)*, *731*, 237–245. https://doi.org/10.1007/978-1-61779-080-5_20

191. Aguilar JS, Roy D, Ghazal P, Wagner EK. Dimethyl sulfoxide blocks herpes simplex virus-1 productive infection in vitro acting at different stages with positive cooperativity. Application of micro-array analysis. *BMC Infectious Diseases*. 2002;2(1):9. https://doi.org/10.1186/1471-2334-2-9

192. Campoccia D, Bottau G, De Donno A, Bua G, Ravaioli S, Capponi E, et al. Assessing Cytotoxicity, Proteolytic Stability, and Selectivity of Antimicrobial Peptides: Implications for Orthopedic Applications. *International Journal of Molecular Sciences*. 2024;25(24):13241. https://doi.org/10.3390/ijms252413241

193. Yang J, Yan R, Roy A, Xu D, Poisson J, Zhang Y. The I-TASSER Suite: protein structure and function prediction. *Nature Methods*. 2015;12(1):7-8. https://doi.org/10.1038/nmeth.3213

194. Haque MA, Kaur P, Islam A, Hassan MI. Chapter 14 - Application of circular dichroism spectroscopy in studying protein folding, stability, and interaction. In: Tripathi T, Dubey VK, editors. *Advances in Protein Molecular and Structural Biology Methods: Academic Press*; 2022. p. 213-24. https://doi.org/10.1016/B978-0-323-90264-9.00014-3

195. Wang H, Dawber RS, Zhang P, Walko M, Wilson AJ, Wang X. Peptide-based inhibitors of protein–protein interactions: biophysical, structural and cellular consequences of introducing a constraint. *Chemical Science*. 2021;12(17):5977-93. https://doi.org/10.1039/d1sc00165e

196. Huang Y, He L, Li G, Zhai N, Jiang H, Chen Y. Role of helicity of α-helical antimicrobial peptides to improve specificity. *Protein Cell*. 2014;5(8):631-42. https://doi.org/10.1007/s13238-014-0061-0

197. Chen Y, Guarnieri MT, Vasil AI, Vasil ML, Mant CT, Hodges RS. Role of peptide hydrophobicity in the mechanism of action of alpha-helical antimicrobial peptides. *Antimicrob Agents Chemother*. 2007;51(4):1398-406. https://doi.org/10.1128/aac.00925-06

198. Kozakov D, Hall DR, Xia B, Porter KA, Padhorny D, Yueh C, et al. The ClusPro web server for protein-protein docking. *Nat Protoc*. 2017;12(2):255-78. https://doi.org/10.1038/nprot.2016.169

199. Yan Y, Zhang D, Zhou P, Li B, Huang SY. HDOCK: a web server for protein-protein and protein-DNA/RNA docking based on a hybrid strategy. *Nucleic Acids Res*. 2017;45(W1):W365-w73. https://doi.org/10.1093/nar/gkx407

200. Hu X, Compton JR, Leary DH, Olson MA, Lee MS, Cheung J, et al. Kinetic, Mutational, and Structural Studies of the Venezuelan Equine Encephalitis Virus Nonstructural Protein 2 Cysteine Protease. *Biochemistry*. 2016;55(21):3007-19. https://doi.org/10.1021/acs.biochem.5b00992

201. Wu L, Yan Y, Yuan Y, Zhao Z, Qu W, Huang X, et al. Viral protease binds to nucleosomal DNA and cleaves nuclear cGAS that attenuates type I interferon. *mBio*. 2025;16(4):e0339524. https://doi.org/10.1128/mbio.03395-24

202. Yin J, Chen R, Liu C. Nucleic acid induced protein aggregation and its role in biology and pathology. *FBL*. 2009;14(13):5084-106. https://doi.org/10.2741/3588

203. Cruceanu M, Urbaneja MA, Hixson CV, Johnson DG, Datta SA, Fivash MJ, et al. Nucleic acid binding and chaperone properties of HIV-1 Gag and nucleocapsid proteins. *Nucleic Acids Res*. 2006;34(2):593-605. https://doi.org/10.1093/nar/gkj458

204. Pavletich NP, Pabo CO. Zinc finger-DNA recognition: crystal structure of a Zif268-DNA complex at 2.1 A. *Science*. 1991;252(5007):809-17. https://doi.org/10.1126/science.2028256

205. Dougherty DA. The Cation-π Interaction in Chemistry and Biology. *Chem Rev*. 2025;125(5):2793-808. https://doi.org/10.1021/acs.chemrev.4c00707

206. Kutnowski N, Shmulevich F, Davidov G, Shahar A, Bar-Zvi D, Eichler J, et al. Specificity of protein–DNA interactions in hypersaline environment: structural studies on complexes of Halobacterium salinarum oxidative stress-dependent protein hsRosR. *Nucleic Acids Research*. 2019;47(16):8860-73. https://doi.org/10.1093/nar/gkz604

207. Drees A, Trinh TL, Fischer M. The Influence of Protein Charge and Molecular Weight on the Affinity of Aptamers. *Pharmaceuticals*. 2023;16(3):457. https://doi.org/10.3390/ph16030457

208. Onufriev AV. Biologically relevant small variations of intra-cellular pH can have significant effect on stability of protein-DNA complexes, including the nucleosome. *Front Mol Biosci*. 2023;10:1067787. https://doi.org/10.3389/fmolb.2023.1067787

209. Markham NR, Zuker M. DINAMelt web server for nucleic acid melting prediction. *Nucleic Acids Research.* 2005;33(suppl_2):W577-W81. https://doi.org/10.1093/nar/gki591

210. Kypr J, Kejnovská I, Renčiuk D, Vorlíčková M. Circular dichroism and conformational polymorphism of DNA. *Nucleic Acids Research*. 2009;37(6):1713-25. https://doi.org/10.1093/nar/gkp026

211. Sosnick TR, Fang X, Shelton VM. [24] Application of circular dichroism to study RNA folding transitions. Methods in Enzymology. 317: *Academic Press*. 2000. p. 393-409. https://doi.org/10.1016/s0076-6879(00)17026-0